

Computational Pathology: A Survey Review and The Way Forward

Mahdi S. Hosseini^{a,*}, Babak Ehteshami Bejnordi^{b,1}, Vincent Quoc-Huy Trinh^c, Lyndon Chan^d, Danial Hasan^d, Xingwen Li^d, Stephen Yang^d, Taehyo Kim^d, Haochen Zhang^d, Theodore Wu^d, Kajanan Chinniah^d, Sina Maghsoudlou^a, Ryan Zhang^d, Jiadai Zhu^d, Samir Khaki^d, Andrei Buin^e, Fatemeh Chaji^a, Ala Salehi^f, Bich Ngoc Nguyen^g, Dimitris Samaras^h, Konstantinos N. Plataniotis^d

^aDepartment of Computer Science and Software Engineering (CSSE), Concordia University, Montreal, QC H3H 2R9, Canada

^bQualcomm AI Research, Qualcomm Technologies Netherlands B.V., Amsterdam, The Netherlands

^cInstitute for Research in Immunology and Cancer of the University of Montreal, Montreal, QC H3T 1J4, Canada

^dThe Edward S. Rogers Sr. Department of Electrical & Computer Engineering (ECE), University of Toronto, Toronto, ON M5S 3G4, Canada

^eHuron Digital Pathology, St. Jacobs, ON N0B 2N0, Canada

^fDepartment of Electrical and Computer Engineering, University of New Brunswick, Fredericton, NB E3B 5A3, Canada

^gUniversity of Montreal Hospital Center, Montreal, QC H2X 0C2, Canada

^hDepartment of Computer Science, Stony Brook University, Stony Brook, NY 11794, United States

This work is dedicated to the beloved memories of Kuanhou Fang, Shahnaz Habibpanah, Zakiyeh Khaliji-Oskoui, James Liang, Mahsa MohammadiMoghaddam, Vily Panoutsakopoulou, Athanasia Samara, Huoyuan Yu, Dexi Zhang and all people around the world who have lost their lives because of cancer

Abstract. Computational Pathology (CPath) is an interdisciplinary science that augments developments of computational approaches to analyze and model medical histopathology images. The main objective for CPath is to develop infrastructure and workflows of digital diagnostics as an assistive CAD system for clinical pathology, facilitating transformational changes in the diagnosis and treatment of cancer that are mainly address by CPath tools. With evergrowing developments in deep learning and computer vision algorithms, and the ease of the data flow from digital pathology, currently CPath is witnessing a paradigm shift. Despite the sheer volume of engineering and scientific works being introduced for cancer image analysis, there is still a considerable gap of adopting and integrating these algorithms in clinical practice. This raises a significant question regarding the direction and trends that are undertaken in CPath. In this article we provide a comprehensive review of more than 700 papers to address the challenges faced in problem design all-the-way to the application and implementation viewpoints. We have catalogued each paper into a model-card by examining the key works and challenges faced to layout the current landscape in CPath. We hope this helps the community to locate relevant works and facilitate understanding of the field's future directions. In a nutshell, we oversee the CPath developments in cycle of stages which are required to be cohesively linked together to address the challenges associated with such multidisciplinary science. We overview this cycle from different perspectives of data-centric, model-centric, and application-centric problems. We finally sketch remaining challenges and provide directions for future technical developments and clinical integration of CPath. For updated information on this survey review paper and accessing to the original model cards repository, please refer to GitHub.

Keywords: digital pathology, whole slide image (WSI), deep learning, computer aided diagnosis (CAD), clinical pathology, survey

Contents

| | | | |
|--|----------|---|-----------|
| 1 Introduction | 2 | 3.2 Whole Slide Imaging (WSI) | 10 |
| 2 Clinical Applications for CPath | 4 | 3.3 Cohort Selection, Scale, and Challenges | 11 |
| 2.1 Clinical Pathology Workflow | 4 | 4 Domain Expert Knowledge Annotation | 13 |
| 2.2 Diagnostic Tasks | 5 | 4.1 Supervised Annotation | 13 |
| 2.3 Prognosis | 6 | 4.2 Optimum Labeling Workflow Design | 15 |
| 2.4 Prediction of treatment response | 6 | 5 Model Learning for CPath | 16 |
| 2.5 Organs and Diseases | 6 | 5.1 Classification Architectures | 17 |
| 3 Data Collection for CPath | 9 | 5.2 Segmentation Architectures | 17 |
| 3.1 Tissue Slide Preparation | 10 | 5.3 Object Detection Architectures | 17 |
| | | 5.4 Multi-Task Learning | 18 |
| | | 5.5 Multi-Modal Learning | 18 |
| | | 5.6 Vision-Language Models | 18 |
| | | 5.7 Sequential Models | 19 |
| | | 5.8 Synthetic Data and Generative Models | 19 |
| | | 5.9 Multi-Instance Learning (MIL) Models | 19 |

*Corresponding author.

E-mail address: mahdi.hosseini@concordia.ca

¹Qualcomm AI Research is an initiative of Qualcomm Technologies, Inc.

| | | |
|----------|--|-----------|
| 5.10 | Contrastive Self-Supervised Learning for Few-Shot Generalization | 20 |
| 5.11 | Novel CPath Architectures | 20 |
| 5.12 | Model Comparison | 20 |
| 6 | Evaluation and Regulations | 21 |
| 6.1 | Clinical Validation | 21 |
| 6.2 | FDA Regulations | 22 |
| 7 | Emerging Trends in CPath Research | 22 |
| 7.1 | Contrastive Self-Supervised Learning becomes Mainstream | 22 |
| 7.2 | Prediction becoming increasingly High-Level | 22 |
| 7.3 | Spatial and Hierarchical Relationships receiving Attention | 22 |
| 7.4 | Vision-Language Models for Explainable Predictions | 22 |
| 7.5 | Synthetic Data now Realistic Enough | 23 |
| 8 | Existing Challenges and Future Opportunities | 23 |
| 8.1 | CPath as Anomaly Detection | 23 |
| 8.2 | Leveraging Existing Datasets | 23 |
| 8.3 | Creating New Datasets | 24 |
| 8.4 | Pre- and Post-Analytical CAD Tools | 24 |
| 8.5 | Multi Domain Learning | 24 |
| 8.6 | Federated Learning for Multi-Central CPath | 24 |
| 8.7 | CPath-specific Architecture Designs | 25 |
| 8.8 | Digital and Computational Pathology Adoption | 25 |
| 8.9 | Institutional Challenges | 26 |
| 8.10 | Clinical Alignment of CPath Tasks | 26 |
| 8.11 | Concluding Remarks | 26 |
| 9 | Appendix | 51 |
| 9.1 | Clinical Pathology Workflow | 51 |
| 9.2 | Diagnostic Tasks | 52 |
| 9.3 | Prognosis | 53 |
| 9.4 | Prediction of Treatment Response | 54 |
| 9.5 | Cancer Statistics | 54 |
| 9.6 | Whole Slide Imaging | 55 |
| 9.7 | Organs and Diseases | 56 |
| 9.8 | Ground Truth Labelling and Annotation | 58 |
| 9.9 | Surveyed Datasets | 59 |
| 9.9.1 | Table Creation Details | 59 |
| 9.10 | Organ Overview | 59 |
| 9.11 | Technicalities by Task | 59 |
| 9.12 | Model Card Categorization | 81 |
| 9.12.1 | Template | 81 |
| 9.12.2 | Samples | 82 |

1. Introduction

April 2017 marked a turning point for digital pathology when the Philips IntelliSite digital scanner received the US Food & Drugs Administration (FDA) approval (with limited use case) for diagnostic applications in clinical pathology [1, 2]. A subsequent validation guideline was created to help ensure the produced Whole Slide Image (WSI) scans could be used in clinical settings without compromising patient care, while maintaining similar results to the current gold standard of optical microscopy [3, 4, 5, 6]. The use of WSIs offers significant advantages to the pathologist’s workflow: digitally captured images, compared to tissue slides, are immune from accidental physical damage and maintain their quality over time [7, 8].

Clinics and practices can share and store these high-resolution images digitally enabling asynchronous viewing/collaboration worldwide [9, 10]. The development of *digital pathology* shows great promise as a framework to improve work efficiency in the practice of pathology [11, 10]. Adopting a digital workflow also opens immense opportunities for using computational methods to augment and expedite their workflow—the field of *Computational Pathology (CPath)* is dedicated to researching and developing these methods [12, 13, 14, 15, 16, 17].

However, despite the aforementioned advantages, the adoption of digital pathology, and hence computational pathology, has been slow. Some pathologists consider the analysis of WSIs as opposed to glass slides as an unnecessary change in their workflow [18, 19, 9, 20] and recent surveys indicate that the switch to digital pathology does not provide enough financial incentive [21, 22, 23, 24, 25, 8]. This is where advances from CPath can address or overpower many of the concerns in adopting a digital workflow. For example, CPath models to identify morphological features that correlate with breast cancer [26] provide substantial benefits to clinical accuracy. Further, CPath models that identify lymph node metastases with better sensitivity while reducing diagnostic time [27] can streamline workflows to increase pathologist throughput and generate more revenue [28, 29].

Similar to digital pathology, the adoption of CPath methods has also lagged despite the many benefits it offers to improve efficiency and accuracy in pathology [30, 31, 2, 32]. This lack of adoption and integration into clinical practice raises a significant question regarding the direction and trends of current work in CPath. This survey looks to review the field of CPath in a systematic fashion by breaking down the various steps involved in a CPath workflow and categorizing CPath works to both determine trends in the field and provide a resource for the community to reference when creating new works.

Existing survey papers in the field of CPath can be clustered into a few groups. The first focuses on the design and applications of smart diagnosis tools [33, 34, 35, 36, 37, 38, 17, 16, 15, 39, 40, 41, 42, 43]. These works focus on designing novel architectures for artificial intelligence (AI) models with regards to specific clinical tasks, although they may briefly discuss clinical challenges and limitations. A second group of works focus on clinical barriers for AI integration discussing specific certifications and regulations required for the development of medical devices under clinical settings [44, 45, 46, 47, 48, 49]. Lastly, the final group focuses on both the design and the integration of AI tools with clinical applications [50, 51, 12, 13, 52, 29, 53, 54, 14, 55, 56]. These works speak to both the computer vision and pathology communities in developing machine learning (ML) models that can satisfy clinical use cases.

Our work is situated in this final group as we breakdown the end-to-end CPath workflow into stages and systematically review works related to and addressing those stages. We oversee this as a workflow for CPath research that breaks down the process of problem definition, data collection, model creation, and clinical validation into a cycle of stages. A visual representation of this cycle is provided in Figure 1. We review over 700 papers

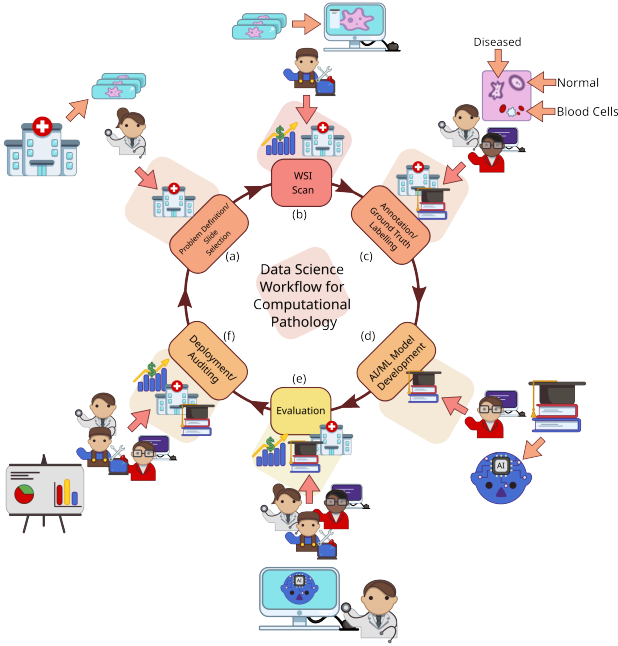


Fig. 1: We divide the data science workflow for pathology into multiple stages, wherein each brings a different level of experience. For example, the annotation/ground truth labelling stage (c) is where domain expert knowledge is consulted as to augment images with associated metadata. Meanwhile, in the evaluation phase (e), we have computer vision scientists, software developers, and pathologists working in concert to extract meaningful results and implications from the representation learning.

from all areas of the CPath field to examine key works and challenges faced. By reviewing the field so comprehensively, our goal is to layout the current landscape of key developments to allow computer scientists and pathologists alike to situate their work in the overall CPath workflow, locate relevant works, and facilitate an understanding of the field’s future directions. We also adopt the idea of generating model cards from [57] and designed a card format specifically tailored for CPath. Each paper we reviewed was catalogued as a model card that concisely describes (1) the organ of application, (2) the compiled dataset, (3) the machine learning model, and (4) the target task. The complete model card categorization of the reviewed publications is provided in Appendix 9.12 for the reader’s use.

In our review of the CPath field, we find that two main approaches emerge in works: 1) a data-centric approach and 2) a model-centric approach. Considering a given application area, such as specific cancers, e.g. breast ductal carcinoma in-situ (DCIS), or a specific task, e.g. segmentation of benign and malignant regions of tissue, researchers in the CPath field focus generally on either improving the data or innovating on the model used.

Works with data-centric approaches focus on collecting pathology data and compiling datasets to train models on certain tasks based on the premise that the transfer of domain expert knowledge to models is captured by the process of collecting and labeling high-quality data [58, 51, 59]. The motivation behind this approach in CPath is driven by the need to 1) ad-

dress the lack of labeled WSI data representing both histology and histopathology cases due to the laborious annotation process [24] and 2) capture a predefined pathology ontology provided by domain expert pathologists for the class definitions and relations in tissue samples. Regarding the lack of labeled WSI data our analysis reveals that there are a larger number of datasets with granular labels, but there is a larger total amount of data available for a given organ and disease application that have weakly supervised labels at the Slide or Patient-level. Although some tasks, such as segmentation and detection, require WSI data to have more granular labels at the region-of-interest (ROI) or image mosaic/tiles (known as patch) levels, to capture more precise information for training models, there is a potential gap to leverage the large amount of weakly-supervised data to train models that can be later used downstream on smaller strongly-supervised datasets for those tasks. When considering the ontology of pathology as compared to the field of computer vision, we note that pathology datasets have far fewer classes than computer vision (e.g. ImageNet-20K contains 20,000 class categories for natural images [60] whereas CAMELYON17 has four annotated classes for breast cancer metastases [61]), but has much more variation within each of these classes in terms of representations and fuzzy boundaries around the *grade* of cancers which subdivides each class into many more in reality. There are also very rare classes in the form of rare diseases and cancers, as presented in Figure 12 and discussed in Section 2, which present a class imbalance challenge when compiling data or training models. If one considers the complexities involved in representational learning of related tissues and diseases, it raises the question of whether there is a clear understanding and consensus in the field of how an efficient dataset should be compiled for model development. Our survey analyzes the availability of CPath datasets along with what area of application they address and their annotation level in detail in Section 3.3, and the complete table of datasets we have covered is available in Appendix 9.9. Section 4 goes into more depth about the various levels of annotation, the annotation process, and selecting the appropriate annotation level for a task.

The model-centric approach, by contrast, is favoured by computer scientists and engineers, who design algorithmic approaches based on the available pathology data. Selection of a modelling approach, such as self-supervised, weakly-supervised, or strongly-supervised learning, is dictated directly by the amount of data available for a given annotation level and task. Currently, many models are developed on datasets with strongly-supervised labels at the ROI, Patch, or Pixel-levels to address tasks such as tissue type classification or disease detection. However, a recent trend is developing to apply self-supervised and weakly-supervised learning methods to leverage the large amount of data with Slide and Patient-level annotations [62]. Models are trained in a self or weakly supervised manner to learn representations on a wider range of pathology data across organs and diseases, which can be leveraged for other tasks requiring more supervision but without the need for massive labeled datasets [63, 64, 65]. This trend points to the future direction of CPath models following a similar trend to that in computer vision, where large-scale models are being

pre-trained using self-supervised techniques to achieve state-of-the-art performance in downstream tasks [66, 67].

Although data and model centric approaches are both important in advancing the performance of models and tools in CPath, we note a need for much more *application* centric work in CPath. We define a study to be application centric if the primary focus is on addressing a particularly impactful task or need in the clinical workflow, ideally including clinical validation of the method or tool. To this end, Section 2 details the clinical pathology workflow from specimen collection to report generation, major task categories in CPath, and specific applications per organ. Particularly, we find that very few works focus on the pre or post-analytical phases of the pathology workflow where many errors can occur, instead focusing on the analytical phase where interpretation tasks take place. Additionally, certain types of cancer with deadly survival rates are underrepresented in CPath datasets and works. Very few CPath models and tools have been validated in a clinical setting by pathologists, suggesting that there may still be massive barriers to actually using CPath tools in practice. All of this points to a severe oversight by the CPath community towards considering the actual application and implementation of tools in a clinical setting. We suspect this to be a major reason as to why there is a slow uptake in adopting CPath tools by pathology labs.

The contributions of this survey include the provision of an end-to-end workflow for developing CPath work which outlines the various stages involved and is reflected within the survey sections. Further, we propose and provide a comprehensive conceptual model card framework for CPath that clearly categorizes works by their application of interest, dataset usage, and model, enabling consistent and easy comparison and retrieval of papers in relevant areas. Based on our analysis of the field, we highlight several challenges and trends, including the availability of datasets, focus on models leveraging existing data, disregard of impactful application areas, and lack of clinical validation. Finally, we give suggestions for addressing these aforementioned challenges and provide directions for future work in the hopes of aiding the adoption and implementation of CPath tools in clinical settings.

The structure of this survey closely follows the CPath data workflow illustrated in Figure 1. Section 2 begins by outlining the clinical pathology workflow and covers the various task domains in CPath, along with organ specific tasks and diseases. The next step of the workflow involves the processes and methods of histopathology data collection, which is outlined in Section 3. Following data collection, Section 4 details the corresponding annotation and labeling methodology and considerations. Section 5 covers deep learning designs and methodologies for CPath applications. Section 6 focuses on regulatory measures and clinical validation of CPath tools. Section 7 explores emerging trends in recent CPath research. Finally, we provide our perceived challenges and future outlook of CPath in Section 8.

2. Clinical Applications for CPath

The field of CPath is dedicated to the creation of tools that address and aid steps in the clinical pathology workflow.

Thus, a grounded understanding of the clinical workflow is of paramount importance before development of any CPath tool. The outcomes of clinical pathology are diagnostics, prognostics, and predictions of therapy response. Computational pathology systems that focus on diagnostic tasks aim to assist the pathologists in tasks such as tumour detection, tumour grading, quantification of cell numbers, etc. Prognostic systems aim to predict survival for individual patients while therapy response predictive models aid personalized treatment decisions based on histopathology images. Figure 3 visualizes the goals pertaining to these tasks. In this section, we provide detail on the clinical pathology workflow, the major application areas in diagnostics, prognostics, and therapy response, and finally detail the cancers and CPath applications in specific organs. The goal is to outline the tasks and areas of application in pathology where CPath tools and systems can be developed and implemented.

2.1. Clinical Pathology Workflow

This subsection provides a general overview of the clinical workflow in pathology covering the collection of a tissue sample, its subsequent processing into a slide, inspection by a pathologist, and compilation of the analysis and diagnosis into a pathology. Figure 2 summarizes these steps at a high level and provides suggestions for corresponding CPath applications. The steps are organized under the conventional pathology phases for samples: pre-analytical, analytical, and post-analytical. These phases were developed to categorize quality control measures, as each phase has its own set of potential sources of errors [68], and thus potential sources of corrections during which CPath and healthcare artificial intelligence tools could prove useful. For details about each step of the workflow, please refer to the Appendix 9.1.

Pre Analytical Phase The first step of the *pre-analytical* phase is a biopsy performed to collect a tissue sample, where the biopsy method is dependent on the type of sample required and the tissue characteristics. Sample collection is followed by accessioning of the sample which involves entering of the patient and specimen information into a Laboratory Information System (LIS) and linking to the Electronic Medical Records (EMR) and potentially a Slide Tracking System (STS). After accessioning, smaller specimens that have not already been preserved by fixation in formalin are fixated. Once the basic specimen preparation has occurred, the tissue is analyzed by the pathology team without the use of a microscope; a step called grossing. Grossing involves cross-referencing the clinical findings and the EMR reports, with the operator localizing the disease, locating the pathological landmarks, describing these landmarks, and measuring disease extent. Specific sampling of these landmarks is performed, and these samples are then put into cassettes for the final fixation. Subsequently, the samples are then sliced using a microtome, stained using the relevant stains for diagnosis, and covered with a glass slide.

Analytical Phase After a slide is processed and prepared, a pathologist views the slide to analyze and interpret the sample. The approach to interpretation varies depending on the specimen type. Interpretation of smaller specimens is focused on

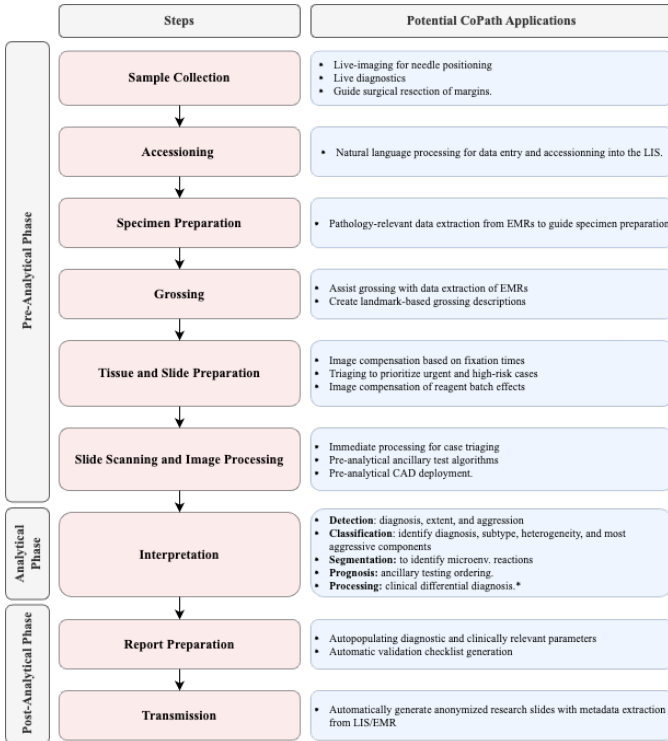


Fig. 2: Quality assurance and control phases developed by pathologists to oversee the clinical pathology workflow into three main phases of pre-analytical, analytical, and post-analytical phases. We further show how each of these processes can be augmented under the potential CPath applications in an end-to-end pipeline.

diagnosis of any disease. Analysis is performed in a decision-tree style approach to add diagnosis-specific parameters, e.g. esophagus biopsy → type of sampled mucosa → presence of foliolar-type mucosa → identify Barrett’s metaplasia → identify degree of dysplasia. Once the main diagnosis has been identified and characterized, the pathologist sweeps the remaining tissue for secondary diagnoses which can also be characterized depending on their nature. Larger specimens are more complex and usually focus on characterizing the tissue and identifying unexpected diagnoses beyond the prior diagnosis from a small specimen biopsy. Microscopic interpretation of large specimens is highly dependent on the quality of the grossing and the appropriate detection and sampling of landmarks. Each landmark (e.g., tumor surface, tumor at deepest point, surgical margins, lymph node in mesenteric fat) is characterized either according to guidelines, if available, or according to the pathologist’s judgment. After the initial microscopic interpretation additional deeper cuts (“levels”), special stains, immunohistochemistry (IHC), and/or molecular testing may be performed to hone the diagnosis by generating new material or slides from the original tissue block.

Post-Analytical Phase The pathologist synthesizes a diagnosis by aggregating their findings from grossing and microscopic examination in combination with the patient’s clinical information, all of which are included in a final pathology report. The

classic sections of a pathology report are patient information, a list of specimens included, clinical findings, grossing report, microscopic description, final diagnosis, and comment. The length and degree of complexity of the report again depends on the specimen type. Small specimen reports are often succinct, clearly and unambiguously listing relevant findings which guide treatment and follow-up. Large specimen reports depend on the disease, for example, in cancer resection specimens the grossing landmarks are specifically targeted at elements that will guide subsequent treatment.

In the past, pathology reports had no standardized format, usually taking a narrative-free text form. Free text reports can omit necessary data, include irrelevant information, and contain inconsistent descriptions [69]. To combat this, synoptic reporting was introduced to provide a structured and standardized reporting format specific to each organ and cancer of interest [69, 70]. Over the last 15 years, synoptic reporting has enabled pathologists to communicate information to surgeons, oncologists, patients, and researchers in a consistent manner across institutions and even countries. The College of American Pathologists (CAP) and the International Collaboration on Cancer Reporting (ICCR) are the two major institutions publishing synoptic reporting protocols. The parameters included in these protocols are determined and updated by CAP and ICCR respectively to remain up-to-date and relevant for diagnosis of each cancer type. For the field of computational pathology, synoptic reporting provides a significant advantage in dataset and model creation, as a pre-normalized set of labels exist across a variety of cases and slides in the form of the synoptic parameters filled out in each report. Additionally, suggestion or prediction of synoptic report values are a possible CPath application area.

2.2. Diagnostic Tasks

Computational pathology systems that focus on diagnostic tasks can broadly be categorized as: (1) disease detection, (2) tissue subtype classification, (3) disease diagnosis, and (4) segmentation. These tasks are visually depicted in Figure 3. Note how the detection tasks all involve visual analysis of the tissue in WSI format. Thus computer vision approach is primarily adopted towards tackling diagnostic tasks in computer aided diagnosis (CAD). For additional detail on some previous works on these diagnostic tasks, we refer the reader to Appendix 9.2

Detection We define the detection task as a binary classification problem where inputs are labeled as positive or negative, indicating the presence or absence of a certain feature. There may be variations in the level of annotation required, e.g. slide-level, patch-level, pixel-level detection depending on the feature in question. Although detection tasks may not provide an immediate disease diagnosis, it is a highly relevant task in many pathology workflows as pathologists incorporate the presence or absence of various histological features into synoptic reports that lead to diagnosis. Broadly, detection tasks fall into two main categories: (1) screening the presence of cancers and (2) detecting histopathological features specific to certain diagnoses.

Cancer detection algorithms can assist the pathologists by filtering obviously normal WSIs and directing pathologist’s focus

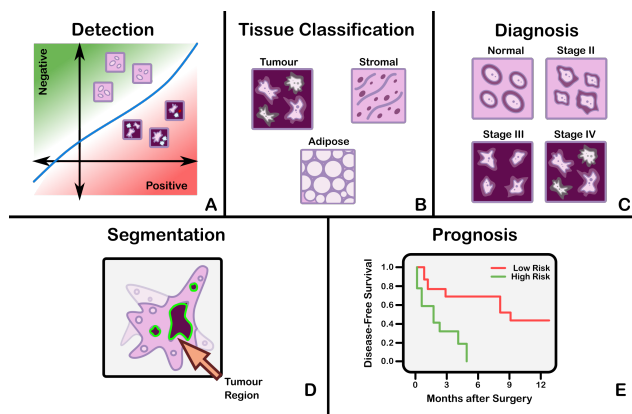


Fig. 3: The categorization of diagnostic tasks in computational pathology along with examples A) **Detection**: common detection task such as differentiating positive from negative classes like malignant from benign, B) **Tissue Subtype Classification**: classification task for tumorous tissue, Stroma, and adipose tissue, C) **Disease Diagnosis**: common disease diagnosis task like cancer staging, D) **Segmentation**: tumor segmentation in WSIs, and E) **Prognosis tasks**: shows a graph comparing survival rate and months after surgery.

to metastatic regions [71]. Although pathologists have to review all the slides to check for multiple conditions regardless of the clinical diagnosis, an accurate cancer detection CAD would expedite the workflow by pinpointing the ROIs and summarizing results into synoptic reports, ultimately leading to a reduces time per slide. Due to this potential impact, cancer detection tasks have been explored in a broad set of organs. Additionally, the simple labeling in binary detection tasks allows for deep learning methods to generalize across different organs where similar cancers form [72, 73, 74].

Tissue Subtype Classification Treatment and patient prognosis can vary widely depending on the stage of cancer, and finely classifying specific tissue structures associated with a specific disease type provides essential diagnostic and prognostic information [75]. Accordingly, accurately classifying tissue subtypes is a crucial component of the disease diagnosis process. As an example, discriminating between two forms of glioma (a type of brain cancer), glioblastoma multiforme and lower grade glioma, is critical as they differ by over 45% in patient survival rates [76]. Additionally, accurate classification is key in colorectal cancer (CRC) diagnosis, as high morphological variation in tumor cells [77] makes certain forms of CRC difficult to diagnose by pathologists [78]. We define this classification of histological features as tissue subtype classification.

Disease Diagnosis The most frequently explored design of deep learning in digital pathology involves emulating pathologist diagnosis. We define this multi-class diagnosis problem as a disease diagnosis task. Note the similarity with detection—disease diagnosis can be considered a fine-grained classification problem which subdivides the general positive disease class into finer disease-specific labels based on the organ and patient context.

Segmentation The segmentation task moves one step beyond classification by adding an element of spatial localization to the predicted label(s). In semantic segmentation, objects of interest are delineated in an image by assigning class labels to every pixel. These class labels can be discrete or non-discrete, the lat-

ter being a more difficult task [79]. Another variant of the segmentation task is instance segmentation, which aims to achieve both pixel-level segmentation accuracy as well as clearly defined object (instance) boundaries. Segmentation approaches can accurately capture many morphological statistics [80] and textural features [81], both of which are relevant for cancer diagnosis and prognosis. Most frequently, segmentation is used to capture characteristics of individual glands, nuclei, and tumor regions in WSIs. For instance, glandular structure is a critical indicator of the severity of colorectal carcinoma [82], thus accurate segmentation could highlight particularly abnormal glands to the pathologist as demonstrated in [82, 83, 84]. Overall, segmentation provides localization and classification of cancer-specific tumors and of specific histological features that can be meaningful for the pathologist’s clinical interpretation.

2.3. Prognosis

Prognosis involves predicting the likely development of a disease based on given patient features. For accurate survival prediction, models must learn to both identify and infer the effects of histological features on patient risk. Prognosis represents a merging of the diagnosis classification task and the disease-survivability regression task.

Training a model for prognosis requires a comprehensive set of both histopathology slides and patient survival data (i.e. a variant of multi-modal representation learning). Despite the complexity of the input data, ML models are still capable of extracting novel histological patterns for disease-specific survivability [85, 86, 87]. Furthermore, strong models can discover novel prognostically-relevant histological features from WSI analysis [88, 89]. As the quality and comprehensiveness of data improves, additional clinical factors could be incorporated into deep learning analysis to improve prognosis.

2.4. Prediction of treatment response

With the recent advances in targeted therapy for cancer treatment, clinicians are able to use treatment options that precisely identify and attack certain types of cancer cells. While the number of options for targeted therapy are constantly increasing, it becomes increasingly important to identify patients who are potential therapy responders to a specific therapy option and avoid treating non-responding patients who may experience severe side effects. Deep learning can be used to detect structures and transformations in tumour tissue that could be used as predictive markers of a positive treatment response. Training such deep learning models usually requires large cohorts of patient data for whom the specific type of treatment option and the corresponding response is known.

2.5. Organs and Diseases

This section presents an overview of the various anatomical application areas for computational pathology grouped by the targeted organ. Each organ section gives a brief overview of the types of cancers typically found and the content of the pathology report as noted from the corresponding CAP synoptic reporting outline (discussed at 2.1). Figure 4 highlights the intersection between the major diagnostic tasks and the anatomical

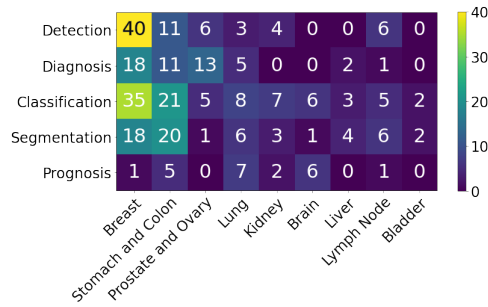


Fig. 4: Distribution of diagnostic tasks in CPath for different organs from Table 9.11. This distribution includes more than 400 cited works from 2018 to 2022 inclusive. The x-axis covers different organs, the y-axis displays different diagnostic tasks, and the height of the bars along the vertical axis measures the number of works that have examined the specific task and organ. Please refer to Table 9.11 in the supplementary section for more information.

focuses in state-of-the-art research. The majority of papers are dedicated to the four most common cancer sites: breast, colon, prostate, and lung [90]. Additionally, a significant amount of research is also done on cancer types with highest mortality, brain and liver. [90]. Note that details of some additional works that may be of interest for each organ type can be found in Appendix 9.7

Breast Breast cancers can start from different parts of the breast and majorly consist of 1) Lobular cancers that start from lobular glands, 2) Ductal cancers, 3) Paget cancer which involves the nipple, 4) Phyllodes tumor that stems from fat and connective tissue surrounding the ducts and lobules, and 5) Angiosarcoma which starts in the lining of the blood and lymph vessels. In addition, based on whether the cancer has spread or not, breast cancers can be categorized into *in situ* or *invasive/infiltrating* forms. DCIS is a precancerous state and is still confined to the ducts. Once the cancerous cells grow out of the ducts, the carcinoma is now considered *invasive* or *infiltrative* and can metastasize [91].

Synoptic reports for breast cancer diagnosis are divided based on the type of cancers mentioned above. For DCIS and invasive breast cancers, synoptic reports focus on the histologic type and grade, along with the nuclear grade, evidence of necrosis, margin, involvement of regional lymph nodes, and biomarker status. Notably, architectural patterns are no longer a valuable predictive tool compared to nuclear grade and necrosis to determine a relative ordering of diagnostic importance for DCIS [92]. In contrast to DCIS and invasive cancers, Phyllodes tumours vary due to their differing origin in the fat and connective tissue, focusing on analyzing the stroma characteristics, existence of heterologous elements, mitotic rate, along with the involvement of lymph nodes. Finally, to determine therapy response and treatments, biomarker tests for Estrogen, Progesterone [93] and HER-2 [94] receptors are recommended, along with occasional tests for Ki67 antigens [95, 96].

Most breast cancer-focused works in CPath propose various solutions for carcinoma detection and metastasis detection, an important step for assessing cancer stage and morbidity. Metastasis detection using deep learning methods was shown to outperform pathologists' exhaustive diagnosis by 9% free-

response receiver operating characteristic (FROC) in [97].

Prostate Prostate cancer is the second most prevalent cancer among the total population and the most common cancer among men (both excluding non-melanoma skin cancers). However, most prostate cancers are not lethal. Prostate cancer can occur in any of the three prostate zones: Central (CZ), Peripheral (PZ), and Transition (TZ), in increasing order of aggressiveness. Prostate cancers are almost always adenocarcinomas, which develop from the gland cells that make prostate fluid. The other types of prostate cancers are small cell carcinomas, neuroendocrine tumors, transitional cell carcinomas, isolated intraductal carcinoma, and sarcomas (which are very rare). Other than cancers, there are multiple conditions that are important to identify or diagnose as precursors to cancer or not. Prostatic intraepithelial neoplasia (PIN) is diagnosed as either low-grade PIN or high-grade PIN. Men with high-grade PIN need closely monitored follow-up sessions to screen for prostate cancer. Similarly, atypical small acinar proliferation (ASAP) is another precancerous condition requiring follow-up biopsies. [98]

To grade and score tumours, pathologists use a Tumor, Nodes, Metastasis (TNM) framework. In the synoptic report, pathologists identify and report the histologic type and grades, and involvement of regional lymph nodes to help grade and provide prognosis for any tumours. Specifically for prostate analysis, tumour size and volume are both important factors in prognosis according to multiple studies [99, 100, 101, 102]. Similarly, location is important to note for both prognosis and therapy response [103]. Invasion to nearby (except perineural invasion) tissues is noted and can correlate to TMN classification [104]. Additionally, margin analysis is especially important in prostate cancers as the presence of a positive margin increases the risk of cancer recurrence and metastasis [105]. Finally, intraductal carcinoma (IDC) must be identified and distinguished from PIN and PIA; as it is strongly associated with a high Gleason score, a high-volume tumor, and metastatic disease [106, 107, 108, 109, 110].

After a prostate cancer diagnosis is established, pathologists assign a Gleason Score to determine the cancer's grade: a grade from 1 to 5 is assigned to the two most common areas and those two grades are summed to make a final Gleason Score [111]. For Gleason scores of 7, where survival and clinical outcomes demonstrate large variance, the identification of Cribiform glands is key in helping to narrow possible outcomes [112, 113].

Ovary Ovarian cancer is the deadliest gynecologic malignancy and accounts for more than 14,000 deaths each year [114]. Ovarian cancer manifests in three types: 1) epithelial cell tumors that start from the epithelial cells covering the outer surface of the ovary, 2) germ cell tumors which start from the cells that produce eggs, and 3) stromal tumors which start from cells that hold the ovary together and produce the hormones estrogen and progesterone. Each of these cancer types can be classified into benign, intermediate and malignant categories. Overall, epithelial cell tumors are the most common ovarian cancer and have the worst prognosis [115].

When compiling a synoptic report for ovarian cancer diag-

nosis, pathologists focus on histologic type and grade, extra-organ involvement, regional lymph nodes, T53 gene mutations, and serous tubal intraepithelial carcinoma (STIC). Varying histologic tissue types are vital to determine the pathology characteristics and determining eventual prognosis. For example, generally endometrioid, mucinous, and clear cell carcinomas have better outcomes than serous carcinomas [116]. Additionally, lymph node involvement and metastasis in both regional and distant nodes has a direct correlation to patient survival, grading, and treatment. Determining the presence of STICs correlates directly to the presence of ovarian cancer, as 60% of ovarian cancer patients will also have an associated STIC [114]. Finally, T53 gene mutations are the most common in epithelial ovarian cancer; which has the worst prognosis among ovarian cancers, so determining their presence is critical to patient cancer risk and therapy response [117, 118]. There are not a large number of works dedicated to the ovary specifically, but most works on ovary focus on classification of its five most common cancer subtypes: high-grade serous (HGSC), low-grade serous (LGSC), endometrioid (ENC), clear cell (CCC), and mucinous (MUC) [119, 120].

Lung Lung cancer is the third most common cancer type, next to breast and prostate cancer [121]. Lung cancers mostly start in the bronchi, bronchioles, or alveoli and are divided into two major types, non-small cell lung carcinomas (NSCLC) (80–85%) and small cell lung carcinomas (SCLC) (10–15%). Although NSCLC cancers are different in terms of origin, they are grouped because they have similar outcomes and treatment plans. Common NSCLC cancers are 1) adenocarcinoma, 2) squamous cell carcinoma 3) large cell carcinoma, and some other uncommon subtypes [122].

For reporting, histologic type helps determine NSCLC vs SCLC and the subtype of NSCLC. Although NSCLC generally has favourable survival rates and prognosis as compared to SCLC, certain subtypes of NSCLC can have lower survival rates due to co-factors [123]. Histologic patterns are applicable in adenocarcinomas, consisting of favourable types: lepidic, intermediate: acinar and papillary, and unfavourable: micropapillary and solid [124]. Grading each histologic type aids in categorization but is differentiated based on each type, and thus is out of scope for this paper. Importantly for lung cancers, tumour size is an independent prognostic factor for early cancer stages, lymph node positivity, and locally invasive disease. Additionally, the size of the invasive portion is an important factor for prognosis of nonmucinous adenocarcinoma with lepidic pattern [125, 126, 127, 128, 129, 123]. Other important lung specific features are visceral pleural invasion, which is associated with worse prognosis in early-stage lung cancer even with tumors < 3cm [130], and lymphatic invasion which indicates an unfavourable prognostic finding [125, 131].

Colon and Rectum Colorectal cancers are two of the five most common cancer types [90]. Cancer cells usually start to develop in the innermost layer of the colon and rectum walls, known as the mucosa, and continue their way up to other layers. In other layers, there are lymph and blood vessels that can be used by cancer cells to travel to nearby lymph nodes or other organs [132]. Colorectal cancers usually start with the creation

of different types of polyps, each possessing a unique risk of developing into cancer. Most colorectal cancers are adenocarcinomas, which are split into three well-studied subtypes: classic adenocarcinoma (AC), signet ring cell carcinoma (SRCC), and mucinous adenocarcinoma (MAC). In most cases, AC has a better prognosis than MAC or SRCC. Other types, albeit uncommon, of colorectal cancers are: carcinoid tumors, gastrointestinal stromal tumors (GISTs), lymphomas, and sarcomas [133].

As in other cancers, histologic grade is the most important factor in cancer prognosis along with regional lymph node status and metastasis. The tumor site is also important in determining survival rates and prognosis [134]. Vascular invasion of both small and large vessels are important factors in adverse outcomes and metastasis [135, 136, 137], and perineural invasion has been shown in multiple studies to be an indicator of poor prognosis [138, 139, 137]. Additionally, microsatellite instability (MSI) is shown to be a good indicator of prognosis and is divided into three stages in decreasing adversity of Stable (MSI-S), Low (MSI-L), and High (MSI-H) [140]. Finally, some studies have indicated the usefulness of biomarkers in colorectal cancer treatment, with biomarkers such as BRAF mutations, KRAS mutations, MSI, APC, Micro-RNA, and PIK3CA [141].

Works are relatively well-distributed among various tasks including disease diagnosis, segmentation, and detection. Expanding on colorectal cancer detection, work from [142] used feature analysis for colorectal and mucinous adenocarcinomas using heatmap visualizations. They discovered that adenocarcinoma is often detected by ill-shaped epithelial cells and that misclassification can occur due to lumen regions that resemble the malformed epithelial cells. Similarly for mucinous carcinoma, the model again recognizes the dense epithelium, but this time ignores the primary characteristic of the carcinoma (abundance of extracellular mucin). These findings suggest that a thorough analysis of class activation maps can be helpful for improving the classifier's accuracy and intuitiveness.

Bladder There are several layers within the bladder wall with most cancers starting in the internal layer, called the urothelium or transitional epithelium. Cancers remaining in the inner layer are non-invasive or carcinoma in situ (CIS) or stage 0. If they grow into other layers such as the muscle or fatty layer, the cancer is now *invasive*. Nearly all bladder cancers are urothelial carcinomas or transitional cell carcinomas (TCC). However, there are other types of cancer such as squamous cell carcinomas, adenocarcinomas, small cell carcinomas, and sarcomas which all are very rare. In the early stages, all types of bladder cancers are treated similarly but as their stage progresses, and chemotherapy is needed, different drugs might be used based on the type of the cancer [143]. As with other organs, histologic type and grade also play a role in prognosis and treatment [144], and lymphovascular invasion is independently associated with poor prognosis and recurrence [145].

Works focusing on the bladder display promising results that could lead to rapid clinical application. For example, a prediction method for four molecular subtypes (basal, luminal, luminal p53, and double negative) of muscle-invasive bladder cancer was proposed in [146], outperforming pathologists by 30% in classification accuracy when restricted to a tissue morphology-

based assessment. Further improvements in accuracy could help expedite diagnosis by complementing traditional molecular testing methods.

Kidney Each kidney is made up of thousands of glomeruli which feed into the renal tubules. Kidney cancer can occur in the cells that line the tubules (renal cell carcinoma (RCC)), blood vessels and connective tissue (sarcomas), or urothelial cells (Urothelial carcinoma). RCC accounts for about 90% of kidney cancers and comes in two types: 1) clear cell renal carcinoma, which are most common and 2) non-clear cell renal carcinoma consisting of papillary, chromophobe and some very rare subtypes [147]. The CAP’s cancer protocol template for the kidney is solely focused on RCCs [148], likely due to their high probability. Tumour size is directly associated with malignancy rates, with 1cm size increases resulting in 16% increases in malignancy [149]. Additionally, the RCC histologic type is correlated with metastasis, with clear cell, capillary, collecting ducts (Bellini), and medullary being the most aggressive [150].

Many works are focused on glomeruli segmentation, as the number of glomeruli and glomerulosclerosis constitute standard components of a renal pathology report [151]. In addition to glomeruli detection, some works have also detected other relevant features such as tubules, Bowman’s capsules, and arteries [152]. The results display strong performance on PAS-stained nephrectomy samples and tissue transplant biopsies, and there seems to be a strong correlation between the visual elements identified by the network and those identified by renal pathologists.

Brain There are two main types of brain tumors: malignant and non-malignant. Malignant tumors can be classified as primary tumors (originating from the brain) or secondary (metastatic) [153, 154]. The most common type of brain cancers are gliomas, occurring 50.4% of the time, and are classified into four grades [155]. In the synoptic reporting, tumour location is noted as it has some impact on the prognosis, with parietal tumours showing better prognosis compared to other locations [153]. Additionally, focality of glioblastomas (a subtype of gliomas) is important to determine as multifocal glioblastoma is far more aggressive and resistant to chemotherapy as compared to unifocal [154]. A recent summary of the World Health Organization’s (WHO) classification of tumors of the central nervous system has indicated that biomarkers as both ancillary and diagnostic predictive tools [156]. Additionally, in a recent WHO edition of classification of tumours of the central nervous system, molecular information is now integrated with histologic information into tumor diagnosis for cases such as diffuse gliomas and embryonal tumors [157].

Accordingly, most works focus on gliomas and more specifically glioblastoma, the most aggressive and invasive form of glioma. Due to glioblastoma’s extremely low survival rate of 5% after 5 years, compared to a low grade glioma’s survival rate of over 50% after 5 years [158, 76], it is critical to distinguish the two forms for improved patient care and prognosis.

Liver Liver cancer is one of the most common causes of cancer death [159]. In particular, hepatocellular carcinoma (HCC) is the most common type of primary liver cancer and has various subtypes, but they generally have little impact on treat-

ment [160]. Histological grade is divided into nuclear features and differentiation, which directly correlate to tumour size, presentation, and metastatic rate [161, 162]. Notably, high-grade dysplastic nodules are included in synoptic reports for HCC but are difficult to assess and have high inter-observer disagreement [163], and thus is an area where CAD systems could be leveraged to normalize assessments. Current grading of this cancer suffers from an unsatisfactory level of standardization [164], likely due to the diversity and complexity of the tissue. This could explain why relatively low number of works are dedicated to liver disease diagnosis and prognosis. Instead, most works focus on the segmentation of cancerous tissues.

Lymph Nodes There are hundreds of lymph nodes in the human body that contain immune cells capable of fighting infections. Cancer manifests in lymph nodes in two ways: 1) cancer that originates in the lymph node itself known as lymphoma and 2) cancer cells from different origins that invade lymph nodes [165]. As mentioned in the prior organ sections, lymphocytic infiltration is correlated with cancer recurrence on multiple organs and lymph nodes are the most common site for metastasis. The generalizable impact to multiple organs and importance of detecting lymphocytic infiltration is why many works focused on lymph nodes address metastasis detection [166].

Organ Agnostic The remaining papers focus on segmentation, diagnosis, and prognosis tasks that attempt to generalize to multiple organs, or target organ agnostic applications. An interesting approach to increase the generalization capability of deep learning in histopathology is proposed in [167]. Currently, publicly available datasets with thorough histological tissue type annotations are organ specific or disease specific and thus constrain the generalizability of CPath research. To fill this gap, a novel dataset called Atlas of Digital Pathology (ADP) is proposed [167]. This dataset contains multi-label patch-level annotations of Histological Tissue Types (HTTs) arranged in a hierarchical taxonomy. Through supervised training on ADP, high performance on multiple tasks is achieved even on unseen tissue types.

3. Data Collection for CPath

One of the first steps in the workflow for any CPath research is the collection of a representative dataset. This procedure often requires large volumes of data that should be annotated with ground-truth labels for further analysis [62, 168, 64]. However, creating a meaningful dataset with corresponding annotations is a significant challenge faced in the CPath community [62, 168, 169, 64, 170].

This section outlines the entire process of the data-centric design approach in CPath, including tissue slide preparation and WSI scanning—the first two stages in the proposed workflow shown in Figure 1. Additionally, the trend in dataset compilation across the 700 papers surveyed is discussed regarding dataset sizes, public availability, and annotation types; see Table 9.11 in the Supplementary Material for information regarding the derivations and investigation of said trends.

3.1. Tissue Slide Preparation

For the application development stages in CPath, the creation of a new WSI dataset must begin with selection of relevant glass slides. High quality WSIs are required for effective analysis, however, considerations must be made for potential slide artifacts and variations inherently present. As described in Section 2.1, pathology samples are categorized as either biopsy or resection samples, with most samples being prepared as *permanent* samples and some intra-operative resection samples being prepared as *frozen* samples.

Variations and Irregularities Throughout the slide sectioning process, artifacts and irregularities can occur which reduce the slide quality, including: uncovered portions, air bubbles in between the glass seal, tissue chatter artifacts, tissue folding and tears, ink markings present on the slide, and dirt, debris, microorganisms, or cross-contamination of slides by unrelated tissue from other organs [171, 172, 173]. Frozen sections can present unique irregularities and variations, such as freezing artifacts, cracks in the tissue specimen block, or delay of fixation causing drying artifacts [174, 175]. Beyond these irregularities, glass slides may vary in stain colouring, occurring due to differences in slide thickness, tissue thickness, fixation, tissue processing schedule, patient variation, stain variation, and lab variation [176, 174, 177, 178, 179, 180].

All such defects and variations are important to keep in mind when selecting glass slides for the development and application process in CPath, as they can both reduce the quality of the WSI as well as impact the performance of developed CAD tools trained with these WSIs [171, 172, 177]. A more detailed discussion on the surveyed works in CPath which seek to identify and correct issues in slide artifacts and colour variation in WSIs is found in Section 3.2. However, prior to digitization, artifacts, and irregularities can be kept at a minimum by following good pathology practices. While an in-depth discussion of this topic is outside the scope of this paper, some research provides an extensive list of recommendations for reducing such errors in slide sectioning [173].

3.2. Whole Slide Imaging (WSI)

WSI Scan Once a glass slide is prepared, it must be digitized into a WSI. The digitization and processing workflow for WSIs can be summarized as a four-step process [181]: (1) Image acquisition via scanning; (2) Image storage; (3) Image editing and annotation; (4) Image display [182]. As the first two steps of the digitization workflow are the most relevant for WSI collection and with regards to the CPath workflow, they are discussed to a greater extent below.

Slide scanning is carried out through a dedicated slide scanner device. A plethora of such devices currently exist or are in development; see Appendix Table 1 for a collection of commercially available WSI scanners. Additionally, some research has investigated and compared the capabilities and performances of various WSI scanners [183, 184, 185, 186].

In order to produce a WSI that is in focus, which is especially important for CPath works, appropriate focal points must be chosen across the slide either using a depth map or by selecting arbitrarily spaced tiles in a subset [187]. Once focal points are

chosen, the image is scanned by capturing tiles or linear scans of the image, which are stitched together to form the full image [180, 187]. Slides can be scanned at various magnification levels depending on the downstream task and analysis required, with the vast majority being scanned at $20\times$ ($\sim 0.5\mu\text{m}/\text{pixel}$) or $40\times$ ($\sim 0.25\mu\text{m}/\text{pixel}$) magnification [180].

WSI Storage and Standards WSIs are in giga-pixel dimension format [30, 188]. For instance a tissue in $1\text{cm} \times 1\text{cm}$ size scanned @ $0.25\mu\text{m}/\text{pixel}$ resolution can produce a 4.8GB image (uncompressed) with $50,000 \times 50,000$ pixels. Due to this large size, hardware constraints may not support viewing entire WSIs at full resolution, thus WSIs are most often stored in a tiled format so only the viewed portion of the image (tile) is loaded into memory and rendered [189]. When building CAD tools for CPath, this large WSI dimensionality must be taken into account in determining how much compute is required to analyze a WSI. Alongside the WSI, metadata regarding patient, tissue specimen, scanner, and WSI information is stored for reference [30, 188, 190]. Due to their clinical use, it is important to develop effective storage solutions for WSI images and metadata, allowing for robust data management, querying of WSIs, and efficient data retrieval [191, 192]. Further details on WSI image formats and storage methods are discussed in Appendix 9.6

To develop CPath CAD tools in a widespread and general manner, a standardized format for WSIs and their corresponding metadata is essential [188]. However, there is a general lack of standardization for WSI formats outputted by various scanners, as shown in Table 1, especially regarding metadata storage. The Digital Imaging and Communications in Medicine (DICOM) standard provides a format for CPath image formatting and data management through Supplement 145 [190, 193], and has been shown in research to allow for efficient access and interoperability of data between varying medical centers and devices [188]. However, few scanners are DICOM-compliant and thus there are challenges to using different models of scanners, thus different image formats and metadata structures, in the context of dataset aggregation and processing.

Apart from storage format, a general framework for storing and distributing WSIs is also an important pillar for CPath. In other medical imaging fields such as radiology, images are often stored in a picture archiving and communications systems (PACS) in a standardized DICOM format, with DICOM storage and retrieval protocols to interface with other systems [189]. The need for standardization persists in pathology for WSI storage solutions; few works have proposed solutions to incorporate DICOM-based WSIs in a PACS, although some research has successfully implemented a WSI PACS consistent using the DICOM standard using a web-based service for viewing and image querying [189].

WSI Defects and Variations Certain aspects of the slide scanning process can introduce unfavorable irregularities and variations [194]. A major source of defects is out-of-focus regions in a generated WSI; often caused by glass slide artifacts, such as air bubbles and tissue folds, which interfere with selection of focus points for a slide [171, 195]. Out-of-focus regions degrade WSI quality and are detrimental to the performance of CAD tools developed with these WSIs, presenting concerns

for performance with studies showing high false-positive errors [196, 172]. Additionally, as WSIs are scanned in strips or tiles, any misalignment between sections can introduce striping/stitching errors in the final image [197]. Another source of error may appear during tissue-background segmentation where the scanner may misidentify some tissue regions as background, potentially missing crucial tissue areas on the glass slide from being digitized [198].

Variations in staining refers to differences in colour and contrast of the tissue structures in the final WSI occurring due to differences in the staining process, staining chemicals, and tissue state. Variations in colour can lead to difficulty in generalizing CAD tools to WSIs from different labs, institutions, and settings [199, 200]. Even identical staining techniques can yield different WSIs due to scanner differences in sensor design, light source and calibration [180, 201], creating challenges for cross-laboratory dataset generation. These additional sources of variation add layers of complexity to the WSI processing workflow, and must be kept in mind during slide selection and dataset curation for CAD tool development and deployment.

Addressing Irregularities and Variations Much work has gone into identifying areas of irregularities within WSIs, most notably blur and tissue fold detection [195, 196]. Some research has explored automated deep learning tools to identify these irregularities at a more efficient pace than manual inspection [195, 196]. Developing techniques for addressing staining variation has also been a significant research area [202, 203, 204, 177, 205, 206, 207] as the use of techniques addressing stain variation is important for all future works. We list some computational approaches proposed to address these issues: An example method proposed in [202] uses a stain normalization technique, attempting to map the original WSI onto a target color profile. In this technique, a color deconvolution matrix is estimated to convert each image to a target hematoxylin and eosin (H&E) color space and each image is normalized to a target image colour profile through spline interpolation [202]. A second approach applies color normalization using the H channel with a threshold on the H channel on a Lymphocyte Detection dataset[205]. Recent studies have shown promise in having deep neural networks accomplish the stain normalization in contrast to the previous classical approaches [208, 209, 203, 210], commonly applying generative models such as generative adversarial networks (GANs) to stain normalization. Furthermore, Histogram Equalization (HE) technique for contrast enhancement is used in [211], where novel preprocessing technique is proposed to select and enhance a portion of the images instead of the whole dataset, resulting in improved performance and computational efficiency.

An alternative approach to address the impact of stain variation on training CAD tools is data augmentation. Such methods augment the data with duplicates of the original data, containing adjustments to the color channels of the image, creating images of varying stain coloration, and training train models that are accustomed to stain variations[200]. This method has been frequently used as a pre-processing step in the development of training datasets for deep learning [212, 213, 214]. A form of medically-irrelevant data augmentation based on random style

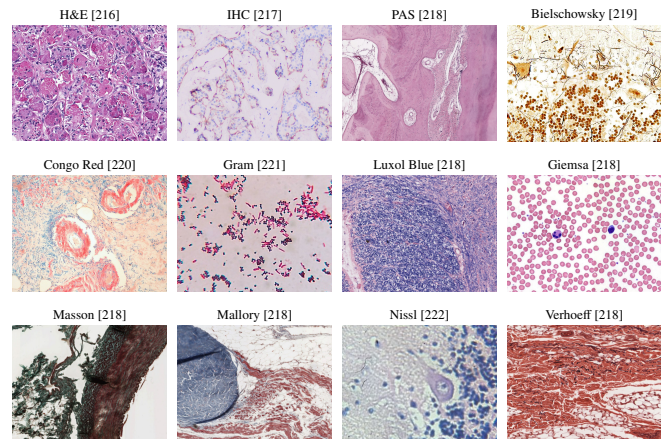


Fig. 5: WSI tissue images with different types of histological stains. Each stain highlights different areas and structures of the tissue in order to aid in visualizing underlying characteristics. Amongst this diversity, there is Hematoxylin and Eosin or H&E which is mainly used in studies as most histopathological processes can be understood from this stain. All images provided are under a Creative Commons license, specifics on the license can be found in the references.

transfer, called STRAP, was proposed by researchers and outperformed stain normalization [206]. Similar to style transfer, [215] proposes stain transfer which allows one to virtually generate multiple types of staining from a single stained WSI.

3.3. Cohort Selection, Scale, and Challenges

The data used to create/train CPath CAD tools can greatly impact the performance and success of the tool. Curating the ideal dataset, and thus selecting the ideal set of WSIs for the development of a CAD tool is a nontrivial task. Several works suggest that datasets for deep learning in CPath should include a large quantity of data with a degree of variation and artifacts in the WSIs [62, 172]. Some works also recommend the inclusion of difficult or rarely diagnosed cases; other works indicate that inclusion of extremely difficult cases may decrease the performance of advanced models [172, 223].

A study highlighting the results of the 2016 Dataset Session at the first annual Conference on Machine Intelligence in Medical Imaging outlines several key attributes to create an ideal medical imaging dataset [224], including: having a large amount of data to achieve high performance on the desired task, quality ground truth annotations, and being reusable for further efforts in the field. While the scope of this conference did not include CPath, many of the points made regarding medical imaging datasets are also relevant to the development of CPath datasets. The session also outlined the impact that class imbalances can have on ML models, an issue also prevalent in CPath as healthy or benign regions often outnumber diseased regions by a significant margin [225].

Our survey of past works in the literature reveals some trends in CPath datasets. Currently, the majority of datasets presented in the literature for CAD tool development are small-scale datasets [62], using a small number of images, and/or images from a small number of pathology laboratories. Examples of these smaller datasets include a dataset with 596 WSIs

(401 training, 195 testing) from four centres for breast cancer detection [226] and the Breast Cancer Histology (BACH2018) dataset, which has 500 ROI images (400 training, 100 testing) and 40 WSIs (30 training, 10 testing) [227]. Although curating a dataset from fewer pathology laboratories may be simpler, these smaller scale datasets may not be able to effectively generalize to data from other pathology centres [199, 120]. An example of this can be seen in which data from different pathology centres are clustered disjointly in a t-distributed stochastic neighbor embedding (t-SNE) representation demonstrated in [172]. Another alternative was proposed in [228]: using a swarm learning technique multiple AI models were trained on different small data sets separately and then unified into one central model.

Additionally, stain variations, slide artifacts, and variation of disease prevalence may sufficiently shift the feature space such that a deep learning model may not sustain high performance on unseen data in new settings [120, 229]. As artifacts in WSIs are inevitable, with some artifacts, such as ink mark-up on glass slides, being an important part of the pathology workflow [230], the ability of CAD tools to become robust to these artifacts through exposure to a diverse set of images is an important consideration.

Compared to the number of studies conducted on small-scale datasets, relatively fewer studies have been performed using large-scale, multi-centre datasets [62, 231, 172]. One study uses over 44,715 WSIs from three organ types, with very little curation of the WSIs for multi-instance learning detailed in [62]. Stomach and colon epithelial tumors were classified using 8,164 WSIs in [231]. A similar study uses 13,537 WSIs from three laboratories to test a machine learning model trained on 5,070 WSIs and achieves high performance [62].

Despite some advancements, there exist major barriers to using such large, multi-centre datasets in CAD development. Notably, for strongly supervised methods of learning, an immense amount of time is needed to acquire granular ground truth annotations on a large amount of data [231]. To combat this, some researchers have implemented weakly-supervised learning by harvesting existing slide level annotations to forego the need for further annotation [62]. Additionally, it may be difficult to aggregate data from multiple pathology centres due to regulatory, privacy, and attribution concerns, despite the improvements that diverse datasets offer. section 5 discusses model architectures and training techniques that harness curated datasets of various annotation levels.

Dataset Availability In general computer vision, progress can be tracked by the increasing size and availability of datasets used to train models, e.g. ImageNet grew from 3.2 million images and 5000 classes in 2009 to 14 million images and 21,000 classes in 2021 [232]. We infer a similar trend in dataset growth and availability indicates progress in CPath. In our survey of over 700 CPath papers, we determine the current landscape by noting the dataset(s) used in work, along with dataset details such as the organ(s) of interest, annotation level, and stain type, tabulating the results into Table 9.11 of the supplementary materials, with summarized findings from Table 9.11 are shown in Figure 6.

From Figure 6 we can clearly see that the majority of datasets used for research developments in computational pathology are privately sourced or require additional registration/request. With organs represented in a small number of datasets, such as the liver, thyroid, brain, etc, having a smaller proportion of freely accessible datasets as compared to the Breast, Colon, or Prostate. This can be problematic when trying to create CAD tools for cancers in these organs due to a lack of accessible data. We additionally note that although data sets requiring registration/request for access can be easily accessible, as in the case of Breast Cancer Histopathological Database (BreakHis) [233] being used in multiple works [234, 235, 236], the need for registration presents a barrier to access as requests may go unanswered or take much time to review.

In our categorization of CPath datasets, we find that a few prominent datasets have been released publicly for use by the research community. Many such datasets are made available through grand challenges in computational pathology [237], such as the CAMELYON16 and CAMELYON17 challenges for breast lymph node metastases detection [238, 61, 239], and the Gland Segmentation in Colon Histology Images Challenge (GLaS) competition for colon gland segmentation in conjunction with Medical Image Computing and Computer Assisted Intervention (MICCAI) 2015 [240, 241]. Notable amongst publicly available data repositories is the cancer genome atlas (TCGA) [242], a very large-scale repository of WSI-data containing many organs and diseases, along with covering a variety of stain types, magnification levels, and scanners. Data collected from TCGA has been used in a large number of works in the literature for the development of CAD tools [200, 243, 244]. As such, TCGA represents an essential repository for the development of computational pathology. While patient confidentiality is a general concern when compiling and releasing a CPath dataset, large-scale databases such as TCGA prove that it is possible to provide relatively unrestricted data access without compromising patient confidentiality. Further evaluating public source datasets, it seems that the majority of them use data extracted from large data repositories, such as TCGA, without specifying the IDs of the images used, which provides a challenge in comparing datasets or CAD tool performance across works. However, there are a few datasets that are exceptions to that phenomenon [245, 246, 247, 64].

Figure 6 also provides some insights on the dataset breakdown by organ, stain type, and annotation level. Per organ, it can be seen that the breast, colon, prostate/ovary, and lung tissue datasets are amongst the most common, understandably since cancer occurrence in these regions is the most frequent [90]—complying with cancer statistics findings in 9.5. Multi-organ datasets are the other most common type, where we have designated a dataset to be multi-organ if it compiles WSIs from several different organs. To note, multi-organ datasets are especially useful for the development of generalized image analysis tools in computational pathology. The annotation level provided in the datasets did not indicate any pattern across most organs.

Dataset Bias It is also important to note the potential for bias in datasets that may influence the ability of any deep learning

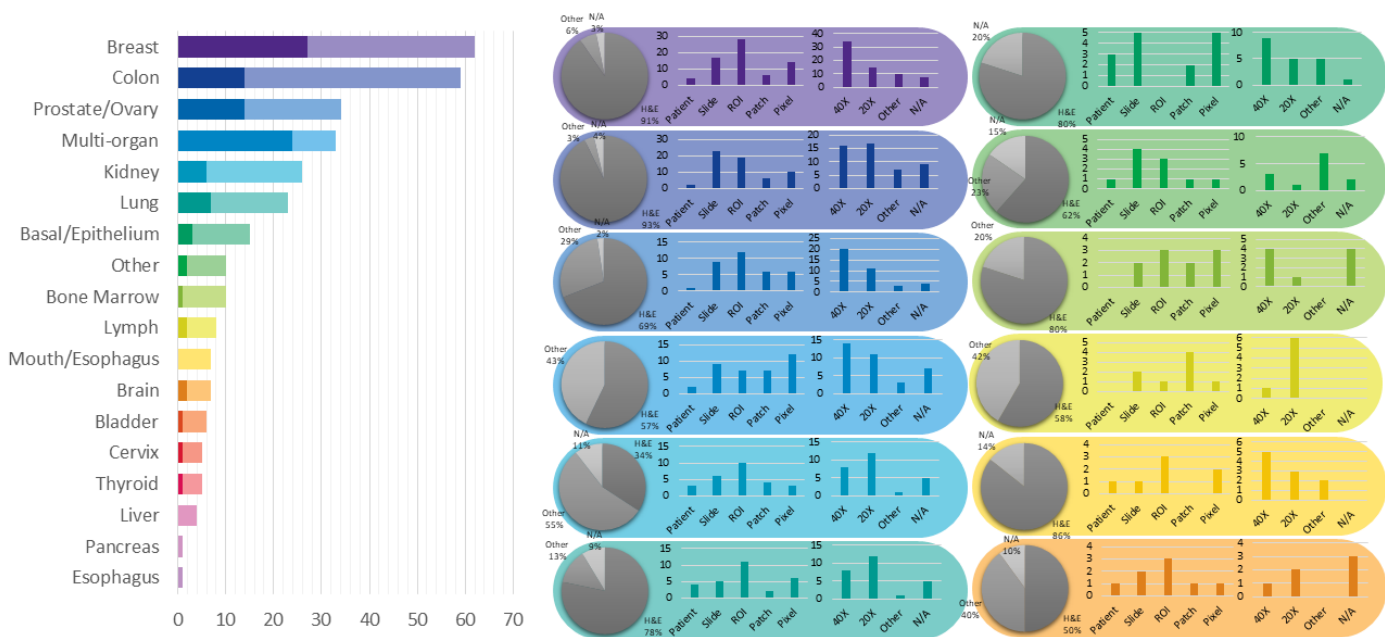


Fig. 6: (left) shows the distribution of datasets per organ as a capture of the current trend in datasets, although the number of datasets can change over time an understanding of what organs have more available data is important for developing CAD tools. Along the vertical axis, we list different organs, while the horizontal axis shows the number of datasets; wherein the darker color denotes public availability while the light color includes unavailable or by request statuses. (right) Distribution of staining types, annotation levels, and magnification details per organ color coded consistently with the bar graph. Organs have been sorted based on the abundance of datasets. For more details, please refer to Table 9.11 in the supplementary section.

algorithm to generalize on unseen data [248, 249]. This problem is a prevalent issue in general machine learning applications [250, 251, 252, 253], and CPath is not immune to it. The survey review in [254] reviews a large number of other examples in machine learning that exhibit such bias, both from a dataset-standpoint and an algorithm-standpoint.

Such a lack of generalizability in CPath can impact the ability of machine learning models trained on biased data to meet the needs of patients. As noted in [248], minority groups may be disproportionately negatively impacted if care is not taken in curating a diverse dataset that adequately reflects the relevant demographics for the problem to be solved.

Several works have delved into the issue of dataset bias in CPath specifically [255, 256]. A notable example is in [256], where the study was able to demonstrate that deep learning models trained on WSIs from TCGA were able to infer the organization that contributed the slide sample. Notably, some features, such as genetic ancestry, patient prognosis, and several key genomic markers were significantly correlated with the site the WSI was provided from. As the vast majority of data in TCGA is acquired from 24 origin centers [255], such site-specific factors may impact the ability of a DL model to perform well on patient data from different sites.

As discussed previously, having a large set of diverse data may help to mitigate generalization issues [199, 120, 248]. Additionally, the study [256] makes the suggestion that training data should be from separate sites than validation data, and that per-site performance of a model should be reported when validating a model. In doing this, the robustness of the model to site-specific variation, including both stain and demographic related variation, can be evaluated.

4. Domain Expert Knowledge Annotation

A primary goal of CPath is to capture and distill domain expert knowledge, in this case the expertise of pathologists, into increasingly efficient and accurate CAD tools to aid pathologists everywhere. Much of the domain knowledge transfer is encompassed within the process of human experts, in this case pathologists, generating diagnostically-relevant annotations and labels for WSIs. It must be emphasized, that without some level of label, a WSI dataset is not directly usable to train a model for most CAD tasks that involve the generation of diagnoses, prognoses, or suggestions for pathologists. Thus, the process of obtaining and/or using annotations at the appropriate granularity and quality is paramount in the field. This section focuses on describing various types of ground-truth annotation to cover the spectrum of weak to strong supervision of labels, discussing the practicality of labeling across this supervision spectrum, and how a labeling workflow can be potentially designed to optimize related annotation tasks.

4.1. Supervised Annotation

In contrast to general computer vision, computer scientists do not have expert-level knowledge of histopathology and thus they are not as efficient at generating annotations or labels of pathology images. Further, labels cannot be easily obtained by outsourcing the task to the general public. As a result, pathologists must be leveraged to obtain labels at some stage of the data collection and curation process, and in many annotation pipelines the first step involves recruiting the help of pathologists for their expertise in labelling.

Obtaining Expert Domain Knowledge The knowledge of pathologists is essential in the development of accurate ground

truth annotations—a process most commonly completed by encircling ROI [226]. However, there are studied instances of inter-observer variance between pathologists when determining a diagnosis [257, 258, 259]. As obtaining the most correct label is essential when training a model for CAD, this issue must be addressed and a review of the data by several pathologists can result in higher quality ground truth data as compared to that of a single pathologist. As a result, most datasets are curated by involving a group of pathologists in the annotation process. If there exists a disagreement between the expert pathologists on the annotation of a ground truth, one of several methods is usually employed to rectify the discrepancy. A consensus can be reached on the annotation label through discussion amongst pathologists, as is done in the triple negative breast cancer (TNBC-CI) dataset [260], the Breast Cancer Surveillance Consortium (BCSC) dataset [261] and the minimalist histopathology image analysis dataset (MHIST) dataset [262]. Alternatively, images, where disagreements occur, can be discarded, as is done in some works [263, 264]. Further, the disagreement between annotators can be recorded to determine the difficulty level of the images, as is done in the MHIST dataset [223]. This extra metadata aids in the development of CAD tools for analysis.

Pathologists can also be involved indirectly in dataset annotation. Both the Multi-organ nuclear segmentation dataset (MoNuSeg) [265] and ADP [167] have non-expert labelers annotate their respective datasets. A board-certified pathologist is then tasked with reviewing the annotations for correctness. Alternatively, some researchers have employed a pathologist in performing quality control on WSIs for curating a high-quality dataset with minimal artifacts [87, 266]. To enable the large scale collection of accurate annotated data, Lizard [267] was developed using a multi-stage pipeline with several significant “pathologist-in-the-loop” refinement steps.

Existing pathological reports, along with the metadata that comes from public large-scale databases like TCGA, can also be leveraged as additional sources of task-dependent annotations without the use of further annotation. For example, TCGA metadata was used to identify desirable slides in [26], while pathological diagnostic reports were used for breast ductal carcinoma in-situ grading in [268].

To note, there are some tasks where manual annotation by pathologists can be bypassed altogether. For instance, IHC was applied to generate mitosis figure labels using a Phospho-Histone H3 (PHH3) slide-restaining approach in [269], while immunofluorescence staining was used as annotations to identify nuclei associated with pancreatic adenocarcinoma [270]. These works parallel the techniques that pathologists often use in clinical practice, such as the use of IHC staining as a supplement to H&E stained slides for difficult to diagnose cases [271]. They demonstrate high performance on their respective tasks wherein the top-performing models on the Tumor Proliferation Assessment Challenge 2016 (TUPAC16) [272] dataset were achieved [269]. Importantly, these techniques still utilize supervision, albeit weakly, by leveraging lab techniques that have been developed and refined to identify the desired regions visually.

Ground-Truth Diagnostic Information Understanding different annotation levels and their impact on the procedural development of ML pipelines is an important step in solving tasks within CPath. There are five possible levels of annotation, in order of increasing granularity (from weakly-supervised to fully-supervised): patient, slide, ROI, patch, and pixel. Figure 7 overviews the benefits and limitations of each level. For additional information regarding each annotation level please refer to Appendix 9.8.

Picking the Annotation Level Selecting an annotation level depends largely on the specific CPath task being addressed, as shown in Figure 8. For example, segmentation tasks tend to favor pixel-level annotations as they require precise delineation of a nucleus or tissue ROI. Conversely, disease diagnosis tends to favor datasets with ROI-level annotations, as diagnosis tasks are predominantly associated with the classification of diseased tissue, the higher-level annotations may provide a sufficient level of detail and context for this task [273].

Figure 8 shows that tasks that use stronger supervision are more likely to be used in CAD tool model development. However, due to the high cost of pixel-level annotation, fully supervised annotations are challenging to develop. Even patch-based annotations often require the division and analysis of a WSI into many small individual sub-images resulting in a similar problem to pixel-based annotations [63, 212]. In contrast, WSI data is most often available with an accompanying slide-level pathology report regarding diagnosis thus making such weakly labeled information at the WSI level significantly more abundant than ROI, patches, or pixel-level data [274, 275]. Different levels of annotation can be leveraged together, as demonstrated by a framework to use both pixel and slide level annotations to generate pseudo labels in [276]. Additionally, it is common in CPath to further annotate the slide-level WSIs on an ROI or patch level structure [85, 277, 278, 32].

Active Learning Tools Active learning annotation tools bridge the gap between the need for highly supervised labels and the current abundance of less informative annotations. Such works seek to ease the annotation process by using computational approaches to assist the human annotator. For example, in [168], a platform was developed for creating nuclei and gland segmentation ground truth labels quickly and efficiently. A convolutional neural network (CNN), trained on similar cohort data, was used to segment nuclei and glands with different mouse actions [168]. Alternatively, Awan et al. [169] presented the HistoMapr™ platform to assist in diagnosis and ground truth data collection. Through this tool, a pathologist selects one of several proposed classes for each given ROI, thus mitigating the need for hand-drawn annotations or manual textual input [169]. Similarly, an active learning model called the Human-Augmenting Labeling System (HALS) [279] was developed to increase data efficiency by guiding annotators to more informative slide sections. Quick Annotator (QA) [280] is another tool which provides an easy-to-use online interface for annotating ROIs and was designed to create a significant improvement in the annotation efficiency of histological structures by several orders of magnitude.

There are other active learning annotation tools proposed for

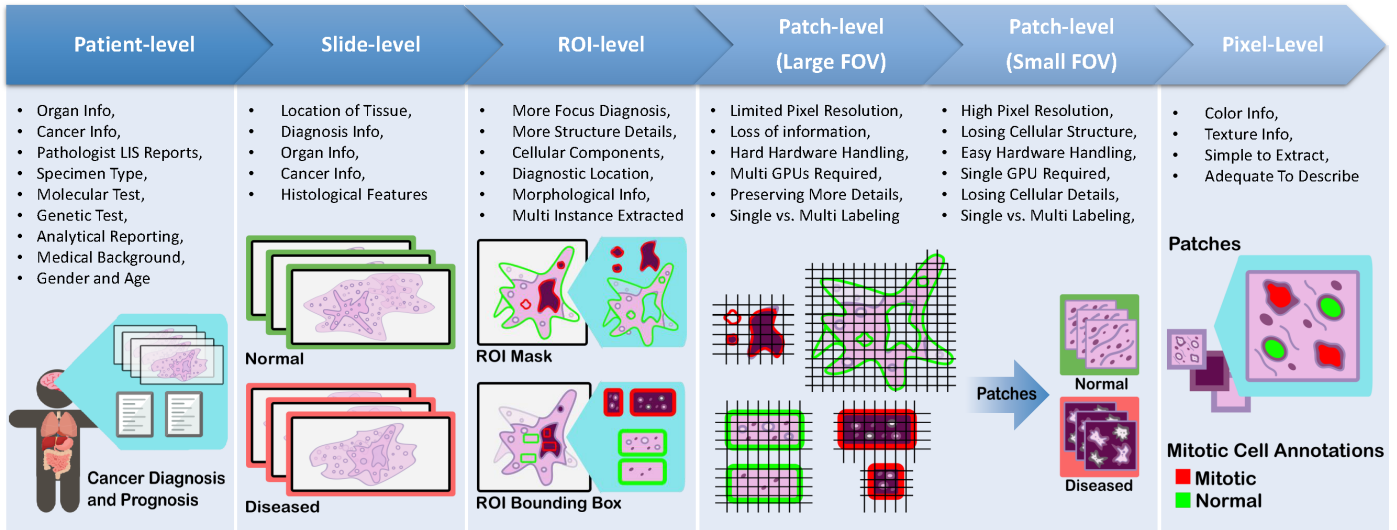


Fig. 7: Details of the five different types of annotations in computational pathology. From left to right: a) **Patient-level annotations**: can include high level information about the patient like status of cancer, test results, etc. b) **Slide-level**: are annotations associated with the whole slide, like a slide of normal tissue or a diseased one c) **ROI-level annotations**: are more focused on diagnosis and structure details d) **Patch-level**: are separated into Large FOV (field of view) and small FOV, each having different computational requirements for processing, and finally e) **Pixel-level**: includes information about color, texture and brightness

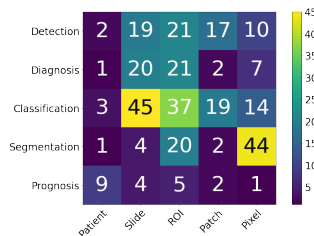


Fig. 8: A snapshot of the distribution of different annotation levels based on the CPath task being addressed in the surveyed literature for the purposes of highlighting the trend of datasets. The x-axis displays the different annotation levels studied in the papers (from left to right): Patient, Slide, ROI, Patch, and Pixel. The y-axis shows the different tasks (top to bottom): Detection, Diagnosis, Classification, Segmentation, and Prognosis. The height of the bars along the vertical axis measures the number of works that have examined the specific task and annotation level.

different applications in computer vision that can be investigated for use in the pathology datasets. Such examples include methods to produce object segmentation masks for still images [281, 282] as well as video [283]. One notable example is DatasetGAN [282]; the model is proposed as a training data creator, and it is shown that the model can produce segmentation masks with a small number of labelled images in the training data. While these systems are for general computer vision, they may be adoptable in computational pathology, and would facilitate the necessary relationship between pathologists and computer scientists in the development of CAD tools. As such, they may prove to be a valuable contributor to the CAD system development workflow.

Tissue-Class and Disease Complexity Much of the current CPath research operates under the umbrella of supervised learning tasks, and correspondingly uses labeled data to develop automated CAD tools. We refer to supervised learning to include a diverse spectrum of annotation i.e. weak-supervision (e.g. patient-level) all the way to strong-supervision (e.g. pixel-

level). Classes within a dataset can be task-dependent, for example as shown in Table 9.11 of the supplementary material, datasets primarily used for segmentation such as MoNuSeg [265] and CPM-17 [284] have classes for each annotated pixel indicating the presence or absence of nuclei. However, classes need not be task-dependent; datasets such as CAMELYON16 [238] outline metastases present in WSIs that can be used for a variety of applications, including disease detection [238] and segmentation tasks [285].

The current paradigm for dataset compilation in computational pathology, particularly for disease detection and diagnosis, treats different disease tissue types as separate independent classes. For example, BreakHis divides all data into benign/malignant breast tumours [233]. At the ROI level, GLaS divides colon tissue into five classes: healthy, adenomatous, moderately differentiated, moderately-to-poorly differentiated, and poorly differentiated [240]. So far, this approach to class categorization has resulted in high-performing CAD tools [80, 235, 236, 286, 83, 84]. However, the treatment of different disease tissue types as an independent class is perceived differently in computer vision domain where the representation learning of normal objects is done differently compared to anomalies. A similar synergy can be found by differentiating healthy tissue classes from diseased ones and one should be mindful about defining meaningful tissue ontology for annotation and labeling.

4.2. Optimum Labeling Workflow Design

This section focuses on the steps required for compilation of a CPath dataset which is broken into three main sub-tasks: Data Acquisition, Data Annotation, and Data Management, as per Figure 9. Each sub-task is discussed below with reference to its individual components in the hierarchical structure in Figure 9.

Data Acquisition Database compilation starts from data acquisition. When collecting data, it is vital that there are large amounts of data [287], along with having sufficient diversity [62, 172]. Specifically, diversity in CPath data occurs in multiple ways, such as staining methods, tissue types and regions, laboratory processes, and digital scanners. We advise that CPath researchers consult expert pathologists on the diversity of data required for various tasks. Ideally, all the data acquired in pathology should be perfect without any irregularity and artifacts. However, some level of artifacts and irregularity are unavoidable and introducing realistic artifacts that are representative of real-world scenarios into the data increases the robustness and generalizability of CAD tools.

Data Annotation After collecting sufficient data, the next task is annotation of the data. Data annotation is a costly process in both time and money, thus a budget and schedule should always be established when generating labels. There are often various approaches for annotating different structures [288], so a specific labelling taxonomy should be defined *a priori*. As mentioned previously, annotation should involve expert pathologists due to the domain knowledge requirement and importance of label correctness. A table of commonly used commercially available annotation software for annotating different slide formats are show in Table 2, along with their compatible image formats which is important to note when trying to build compatible and accessible datasets.

Once the ontology of class-definitions is defined (in collaboration with expert pathologists), there will be two ways to generate labels or annotations in general: domain expert labelling or non-expert labelling. The domain expert labelling refers to having pathologists annotate data that they are specialized at, which is labor-extensive. On the other hand, non-expert labelling can use crowdsourcing techniques to generate weak labels or have non-experts, such as junior pathologists or students, label the data. This process is cheaper and quicker, but it may be harder to maintain the same level of quality as domain expert labeling [288]. Regardless of the labelling methodology used, labels generated from both should be validated. Finally, to determine the sufficiency of label quantity, one should consider the balance between the number of classes, representation size of each class, and complexity of class representation. Techniques from active-learning could be also leveraged to compensate for lack of resource management as well as maintain the quality of labeling as discussed above.

Data Management Data management is an important aspect of any dataset creation process, and is the one that is most likely to be overlooked. Proper data management should have considerations for reusability, medical regulations/procedures, and continuous integration and development.

Reusability can be broken down into detailed documentation of the data, accessible and robust hosting of data, and consideration for image standards. Poor cross-organizational documentation can lead to missing metadata, ultimately resulting in discarding entire datasets [289]. Adherence to an established image standard, such as DICOM, can help resolve some of these issues in reusability. Medical regulations/procedures can be broken down into the construction of a Research Ethics

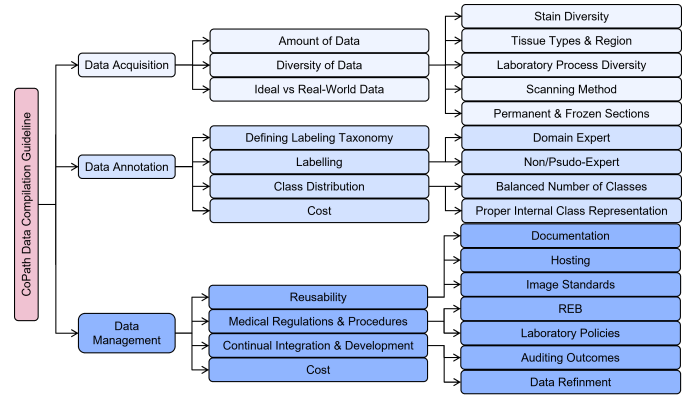


Fig. 9: Tree diagram for the optimum labeling workflow, where a CPath dataset is divided into tasks and sub-tasks based on its initial characteristics.

Board (REB) and proper consideration for whom is curating the data. Through incentives for data excellence for medical practitioners, the issue of misaligned priorities between data scientists, domain experts, and field partners can be resolved [289]. To ensure that models used on actual patients remain relevant and hidden errors do not propagate, continuous integration/development (CI/CD) must be implemented. These systems must include at least two components, a method to audit predictions from the model, as well as a way to refine the training data accounting for discrepancies found through auditing. Several algorithms deployed in high-risk environments, including medical diagnosis, proved to only work well when data was updated after initial deployment [290, 289]. Throughout the data management process, consultation with domain experts is a vital step in ensuring the success of data compilations [291].

5. Model Learning for CPath

Once an application domain and corresponding dataset have been chosen, the next step of developing a CPath tool involves designing of an appropriate model and representation learning paradigm. Representation learning refers to a set of algorithmic techniques dedicated to learning feature representations of a certain data domain that can be used in downstream tasks [292]. In CPath, the amount of data available for a given annotation level and task are the key determinants to designing a model and learning technique. The last decade has shown neural network architectures to become the dominant method in many machine-learning domains because they are rich enough to avoid handcrafted features and offer superior performance. [293]. The annotation level of the data pertaining to the task corresponds to the level of supervision for the learning technique applied. This relationship between data annotation level and learning supervision level is surveyed in Figure 11.

This section details the various types of models and learning techniques, along with the tasks they have been applied to in CPath. Figure 10 highlights the most common backbone architectures used for feature encoding in SOTA research, based on the corresponding tasks. More details are provided in Table 9.11 from the supplementary materials. The selection of

architectures is then compared to draw useful insights into accuracy, computational complexity, and limitations. Lastly, existing challenges in model design are investigated.

5.1. Classification Architectures

In CPath, general classification architectures are the most prevalent due to their straightforward applicability to a wide range of tasks including tissue subtype classification, disease diagnosis and detection (more details in Section 2 and Figure 4). Architectures commonly used for natural images, in particular CNNs, are widely adopted for CPath. To maximize model performance, it is a common approach to pre-train the model on large datasets like ImageNet before subsequent fine-tuning them to perform well for the specific CPath task, a task known as transfer learning [294, 295, 296, 297, 274, 298, 299, 87, 300, 301, 302, 303, 304, 305, 86, 306, 307, 257, 308, 268, 309, 310, 64, 311, 312, 313, 314, 206, 315, 316, 317, 318, 319]. Transfer learning for CPath allows for: 1) improved generalizability, particularly for tasks with limited amount of data; and 2) improved ease in finetuning a model compared to training from scratch [320].

Graph Convolutional Neural Networks (GCN) [321, 322] is an alternative architecture that can be used to improve the learning of context-aware features across the WSI. GCNs typically consist of nodes representing elements and edges defining relationships between nodes. In [323], a GCN was defined on a WSI, where the nodes represent patches and edges represent the connections among patches; this work obtained remarkable results on cancer prognosis task outperforming the SOTA in four out of five cancer types [323].

Vision Transformers (ViT) [324], have recently emerged as a direct application of Transformer models [325] to the image domain. In ViT, images are sub-patched and flattened into a 1D embedding along with a positional encoding which is then classified by an MLP head. By using the positional encoding, the model’s attention mechanism can focus computation on the most relevant areas of the image. ViT models have been applied with great success to CPath tasks, especially in conjunction with pre-trained CNN models [326]. We refer the reader to a comprehensive survey of transformer methods in medical image analysis for more details [327].

General classification architectures are also commonly used as a foundation for novel architectural designs. For example, Squeeze-and-Excitation (SE) modules were introduced to reduce the number of parameters in ResNet and DenseNet blocks while maintaining high accuracy [328, 236]. A fully-connected conditional random field (CRF) was incorporated on top of a CNN encoder to improve performance while maintaining the same level of computational complexity [329]. Lastly, patch sampling and pooling were used with AlexNet to perform slide-level disease diagnosis and segmentation [142].

Finally, in order to achieve superior performance, many researchers often rely on ensemble or multi-stage techniques which combine the predictive power or feature extraction abilities of multiple models to form a final output. These approaches have shown performance improvements compared to traditional single model classifiers [330, 331, 332, 333, 334, 335]. How-

ever, this often comes at the expense of higher computational requirements.

5.2. Segmentation Architectures

Segmentation is widely used in CPath, as shown in Figure 4, and enable localizing the area of interest at the pixel level [336]. U-Net was initially developed for neuronal structure segmentation in electron microscopy image stacks [336], but has become one of the most common architectures for segmentation in CPath [337, 338, 339, 340, 244, 341, 342, 285, 330, 343, 344, 345, 346, 347, 152, 280, 348, 349, 350, 311, 351, 352, 353, 354, 355, 205, 356, 207]. U-Net has an encoder-decoder structure: an encoder to contract features spatially and a decoder to expand them again to capture semantically related context and generate pixel-level predictions [336]. The U-Net model has been used to segment nuclei for creating a novel dataset with unsupervised learning [244], but it should be noted that this process also relies on the Mask R-CNN framework and pathologists for quality-checking purposes.

Another common approach for segmentation is to use fully convolutional networks (FCNs) [357, 265, 358, 359, 80, 360, 198, 277, 84, 361, 362, 356], customized architectures constructed by combining multiple components of various architectures, or introducing new components to pre-existing architectures [241, 363, 168, 364, 365, 366, 367, 368, 369, 370, 266, 371, 307, 84, 372, 373, 374, 350, 375, 351, 276, 273, 376, 316]. For example, one work used a custom CNN to predict whether each pixel was benign or malignant, while a second CNN was used to refine the initial prediction through probability fusion [84].

5.3. Object Detection Architectures

In this section, we specifically focus on architectures that are used for object detection in CPath, where bounding boxes are predicted around regions of interest. A major CPath application for object detection is mitosis detection with the primary goal for counting the number of mitosis instances. To this end, a large number of studies has been dedicated to this application [377, 199, 225, 269, 378, 344, 379, 200, 380, 381, 382, 383, 384, 385, 350, 386]. Object detection has been additionally applied for nuclei [387, 388, 77, 389, 390, 391, 392], colorectal gland [80, 393, 348] and glomeruli detection [394, 395, 396]; however, it can also be applied to the detection of a variety of histopathological objects including tumor-infiltrating lymphocytes [397] or keratin pearls [371].

In CPath, object detection employs a combination of pre-existing off-the-shelf architectures and customized neural networks to perform object detection tasks, as shown in Figure 10. A model called CircleNet, which uses a deep layer aggregation network as a backbone, was proposed to detect round objects [395]. Their approach involves using an anchor-free “center point localization” framework in order to output a heatmap with center points followed by a conversion into a bounding circle for the detection of kidney glomeruli. A multi-stage deep learning detection model based on Fast R-CNN was proposed in [379]. First, a modified Fast R-CNN generated region proposals, then a ResNet-50 model eliminated false positives, and

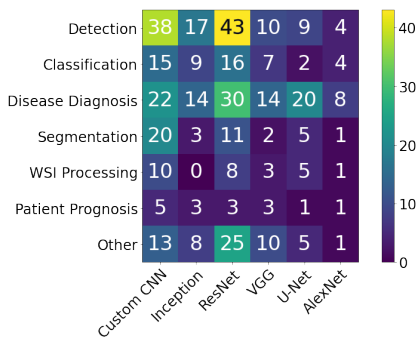


Fig. 10: Distribution of the most common Neural Network architectures used in the surveyed literature, based on the CPath task. The x-axis displays the Neural Network architectures used in the papers (from left to right): Custom CNN, Inception, ResNet, VGG, U-Net, and AlexNet. The y-axis shows the different tasks (top to bottom): Detection, Classification, Disease Diagnosis, Segmentation, WSI Processing, Patient Prognosis, and Others. For more details, please refer to Table 9.11 in the supplementary section.

a Feature Pyramid Network detected mitosis in sparsely annotated images using a ResNet backbone [385].

5.4. Multi-Task Learning

Multi-task models are individual models predicting for multiple tasks at once (e.g. classification and segmentation), as defined in Section 2. Multi-task learning (MTL) can be beneficial over independent task learning because sharing representations between related tasks can create more generalizable representations and encourage the task heads to make logically consistent predictions. This type of model, however, is uncommon in CPath, as it requires annotating multiple tasks for each image [120, 398, 82, 384, 399, 32, 400]. We discuss some of these papers in further detail below.

In one work, a ResNet-50 backbone followed by independent decoders (a pyramid scene parsing network for segmentation and a fully-connected layer for classification) was used to solve 11 different tasks (4 segmentation based and 7 classification based) [120]. With significantly less computation, the MTL model achieved comparable or better results to single task learning in classification, but comparatively worse results in segmentation. Similarly, in [82], a ResNet-50 with two parallel branches to perform segmentation and classification, was able to achieve comparable results on both tasks through an MTL approach.

While the results are impressive, there is still work to be done in this field. One work found that model performance may be sensitive to the number and type of tasks used during training [398]. If the tasks are unrelated, this could deteriorate the performance compared to a single-task setting. How to weigh different task objectives and select optimal tasks to be trained together is yet an active area of research [401, 402]. MTL represents an interesting field of research in CPath as it may reduce the necessity to train multiple deep neural networks to perform different tasks.

5.5. Multi-Modal Learning

As opposed to multi-task networks where multiple tasks are learned simultaneously, the multi-modal approach involves us-

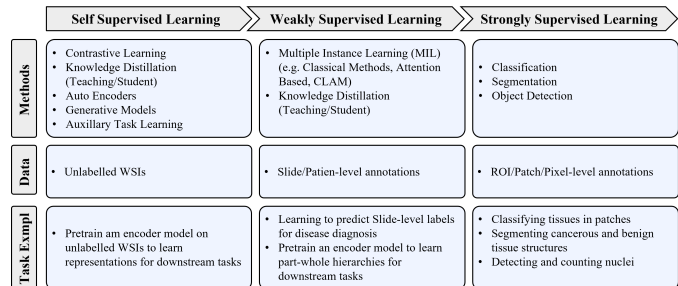


Fig. 11: Details of types of learning using varying levels of supervision. Note that the types of tasks each type of learning can address vary based on the data that is available, as noted in the *Example Task* portion of the figure. However, from left to right, models trained with less supervision can still learn salient representations of the data that can be used to fine-tune models for tasks requiring more supervision. In that sense, for CPath there is a *spectrum* of supervision from self to strongly supervised learning that aligns well with the annotation levels shown in Figure 7.

ing network input features from multiple domains/modalities at once [403]. In the case of CPath, modalities can be represented as pathologists’ reports, gene expression data, or even WSI images. Most commonly, immunohistochemistry (IHC) stains alongside the H&E stain to better visualize specific proteins [404, 405, 406]. As a result, models can learn better unified/shared latent representations which capture correlations from multiple indicators, since some information may not be captured by individual indicators [407]. This approach can be viewed as adding hand-crafted features to boost performance. While the use of deep learning normally implies using learned features to replace hand-crafted ones, using hand-crafted features can nonetheless improve performance compared to strictly deep learning approaches when data is limited [408]. Indeed, many works have obtained best performance by combining manual and learned features [378, 390, 409]. This was demonstrated in the case of mitotic cell classification when an ensemble classifier model using hand-crafted features set a new record for the MITOS-ATYPIA 2014 challenge with an F-score of 86% [410]. However, where data is plentiful, CNNs alone can outperform all other hand-crafted features. In the same MITOS-ATYPIA 2014 challenge, the previous record was broken this way with a new F-score of 96% [411]. Although one cannot compare these two works directly as they use different classifier heads and dataset balancing methods, one can argue that the optimal choice of approaches from deep learning, classical ML, and different modalities should depend on the situation. Multi-modal approaches are gaining traction in CPath for specific problems, especially where useful additional data is available [412, 413]. For example, gene expression data and WSI images are often combined to improve cancer prognosis prediction [414, 415].

5.6. Vision-Language Models

Following its successful use in the natural image domain, vision-language data (consisting of histopathology images paired with relevant natural language text) is becoming increasingly prominent in CPath. Whether it be the development of foundational models [416] extending to CPath, or fine tuning state-of-art large large models for use in downstream tasks

[417, 418, 419], leveraging the semantic information embedded in the natural language data is becoming more evidently beneficial. It was only recently that foundational language models advanced enough to become useful in CPath, and this has triggered an explosion of interest into building models at the intersection of visual and language information. At the moment, language data is primarily used to address Multi-Instance Learning, although this is still an extremely new field and we anticipate that future works will surely address more advanced tasks (see Section 7.4 for further discussion).

5.7. Sequential Models

Recurrent Neural Networks (RNNs) are typically used in tasks with temporally-correlated sequential data, such as speech or time series [420]. Since RNNs consider the past through the hidden state, they are suited for handling contextual information. While images are the default data format in CPath (and hence poorly-suited for RNNs), some works opt to combine RNNs with CNNs as a feature extractor [62, 88, 421, 231, 422, 266, 423, 264, 424, 425, 213, 426, 427], most commonly by aggregating patches or processing feature sequences [62, 231, 266, 425, 428]. Another application of RNNs is to consider spatial relations between patches, which can be lost after extracting from the slide [264, 213].

A particularly exciting use of RNNs is in deciding which region within an image should be examined next [424, 429]. In the “Look, Investigate, and Classify” 3-stage model, a long short-term memory (LSTM) was used to classify the ROI cropped from the current patch and predict the next region to be analyzed, and achieved good performance while only using 15% of pixels from the original image [424]. Similarly, an LSTM network was used to better predict ROIs by treating state features similar to time-series data, thus identifying only relevant examples to use for training [429]. And an LSTM transformer with “Feature Aware Normalization” (FAN) units for stain normalization was used in parallel with a VGG-19 network [325]. More recently, transformers using attention mechanisms have been used to allow parallelization and better sequence translation compared to older RNNs or LSTM networks [430].

5.8. Synthetic Data and Generative Models

With annotated data difficult to obtain in CPath, especially with granular labels (see Section 3.3 for more discussion), this is problematic for training generalizable models. Hence, generating *synthetic* data from a controlled environment (either via simulation or a trained model) for augmenting the available training set of annotated data shows much promise. Originally developed for visual style transfer in general computer vision, generative models learn to create novel instances of samples from a given data distribution - they form the dominant approach in CPath.

Initial works primarily utilized Generative Adversarial Networks (GANs) for patch synthesis [337, 431, 432, 433], stain normalization, [434, 208, 209, 210, 435, 206], style transfer [436, 437, 438, 206], and various other tasks [212]. One unsupervised pipeline relied on a non-GAN model to create an initial

patch that was refined by a GAN [337]. In another work, one CycleGAN generated tumor images and another non-tumor, in order to train a classification network [439]. One work used neural image compression to learn the optimal encoder to map image patches to spatially consistent feature vectors [212]. Another work first classified bone marrow cell representations and then used an unsupervised GAN to generate more instances from each cluster [440]. A self-supervised CycleGAN was also used for stain normalization, and shown to improve model performance in subsequent detection and segmentation tasks [210]. Similarly, a CycleGAN pipeline was applied to perform artificial IHC re-staining [441]. Recent works in GANs attempt to model spatial awareness of tissues and improve the realism of the generated samples [442].

Lately, diffusion models have become the SOTA in general computer vision and now produce far more semantically plausible and noise-free images than GANs. These improvements promise to make synthetic data finally accepted by pathologists and the broader CPath community as reliable training data and significantly improve the generalizability of models trained on them [443].

5.9. Multi-Instance Learning (MIL) Models

Multi-instance learning (MIL) involves training from data that is labelled as high-level bags consisting of numerous unlabelled instances. In the context of CPath, these labelled bags often represent annotated slides of far more unlabelled patch instances [444]. As labels at the WSI level are much easier to obtain (and hence more prevalent) than patch-level annotations, MIL has been applied to CPath by a significant number of papers [62, 425, 445, 446, 63, 447, 448, 449, 444, 274, 450, 451, 452, 453, 454, 455, 456, 315, 275, 323, 457, 64, 456, 458, 459, 460, 461, 462, 463]. Since both utilize coarser annotations for training on massive images, MIL is similar to weakly-supervised learning. However, weak supervision predicts at a finer level (e.g. pixel segmentation from labelled patches) than the provided annotation while MIL prediction is typically at the same level.

One notable work used a two stage approach to first encode patches with a CNN from a slide into feature vectors and then pass the most cancer-likely ones to a slide-level classification RNN. A similar work first detected abnormal regions in the WSI before adaptively fusing the instance-level features with an importance coefficient [446]. Adding additional instance-specific attributes tends to improve MIL performance. One work applied a nuclei grading network to provide a cell-level prediction for each patch, and demonstrate this out-performs hand-crafted cell features for overall slide classification [326]. Recent works explore the morphological and spatial relationships between instances, which conforms with pathologist diagnostic intuitions and have demonstrably improved performance, especially with unbalanced data [463].

As not all instances are equally relevant to the bag label, many works focus on building attention mechanisms to adaptively focus on more relevant instances. One work used such a mechanism to highlight regions of interest and improve localization relative to other SOTA CNNs [444]. MIL models can

be improved by considering multi-scale information: one work notably used embeddings from different magnification levels and self-supervised contrastive learning to learn WSI classifiers [275]. Some works explicitly encode the patient-slide-patch hierarchy in the attention mechanism [464, 465], with one work using a cellular graph for top-down attention [466]. Graph Neural Networks (GNNs) have been explored to leverage intra- and inter-cell relationships, enabling cancer grading [467], classification [468], and survival prediction [469, 470]. These hierarchy- and morphology-aware models are the current SOTA and pave the way for future improvements.

One persistent challenge with using MIL in CPath, compared to natural image computer vision, is the lack of large-scale WSI datasets [471]. One recent work addressed issues related to small sample cohorts by splitting up large bags (and their labels) into smaller ones through pseudo-bags [472].

5.10. Contrastive Self-Supervised Learning for Few-Shot Generalization

The idea of using contrastive learning (CL) for self-supervised learning (SSL) dates back to 2005, yet only recently gained momentum in CPath [473, 474, 275, 475, 476, 477, 313, 478]. By using a contrastive loss, a feature embedding is learned to ensure similar (positive) examples are close in vector space, while dissimilar (negative) examples are distant [473, 474]. Contrastive learning is an attractive approach for CPath because when used as self-supervision for few-shot learning [275, 475, 313], it does not require labelling the massive self-supervision image set but only labelling the small subset used for training on the downstream task, an approach that has recently achieved SOTA performance in a wide array of tasks in CPath [313]. SimCLR was originally proposed to learn representations invariant to different augmentation transforms (such as crop, noise) for natural images [66], and when applied to CPath, was found to match or outperform SOTA supervised techniques [313]. Self-supervised pre-training has been shown to perform best against fully-supervised pre-training when applied to small but visually-diverse datasets [313]. Recent works have focused on transferring the self-supervised representations to the downstream task more intelligently: through latent space transfers [479], with an awareness of the patient-slide-patch hierarchy [480, 481], or with semi-supervised pseudo-label guidance [482].

5.11. Novel CPath Architectures

In this section, we discuss papers that made significant changes to the model design or completely designed an architecture from scratch for CPath tasks [284, 483, 389, 484, 64, 364, 485, 368, 486]. Typically, model architectures are adapted from the natural image domain and minor changes applied for CPath tasks, rather than being designed from scratch for CPath directly. Unfortunately, general computer vision architectures typically require large computational resources not necessarily available in clinical settings and are prone to overfitting on smaller CPath training sets [483].

More importantly, CPath tasks often comprise of multiple specialized sub-tasks not addressed by common architectures

- in such cases, CPath-specific architectures perform better. “PlexusNet” achieved SOTA performance with significantly fewer parameters [483] and “Hover-Net” used a three-branched architecture for nuclei classification and instance segmentation [284]. Path R-CNN similarly used one branch to generate epithelial region proposals and another to segment tumours [389].

In other cases, custom architectures are designed to obtain better performance with respect to certain metrics [85, 302, 384, 395, 345] or improve computational efficiency and speed [196], where since model inference can be a bottleneck for WSI processing. To automate architecture design, neural architecture search (NAS) is often used. This is an umbrella term covering evolutionary algorithms (EA), deep learning (specifically Reinforcement Learning), and gradient-based NAS searches. There are two approaches to EA: (1) Neuroevolution, which more generally optimizes at the neuron-level to find optimal weights, and (2) Evolutionary-Algorithms based NAS (EANAS), which searches for optimal combinations of mid-sized neural network blocks and conducts training after this architectural search [487, 488]. In CPath, reinforcement learning-based NAS has designed models for cancer prediction which were found to train faster, have fewer parameters, and perform comparably with manually designed models [489]. Another work demonstrated that a significantly smaller model can outperform existing SOTA models on a variety of CPath tasks using an adaptive optimization strategy [486].

We hypothesize that NAS has yet to be explored significantly in CPath due to the lack of annotated data (see Section 3.3) and its relative recency as a research area. According to the “no free lunch theorems” [490, 491], no single model can perform best on all tasks. However, computationally efficient but performant models are crucial for CPath applications, and NAS is the most promising approach to computationally design such architectures without manual engineering.

5.12. Model Comparison

The various model architectures and types discussed above can and should be compared on common benchmarks to determine the best models for a given task [492]. Numerous papers have conducted such benchmarking work on CNNs. One work comparing GoogLeNet, AlexNet, VGG16, and FaceNet on breast cancer metastasis classification found that deeper networks (i.e. GoogLeNet) predictably performed better [199]. Another work found that using ResNet-34 with a custom gradient descent performed best [394]. Finally, VGG-19 performed best in colorectal tissue subtype classification, showing that deeper SOTA networks do not necessarily perform better universally. Which CNN performs best depends on the task, the nature of the data, the metrics used, training time, hyperparameters, and/or hardware constraints.

Likewise, third parties have organized “grand-challenges” to facilitate the fair comparison of different techniques on a common CPath task and dataset. In some cases, SOTA CNNs achieve the best results, such as the adapted GoogLeNet that obtained the highest AUC [238] and the AlexNet that achieved highest accuracy [493] for breast cancer detection in the CAMELYON16 challenge. Likewise, SqueezeNet, which

is an existing SOTA network performs best in colorectal tissue subtype classification [494]. On the contrary, the best performing models for mitosis detection in the TUPAC16 [199] and MITOS12 [345] challenges both relied on custom CNN architectures. For breast cancer diagnosis, a novel Hybrid CNN achieved the best results in the BACH18 (ICIAR18) dataset [495] while the two teams achieving the best classification accuracy in the BreakHis dataset used differing approaches: one directly used ResNet-50 [298] and the other used an ensemble of VGG networks [496]. For nuclei segmentation on the Kumar-TCGA dataset, a novel framework using ResNet and another existing model achieved the highest F1-score [364]. Lastly, a custom CNN achieved the best results for gland segmentation on the GLaS dataset [168].

However, as mentioned in Section 3.3, many grand challenges use private datasets or even extract data from larger public repositories without referencing the original WSIs used. Furthermore, benchmark datasets address different tasks and lack standardization. As models that are hyper-optimized for specific sets of data continue to be released, the lack of more standardized benchmark datasets and model comparison studies make it impossible to systematically compare new models against existing ones or assess their robustness in clinical settings, thus impeding model development in CPath.

6. Evaluation and Regulations

6.1. Clinical Validation

Within the domain of CPath, clinical validation is essential for substantiating the decisions produced by deep learning models so that they are more readily accepted by the medical community. Generally, acceptable clinical criteria are determined by authoritative professional guidelines, consensus, or evidence-based sources. However, in CPath, prediction results are generated by the computer scientists and engineers who build the model, and may not be completely aware of where their work fits into the clinical pathology workflow—the clinical implications of this arrangement are often unknown [169]. By incorporating pathologist expertise, clinical validation can better align the technical work with clinical objectives.

Despite the importance of this step for real-world deployment, very few works have performed clinical validation with expert pathologists. We identify three prominent types of clinical validation in the CPath literature: (1) direct performance comparison of CAD tools with pathologists on a similar task, (2) impact of CAD tool assistance on pathologist performance, and (3) pathologist validation of CAD tool outputs. Each topic is further discussed in the sections alongside notable results.

Direct Performance Comparison with Pathologists To validate the benefits of deep learning methods, it is desirable that they equal or surpass the performance humans to gain the trust of pathologists in their decisions and their willingness to use them as a second opinion [497]. With this in mind, many papers directly compared their models with pathologists in tasks such as prognosis and diagnosis.

One study on cancer detection found that the top computational models from the CAMELYON16 challenge outperformed the 11 pathologists with a two-hour time constraint

and performed similarly to the expert pathologist without a time constraint [238]. This suggests that deep learning models could be particularly useful in clinical scenarios with excessive numbers of time-critical cases to diagnose. Similarly, for tissue subtype classification, another study performed similarly to, or slightly better than individual pathologists. The proposed model agreed with all pathologists 66.6% of the time and agreed with two-thirds of pathologists 76.7% of the time [75]. An additional study claimed their deep learning model outperformed pathologists without gynecology-specific training in ovarian carcinoma classification [119]. This pushes the idea that CAD predictions can be used as a second opinion due to the potential for human error by individual pathologists.

One paper on diagnosis [263] demonstrated that deep learning models can correctly classify images that even individual pathologists failed to correctly identify. However, another paper found that 50% of the examples misclassified by their model were also misclassified by at least one pathologist [498]. This suggests that deep learning models can aid pathologists in decision-making, but as they tend to achieve a specificity and sensitivity similar to pathologists, they must be applied cautiously to avoid reinforcing the biases or errors of individual pathologists.

Deep learning models for prognosis have been shown to achieve performance similar to or better than experts as well [245, 388, 296]. In one study, the best model for renal clear cell carcinoma classification achieved 83% accuracy, outperforming the inter-pathologist accuracy of 80% [296]. This shows that deep learning models and pathologists may perform similarly on patient prognosis.

Overall, AI approaches are not perfect but have approached expert-level ability in a variety of tasks. Deep learning could play an important role as a second opinion and in democratizing the knowledge distilled from many pathologists to other pathology centres. Specifically, deep learning models appear to be best used as a tool to enhance the pathologist workflow, and could provide aid in making quick decisions with high accuracy [14].

Impact of CAD Tool Assistance Much of CPath research is conducted under the assumption that the resulting AI tools will be intuitive, usable, and beneficial to pathologists and patients. However, CAD tools that are developed without feedback from pathologists could fail to integrate into a realistic pathologist workflow or impact the most significant diagnostic tasks. Thus, a valuable validation experiment is to compare and comprehend the performance of expert pathologists in clinical tasks before and after being given the assistance of a CAD tool.

In one study, a CAD system called Paige Prostate Alpha leveraged a weakly-supervised algorithm to highlight patches in a WSI with the highest probability of cancer [62]. When used by pathologists, the model significantly improved sensitivity, average review time, and accuracy over unaided diagnosis. Likewise, another study using the LYNA algorithm examined the performance of six pathologists on breast cancer tumor classification before and after being able to see the LYNA-predicted patch heatmaps. The results indicate using LYNA substantially improved sensitivity, average review time, and the subjective

“obviousness” score for all breast cancer types [72, 27].

These studies suggest that integrating CAD tools into the clinical workflow will greatly improve pathologist efficiency. However, there is a general lack of research on the impact of CAD tools on pathology efficiency. Such studies would shed more light on the impact of CAD tools and identify approaches for implementation in clinical settings.

6.2. FDA Regulations

Despite the ongoing development of CAD tools in CPath and its potential for triaging cases and providing second opinions, the regulations regarding this technology pose an obstacle to the testing and deployment of these devices. The FDA currently provides three levels of clearance on AI/ML-based medical technologies: 510(k) clearance, premarket approval, and the De Novo pathway. While one source lists 64 AI/ML-based medical solutions that are currently FDA-approved or cleared, none of these are in the field of CPath [499]. A few companies, such as Paige AI, hold the 510(k) clearance for their digital pathology image viewer; however, an automated diagnostic system has yet to be approved. This may indicate a reluctance to change, and the lack of clarity in the process of FDA approval has prevented numerous impactful technologies from being deployed. There is a need for collaboration between researchers, doctors, and governmental bodies to establish a clear pathway for these novel technologies to be validated and implemented in clinical settings.

7. Emerging Trends in CPath Research

Computational pathology research has seen a sudden shift of focus in the past year of 2023. Driven by recent technological advances in the field of computer vision for natural images and the release of capable foundational models in natural language processing, formerly difficult research problems in CPath have been solved, opening up exciting new avenues of research, especially the difficulty of training models on adequate annotated data. We will discuss the main research trends below in further detail and make simple predictions of where the field is headed.

7.1. Contrastive Self-Supervised Learning becomes Mainstream

Data annotation for CPath is a persistent problem - it is easy to collect large amounts of visual data but much harder to annotate them. Transfer learning can help but it is difficult to transfer a model trained on one dataset to generalize to another. Whereas past efforts focused on carefully engineered methods, the recent development of contrastive self-supervised learning [66] means that it has become the mainstream approach in CPath [313, 275, 475]. Not only does it utilize the massive amounts of unlabelled images typically available in CPath, but it also as a result only requires finetuning on a small set for the downstream task. We anticipate that this will lead to the development of general-use foundational models in the future to perform the most common CPath tasks, as more pathology images are collected and models become more advanced.

7.2. Prediction becoming increasingly High-Level

We noticed that recent research works are increasingly addressing higher level prediction tasks than before. Whereas patch classification [294, 295, 296, 297, 274] or pixel segmentation [336, 337, 339, 340, 244] was formerly mainstream, these problems appear to have been largely solved, and now there is far more research into higher-level problems dominate, such as multiple-instance learning [444, 62, 464, 465, 466]. As computational methods continue to improve, it is natural that they are applied not merely as attention aids for pathologists (i.e. at the pixel or patch level), but furthermore are used to make intelligent slide- and patient-level decisions on their own. Indeed, they promise to vastly improve pathologist efficiency when used with human pathologists in the loop to validate the automated decisions, especially when paired with modern natural language capabilities.

7.3. Spatial and Hierarchical Relationships receiving Attention

Inspired by the approach taken for natural image computer vision, the mainstream approach in CPath currently requires breaking up large WSIs into smaller patches and perceiving them independently (see Figure 7). However, this ignores the spatial relationships between cells and tissues or between the patches and their parent slides in histopathology images, which are often relevant or even crucial when making decisions. Many works have recently found success in explicitly encoding an awareness of these inter-cell relationships [467, 469, 470] and the patch-slide-patient hierarchy [466, 464, 465], especially using Graph neural networks, but these suffer from higher latency than conventional CNNs. We anticipate future works will seek to speed up GNNs for tasks where spatial and hierarchical relationships are important and continue developing hierarchy-aware attention for MIL techniques.

7.4. Vision-Language Models for Explainable Predictions

One persistent problem in CPath has been developing models that can explain their decisions for human validation. One obvious route is to develop models that produce natural language output (and even converse with the human user to explain their decisions), but until recently, this would have required collecting massive amounts of pathology text paired with images. With foundational vision-language models widely available and able to generalize to great effect in the natural image domain [500, 501, 502], recent works have shown that they perform excellently when applied with minimal re-training to CPath images [417, 418, 419]. Further advances require collecting more pathology-specific data, but we anticipate that crowd sourcing of public pathology annotations will become mainstream and this will lead to the development of foundational vision-language models. As natural language capabilities continue improving, we also anticipate that synoptic report automation will become feasible and reinforcement learning from human feedback (RLHF) [503] will become common for improving CPath language models.

7.5. Synthetic Data now Realistic Enough

Whereas one way to combat the difficulty of annotating CPath data is to develop models that require fewer annotations, another trend is to generate more annotated data for training. Whereas concerns were previously raised about their realism, new advances in generative image models have now been leveraged to produce realistic histopathology images and pixel-accurate annotations simultaneously. However, current works are limited by specific tissues, organs, diseases [337, 439, 212, 440], or stains [210, 441] and are limited by their inability to easily expand to other histopathology content. We note that generating synthetic data via game engines and 3D model assets is a recent trend in the natural image domain [504, 505, 506], but visual modelling of histopathology entities is little explored. We anticipate that future works will attempt to improve synthetic histopathology image generation by: (1) attempting to create generative models that can generalize to a broad variety of histopathology images and (2) create simulation software to generate realistic histopathology images without learned models.

8. Existing Challenges and Future Opportunities

8.1. CPath as Anomaly Detection

Typically in computer vision, the various classes represent distinct normative entities, such as airplanes or bears [507, 508]. There exist abundant “normal” samples and potentially few “anomalous” samples, which are considered data points significantly dissimilar to the majority within a given class [509]. These anomalies are not only out of distribution from the samples in a dataset, there is also a lack of consensus on understanding anomalous representations as effectively identifying anomalies requires ML models to learn a feature space encompassing all “normal” samples within each class [509].

In other words, in general computer vision, each class cannot simply be considered as an anomalous version of any other class. However, in CPath, since each class is often considered a different disease state on a single tissue type, diseased classes are essentially extensions of the “normal” healthy class into the “anomalous” zone. From a pathologist’s perspective, similar to the general computer vision approach, the curriculum learning process of a resident pathologist first involves training on histology and gaining a mastery of normal tissue identification, and then train on diseased tissues, so they are able to flag the sample as anomalous and follow up with possible diagnosis.

In light of this, it may be illuminating to approach the problem from an anomaly detection viewpoint: provided a model has sufficient variety of healthy tissue, any anomalies must then be diseased. The output of such an anomaly detection algorithm is dependent on the task at hand. One source describes several meaningful output types that may be produced [509]: an anomaly score which describes how anomalous a sample is and a binary label indicating whether a sample is normal or anomalous. If only identifying anomalous samples is enough, a binary classification procedure may be sufficient. However, if it is necessary to identify the particular stage of progression of a disease type, then a more granular approach in assigning

some *anomaly score* may be more appropriate as explored in a previous work [510]. This work found that the confidence score in tissue classification was inversely correlated with disease progression, thus the confidence score may act as a proxy for an anomaly score. Theoretically, such approaches may better replicate the behaviour of pathologists. While several works have used an anomaly detection approach on medical image data outside of CPath [511, 512, 513], few works tackle the problem for WSI data in CPath.

8.2. Leveraging Existing Datasets

As mentioned in Section 3.3 of this paper, a minority of datasets in CPath are available to be freely used by the public. Additionally, the level of annotations varies for each dataset. However as can be noted in Table 9.11 of the supplementary material, for prominent public datasets such as CAMELYON16, CAMELYON17, Glas, BreakHis, and TCGA, there is far more available data annotated at the slide level as opposed to more granular predictions. For example, considering breast datasets, there are 399 WSIs annotated at the Slide and ROI levels in CAMELYON16 [514] and 1399 WSIs annotated at the Patient, Slide, and ROI levels in CAMELYON17 [61], in contrast, the TCGA-BRCA dataset contains 1163 diagnostic slides and 1978 tissue slides that are accompanied with labels at the Patient and Slide levels and diagnostic reports with labels for tissue features and tumor grades [242].

The lack of publicly available datasets with granular annotations is a major challenge in CPath. To address this lack some training data, techniques have been proposed to efficiently obtain labels, such as an active deep learning frameworks that use a small amount of labelled data to suggest the most pertinent unlabelled samples to be annotated [515]. Alternatively, other works propose models to synthetically create WSI patches, usually with the use of GANs. For example, Hou et al. [337] introduced an unsupervised pipeline that was capable of synthesizing annotated data at a large scale, noting that even pathologists had difficulty distinguishing between real and synthesized patches. However, despite these promising results, the issue of acquiring accurate and large datasets remains a prevalent issue within CPath.

Generally, tasks such as tissue classification or gland segmentation require labels at the ROI, Patch, or Pixel levels. However, existing data annotated at the patient and slide levels can be used for these tasks by leveraging weakly supervised techniques such as MIL [64, 444], or by learning rich representations using self-supervised techniques such as DINO [516, 65] and contrastive learning [313] that can be used in downstream tasks. Specifically, work is being done to develop training methodologies and architectures that are more data efficient for patient- and slide-level annotations, such as CLAM, which is a MIL technique that is used to train a performant CPath model with as little as 25% of the training data to get over 0.9 AUC [64]. Another recent work used self-supervised learning on WSIs without labels to train a hierarchical vision transformer and used the learned representations to fine-tune for cancer subtyping tasks. This finetuned model outperformed other SOTA methods that used supervised learning methods on both the full

training set and when all models used only 25% of the training set. These examples demonstrate a recent trend in the application of weakly and self-supervised learning techniques to leverage pre-existing and available data with weak labels, showcasing that a large amount of granular labels are not necessarily required for achieving SOTA performance. We urge researchers in the CPath field to follow this trend and focus on how to leverage existing weakly labelled datasets, especially to learn rich representations as a pre-training step for learning on smaller strongly labelled datasets.

8.3. Creating New Datasets

Although we mention the availability of many datasets and comment on how to leverage this existing data, there is still a need for new CPath datasets that address overlooked clinical and diagnostic areas. Therefore, creation of new CPath datasets should focus on addressing two main goals: (1) tasks that are not addressed adequately by existing datasets and (2) accumulating as large a dataset as possible with maximal variety.

Regarding the first goal, there are still organs, diseases, and pathology tasks without freely available data or sufficient annotations to develop CAD tools. For example, in Figure 6, we see that whereas breast tissue datasets are abundant, there are few public datasets for the brain and none for the liver. Collecting and releasing datasets for these organs would have significant impact in enabling further works focusing on these applications. Further, analysis of specific organ synoptic reports can guide CPath researchers to build CAD tools to identify or discriminate the most impactful diagnostic parameters. In the case of the prostate, which is discussed in Section 2.5, the synoptic report requires distinguishing IDC from PIN and PIA as it correlates to high Gleason scores. This is important, as high-grade PIN is a cancer precursor requiring follow-up sessions for screenings. These parameters are identified and noted in the report by the pathologist and factor into the final diagnosis and grading. Thus, collecting annotated datasets for such parameters can be crucial to developing CAD tools that are relevant to clinical workflows and can enrich learned representations.

The second goal is concerned with the scaling laws of deep learning models with respect to the amount of data available and their application to diverse clinical settings. As seen in the general computer vision domain, larger datasets tend to improve model performance, especially when used to learn rich model representations through pre-training that can be used for downstream tasks such as classification and semantic segmentation [517]. Additionally, ensuring that datasets capture the underlying data distribution and thus sufficiently encompass the test distribution has been shown to be especially important in the medical domain [518]. For CPath, this means ensuring a dataset captures the expected variations in tissue structure, disease progression, staining, preparation artifacts, scanner types, and image processing. Collecting a sufficiently large dataset continues to be problematic, however, so recent works have focused on using crowd sourcing to annotate histopathology data posted publicly on Twitter and YouTube [416, 418], a practice that is similar to that commonly used for natural images.

8.4. Pre- and Post-Analytical CAD Tools

In recent years, advances in image analysis, object detection, and segmentation have motivated new approaches to support the analytical phase of the clinical workflow, especially in the two steps where CAD tools could significantly increase efficiency and accuracy: (1) specimen registration and (2) pathology reports. This need is highlighted by a study determining that the pre-analytical and post-analytical phases (as shown in Figure 2 account for up to 77% of medical errors in pathology [519]. Likewise, Meier et al. classify 14% of medical errors as diagnostic errors, with an even smaller proportion being misinterpreted diagnoses in their study [520]. Other authors attribute approximately 15 – 25% of diagnostic errors to slide interpretation [521, 522, 523, 524, 525]. These results reinforce the need for CPath applications that address more than just the analytical phase [526]. Considering post-analytical step of compiling a pathology report, a few natural language processing efforts have been used to analyze completed pathology reports [527, 528, 529], extract primary site codes from reports [530], and generate of captions or descriptive texts for WSI patches [422]. However, to the best of our knowledge, there are no works that reliably extract clinical data from service requests and electronic medical records to automatically generate synoptic or text reports. Developing such a tool that could explicitly identify the most significant parameters for its decisions would directly improve clinical workflow and increase the interpretability of the results at the same time. We encourage the field of CPath to expand its efforts in creating tools for the pre- and post-analytical steps in order to reduce the large proportion of clinical errors attributed to those phases, and suggest some potential applications in Figure 2.

8.5. Multi Domain Learning

Despite being particularly well-suited for CPath, multi-domain learning (MDL) is still a relatively unexplored topic. MDL aims to train a unified architecture that can solve many tasks (e.g. lesion classification, tumour grading) for data coming from different domains (e.g. breast, prostate, liver). During inference, the model receives an input image and the corresponding domain indicator and is able to solve the corresponding task for the given domain. There are two reasons that make MDL attractive for CPath. The first is that the additional information from a source domain (coming from a related organ such as the stomach) can be informative for improving performance in the target domain (e.g. colon). By sharing representations between related domains, the model is enabled to generalize to other domains. The second motivation is to alleviate the data sparsity problem where one domain has a limited number of labeled data. Through MDL, the domain with limited data can benefit from the features that are jointly learned with other related tasks/domains [531, 532].

8.6. Federated Learning for Multi-Central CPath

Data-driven models require a large amount of data to yield strong performance. In CPath, this requires incorporating diverse datasets with varying tissue slide preparations, staining quality, and scanners. An obvious solution to train such models

is to accumulate the data from multiple medical centers into a centralized repository. However, in practice, data privacy regulations may not permit such data sharing between medical institutions, especially between countries. A possible solution lies in privacy-preserving training algorithms, such as federated learning [533, 534], which can make use of decentralized data from multiple institutions while maintaining data privacy. In federated learning, training starts with a generic machine learning model in a centrally located server. But instead of transferring data to a centralized server for training, copies of the model are sent to individual institutions for training on their local data. The learning updates are encrypted and sent to the central server and then aggregated across the institutions. Ming Lu et al. [454] demonstrated the feasibility and effectiveness of applying federated, attention-based weakly supervised learning for general-purpose classification and survival prediction on WSIs using data from different sites. Using such algorithms for CPath can facilitate cross-institutional collaborations and can be a viable solution for future commercial solutions that need to continuously augment and improve their ML models using decentralized data.

8.7. CPath-specific Architecture Designs

Many deep learning architectures are not designed for CPath specifically, which raises a serious question about the optimality of using “borrowed” architectures from general computer vision. For instance, [483] notes that traditional CV architectures may not be well suited for CPath due to a large number of parameters that risk overfitting. Additionally, the field of pathology has much domain-specific knowledge that should be taken into account before choosing an ML model. For example, under varying magnifications different morphological patterns are captured, from cellular-level details to tissue architecture features [335]. Naively applying an architecture without considering such details could discard key visual information and lead to deteriorated performance.

Unlike natural images, WSIs exhibit translational, rotational, and reflective symmetry [535] and CNNs for general vision applications do not exploit this symmetry. The conventional approach to overcome this issue is to train the model with augmented rotations and reflections, but this increases training time and does not explicitly restrict CNN kernels to exploit those symmetries. Rotation-equivariant CNNs, which are inherently equivariant to rotations and reflections were introduced for digital pathology [535], significantly improving over a comparable CNN on slide level classification and tumor localization. Similarly, Lafarge et al. [383] designed a group convolution layer leveraging the rotational symmetry of pathology data to yield superior performance in mitosis detection, nuclei segmentation, and tumor classification tasks. These results motivate the application and further research of rotation-equivariant models for CPath.

In general, we note that the SOTA computer vision architectures used in computational pathology have tended to lag behind those used for natural images by a couple of years. This delay in knowledge propagation from the mainline computer vision research in natural images may be due to the data-centric

nature of the CPath field. As data labelling is specialized and expensive to conduct, annotating more data or clever training tweaks to finetune established architectures is more attractive than developing advanced, specialized architectures. However, we recommend that CPath researchers should still use the most powerful relevant models available for the simple reason that they tend to perform best given the computational resources available. While computational efficiency is generally not as important during training, it is imperative at inference time if models are to be run in real-time on medical devices with limited computational resources.

8.8. Digital and Computational Pathology Adoption

Despite the numerous advantages to the clinical workflow and applications offered by using digital pathology and CPath, the adoption of digital pathology remains the first barrier to clinical use. A major reason for adoption hesitancy is the common opinion that digital slide analysis is an unnecessary step in a pathologist’s workflow which has been refined over decades to produce reproducible and robust diagnoses without digitization [18, 19, 9, 20]. In terms of clinical efficiency, studies have shown mixed results, with two finding that digitization actually decreased efficiency (by increasing turnaround time by 19%) [536, 537]. However, another study demonstrated a clear increase in productivity and reduction of turnaround-time [24]. One of the co-authors (B.N.) has implemented digital pathology at a public tertiary institution, which began as a pilot study over three years including three experienced academic pathologists and showed that digitization reduced turnaround time by 18% for biopsies and 25% for resections, and increased case output by 17%. These trial results led to all pathologists not retiring within two years to transition to a digital pathology workflow in 2019. Due to the varied nature of results and outcomes in studies analyzing the effectiveness of digital pathology there is more work to be done to have a multi-institution and lab analysis for more general and concrete results.

A major factor in the adoption of digital or computational pathology practices is the source of funding and the pay structure of pathologists. A few cost-analysis studies show that the transition to digital pathology becomes financially advantageous in 2 years, with savings projected to be up to \$5M after 5 years in a sizeable tertiary center [538, 9, 539, 540]. The financial impact will also be viewed differently in public vs private healthcare settings. Public healthcare is primarily limited by funding and universal access to healthcare whereas for private lab networks improvements in processes and services are directly linked to the prospects of obtaining additional contracts and increased profitability. However, studies considering multiple institutions and funding settings are still required to fully characterize the financial impact compared to clinical benefit. Additionally, on an individual pathologist level, compensation structures can affect buy in for implementation. For example, at our co-authors’ B.N. and V.Q.T institution, a fee-for-service structure is used to compensate pathologists thus an increase in throughput and productivity has a direct correlation to increased pay. We propose that this fee-for-service model contributes to the widespread embracement of DP at this institution. In contrast, pathologists in a salary-based environment are paid based

based on a combined package of services which includes diagnostics, research, teaching, administration, quality control, etc. An increase in clinical productivity would technically not benefit them directly, as it would translate to a high number of rendered diagnostics over the same amount of time.

Integration CPath into the clinical workflow is relatively understudied as few papers have actually deployed, or performed clinical validation of their results. Works in this area have either proposed methods to deploy their models in the clinic or developed tools to enable the use of their research in the clinic [294, 497, 541]. However, as a primary goal of CPath is the use of CAD tools in clinical settings, more works should consider how to integrate models and tools into the clinical workflow, especially in conjunction with expert clinicians.

8.9. Institutional Challenges

Several institutional challenges may affect the implementation of CPath tools, and similar challenges in implementing digital pathology workflows at medical institutions have been well-described by many studies [542, 543, 544, 545, 546]. As noted by multiple studies considering the digital transition of pathology laboratories [542, 543, 544, 545, 546], the importance of a common shared goal and frequent communication between the involved parties is necessary to successfully deploy a digital system. These lessons are likely extendable in the context of CPath and CAD development as well. Specifically, Cheng et al. [545] reported on their experiences and lessons learned as a 7-point-based system to efficiently deploy a digital pathology system in a large academic center. We believe similar systematic approaches will need to be developed to implement CPath applications in a clinical setting.

Another institutional challenge concerns the regulatory oversight at the departmental, institutional, accrediting agencies, pathology association, state/provincial, and federal levels. Regulatory measures underlying WSI scanners are well established, as well as the technical and clinical validation of their use [547, 548, 549]. On the other hand, patient confidentiality, ethics, medical data storage regulations, and data encryption laws are equally, if not more, time-consuming and intensive to comply with. These issues can be mitigated by deploying a standardized digital pathology system throughout multiple institutions at the state/provincial level. For example, our co-author (B.N.) has obtained governmental approval and funding to distribute a set of digital pathology systems throughout the province's public anatomical pathology laboratories. Similarly, a unified set of standards for processing and digitizing slides, along with unifying storage and access to WSIs for research use in collaborative efforts is paramount in moving forward in both the development and implementation of CAD systems.

8.10. Clinical Alignment of CPath Tasks

Researchers in the CPath field must ensure that the CAD tools they create are clinically relevant and applicable to pathology so that effort and resources are not allocated towards extraneous or clinically irrelevant tasks. For example, certain CADs have been proposed to facilitate case triaging and reduce turnaround time for critical diagnoses [550, 72, 73, 74, 551]].

However, several regulatory agencies in pathology aim for 90% of cases to be completed within a timeframe of 72 hours for signing-out resection specimens and up to 48 hours for biopsies [552, 553]. In this context, triaging becomes extraneous, as signing out cases faster than 48-72 hours has no clinical impact. However, in the context of an institution operating at longer turnaround times or struggling to keep up with the caseload, this method could be lifesaving. Alternatively, identifying mitotic figures and counting positive Ki-67 nuclei are appreciated tools already in use in multiple digital pathology settings, despite these tools being seldom applied to the large caseload proportion of most practicing pathologists.

As noted previously, the overall number of pathologists in the USA has decreased 17% from 2007 to 2017 and caseloads have increased by 41.7% [554]. This trend places further emphasis of developing CAD tools towards specific challenges encountered by pathologists and where sub-specialists may not be readily available. For example, a large consortium generated a prostate cancer CAD that achieved a 86.8% concordance with expert genitourinary pathologists [555], a significant breakthrough for healthcare settings where prostate biopsies are not signed out by sub-specialists. Additionally, targeting specific diagnoses with high rates of medical errors and inter-observer variance, notably in dermatological, gynecological, and gastrointestinal pathology, should be prioritized and integrated into practice quickly to support patient care [556]. Finally, advanced CAD tools capable of diagnosing features out of reach by conventional pathology could have a great impact. For example, identifying the origin of metastases from morphological cues on the WSIs without added IHC [455] or CADs capable of calculating the exact involvement of cancer on a biopsy core for prognostic purposes [555].

8.11. Concluding Remarks

Bringing pathologists and computer scientists together and initiating meaningful collaborations with shared gains between all parties is likely the most efficient path forward for CPath and CAD integration. Opportunities to facilitate collaborations should be promoted by parties such as the Pathology Innovation Collaborative Community and the Digital Pathology Association. Furthermore, we encourage involved pathologists and computer scientists to communicate and collaborate on studies towards the common goal of providing patients with fast, reproducible, and high-quality care.

Acknowledgment

Authors would like to thank Huron Digital Pathology for providing support and insightful discussions related to digital pathology hardware infrastructures. Authors would like to also thank Xin Zhao, Koosha E. Khorasani, Mona Sharifi, Kiana Abtahi, Alejandra Zambrano Luna, Cassandre Notton, Tomas Pereira, and Amirhossein Mohammadi for their help in initial preparation of our model-cards. This work was partly supported from NSERC-CRD (CRDPJ515553-17) funding grant and MITACS-Elevate award (Ref. IT14369).

References

- [1] FDA News Release. Fda allows marketing of first whole slide imaging system for digital pathology. <https://www.fda.gov/news-events/press-announcements/fda-allows-marketing-first-whole-slide-imaging-system-digital-pathology>, 2017.
- [2] Andrew J Evans, Thomas W Bauer, Marilyn M Bui, Toby C Cornish, Helena Duncan, Eric F Glassy, Jason Hipp, Robert S McGee, Doug Murphy, Charles Myers, et al. Us food and drug administration approval of whole slide imaging for primary diagnosis: a key milestone is reached and new questions are raised. *Archives of pathology & laboratory medicine*, 142(11):1383–1387, 2018.
- [3] Anna Luíza Damaceno Araújo, Lady Paola Aristizábal Arboleda, Natalia Rangel Palmier, Jessica Montenegro Fonseca, Mariana de Pauli Paglioni, Wagner Gomes-Silva, Ana Carolina Prado Ribeiro, Thais Bianca Brandao, Luciana Estevam Simonato, Paul M Speight, et al. The performance of digital microscopy for primary diagnosis in human pathology: a systematic review. *Virchows Archiv*, 474(3):269–287, 2019.
- [4] Bethany Jill Williams, Andrew Hanby, Rebecca Millican-Slater, Anju Nijhawan, Eldo Verghese, and Darren Treanor. Digital pathology for the primary diagnosis of breast histopathological specimens: an innovative validation and concordance study on digital pathology validation and training. *Histopathology*, 72(4):662–671, 2018.
- [5] Frederik Großerueschkamp, Hendrik Jütte, Klaus Gerwert, and Andrea Tannapfel. Advances in digital pathology: from artificial intelligence to label-free imaging. *Visceral Medicine*, pages 1–9, 2021.
- [6] Kuo-Hsing Kuo and Joyce M Leo. Optical versus virtual microscope for medical education: a systematic review. *Anatomical Sciences Education*, 12(6):678–685, 2019.
- [7] Robert Pell, Karin Oien, Max Robinson, Helen Pitman, Nasir Rajpoot, Jens Rittscher, David Snead, Clare Verrill, UK National Cancer Research Institute (NCRI) Cellular-Molecular Pathology (CM-Path) quality assurance working group, Owen J Driskell, et al. The use of digital pathology and image analysis in clinical trials. *The Journal of Pathology: Clinical Research*, 5(2):81–90, 2019.
- [8] Shaimaa Al-Janabi, André Huisman, and Paul J Van Diest. Digital pathology: current status and future perspectives. *Histopathology*, 61(1):1–9, 2012.
- [9] Jon Griffin and Darren Treanor. Digital pathology in clinical use: where are we now and what is holding us back? *Histopathology*, 70(1):134–145, 2017.
- [10] Adela Saco, Jose Antoni Bombi, Adriana Garcia, Jose Ramirez, and Jaume Ordí. Current status of whole-slide imaging in education. *Pathobiology*, 83(2-3):79–88, 2016.
- [11] Rajiv Kumar Kaushal, Sathyananarayanan Rajaganesan, Vidya Rao, Akash Sali, Balaji More, and Sangeeta B Desai. Validation of a portable whole-slide imaging system for frozen section diagnosis. *Journal of Pathology Informatics*, 12(1):33, 2021.
- [12] Jeroen Van der Laak, Geert Litjens, and Francesco Ciompi. Deep learning in histopathology: the path to the clinic. *Nature medicine*, 27(5):775–784, 2021.
- [13] Miao Cui and David Y Zhang. Artificial intelligence and computational pathology. *Laboratory Investigation*, 101(4):412–422, 2021.
- [14] Amelie Ehle, Niklas Timon Rindtorff, Titus Josef Brinker, Tom Luedde, Alexander Thomas Pearson, and Jakob Nikolas Kather. Deep learning in cancer pathology: a new generation of clinical biomarkers. *British journal of cancer*, 124(4):686–696, 2021.
- [15] Balázs Acs, Mattias Rantalainen, and Johan Hartman. Artificial intelligence as the next step towards precision pathology. *Journal of internal medicine*, 288(1):62–81, 2020.
- [16] Massimo Salvi, U. Rajendra Acharya, Filippo Molinari, and Kristen M. Meiburger. The impact of pre- and post-image processing techniques on deep learning frameworks: A comprehensive review for digital pathology image analysis. *Computers in Biology and Medicine*, 128:104129, 2021.
- [17] Chetan L. Srinidhi, Ozan Ciga, and Anne L. Martel. Deep neural network models for computational histopathology: A survey. *Medical Image Analysis*, 67:101813, 2021.
- [18] Giovani Lujan, Zaibo Li, and Anil V Parwani. Challenges in implementing a digital pathology workflow in surgical pathology. *Human Pathology Reports*, 29:300673, 2022.
- [19] Yingci Liu and Liron Pantanowitz. Digital pathology: Review of current opportunities and challenges for oral pathologists. *Journal of Oral Pathology & Medicine*, 48(4):263–269, 2019.
- [20] Ana Richelia Jara-Lazaro, Thomas Paulraj Thamboo, Ming Teh, and Puay Hoon Tan. Digital pathology: exploring its applications in diagnostic surgical pathology practice. *Pathology*, 42(6):512–518, 2010.
- [21] Julie Smith, Sys Johnsen, Mette Christa Zeuthen, Lisbeth Koch Thomsen, Niels Marcussen, Stig Hansen, and Charlotte Lerbech Jensen. On the road to digital pathology in denmark—national survey and interviews. *Journal of Digital Imaging*, pages 1–18, 2022.
- [22] Sandhya Sundar, Pratibha Ramani, Herald J Sherlin, Gheena Ranjith, Abilasha Ramasubramani, and Gifrina Jayaraj. Awareness about whole slide imaging and digital pathology among pathologists-cross sectional survey. *Indian Journal of Forensic Medicine & Toxicology*, 14(2), 2020.
- [23] Ali Jasem Buabbas, Tareq Mohammad, Adel K Ayed, Hawraa Mallah, Hamza Al-Shawaf, and Abdulwahed Mohammed Khalfan. Evaluating the success of the tele-pathology system in governmental hospitals in kuwait: an explanatory sequential mixed methods design. *BMC Medical Informatics and Decision Making*, 21(1):1–12, 2021.
- [24] Alexi Baidoshvili, Anca Bucur, Jasper van Leeuwen, Jeroen van der Laak, Philip Kluin, and Paul J van Diest. Evaluating the benefits of digital pathology implementation: time savings in laboratory logistics. *Histopathology*, 73(5):784–794, 2018.
- [25] T Dennis, R. D. Start, and Simon S. Cross. The use of digital imaging, video conferencing, and telepathology in histopathology: a national survey. *Journal of Clinical Pathology*, 58:254–258, 2005.
- [26] Fei Dong, Humayun Irshad, Eun-Yeong Oh, Melinda F Lerwill, Elena F Brachtel, Nicholas C Jones, Nicholas W Knoblauch, Laleh Montaser-Kouhsari, Nicole B Johnson, Luigi KF Rao, et al. Computational pathology to discriminate benign from malignant intraductal proliferations of the breast. *PLoS one*, 9(12):e114885, 2014.
- [27] David F Steiner, Robert MacDonald, Yun Liu, Peter Truszkowski, Jason D Hipp, Christopher Gammage, Florence Thng, Lily Peng, and Martin C Stumpe. Impact of deep learning assistance on the histopathologic review of lymph nodes for metastatic breast cancer. *The American journal of surgical pathology*, 42(12):1636, 2018.
- [28] Lee AD Cooper, Alexis B Carter, Alton B Farris, Fusheng Wang, Jun Kong, David A Gutman, Patrick Widener, Tony C Pan, Sharath R Cholleti, Ashish Sharma, et al. Digital pathology: Data-intensive frontier in medical imaging. *Proceedings of the IEEE*, 100(4):991–1003, 2012.
- [29] Inho Kim, Kyungmin Kang, Youngjae Song, and Tae-Jung Kim. Application of artificial intelligence in pathology: Trends and challenges. *Diagnostics*, 12(11):2794, 2022.
- [30] Esther Abels, Liron Pantanowitz, Famke Aeffner, Mark D Zarella, Jeroen van der Laak, Marilyn M Bui, Venkata NP Vemuri, Anil V Parwani, Jeff Gibbs, Emmanuel Agosto-Arroyo, et al. Computational pathology definitions, best practices, and recommendations for regulatory guidance: a white paper from the digital pathology association. *The Journal of Pathology*, 249(3):286–294, 2019.
- [31] Neeta Kumar, Ruchika Gupta, and Sanjay Gupta. Whole slide imaging (wsi) in pathology: current perspectives and future directions. *Journal of Digital Imaging*, 33(4):1034–1040, 2020.
- [32] Navid Alemi Koohbanani, Balagopal Unnikrishnan, Syed Ali Khurram, Pavitra Krishnaswamy, and Nasir Rajpoot. Self-path: Self-supervision for classification of pathology images with limited annotations. *IEEE Transactions on Medical Imaging*, 40(10):2845–2856, 2021.
- [33] Kaustav Bera, Kurt A Schalper, David L Rimm, Vamsidhar Velcheti, and Anant Madabhushi. Artificial intelligence in digital pathology—new tools for diagnosis and precision oncology. *Nature reviews Clinical oncology*, 16(11):703–715, 2019.
- [34] Muhammad Khalid Khan Niazi, Anil V Parwani, and Metin N Gurcan. Digital pathology and artificial intelligence. *The lancet oncology*, 20(5):e253–e261, 2019.
- [35] Faranak Sobhani, Ruth Robinson, Azam Hamidinekoo, Ioannis Roxanis, Navita Somaiah, and Yinyin Yuan. Artificial intelligence and digital pathology: Opportunities and implications for immunoncology. *Biochimica et Biophysica Acta (BBA)-Reviews on Cancer*, 1875(2):188520, 2021.
- [36] Christophe Klein, Qinghe Zeng, Floriane Arbaretz, Estelle Devèvre, Julien Calderaro, Nicolas Lomenie, and Maria Chiara Maiuri. Artificial intelligence for solid tumour diagnosis in digital pathology. *British Journal of Pharmacology*, 178(21):4291–4315, 2021.

- [37] Heounjeong Go. Digital pathology and artificial intelligence applications in pathology. *Brain Tumor Research and Treatment*, 10(2):76, 2022.
- [38] Jérôme Rony, Soufiane Belharbi, Jose Dolz, Ismail Ben Ayed, Luke McCaffrey, and Eric Granger. Deep weakly-supervised learning methods for classification and localization in histology images: a survey. *arXiv preprint arXiv:1909.03354*, 2019.
- [39] K Abinaya and B Sivakumar. A systematic review: Intellectual detection and prediction of cancer using dl techniques. In *2022 6th International Conference on Trends in Electronics and Informatics (ICOEI)*, pages 1497–1504. IEEE, 2022.
- [40] Mohsin Bilal, Mohammed Nimir, David Snead, Graham S Taylor, and Nasir Rajpoot. Role of ai and digital pathology for colorectal immunoncology. *British Journal of Cancer*, pages 1–9, 2022.
- [41] Lucas Schneider, Sara Laiouar-Pedari, Sara Kuntz, Eva Kriehoff-Henning, Achim Hekler, Jakob N Kather, Timo Gaiser, Stefan Fröhling, and Titus J Brinker. Integration of deep learning-based image analysis and genomic data in cancer pathology: A systematic review. *European Journal of Cancer*, 160:80–91, 2022.
- [42] Yahui Jiang, Meng Yang, Shuhao Wang, Xiangchun Li, and Yan Sun. Emerging role of deep learning-based artificial intelligence in tumor pathology. *Cancer communications*, 40(4):154–166, 2020.
- [43] Cesare Lancellotti, Pierandrea Cancian, Victor Savevski, Soumya Rupa Reddy Kotha, Filippo Frassetto, Paolo Graziano, and Luca Di Tommaso. Artificial intelligence & tissue biomarkers: advantages, risks and perspectives for pathology. *Cells*, 10(4):787, 2021.
- [44] Richard Colling, Helen Pitman, Karin Oien, Nasir Rajpoot, Philip Macklin, CM-Path AI in Histopathology Working Group, Velicia Bachtiar, Richard Booth, Alyson Bryant, Joshua Bull, et al. Artificial intelligence in digital pathology: a roadmap to routine use in clinical practice. *The Journal of pathology*, 249(2):143–150, 2019.
- [45] Vipul Baxi, Robin Edwards, Michael Montalto, and Saurabh Saha. Digital pathology and artificial intelligence in translational medicine and clinical practice. *Modern Pathology*, 35(1):23–32, 2022.
- [46] Taro Sakamoto, Tomoi Furukawa, Kris Lami, Hoa Hoang Ngoc Pham, Wataru Uegami, Kishio Kuroda, Masataka Kawai, Hidenori Sakanashi, Lee Alex Donald Cooper, Andrey Bychkov, et al. A narrative review of digital pathology and artificial intelligence: focusing on lung cancer. *Translational Lung Cancer Research*, 9(5):2255, 2020.
- [47] Jerome Y Cheng, Jacob T Abel, Ulysses GJ Balis, David S McClintock, and Liron Pantanowitz. Challenges in the development, deployment, and regulation of artificial intelligence in anatomic pathology. *The American Journal of Pathology*, 191(10):1684–1692, 2021.
- [48] Romain Brixtel, Sébastien Bougleux, Olivier Lézoray, Yann Caillot, Benoît Lemoine, Mathieu Fontaine, Dalal Nebati, and Arnaud Renouf. Whole slide image quality in digital pathology: review and perspectives. *IEEE Access*, 2022.
- [49] Artem Shmatko, Narmin Ghaffari Laleh, Moritz Gerstung, and Jakob Nikolas Kather. Artificial intelligence in histopathology: enhancing cancer research and clinical oncology. *Nature cancer*, 3(9):1026–1038, 2022.
- [50] Yasmine Makhoulouf, Manuel Salto-Tellez, Jacqueline James, Paul O’Reilly, and Perry Maxwell. General roadmap and core steps for the development of ai tools in digital pathology. *Diagnostics*, 12(5):1272, 2022.
- [51] Yuankai Huo, Ruining Deng, Quan Liu, Agnes B Fogo, and Haichun Yang. Ai applications in renal pathology. *Kidney international*, 99(6):1309–1320, 2021.
- [52] Ahmed Serag, Adrian Ion-Margineanu, Hammad Qureshi, Ryan McMillan, Marie-Judith Saint Martin, Jim Diamond, Paul O’Reilly, and Peter Hamilton. Translational ai and deep learning in diagnostic pathology. *Frontiers in medicine*, 6:185, 2019.
- [53] Alex Ngai Nick Wong, Zebang He, Ka Long Leung, Curtis Chun Kit To, Chun Yin Wong, Sze Chuen Cesar Wong, Jung Sun Yoo, Cheong Kin Ronald Chan, Angela Zaneta Chan, Maribel D Lacambra, et al. Current developments of artificial intelligence in digital pathology and its future clinical applications in gastrointestinal cancers. *Cancers*, 14(15):3780, 2022.
- [54] Manal AlAmir and Manal AlGhamdi. The role of generative adversarial network in medical image analysis: An in-depth survey. *ACM Computing Surveys*, 55(5):1–36, 2022.
- [55] Didem Cifci, Sebastian Foersch, and Jakob Nikolas Kather. Artificial intelligence to identify genetic alterations in conventional histopathology. *The Journal of Pathology*, 257(4):430–444, 2022.
- [56] Sarah Haggenmüller, Roman C Maron, Achim Hekler, Jochen S Utikal, Catarina Barata, Raymond L Barnhill, Helmut Beltraminelli, Carola Berking, Brigid Betz-Stablein, Andreas Blum, et al. Skin cancer classification via convolutional neural networks: systematic review of studies involving human experts. *European Journal of Cancer*, 156:202–216, 2021.
- [57] Margaret Mitchell, Simone Wu, Andrew Zaldivar, Parker Barnes, Lucy Vasserman, Ben Hutchinson, Elena Spitzer, Inioluwa Deborah Raji, and Timnit Gebru. Model cards for model reporting. In *Proceedings of the conference on fairness, accountability, and transparency*, pages 220 – 229, 2019.
- [58] Hongyan Gu, Jingbin Huang, Lauren Hung, and Xiang’Anthony’ Chen. Lessons learned from designing an ai-enabled diagnosis tool for pathologists. *Proceedings of the ACM on Human-Computer Interaction*, 5(CSCW1):1–25, 2021.
- [59] John E Tomaszewski. Overview of the role of artificial intelligence in pathology: the computer as a pathology digital assistant. In *Artificial Intelligence and Deep Learning in Pathology*, pages 237–262. Elsevier, 2021.
- [60] Jia Deng, Wei Dong, Richard Socher, Li-Jia Li, Kai Li, and Li Fei-Fei. Imagenet: A large-scale hierarchical image database. In *IEEE Conference on Computer Vision and Pattern Recognition*, pages 248–255, 2009.
- [61] Geert Litjens, Peter Bandi, Babak Ehteshami Bejnordi, Oscar Geessink, Maschenka Balkenhol, Peter Bult, Altuna Halilovic, Meyke Hermsen, Rob van de Loo, Rob Vogels, Quirine F Manson, Nikolas Stathonikos, Alexi Baidoshvili, Paul van Diest, Carla Wauters, Marcory van Dijk, and Jeroen van der Laak. 1399 h&e-stained sentinel lymph node sections of breast cancer patients: the camelyon dataset. *Gigascience*, 7(6):giy065, 2018.
- [62] Gabriele Campanella, Matthew G Hanna, Luke Geneslaw, Allen Mirafior, Vitor Werneck Krauss Silva, Klaus J Busam, Edi Brogi, Victor E Reuter, David S Klimstra, and Thomas J Fuchs. Clinical-grade computational pathology using weakly supervised deep learning on whole slide images. *Nature medicine*, 25(8):1301–1309, 2019.
- [63] Ming Y Lu, Richard J Chen, and Faisal Mahmood. Semi-supervised breast cancer histology classification using deep multiple instance learning and contrast predictive coding. In *Medical Imaging: Digital Pathology*, volume 11320, page 113200J. International Society for Optics and Photonics, 2020.
- [64] Ming Y Lu, Drew FK Williamson, Tiffany Y Chen, Richard J Chen, Matteo Barbieri, and Faisal Mahmood. Data-efficient and weakly supervised computational pathology on whole-slide images. *Nature Biomedical Engineering*, 5(6):555–570, 2021.
- [65] Richard J Chen, Chengkuan Chen, Yicong Li, Tiffany Y Chen, Andrew D Trister, Rahul G Krishnan, and Faisal Mahmood. Scaling vision transformers to gigapixel images via hierarchical self-supervised learning. In *Proceedings of the IEEE/CVF Conference on Computer Vision and Pattern Recognition*, pages 16144–16155, 2022.
- [66] Ting Chen, Simon Kornblith, Mohammad Norouzi, and Geoffrey Hinton. A simple framework for contrastive learning of visual representations. In *International conference on machine learning*, pages 1597–1607. PMLR, 2020.
- [67] Mathilde Caron, Hugo Touvron, Ishan Misra, Hervé Jégou, Julien Mairal, Piotr Bojanowski, and Armand Joulin. Emerging properties in self-supervised vision transformers. In *Proceedings of the IEEE/CVF International Conference on Computer Vision*, pages 9650–9660, 2021.
- [68] Sarah W Njoroge and James H Nichols. Risk management in the clinical laboratory. *Annals of laboratory medicine*, 34(4):274, 2014.
- [69] Andrew A. Renshaw, Mercy Mena-Allauca, Edwin W. Gould, and S. Joseph Sirintrapun. Synoptic reporting: Evidence-based review and future directions. *JCO Clinical Cancer Informatics*, (2):1–9, 2018. PMID: 30652566.
- [70] Ekkehard Hwer. The oncologist’s guide to synoptic reporting: a primer. *Oncology*, 98(6):396–402, 2020.
- [71] Geert Litjens, Clara I Sánchez, Nadya Timofeeva, Meyke Hermsen, Iris Nagtegaal, Iringo Kovacs, Christina Hulsbergen-Van De Kaa, Peter Bult, Bram Van Ginneken, and Jeroen Van Der Laak. Deep learning as a tool for increased accuracy and efficiency of histopathological diagnosis. *Scientific Reports*, 6:26286, 2016.

- [72] Yun Liu, Timo Kohlberger, Mohammad Norouzi, George E Dahl, Jenny L Smith, Arash Mohtashamian, Niels Olson, Lily H Peng, Jason D Hipp, and Martin C Stumpe. Artificial intelligence-based breast cancer nodal metastasis detection: Insights into the black box for pathologists. *Archives of pathology & laboratory medicine*, 143(7):859–868, 2019.
- [73] Umair Akhtar Hasan Khan, Carolin Stürenberg, Oguzhan Gencoglu, Kevin Sandeman, Timo Heikkinen, Antti Rannikko, and Tuomas Mirtti. Improving prostate cancer detection with breast histopathology images. In *European Congress on Digital Pathology*, pages 91–99. Springer, 2019.
- [74] Javad Noorbakhsh, Saman Farahmand, Sandeep Namburi, Dennis Caruana, David Rimm, Mohammad Soltanieh-ha, Kourosh Zarringhalam, Jeffrey H Chuang, et al. Deep learning-based cross-classifications reveal conserved spatial behaviors within tumor histological images. *Nature communications*, 11(1):1–14, 2020.
- [75] Jason W Wei, Laura J Tafe, Yevgeniy A Linnik, Louis J Vaickus, Naofumi Tomita, and Saeed Hassanpour. Pathologist-level classification of histologic patterns on resected lung adenocarcinoma slides with deep neural networks. *Scientific Reports*, 9(1):1–8, 2019.
- [76] Jocelyn Barker, Assaf Hoogi, Adrien Depeursinge, and Daniel L Rubin. Automated classification of brain tumor type in whole-slide digital pathology images using local representative tiles. *Medical Image Analysis*, 30:60–71, 2016.
- [77] Korsuk Sirinukunwattana, Shan E Ahmed Raza, Yee-Wah Tsang, David RJ Snead, Ian A Cree, and Nasir M Rajpoot. Locality sensitive deep learning for detection and classification of nuclei in routine colon cancer histology images. *IEEE Transactions on Medical Imaging*, 35(5):1196–1206, 2016.
- [78] Bruno Korbar, Andrea M Olofson, Allen P Mirafior, Catherine M Nicka, Matthew A Suriawinata, Lorenzo Torresani, Arief A Suriawinata, and Saeed Hassanpour. Deep learning for classification of colorectal polyps on whole-slide images. *Journal of Pathology Informatics*, 8, 2017.
- [79] Lyndon Chan, Mahdi S Hosseini, and Konstantinos N Plataniotis. A comprehensive analysis of weakly-supervised semantic segmentation in different image domains. *International Journal of Computer Vision*, 129:361–384, 2021.
- [80] Hao Chen, Xiaojuan Qi, Lequan Yu, and Pheng-Ann Heng. Dcan: deep contour-aware networks for accurate gland segmentation. In *IEEE Conference on Computer Vision and Pattern Recognition*, pages 2487–2496, 2016.
- [81] Ramin Nateghi, Habibollah Danyali, and Mohammad-Sadegh Helfroush. A systematic approach for glandular structure segmentation from colon histopathology images. In *Iranian Conference on Electrical Engineering (ICEE)*, pages 1505–1509. IEEE, 2016.
- [82] Chaoyang Yan, Jun Xu, Jiawei Xie, Chengfei Cai, and Haoda Lu. Prior-aware cnn with multi-task learning for colon images analysis. In *IEEE International Symposium on Biomedical Imaging*, pages 254–257. IEEE, 2020.
- [83] Korsuk Sirinukunwattana, David RJ Snead, and Nasir M Rajpoot. A stochastic polygons model for glandular structures in colon histology images. *IEEE Transactions on Medical Imaging*, 34(11):2366–2378, 2015.
- [84] Jon N Marsh, Matthew K Matlock, Satoru Kudose, Ta-Chiang Liu, Thaddeus S Stappenbeck, Joseph P Gaut, and S Joshua Swamidass. Deep learning global glomerulosclerosis in transplant kidney frozen sections. *IEEE Transactions on Medical Imaging*, 37(12):2718–2728, 2018.
- [85] Amin Zadeh Shirazi, Eric Fornaciari, Narjes Sadat Bagherian, Lisa M Ebert, Barbara Koszyca, and Guillermo A Gomez. DeepSurvNet: deep survival convolutional network for brain cancer survival rate classification based on histopathological images. *Medical & Biological Engineering & Computing*, 58(5):1031–1045, 2020.
- [86] Jakob Nikolas Kather, Johannes Krisam, Pornpimol Charoentong, Tom Luedde, Esther Herpel, Cleo-Aron Weis, Timo Gaiser, Alexander Marx, Nektarios A Valous, Dyke Ferber, et al. Predicting survival from colorectal cancer histology slides using deep learning: A retrospective multicenter study. *PLoS medicine*, 16(1):e1002730, 2019.
- [87] Pierre Courtiol, Charles Maussion, Matahi Moarii, Elodie Pronier, Samuel Pilcer, Meriem Sefta, Pierre Manceron, Sylvain Toldo, Mikhail Zaslavskiy, Nolwenn Le Stang, et al. Deep learning-based classification of mesothelioma improves prediction of patient outcome. *Nature medicine*, 25(10):1519–1525, 2019.
- [88] Dmitrii Bychkov, Nina Linder, Riku Turkki, Stig Nordling, Panu E Kovanen, Clare Verrill, Margarita Walliander, Mikael Lundin, Caj Haglund, and Johan Lundin. Deep learning based tissue analysis predicts outcome in colorectal cancer. *Scientific Reports*, 8(1):1–11, 2018.
- [89] Xiangxue Wang, Andrew Janowczyk, Yu Zhou, Rajat Thawani, Pingfu Fu, Kurt Schalper, Vamsidhar Velcheti, and Anant Madabhushi. Prediction of recurrence in early stage non-small cell lung cancer using computer extracted nuclear features from digital h&e images. *Scientific Reports*, 7(1):1–10, 2017.
- [90] Rebecca L. Siegel, Kimberly D. Miller, and Ahmedin Jemal. Cancer statistics, 2020. *CA: A Cancer Journal for Clinicians*, 70(1):7–30, 2020.
- [91] American Cancer Society. What is breast cancer? Available at: <https://www.cancer.org/cancer/breast-cancer/about/what-is-breast-cancer.html> (accessed Jan 22, 2023).
- [92] Connolly Fitzgibbons. Protocol for the examination of resection specimens from patients with ductal carcinoma in situ (dcis) of the breast. *College of American Pathologists*, Jun 2021.
- [93] Kimberly H Allison, M Elizabeth H Hammond, Mitchell Dowsett, Shannon E McKernin, Lisa A Carey, Patrick L Fitzgibbons, Daniel F Hayes, Sunil R Lakhani, Mariana Chavez-MacGregor, Jane Perlmutter, et al. Estrogen and progesterone receptor testing in breast cancer: Asco/cap guideline update. *Journal of Clinical Oncology*, 38(12):1346–1366, 2020.
- [94] Antonio C Wolff, M Elizabeth Hale Hammond, Kimberly H Allison, Brittany E Harvey, Lisa M McShane, and Mitchell Dowsett. Her2 testing in breast cancer: American society of clinical oncology/college of american pathologists clinical practice guideline focused update summary. *Journal of oncology practice*, 14(7):437–441, 2018.
- [95] Mitch Dowsett, Torsten O Nielsen, Roger A'Hern, John Bartlett, R Charles Coombes, Jack Cuzick, Matthew Ellis, N Lynn Henry, Judith C Hugh, Tracy Lively, et al. Assessment of ki67 in breast cancer: recommendations from the international ki67 in breast cancer working group. *Journal of the National Cancer Institute*, 103(22):1656–1664, 2011.
- [96] Megan A Healey, Kelly A Hirko, Andrew H Beck, Laura C Collins, Stuart J Schmitt, A Heather Eliassen, Michelle D Holmes, Rulla M Tamimi, and Aditi Hazra. Assessment of ki67 expression for breast cancer subtype classification and prognosis in the nurses' health study. *Breast cancer research and treatment*, 166(2):613–622, 2017.
- [97] Yun Liu, Krishna Gadepalli, Mohammad Norouzi, George E Dahl, Timo Kohlberger, Aleksey Boyko, Subhashini Venugopalan, Aleksei Timofeev, Philip Q Nelson, Greg S Corrado, et al. Detecting cancer metastases on gigapixel pathology images. *arXiv preprint arXiv:1703.02442*, 2017.
- [98] American Cancer Society. What is prostate cancer? Available at: <https://www.cancer.org/cancer/prostate-cancer/about/what-is-prostate-cancer.html> (accessed Jan 21, 2023).
- [99] Yujiro Ito, Emily A Vertosick, Daniel D Sjoberg, Andrew J Vickers, Hikmat A Al-Ahmadie, Ying-Bei Chen, Anuradha Gopalan, S Joseph Sirintrapun, Satish K Tickoo, James A Eastham, et al. In organ-confined prostate cancer, tumor quantitation not found to aid in prediction of biochemical recurrence. *The American journal of surgical pathology*, 43(8):1061, 2019.
- [100] Jonathan I Epstein. Prognostic significance of tumor volume in radical prostatectomy and needle biopsy specimens. *The Journal of urology*, 186(3):790–797, 2011.
- [101] Laurent Salomon, Olivier Levlre, Aristotelis G Anastasiadis, Jacques Irani, Alexandre De La Taille, Fabien Saint, Dimitri Vordos, Antony Cicco, Andras Hoznek, Dominique Chopin, et al. Prognostic significance of tumor volume after radical prostatectomy: a multivariate analysis of pathological prognostic factors. *European urology*, 43(1):39–44, 2003.
- [102] Thomas A Stamey, John E McNeal, Cheryl M Yemoto, Bronislava M Sigal, and Iain M Johnstone. Biological determinants of cancer progression in men with prostate cancer. *Jama*, 281(15):1395–1400, 1999.
- [103] J Joy Lee, I-Chun Thomas, Rosalie Nolley, Michelle Ferrari, James D Brooks, and John T Leppert. Biologic differences between peripheral and transition zone prostate cancer. *The Prostate*, 75(2):183–190, 2015.
- [104] Strigley Paner. Protocol for the examination of radical prostatectomy specimens from patients with carcinoma of the prostate gland, Nov 2021.
- [105] Jonathan L Wright, Bruce L Dalkin, Lawrence D True, William J Ellis, Janet L Stanford, Paul H Lange, and Daniel W Lin. Positive surgical margins at radical prostatectomy predict prostate cancer specific mortality. *The Journal of urology*, 183(6):2213–2218, 2010.

- [106] Murali Varma. Intraductal carcinoma of the prostate: a guide for the practicing pathologist. *Advances in Anatomic Pathology*, 28(4):276–287, 2021.
- [107] Rodolfo Montironi, Ming Zhou, Cristina Magi-Galluzzi, and Jonathan I Epstein. Features and prognostic significance of intraductal carcinoma of the prostate. *European Urology Oncology*, 1(1):21–28, 2018.
- [108] Ming Zhou. Intraductal carcinoma of the prostate: the whole story. *Pathology*, 45(6):533–539, 2013.
- [109] Ronald J Cohen, Thomas M Wheeler, Helmut Bonkhoff, and Mark A Rubin. A proposal on the identification, histologic reporting, and implications of intraductal prostatic carcinoma. *Archives of pathology & laboratory medicine*, 131(7):1103–1109, 2007.
- [110] Charles C Guo and Jonathan I Epstein. Intraductal carcinoma of the prostate on needle biopsy: histologic features and clinical significance. *Modern pathology*, 19(12):1528–1535, 2006.
- [111] American Cancer Society. Tests to diagnose and stage prostate cancer. Available at: <https://www.cancer.org/cancer/prostate-cancer/detection-diagnosis-staging/how-diagnosed.html> (accessed Jan 21, 2023).
- [112] Charlotte F Kweldam, Mark F Wildhagen, Ewout W Steyerberg, Chris H Bangma, Theodorus H Van Der Kwast, and Geert Jlh Van Leenders. Cribriform growth is highly predictive for postoperative metastasis and disease-specific death in gleason score 7 prostate cancer. *Modern pathology*, 28(3):457–464, 2015.
- [113] Thomas K Lee and Jae Y Ro. Spectrum of cribriform proliferations of the prostate: from benign to malignant. *Archives of Pathology & Laboratory Medicine*, 142(8):938–946, 2018.
- [114] S Emily Bachert, Anthony McDowell Jr, Dava Piecoro, and Lauren Baldwin Branch. Serous tubal intraepithelial carcinoma: a concise review for the practicing pathologist and clinician. *Diagnostics*, 10(2):102, 2020.
- [115] American Cancer Society. What is ovarian cancer? Available at: <https://www.cancer.org/cancer/ovarian-cancer/about/what-is-ovarian-cancer.html> (accessed Jan 21, 2023).
- [116] Shi-Ping Yang, Hui-Luan Su, Xiu-Bei Chen, Li Hua, Jian-Xian Chen, Min Hu, Jian Lei, San-Gang Wu, Juan Zhou, et al. Long-term survival among histological subtypes in advanced epithelial ovarian cancer: population-based study using the surveillance, epidemiology, and end results database. *JMIR Public Health and Surveillance*, 7(11):e25976, 2021.
- [117] Lisa Vermij, Alicia León-Castillo, Naveena Singh, Melanie E Powell, Richard J Edmondson, Catherine Genestie, Pearly Khaw, Jan Pyman, C Meg McLachlin, Prafull Ghatage, et al. p53 immunohistochemistry in endometrial cancer: clinical and molecular correlates in the portec-3 trial. *Modern Pathology*, 35(10):1475–1483, 2022.
- [118] Yu Zhang, Lan Cao, Daniel Nguyen, and Hua Lu. Tp53 mutations in epithelial ovarian cancer. *Translational cancer research*, 5(6):650, 2016.
- [119] Yiping Wang, David Farnell, Hossein Farahani, Mitchell Nursey, Basile Tessier-Cloutier, Steven JM Jones, David G Huntsman, C Blake Gilks, and Ali Bashashati. Classification of epithelial ovarian carcinoma whole-slide pathology images using deep transfer learning. In *Medical Imaging with Deep Learning*, 2020.
- [120] Jevgenij Gamper, Navid Alemi Koochbanani, and Nasir Rajpoot. Multi-task learning in histo-pathology for widely generalizable model. *arXiv preprint arXiv:2005.08645*, 2020.
- [121] National Cancer Institute. Common cancer types. Available at: <https://www.cancer.gov/types/common-cancers#:~:text=Themostcommontypeof,arecombinedforthelist/> (accessed June 10, 2021).
- [122] American Cancer Society. Tests to diagnose and stage prostate cancer. Available at: <https://www.cancer.org/cancer/lung-cancer/about/what-is.html> (accessed Jan 21, 2023).
- [123] Akihiko Yoshizawa, Noriko Motoi, Gregory J Riely, Cami S Sima, William L Gerald, Mark G Kris, Bernard J Park, Valerie W Rusch, and William D Travis. Impact of proposed iaslc/ats/ers classification of lung adenocarcinoma: prognostic subgroups and implications for further revision of staging based on analysis of 514 stage i cases. *Modern pathology*, 24(5):653–664, 2011.
- [124] Andre L Moreira, Paolo SS Ocampo, Yuhe Xia, Hua Zhong, Prudence A Russell, Yuko Minami, Wendy A Cooper, Akihiko Yoshida, Lukas Bubendorf, Mauro Papotti, et al. A grading system for invasive pulmonary adenocarcinoma: a proposal from the international association for the study of lung cancer pathology committee. *Journal of Thoracic Oncology*, 15(10):1599–1610, 2020.
- [125] Yasuhiro Tsutani, Yoshihiro Miyata, Haruhiko Nakayama, Sakae Okumura, Shuji Adachi, Masahiro Yoshimura, and Morihito Okada. Prognostic significance of using solid versus whole tumor size on high-resolution computed tomography for predicting pathologic malignant grade of tumors in clinical stage ia lung adenocarcinoma: a multicenter study. *The Journal of thoracic and cardiovascular surgery*, 143(3):607–612, 2012.
- [126] Tatsuo Maeyashiki, Kenji Suzuki, Aritoshi Hattori, Takeshi Matsunaga, Kazuya Takamochi, and Shiaki Oh. The size of consolidation on thin-section computed tomography is a better predictor of survival than the maximum tumour dimension in resectable lung cancer. *European Journal of Cardio-Thoracic Surgery*, 43(5):915–918, 2013.
- [127] Mahul B Amin, Frederick L Greene, Stephen B Edge, Carolyn C Compton, Jeffrey E Gershenwald, Robert K Brookland, Laura Meyer, Donna M Gress, David R Byrd, and David P Winchester. The eighth edition ajcc cancer staging manual: continuing to build a bridge from a population-based to a more “personalized” approach to cancer staging. *CA: a cancer journal for clinicians*, 67(2):93–99, 2017.
- [128] Liang Wang, Xuejun Dou, Tao Liu, Weiqiang Lu, Yunlei Ma, and Yue Yang. Tumor size and lymph node metastasis are prognostic markers of small cell lung cancer in a chinese population. *Medicine*, 97(31), 2018.
- [129] Jianjun Zhang, Kathryn A Gold, Heather Y Lin, Stephen G Swisher, Yan Xing, J Jack Lee, Edward S Kim, and William N William Jr. Relationship between tumor size and survival in non-small-cell lung cancer (nsccl): an analysis of the surveillance, epidemiology, and end results (seer) registry. *Journal of Thoracic Oncology*, 10(4):682–690, 2015.
- [130] Yina Gao, Yangyang Dong, Yingxu Zhou, Gongyan Chen, Xuan Hong, Qingyuan Zhang, et al. Peripheral tumor location predicts a favorable prognosis in patients with resected small cell lung cancer. *International Journal of Clinical Practice*, 2022, 2022.
- [131] Mahul B Amin, Stephen B Edge, Frederick L Greene, David R Byrd, Robert K Brookland, Mary Kay Washington, Jeffrey E Gershenwald, Carolyn C Compton, Kenneth R Hess, Daniel C Sullivan, et al. *AJCC cancer staging manual*, volume 1024. Springer, 2017.
- [132] American Cancer Society. Colorectal cancer facts & figures 2020–2022. *American Cancer Society*, page 48, 2020.
- [133] American Cancer Society. What is colorectal cancer? Available at: <https://www.cancer.org/cancer/colon-rectal-cancer/about/what-is-colorectal-cancer.html> (accessed Jan 21, 2023).
- [134] Y Nancy You, Karin M Hardiman, Andrea Bafford, Vitaliy Poylin, Todd D Francone, Kurt Davis, Ian M Paquette, Scott R Steele, Daniel L Feingold, et al. The american society of colon and rectal surgeons clinical practice guidelines for the management of rectal cancer. *Diseases of the Colon & Rectum*, 63(9):1191–1222, 2020.
- [135] Seok-Byung Lim, Chang Sik Yu, Se Jin Jang, Tae Won Kim, Jong Hoon Kim, and Jin Cheon Kim. Prognostic significance of lymphovascular invasion in sporadic colorectal cancer. *Diseases of the colon & rectum*, 53(4):377–384, 2010.
- [136] C Santos, A López-Doriga, M Navarro, J Mateo, S Biondo, M Martínez Villacampa, G Soler, X Sanjuan, MJ Paules, B Laquente, et al. Clinicopathological risk factors of stage ii colon cancer: results of a prospective study. *Colorectal Disease*, 15(4):414–422, 2013.
- [137] Dhanwant Gomez, Abed M Zaitoun, Antonella De Rosa, Sina Hossaini, Ian J Beckingham, Adam Brooks, and Iain C Cameron. Critical review of the prognostic significance of pathological variables in patients undergoing resection for colorectal liver metastases. *HPB*, 16(9):836–844, 2014.
- [138] Catherine Liebig, Gustavo Ayala, Jonathan Wilks, Gordana Verstovsek, Hao Liu, Neeti Agarwal, David H Berger, and Daniel Albo. Perineural invasion is an independent predictor of outcome in colorectal cancer. *Journal of clinical oncology*, 27(31):5131, 2009.
- [139] H Ueno, K Shirouzu, Y Eishi, K Yamada, T Kusumi, R Kushima, M Ikegami, A Murata, K Okuno, T Sato, et al. Study group for perineural invasion projected by the japanese society for cancer of the colon and rectum (jsscrr). characterization of perineural invasion as a component of colorectal cancer staging. *Am J Surg Pathol*, 37(10):1542–9, 2013.
- [140] Amanda I Phipps, Noralane M Lindor, Mark A Jenkins, John A Baron, Aung Ko Win, Steven Gallinger, Robert Gryfe, and Polly A Newcomb. Colon and rectal cancer survival by tumor location and microsatellite instability: the colon cancer family registry. *Diseases of the colon and*

- rectum*, 56(8):937, 2013.
- [141] Marco Vacante, Antonio Maria Borzì, Francesco Basile, and Antonio Biondi. Biomarkers in colorectal cancer: Current clinical utility and future perspectives. *World journal of clinical cases*, 6(15):869, 2018.
- [142] Yan Xu, Zhipeng Jia, Liang-Bo Wang, Yuqing Ai, Fang Zhang, Maode Lai, I Eric, and Chao Chang. Large scale tissue histopathology image classification, segmentation, and visualization via deep convolutional activation features. *BMC bioinformatics*, 18(1):1–17, 2017.
- [143] American Cancer Society. What is bladder cancer? Available at: <https://www.cancer.org/cancer/bladder-cancer/about/what-is-bladder-cancer.html> (accessed Jan 25, 2023).
- [144] Venu Chalasani, Joseph L Chin, and Jonathan I Izawa. Histologic variants of urothelial bladder cancer and nonurothelial histology in bladder cancer. *Canadian Urological Association Journal*, 3(6 Suppl 4):S193, 2009.
- [145] Yair Lotan, Amit Gupta, Shahrokh F Shariat, Ganesh S Palapattu, Amnon Vazina, Pierre I Karakiewicz, Patrick J Bastian, Craig G Rogers, Gilad Amiel, Paul Perotte, et al. Lymphovascular invasion is independently associated with overall survival, cause-specific survival, and local and distant recurrence in patients with negative lymph nodes at radical cystectomy. *Journal of clinical oncology*, 23(27):6533–6539, 2005.
- [146] Ann-Christin Woerl, Markus Eckstein, Josephine Geiger, Daniel C Wagner, Tamas Daher, Philipp Stenzel, Aurélie Fernandez, Arndt Hartmann, Michael Wand, Wilfried Roth, et al. Deep learning predicts molecular subtype of muscle-invasive bladder cancer from conventional histopathological slides. *European urology*, 78(2):256–264, 2020.
- [147] American Cancer Society. What is kidney cancer? Available at: <https://www.cancer.org/cancer/kidney-cancer/about/what-is-kidney-cancer> (accessed Jan 25, 2023).
- [148] John R Srigley, M Zhou, R Allan, et al. Protocol for the examination of resection specimens from patients with invasive carcinoma of renal tubular origin. *The College of American Pathologists (CAP) Cancer Protocols*, v4, 1(0), 2020.
- [149] Stephen M Bonsib. Renal lymphatics, and lymphatic involvement in sinus vein invasive (pt3b) clear cell renal cell carcinoma: a study of 40 cases. *Modern pathology*, 19(5):746–753, 2006.
- [150] Valdair F Muglia and Adilson Prando. Renal cell carcinoma: histological classification and correlation with imaging findings. *Radiologia brasileira*, 48:166–174, 2015.
- [151] Shruti Kannan, Laura A Morgan, Benjamin Liang, McKenzie G Cheung, Christopher Q Lin, Dan Mun, Ralph G Nader, Mostafa E Belghasem, Joel M Henderson, Jean M Francis, et al. Segmentation of glomeruli within trichrome images using deep learning. *Kidney international reports*, 4(7):955–962, 2019.
- [152] Meyke Hermsen, Thomas de Bel, Marjolijn Den Boer, Eric J Steenbergen, Jesper Kers, Sandrine Florquin, Joris JTH Roelofs, Mark D Stegall, Mariam P Alexander, Byron H Smith, et al. Deep learning–based histopathologic assessment of kidney tissue. *Journal of the American Society of Nephrology*, 30(10):1968–1979, 2019.
- [153] Edmund A Gehan and Michael D Walker. Prognostic factors for patients with brain tumors. *National Cancer Inst Monograph*, 46:189–195, 1977.
- [154] Yao Li, Zuo-Xin Zhang, Guo-Hao Huang, Yan Xiang, Lin Yang, Yu-Chun Pei, Wei Yang, and Sheng-Qing Lv. A systematic review of multifocal and multicentric glioblastoma. *Journal of Clinical Neuroscience*, 83:71–76, 2021.
- [155] American Cancer Society. Brain tumors – classifications, symptoms, diagnosis and treatments. Available at: <https://www.aans.org/en/Patients/Neurosurgical-Conditions-and-Treatments/Brain-Tumors> (accessed Jan 30, 2023).
- [156] David N Louis, Arie Perry, Pieter Wesseling, Daniel J Brat, Ian A Cree, Dominique Figarella-Branger, Cynthia Hawkins, HK Ng, Stefan M Pfister, Guido Reifenberger, et al. The 2021 who classification of tumors of the central nervous system: a summary. *Neuro-oncology*, 23(8):1231–1251, 2021.
- [157] WHO Classification of Tumours Editorial Board. *Central Nervous System Tumours*. World Health Organization, 2021.
- [158] Canadian Cancer Society. Survival statistics for brain and spinal cord tumours. Available at: <https://www.cancer.ca/en/cancer-information/cancer-type/brain-spinal/prognosis-and-survival/survival-statistics/?region=on#:~:text=InCanada,the5-year,surviveatleast5years.> (accessed June 10, 2021).
- [159] World Health Organization. Cancer. Available at: <https://www.who.int/news-room/fact-sheets/detail/cancer> (accessed June 10, 2021).
- [160] Haeryoung Kim, Mi Jang, and Young Nyun Park. Histopathological variants of hepatocellular carcinomas: an update according to the 5th edition of the who classification of digestive system tumors. *Journal of Liver Cancer*, 20(1):17–24, 2020.
- [161] Gregory Y Lauwers, Benoit Terris, Ulysses J Balis, Kenneth P Batts, Jean-Marc Regimbeau, Yuchiao Chang, Fiona Graeme-Cook, Hirohiko Yamabe, Iwao Ikai, Karen R Cleary, et al. Prognostic histologic indicators of curatively resected hepatocellular carcinomas: a multi-institutional analysis of 425 patients with definition of a histologic prognostic index. *The American journal of surgical pathology*, 26(1):25–34, 2002.
- [162] Gaya Spolverato, Yuhree Kim, Sorin Alexandrescu, Irinel Popescu, Hugo P Marques, Luca Aldrighetti, T Clark Gamblin, John Miura, Shishir K Maithel, Malcolm H Squires, et al. Is hepatic resection for large or multifocal intrahepatic cholangiocarcinoma justified? results from a multi-institutional collaboration. *Annals of surgical oncology*, 22:2218–2225, 2015.
- [163] Ian R Wanless et al. Terminology of nodular hepatocellular lesions. *Hepatology*, 22(3):983–993, 1995.
- [164] Sebastiao N Martins-Filho, Caterina Paiva, Raymundo Soares Azevedo, and Venancio Avancini Ferreira Alves. Histological grading of hepatocellular carcinoma—a systematic review of literature. *Frontiers in medicine*, 4:193, 2017.
- [165] American Cancer Society. Lymph nodes and cancer. Available at: <https://www.cancer.org/treatment/understanding-your-diagnosis/lymph-nodes-and-cancer.html> (accessed Jan 25, 2023).
- [166] Zhihua Wang, Lequan Yu, Xin Ding, Xuehong Liao, and Liansheng Wang. Lymph node metastasis prediction from whole slide images with transformer-guided multi-instance learning and knowledge transfer. *IEEE Transactions on Medical Imaging*, 2022.
- [167] Mahdi S Hosseini, Lyndon Chan, Gabriel Tse, Michael Tang, Jun Deng, Sajad Norouzi, Corwyn Rowsell, Konstantinos N Plataniotis, and Savvas Damaskinos. Atlas of digital pathology: A generalized hierarchical histological tissue type-annotated database for deep learning. In *IEEE Conference on Computer Vision and Pattern Recognition*, pages 11747–11756, 2019.
- [168] Navid Alemi Koohbanani, Mostafa Jahanifar, Neda Zamani Tajadin, and Nasir Rajpoot. Nuclick: a deep learning framework for interactive segmentation of microscopic images. *Medical Image Analysis*, 65:101771, 2020.
- [169] Ruqayya Awan, Korsuk Sirinukunwattana, David Epstein, Samuel Jeffrey, Uvais Qidwai, Zia Aftab, Imaad Mujeeb, David Snead, and Nasir Rajpoot. Glandular morphometrics for objective grading of colorectal adenocarcinoma histology images. *Scientific Reports*, 7(1):1–12, 2017.
- [170] Wenyan Li, Jiayun Li, Zichen Wang, Jennifer Polson, Anthony E Sisk, Dipti P Sajed, William Speier, and Corey W Arnold. Pathal: An active learning framework for histopathology image analysis. *IEEE Transactions on Medical Imaging*, 41(5):1176–1187, 2021.
- [171] Farzad Ghaznavi, Andrew Evans, Anant Madabhushi, and Michael Feldman. Digital imaging in pathology: whole-slide imaging and beyond. *Annual Review of Pathology: Mechanisms of Disease*, 8:331–359, 2013.
- [172] Julianna D Ianni, Rajath E Soans, Sivaramkrishnan Sankarapandian, Ramachandra Vikas Chamathi, Devi Ayyagari, Thomas G Olsen, Michael J Bonham, Coleman C Stavish, Kiran Motaparthi, Clay J Cockerell, et al. Tailored for real-world: a whole slide image classification system validated on uncurated multi-site data emulating the prospective pathology workload. *Scientific Reports*, 10(1):1–12, 2020.
- [173] Geoffrey Rolls. *101 Steps to Better Histology - a Practical Guide to Good Histology Practice*. Leica Biosystems, 2016.
- [174] S. Kim Suvarna, Christopher Layton, and John D. Bancroft. *Bancroft's theory and practice of histological techniques*. Elsevier, 8 edition, 2019.
- [175] Stephen R. Peters. *A Practical guide to Frozen Section Technique*. SPRINGER, 2016.
- [176] Yukako Yagi. Color standardization and optimization in whole slide imaging. In *Diagnostic pathology*, volume 6, pages 1–12. Springer, 2011.
- [177] Babak Ehteshami Bejnordi, Geert Litjens, Nadya Timofeeva, Irene Otte-Höller, André Homeyer, Nico Karssemeijer, and Jeroen AWM van der Laak. Stain specific standardization of whole-slide histopathological images. *IEEE Transactions on Medical Imaging*, 35(2):404–415, 2015.
- [178] Babak Ehteshami Bejnordi, Nadya Timofeeva, Irene Otte-Höller, Nico

- Karssemeijer, and Jeroen AWM van der Laak. Quantitative analysis of stain variability in histology slides and an algorithm for standardization. In *Medical Imaging: Digital Pathology*, volume 9041, page 904108. International Society for Optics and Photonics, 2014.
- [179] Daisuke Komura and Shumpei Ishikawa. Machine learning methods for histopathological image analysis. *Computational and structural biotechnology journal*, 16:34–42, 2018.
- [180] Mark D Zarella, Douglas Bowman, Famke Aeffner, Navid Farahani, Albert Xthona, Syeda Fatima Absar, Anil Parwani, Marilyn Bui, and Douglas J Hartman. A practical guide to whole slide imaging: a white paper from the digital pathology association. *Archives of pathology & laboratory medicine*, 143(2):222–234, 2019.
- [181] Liron Pantanowitz. Digital images and the future of digital pathology. *Journal of Pathology Informatics*, 1, 2010.
- [182] Liron Pantanowitz, Ashish Sharma, Alexis B Carter, Tahsin Kurc, Alan Sussman, and Joel Saltz. Twenty years of digital pathology: an overview of the road travelled, what is on the horizon, and the emergence of vendor-neutral archives. *Journal of pathology informatics*, 9, 2018.
- [183] Md Shakhawat Hossain, Toyama Nakamura, Fumikazu Kimura, Yukako Yagi, and Masahiro Yamaguchi. Practical image quality evaluation for whole slide imaging scanner. In *Biomedical Imaging and Sensing Conference*, volume 10711, page 107111S. International Society for Optics and Photonics, 2018.
- [184] Kazuhiro Tabata, Naohiro Uraoka, Jamal Benhamida, Matthew G Hanna, Sahussapont Joseph Sirintrapun, Brandon D Gallas, Qi Gong, Rania G Aly, Katsura Emoto, Kant M Matsuda, et al. Validation of mitotic cell quantification via microscopy and multiple whole-slide scanners. *Diagnostic pathology*, 14(1):1–9, 2019.
- [185] Wei-Chung Cheng, Firdous Saleheen, and Aldo Badano. Assessing color performance of whole-slide imaging scanners for digital pathology. *Color Research & Application*, 44(3):322–334, 2019.
- [186] Paul Lemaillet, Kazuyo Takeda, Andrew C Lamont, and Anant Agrawal. Colorimetric uncertainty estimation for the performance assessment of whole slide imaging scanners. *Journal of Medical Imaging*, 8(5):057501, 2021.
- [187] M Indu, R Rathy, and MP Binu. “slide less pathology”: Fairy tale or reality? *Journal of oral and maxillofacial pathology: JOMFP*, 20(2):284, 2016.
- [188] Markus D Herrmann, David A Clunie, Andriy Fedorov, Sean W Doyle, Steven Pieper, Veronica Klepeis, Long P Le, George L Mutter, David S Milstone, Thomas J Schultz, et al. Implementing the dicom standard for digital pathology. *Journal of Pathology Informatics*, 9, 2018.
- [189] Tiago Marques Godinho, Rui Lebre, Luís Bastião Silva, and Carlos Costa. An efficient architecture to support digital pathology in standard medical imaging repositories. *Journal of biomedical informatics*, 71:190–197, 2017.
- [190] David A Clunie. Dicom format and protocol standardization—a core requirement for digital pathology success. *Toxicologic Pathology*, 49(4):738–749, 2021.
- [191] Fusheng Wang, Tae W Oh, Cristobal Vergara-Niedermayr, Tahsin Kurc, and Joel Saltz. Managing and querying whole slide images. In *Medical Imaging 2012: Advanced PACS-Based Imaging Informatics and Therapeutic Applications*, volume 8319, pages 137–148. SPIE, 2012.
- [192] Daniel E Lopez Barron, Dig Vijay Kumar Yarlagadda, Praveen Rao, Osama Tawfik, and Deepthi Rao. Scalable storage of whole slide images and fast retrieval of tiles using apache spark. In *Medical Imaging: Digital Pathology*, volume 10581, page 1058113. International Society for Optics and Photonics, 2018.
- [193] Rajendra Singh, Lauren Chubb, Liron Pantanowitz, and Anil Parwani. Standardization in digital pathology: Supplement 145 of the dicom standards. *Journal of Pathology Informatics*, 2, 2011.
- [194] Neel Kanwal, Fernando Pérez-Bueno, Arne Schmidt, Kjersti Egan, and Rafael Molina. The devil is in the details: Whole slide image acquisition and processing for artifacts detection, color variation, and data augmentation: A review. *IEEE Access*, 10:58821–58844, 2022.
- [195] Gabriele Campanella, Arjun R Rajanna, Lorraine Corsale, Peter J Schüffler, Yukako Yagi, and Thomas J Fuchs. Towards machine learned quality control: A benchmark for sharpness quantification in digital pathology. *Computerized Medical Imaging and Graphics*, 65:142–151, 2018.
- [196] Zhongling Wang, Mahdi S. Hosseini, Adyn Miles, Konstantinos N. Plataniotis, and Zhou Wang. Focuslitenn: High efficiency focus quality assessment for digital pathology. In Anne L Martel, Purang Abolmaesumi, Danail Stoyanov, Diana Mateus, and Maria A. Zuluaga, editors, *Medical Image Computing and Computer-Assisted Intervention – MICCAI*, volume 12265 of *Lecture Notes in Computer Science*, page 403–413. Springer, 2020.
- [197] Simon Cross, Peter Furness, Laszlo Igali, David Snead, and Darren Treanor. Best practice recommendations for implementing digital pathology. Technical Report G162, The Royal College of Pathologists, 4th Floor 21 Prescott Street, London, United Kingdom E1 8BB, September 2018.
- [198] Péter Bándi, Maschenka Balkenhol, Bram van Ginneken, Jeroen van der Laak, and Geert Litjens. Resolution-agnostic tissue segmentation in whole-slide histopathology images with convolutional neural networks. *PeerJ*, 7:e8242, 2019.
- [199] David Tellez, Geert Litjens, Péter Bándi, Wouter Bulten, John-Melle Bokhorst, Francesco Ciompi, and Jeroen Van Der Laak. Quantifying the effects of data augmentation and stain color normalization in convolutional neural networks for computational pathology. *Medical Image Analysis*, 58:101544, 2019.
- [200] Sebastian Otálora, Manfredo Atzori, Vincent Andrearczyk, Amjad Khan, and Henning Müller. Staining invariant features for improving generalization of deep convolutional neural networks in computational pathology. *Frontiers in Bioengineering and Biotechnology*, page 198, 2019.
- [201] Savannah R. Duenweg, Samuel A. Bobholz, Allison K. Lowman, Margaret A. Stebbins, Aleksandra Winiarz, Biprojit Nath, Fitzgerald Kyereme, Kenneth A. Iczkowski, and Peter S. LaViolette. Whole slide imaging (wsi) scanner differences influence optical and computed properties of digitized prostate cancer histology. *Journal of Pathology Informatics*, 14:100321, 2023.
- [202] Adnan Mujahid Khan, Nasir Rajpoot, Darren Treanor, and Derek Magee. A nonlinear mapping approach to stain normalization in digital histopathology images using image-specific color deconvolution. *IEEE Transactions on Biomedical Engineering*, 61(6):1729–1738, 2014.
- [203] Farhad Ghazvinian Zanjani, Svitlana Zinger, Babak E Bejnordi, Jeroen AWM van der Laak, et al. Histopathology stain-color normalization using deep generative models. In *1st Conference on Medical Imaging with Deep Learning (MIDL)*, pages 1–11, 2018.
- [204] Amit Sethi, Lingdao Sha, Abhishek Ramnath Vahadane, Ryan J Deaton, Neeraj Kumar, Virgilia Macias, and Peter H Gann. Empirical comparison of color normalization methods for epithelial-stromal classification in h and e images. *Journal of Pathology Informatics*, 7, 2016.
- [205] Rodrigo Escobar Diaz Guerrero and José Luís Oliveira. Improvements in lymphocytes detection using deep learning with a preprocessing stage. pages 178–182, 2021.
- [206] Rikiya Yamashita, Jin Long, Snikitha Banda, Jeanne Shen, and Daniel L Rubin. Learning domain-agnostic visual representation for computational pathology using medically-irrelevant style transfer augmentation. *IEEE Transactions on Medical Imaging*, 40(12):3945–3954, 2021.
- [207] Abhishek Vahadane, B Atheeth, and Shantanu Majumdar. Dual encoder attention u-net for nuclei segmentation. pages 3205–3208, 2021.
- [208] Ida Arvidsson, Niels Christian Overgaard, Kalle Åström, and Anders Heyden. Comparison of different augmentation techniques for improved generalization performance for gleason grading. In *IEEE International Symposium on Biomedical Imaging*, pages 923–927. IEEE, 2019.
- [209] M Tarek Shaban, Christoph Baur, Nassir Navab, and Shadi Albarqouni. Staining: Stain style transfer for digital histological images. In *IEEE International Symposium on Biomedical Imaging*, pages 953–956. IEEE, 2019.
- [210] Dwarikanath Mahapatra, Behzad Bozorgtabar, Jean-Philippe Thiran, and Ling Shao. Structure preserving stain normalization of histopathology images using self supervised semantic guidance. In *International Conference on Medical Image Computing and Computer-Assisted Intervention*, pages 309–319. Springer, 2020.
- [211] Shahid Mehmood, Taher M Ghazal, Muhammad Adnan Khan, Muhammad Zubair, Muhammad Tahir Naseem, Tauqeer Faiz, and Munir Ahmad. Malignancy detection in lung and colon histopathology images using transfer learning with class selective image processing. *IEEE Access*, 10:25657–25668, 2022.
- [212] David Tellez, Geert Litjens, Jeroen van der Laak, and Francesco Ciompi. Neural image compression for gigapixel histopathology image analysis. *IEEE Transactions on Pattern Analysis and Machine Intelligence*, 43(2):567–578, 2019.

- [213] Rui Yan, Fei Ren, Zihao Wang, Lihua Wang, Tong Zhang, Yudong Liu, Xiaosong Rao, Chunhou Zheng, and Fa Zhang. Breast cancer histopathological image classification using a hybrid deep neural network. *Methods*, 173:52–60, 2020.
- [214] Shidan Wang, Ruichen Rong, Donghan M Yang, Junya Fujimoto, Shirley Yan, Ling Cai, Lin Yang, Danni Luo, Carmen Behrens, Edwin R Parra, et al. Computational staining of pathology images to study the tumor microenvironment in lung cancer. *Cancer research*, 80(10):2056–2066, 2020.
- [215] Yiyang Lin, Bowei Zeng, Yifeng Wang, Yang Chen, Zijie Fang, Jian Zhang, Xiangyang Ji, Haoqian Wang, and Yongbing Zhang. Unpaired multi-domain stain transfer for kidney histopathological images. 2022.
- [216] LESTERTHEINVESTOR. High power h&e stained image of a parotid sclerosing polycystic adenoma, 2019. License: CC BY-SA 4.0.
- [217] Mikael Häggström. Chromogenic immunohistochemistry for calponin in sclerosing adenosis, 2021. License: CC0.
- [218] Kent Christensen, Matthew Velkey, Lloyd M. Stoolman, Laura Hessler, and Diedra Mosley-Brower. Michigan histology and virtual microscopy learning resources - virtual slide list. License: CC BY-NC-SA 3.0.
- [219] Nephron. Very high magnification micrograph of the cerebellum (cerebellar cortex). bielschowsky stain., 2010. License: CC BY-SA 3.0.
- [220] Ed Uthman. Gastric amyloidosis (congo red stain), 2009. License: CC BY 2.0.
- [221] Microrao. Gram positive cocci and gram negative bacilli, 2018. License: CC BY-SA 4.0.
- [222] Andresja3. Nissl cerebello ampliado, 2011. License: CC BY-SA 3.0.
- [223] Jerry Wei, Arief Suriawinata, Bing Ren, Xiaoying Liu, Mikhail Lisovsky, Louis Vaickus, Charles Brown, Michael Baker, Mustafa Nasir-Moin, Naofumi Tomita, et al. Learn like a pathologist: curriculum learning by annotator agreement for histopathology image classification. In *IEEE/CVF Conference on Computer Vision*, pages 2473–2483, 2021.
- [224] Marc D Kohli, Ronald M Summers, and J Raymond Geis. Medical image data and datasets in the era of machine learning—whitepaper from the 2016 c-mimi meeting dataset session. *Journal of digital imaging*, 30(4):392–399, 2017.
- [225] Noorul Wahab, Asifullah Khan, and Yeon Soo Lee. Two-phase deep convolutional neural network for reducing class skewness in histopathological images based breast cancer detection. *Computers in Biology and Medicine*, 85:86–97, 2017.
- [226] Angel Cruz-Roa, Hannah Gilmore, Ajay Basavanahally, Michael Feldman, Shridar Ganesan, Natalie Shih, John Tomaszewski, Anant Madabhushi, and Fabio González. High-throughput adaptive sampling for whole-slide histopathology image analysis (hashi) via convolutional neural networks: Application to invasive breast cancer detection. *PLoS one*, 13(5):e0196828, 2018.
- [227] Guilherme Aresta, Teresa Araújo, Scotty Kwok, Sai Saketh Chennamsetty, Mohammed Safwan, Varghese Alex, Bahram Marami, Marcel Prastawa, Monica Chan, Michael Donovan, et al. Bach: Grand challenge on breast cancer histology images. *Medical Image Analysis*, 56:122–139, 2019.
- [228] Oliver Lester Saldanha, Philip Quirke, Nicholas P West, Jacqueline A James, Maurice B Loughrey, Heike I Grabsch, Manuel Salto-Tellez, Elizabeth Alwers, Didem Cifci, Narmin Ghaffari Laleh, et al. Swarm learning for decentralized artificial intelligence in cancer histopathology. *Nature Medicine*, pages 1–8, 2022.
- [229] Martin J Willeminck, Wojciech A Koszek, Cailin Hardell, Jie Wu, Dominik Fleischmann, Hugh Harvey, Les R Folio, Ronald M Summers, Daniel L Rubin, and Matthew P Lungren. Preparing medical imaging data for machine learning. *Radiology*, 295(1):4–15, 2020.
- [230] Sharib Ali, Nasullah Khalid Alham, Clare Verrill, and Jens Rittscher. Ink removal from histopathology whole slide images by combining classification, detection and image generation models. In *IEEE International Symposium on Biomedical Imaging*, pages 928–932. IEEE, 2019.
- [231] Osamu Iizuka, Fahdi Kanavati, Kei Kato, Michael Rambeau, Koji Arihiro, and Masayuki Tsuneki. Deep learning models for histopathological classification of gastric and colonic epithelial tumours. *Scientific Reports*, 10(1):1–11, 2020.
- [232] J. Deng, W. Dong, R. Socher, L.-J. Li, K. Li, and L. Fei-Fei. ImageNet: A Large-Scale Hierarchical Image Database. In *CVPR09*, 2009.
- [233] Fabio A Spanhol, Luiz S Oliveira, Caroline Petitjean, and Laurent Heutte. A dataset for breast cancer histopathological image classification. *IEEE Transactions on Biomedical Engineering*, 63(7):1455–1462, 2015.
- [234] Dalal Bardou, Kun Zhang, and Sayed Mohammad Ahmad. Classification of breast cancer based on histology images using convolutional neural networks. *IEEE Access*, 6:24680–24693, 2018.
- [235] Neslihan Bayramoglu, Juho Kannala, and Janne Heikkilä. Deep learning for magnification independent breast cancer histopathology image classification. In *International Conference on Pattern Recognition*, pages 2440–2445. IEEE, 2016.
- [236] Xia Li, Xi Shen, Yongxia Zhou, Xiuhui Wang, and Tie-Qiang Li. Classification of breast cancer histopathological images using interleaved densenet with senet (idsnet). *PLoS one*, 15(5):e0232127, 2020.
- [237] Douglas Joseph Hartman, Jeroen AWM Van Der Laak, Metin N Gurcan, and Liron Pantanowitz. Value of public challenges for the development of pathology deep learning algorithms. *Journal of Pathology Informatics*, 11, 2020.
- [238] Babak Ehteshami Bejnordi, Mitko Veta, Paul Johannes Van Diest, Bram Van Ginneken, Nico Karssemeijer, Geert Litjens, Jeroen AWM Van Der Laak, Meyke Hermesen, Quirine F Manson, Maschenka Balkenhol, et al. Diagnostic assessment of deep learning algorithms for detection of lymph node metastases in women with breast cancer. *JAMA network open*, 318(22):2199–2210, 2017.
- [239] Péter Bándi, Oscar Geessink, Quirine Manson, Marcory Van Dijk, Maschenka Balkenhol, Meyke Hermesen, Babak Ehteshami Bejnordi, Byungjae Lee, Kyunghyun Paeng, Aoxiao Zhong, Quanzheng Li, Farhad Ghazvinian Zanjani, Svitlana Zinger, Keisuke Fukuta, Daisuke Komura, Vlado Ovtcharov, Shenghua Cheng, Shaoqun Zeng, Jeppe Thagaard, Anders B. Dahl, Huangjing Lin, Hao Chen, Ludwig Jacobsson, Martin Hedlund, Melih Çetin, Eren Halıcı, Hunter Jackson, Richard Chen, Fabian Both, Jörg Franke, Heidi Küsters-Vandeveldel, Willem Vreuls, Peter Bult, Bram van Ginneken, Jeroen van der Laak, and Geert Litjens. From detection of individual metastases to classification of lymph node status at the patient level: The camelyon17 challenge. *IEEE Transactions on Medical Imaging*, 38(2):550–560, 2019.
- [240] Korsuk Sirinukunwattana, Josien PW Pluim, Hao Chen, Xiaojuan Qi, Pheng-Ann Heng, Yun Bo Guo, Li Yang Wang, Bogdan J Matuszewski, Elia Bruni, Urko Sanchez, et al. Gland segmentation in colon histology images: The glas challenge contest. *Medical Image Analysis*, 35:489–502, 2017.
- [241] Le Hou, Vu Nguyen, Ariel B Kanevsky, Dimitris Samaras, Tahsin M Kurc, Tianhao Zhao, Rajarsi R Gupta, Yi Gao, Wenjin Chen, David Foran, et al. Sparse autoencoder for unsupervised nucleus detection and representation in histopathology images. *Pattern Recognition Letters*, 86:188–200, 2019.
- [242] Robert L Grossman, Allison P Heath, Vincent Ferretti, Harold E Varanus, Douglas R Lowy, Warren A Kibbe, and Louis M Staudt. Toward a shared vision for cancer genomic data. *New England Journal of Medicine*, 375(12):1109–1112, 2016.
- [243] Kyung-Ok Cho, Sung Hak Lee, and Hyun-Jong Jang. Feasibility of fully automated classification of whole slide images based on deep learning. *The Korean Journal of Physiology & Pharmacology*, 24(1):89–99, 2020.
- [244] Le Hou, Rajarsi Gupta, John S Van Arnam, Yuwei Zhang, Kaustubh Sivalenka, Dimitris Samaras, Tahsin M Kurc, and Joel H Saltz. Dataset of segmented nuclei in hematoxylin and eosin stained histopathology images of ten cancer types. *Scientific data*, 7(1):1–12, 2020.
- [245] Pooya Mobadersany, Safoora Yousefi, Mohamed Amgad, David A Gutmán, Jill S Barnholtz-Sloan, José E Velázquez Vega, Daniel J Brat, and Lee AD Cooper. Predicting cancer outcomes from histology and genomics using convolutional networks. *National Academy of Sciences*, 115(13):E2970–E2979, 2018.
- [246] Will Fischer, Sanketh S Moudgalya, Judith D Cohn, Nga TT Nguyen, and Garrett T Kenyon. Sparse coding of pathology slides compared to transfer learning with deep neural networks. *BMC bioinformatics*, 19(18):9–17, 2018.
- [247] Arkadiusz Gertych, Zaneta Swiderska-Chadaj, Zhaoxuan Ma, Tomasz Markiewicz, Szczepan Cierniak, Hootan Salemi, Samuel Guzman, Ann E Walts, Beatrice S Knudsen, et al. Convolutional neural networks can accurately distinguish four histologic growth patterns of lung adenocarcinoma in digital slides. *Scientific Reports*, 9(1):1–12, 2019.
- [248] Keisuke Nakagawa, Lama Moukheiber, Leo A. Celi, Malhar Patel, Faisal Mahmood, Dibson Gondim, Michael Hogarth, and Richard Levenson. Ai in pathology: What could possibly go wrong? *Seminars in Diagnostic Pathology*, 40(2):100–108, 2023. Artificial Intelligence

- (AI), machine learning (ML) and digital pathology integration are the next major chapter in our diagnostic pathology and laboratory medicine arena.
- [249] Chhavi Chauhan and Rama Gullapalli. Ethics of ai in pathology: Current paradigms and emerging issues. *The American journal of pathology*, 191(10):1673–1683, 2021.
- [250] Zeyu Wang, Klint Qinami, Ioannis Christos Karakozis, Kyle Genova, Prem Nair, Kenji Hata, and Olga Russakovsky. Towards fairness in visual recognition: Effective strategies for bias mitigation. In *Proceedings of the IEEE/CVF Conference on Computer Vision and Pattern Recognition (CVPR)*, June 2020.
- [251] Tian Xu, Jennifer White, Sinan Kalkan, and Hatice Gunes. Investigating bias and fairness in facial expression recognition. In Adrien Bartoli and Andrea Fusiello, editors, *Computer Vision – ECCV 2020 Workshops*, pages 506–523, Cham, 2020. Springer International Publishing.
- [252] Simone Fabbrizzi, Symeon Papadopoulos, Eirini Ntoutsis, and Ioannis Kompatsiaris. A survey on bias in visual datasets. *Computer Vision and Image Understanding*, 223:103552, 2022.
- [253] Markos Georgopoulos, Yannis Panagakis, and Maja Pantic. Investigating bias in deep face analysis: The kanface dataset and empirical study. *Image and Vision Computing*, 102:103954, 2020.
- [254] Ninareh Mehrabi, Fred Morstatter, Nripsuta Saxena, Kristina Lerman, and Aram Galstyan. A survey on bias and fairness in machine learning. *ACM Comput. Surv.*, 54(6), jul 2021.
- [255] Taher Dehkharghanian, Azam Asilian Bidgoli, Abtin Riasatian, Pooria Mazaheri, Clinton J. Campbell, Liron Pantanowitz, H. R. Tizhoosh, and Shahryar Rahnamayan. Biased data, biased ai: Deep networks predict the acquisition site of tcga images. *Diagnostic Pathology*, 18(67), May 2023.
- [256] Frederick M. Howard, James Dolezal, Sara Kochanny, Jefree Schulte, Heather Chen, Lara Heij, Dezheng Huo, Rita Nanda, Olufunmilayo I. Olopade, Jakob N. Kather, and et al. The impact of site-specific digital histology signatures on deep learning model accuracy and bias. *Nature Communications*, 12(1), 2021.
- [257] Kevin Faust, Sudarshan Bala, Randy Van Ommeren, Alessia Portante, Raniah Al Qawahmed, Ugljesa Djuric, and Phedias Diamandis. Intelligent feature engineering and ontological mapping of brain tumour histomorphologies by deep learning. *Nature Machine Intelligence*, 1(7):316–321, 2019.
- [258] Kun-Hsing Yu, Ce Zhang, Gerald J Berry, Russ B Altman, Christopher Ré, Daniel L Rubin, and Michael Snyder. Predicting non-small cell lung cancer prognosis by fully automated microscopic pathology image features. *Nature communications*, 7(1):1–10, 2016.
- [259] Akash Parvatikar, Om Choudhary, Arvind Ramanathan, Olga Navolotkskaia, Gloria Carter, Akif Burak Tosun, Jeffrey L. Fine, and S. Chakra Chennubhotla. Modeling histological patterns for differential diagnosis of atypical breast lesions. In *Medical Image Computing and Computer Assisted Intervention – MICCAI*, volume 12265 of *Lecture Notes in Computer Science*, pages 550–560. Springer, 2020.
- [260] Peter Naylor, Marick Laé, Fabien Reyat, and Thomas Walter. Segmentation of nuclei in histopathology images by deep regression of the distance map. *IEEE Transactions on Medical Imaging*, 38(2):448–459, 2018.
- [261] Breast Cancer Surveillance Consortium. Available at: <https://www.bcsr-research.org/> (accessed June 10, 2021).
- [262] Jerry Wei, Arief Suriawinata, Bing Ren, Xiaoying Liu, Mikhail Lisovsky, Louis Vaickus, Charles Brown, Michael Baker, Naofumi Tomita, Lorenzo Torresani, et al. A petri dish for histopathology image analysis. In *International Conference on Artificial Intelligence in Medicine*, pages 11–24. Springer, 2021.
- [263] Teresa Araújo, Guilherme Aresta, Eduardo Castro, José Rouco, Paulo Aguiar, Catarina Eloy, António Polónia, and Aurélio Campilho. Classification of breast cancer histology images using convolutional neural networks. *PLoS one*, 12(6):e0177544, 2017.
- [264] Rui Yan, Fei Ren, Zihao Wang, Lihua Wang, Yubo Ren, Yudong Liu, Xiaosong Rao, Chunhou Zheng, and Fa Zhang. A hybrid convolutional and recurrent deep neural network for breast cancer pathological image classification. In *IEEE International Conference on Bioinformatics and Biomedicine (BIBM)*, pages 957–962. IEEE, 2018.
- [265] Neeraj Kumar, Ruchika Verma, Sanuj Sharma, Surabhi Bhargava, Abhishek Vahadane, and Amit Sethi. A dataset and a technique for generalized nuclear segmentation for computational pathology. *IEEE Transactions on Medical Imaging*, 36(7):1550–1560, 2017.
- [266] Joel Saltz, Rajarsi Gupta, Le Hou, Tahsin Kurc, Pankaj Singh, Vu Nguyen, Dimitris Samaras, Kenneth R Shroyer, Tianhao Zhao, Rebecca Batiste, et al. Spatial organization and molecular correlation of tumor-infiltrating lymphocytes using deep learning on pathology images. *Cell reports*, 23(1):181–193, 2018.
- [267] Simon Graham, Mostafa Jahanifar, Ayesha Azam, Mohammed Nimir, Yee-Wah Tsang, Katherine Dodd, Emily Hero, Harvir Sahota, Atisha Tank, Ksenija Benes, et al. Lizard: A large-scale dataset for colonic nuclear instance segmentation and classification. In *IEEE/CVF International Conference on Computer Vision*, pages 684–693, 2021.
- [268] Ferdaous Idlahcen, Mohammed Majid Himmi, and Abdelhak Mahmoudi. Cnn-based approach for cervical cancer classification in whole-slide histopathology images. *arXiv preprint arXiv:2005.13924*, 2020.
- [269] David Tellez, Maschenka Balkenhol, Irene Otte-Höller, Rob van de Loo, Rob Vogels, Peter Bult, Carla Wauters, Willem Vreuls, Suzanne Mol, Nico Karssemeijer, et al. Whole-slide mitosis detection in h&e breast histology using phh3 as a reference to train distilled stain-invariant convolutional networks. *IEEE Transactions on Medical Imaging*, 37(9):2126–2136, 2018.
- [270] Young Hwan Chang, Guillaume Thibault, Owen Madin, Vahid Azimi, Cole Meyers, Brett Johnson, Jason Link, Adam Margolin, and Joe W Gray. Deep learning based nucleus classification in pancreas histological images. In *International Conference of the IEEE Engineering in Medicine and Biology Society (EMBC)*, pages 672–675. IEEE, 2017.
- [271] Peter Bandi, Oscar Geessink, Quirine Manson, Marcory Van Dijk, Maschenka Balkenhol, Meyke Hermsen, Babak Ehteshami Bejnordi, Byungjae Lee, Kyunghyun Paeng, Aoxiao Zhong, et al. From detection of individual metastases to classification of lymph node status at the patient level: the camelyon17 challenge. *IEEE Transactions on Medical Imaging*, 38(2):550–560, 2018.
- [272] Mitko Veta, Yujing J Heng, Nikolas Stathonikos, Babak Ehteshami Bejnordi, Francisco Beca, Thomas Wollmann, Karl Rohr, Manan A Shah, Dayong Wang, Mikael Rousson, et al. Predicting breast tumor proliferation from whole-slide images: the tupac16 challenge. *Medical Image Analysis*, 54:111–121, 2019.
- [273] Michał Koziarski, Bogusław Cyganek, Bogusław Olborski, Zbigniew Antosz, Marcin Żydek, Bogdan Kwolek, Paweł Wąsowicz, Andrzej Bukala, Jakub Swadźba, and Piotr Sitkowski. Diagset: a dataset for prostate cancer histopathological image classification. *arXiv preprint arXiv:2105.04014*, 2021.
- [274] Hans Pinckaers, Wouter Bulten, Jeroen van der Laak, and Geert Litjens. Detection of prostate cancer in whole-slide images through end-to-end training with image-level labels. *IEEE Transactions on Medical Imaging*, 40(7):1817–1826, 2021.
- [275] Bin Li, Yin Li, and Kevin W Eliceiri. Dual-stream multiple instance learning network for whole slide image classification with self-supervised contrastive learning. In *IEEE/CVF Conference on Computer Vision and Pattern Recognition*, pages 14318–14328, 2021.
- [276] Jiahui Li, Wen Chen, Xiaodi Huang, Shuang Yang, Zhiqiang Hu, Qi Duan, Dimitris N Metaxas, Hongsheng Li, and Shaoting Zhang. Hybrid supervision learning for pathology whole slide image classification. In *International Conference on Medical Image Computing and Computer-Assisted Intervention*, pages 309–318. Springer, 2021.
- [277] Adon Phillips, Iris Teo, and Jochen Lang. Fully convolutional network for melanoma diagnostics. *arXiv preprint arXiv:1806.04765*, 2018.
- [278] Hongming Xu, Sunho Park, Jean René Clemenceau, Nathan Radakovich, Sung Hak Lee, and Tae Hyun Hwang. Deep transfer learning approach to predict tumor mutation burden (tmb) and delineate spatial heterogeneity of tmb within tumors from whole slide images. *Cold Spring Harbor Lab*, 1:554527, 2020.
- [279] James A Diao, Richard J Chen, and Joseph C Kvedar. Efficient cellular annotation of histopathology slides with real-time ai augmentation. *NPJ Digital Medicine*, 4(1):161, 2021.
- [280] Runtian Miao, Robert Toth, Yu Zhou, Anant Madabhushi, and Andrew Janowczyk. Quick annotator: an open-source digital pathology based rapid image annotation tool. *The Journal of Pathology*, 7(6):542–547, 2021.
- [281] Ziyu Zhang, Sanja Fidler, and Raquel Urtasun. Instance-level segmentation for autonomous driving with deep densely connected mrfs. In *IEEE Conference on Computer Vision and Pattern Recognition*, pages 669–677, 2016.

- [282] Yuxuan Zhang, Huan Ling, Jun Gao, Kangxue Yin, Jean-Francois Lafleche, Adela Barriuso, Antonio Torralba, and Sanja Fidler. Datasetgan: Efficient labeled data factory with minimal human effort. In *IEEE/CVF Conference on Computer Vision and Pattern Recognition*, pages 10145–10155, 2021.
- [283] Bowen Chen, Huan Ling, Xiaohui Zeng, Jun Gao, Ziyue Xu, and Sanja Fidler. Scribblebox: Interactive annotation framework for video object segmentation. In *European Conference on Computer Vision*, pages 293–310. Springer, 2020.
- [284] Simon Graham, Quoc Dang Vu, Shan E Ahmed Raza, Ayesha Azam, Yee Wah Tsang, Jin Tae Kwak, and Nasir Rajpoot. Hover-net: Simultaneous segmentation and classification of nuclei in multi-tissue histology images. *Medical Image Analysis*, 58:101563, 2019.
- [285] Shusuke Takahama, Yusuke Kurose, Yusuke Mukuta, Hiroyuki Abe, Masashi Fukayama, Akihiko Yoshizawa, Masanobu Kitagawa, and Tatsuya Harada. Multi-stage pathological image classification using semantic segmentation. In *IEEE/CVF International Conference on Computer Vision*, pages 10702–10711, 2019.
- [286] Sajid Javed, Arif Mahmood, Muhammad Moazam Fraz, Navid Alemi Koohbanani, Ksenija Benes, Yee-Wah Tsang, Katherine Hewitt, David Epstein, David Snead, and Nasir Rajpoot. Cellular community detection for tissue phenotyping in colorectal cancer histology images. *Medical Image Analysis*, 63:101696, 2020.
- [287] Yuji Roh, Geon Heo, and Steven Euijong Whang. A survey on data collection for machine learning: a big data-ai integration perspective. *IEEE Transactions on Knowledge and Data Engineering*, 33(4):1328–1347, 2019.
- [288] Noorul Wahab, Islam M Miligy, Katherine Dodd, Harvir Sahota, Michael Toss, Wenqi Lu, Mostafa Jahanifar, Mohsin Bilal, Simon Graham, Young Park, et al. Semantic annotation for computational pathology: Multidisciplinary experience and best practice recommendations. *The Journal of Pathology: Clinical Research*, 8(2):116–128, 2022.
- [289] Nithya Sambasivan, Shivani Kapania, Hannah Highfill, Diana Akrong, Praveen Kumar Paritosh, and Lora Mois Aroyo. "everyone wants to do the model work, not the data work": Data cascades in high-stakes ai. 2021.
- [290] Cathy O'Neil. *Weapons of Math Destruction: How Big Data Increases Inequality and Threatens Democracy*. Crown Publishing Group, USA, 2016.
- [291] Michael A Lones. How to avoid machine learning pitfalls: a guide for academic researchers. *arXiv preprint arXiv:2108.02497*, 2021.
- [292] Yoshua Bengio, Aaron Courville, and Pascal Vincent. Representation learning: A review and new perspectives, 2012.
- [293] Yann LeCun, Yoshua Bengio, and Geoffrey Hinton. Deep learning. *nature*, 521(7553):436–444, 2015.
- [294] Jakob Nikolas Kather, Alexander T Pearson, Niels Halama, Dirk Jäger, Jeremias Krause, Sven H Loosen, Alexander Marx, Peter Boor, Frank Tacke, Ulf Peter Neumann, et al. Deep learning can predict microsatellite instability directly from histology in gastrointestinal cancer. *Nature medicine*, 25(7):1054–1056, 2019.
- [295] Naofumi Tomita, Behnaz Abdollahi, Jason Wei, Bing Ren, Arief Suriawinata, and Saeed Hassanpour. Attention-based deep neural networks for detection of cancerous and precancerous esophagus tissue on histopathological slides. *JAMA network open*, 2(11):e1914645–e1914645, 2019.
- [296] Stefan Bauer, Nicolas Carion, Peter Schüffler, Thomas Fuchs, Peter Wild, and Joachim M Buhmann. Multi-organ cancer classification and survival analysis. *arXiv preprint arXiv:1606.00897*, 2016.
- [297] Mehdi Habibzadeh Motlagh, Mahboobeh Jannesari, HamidReza Aboulkheyr, Pegah Khosravi, Olivier Elemento, Mehdi Totonchi, and Iman Hajirasouliha. Breast cancer histopathological image classification: A deep learning approach. *BioRxiv*, page 242818, 2018.
- [298] Yusuf Celik, Muhammed Talo, Ozal Yildirim, Murat Karabatak, and U Rajendra Acharya. Automated invasive ductal carcinoma detection based using deep transfer learning with whole-slide images. *Pattern Recognition Letters*, 133:232–239, 2020.
- [299] Bo Liu, Kelu Yao, Mengmeng Huang, Jiahui Zhang, Yong Li, and Rong Li. Gastric pathology image recognition based on deep residual networks. In *IEEE Annual Computer Software and Applications Conference (COMPSAC)*, volume 2, pages 408–412. IEEE, 2018.
- [300] Jason W Wei, Jerry W Wei, Christopher R Jackson, Bing Ren, Arief A Suriawinata, and Saeed Hassanpour. Automated detection of celiac disease on duodenal biopsy slides: A deep learning approach. *Journal of Pathology Informatics*, 10, 2019.
- [301] Shweta Saxena, Sanyam Shukla, and Manasi Gyanchandani. Pre-trained convolutional neural networks as feature extractors for diagnosis of breast cancer using histopathology. *International Journal of Imaging Systems and Technology*, 30(3):577–591, 2020.
- [302] Rene Bidart and Alexander Wong. Triresnet: A deep triple-stream residual network for histopathology grading. In *International Conference on Image Analysis and Recognition*, pages 369–382. Springer, 2019.
- [303] Lorne Holland, Dongguang Wei, Kristin A Olson, Anupam Mitra, John Paul Graff, Andrew D Jones, Blythe Durbin-Johnson, Ananya Datta Mitra, and Hooman H Rashidi. Limited number of cases may yield generalizable models, a proof of concept in deep learning for colon histology. *Journal of Pathology Informatics*, 11, 2020.
- [304] Achim Hekler, Jochen S Utikal, Alexander H Enk, Wiebke Solass, Max Schmitt, Joachim Klode, Dirk Schadendorf, Wiebke Sondermann, Cindy Franklin, Felix Bestvater, et al. Deep learning outperformed 11 pathologists in the classification of histopathological melanoma images. *European Journal of Cancer*, 118:91–96, 2019.
- [305] Byungjae Lee and Kyunghyun Paeng. A robust and effective approach towards accurate metastasis detection and pn-stage classification in breast cancer. In *International Conference on Medical Image Computing and Computer-Assisted Intervention*, pages 841–850. Springer, 2018.
- [306] Abhinav Kumar, Sanjay Kumar Singh, Sonal Saxena, K Lakshmanan, Arun Kumar Sangaiah, Himanshu Chauhan, Sameer Shrivastava, and Raj Kumar Singh. Deep feature learning for histopathological image classification of canine mammary tumors and human breast cancer. *Information Sciences*, 508:405–421, 2020.
- [307] Lyndon Chan, Mahdi S Hosseini, Corwyn Rowsell, Konstantinos N Plataniotis, and Savvas Damaskinos. Histosegnet: Semantic segmentation of histological tissue type in whole slide images. In *IEEE/CVF International Conference on Computer Vision*, pages 10662–10671, 2019.
- [308] Zeya Wang, Nanqing Dong, Wei Dai, Sean D Rosario, and Eric P Xing. Classification of breast cancer histopathological images using convolutional neural networks with hierarchical loss and global pooling. In *International Conference Image Analysis and Recognition*, pages 745–753. Springer, 2018.
- [309] Ming Y Lu, Tiffany Y Chen, Drew FK Williamson, Melissa Zhao, Maha Shady, Jana Lipkova, and Faisal Mahmood. Ai-based pathology predicts origins for cancers of unknown primary. *Nature*, 594(7861):106–110, 2021.
- [310] Pushpanjali Gupta, Yenlin Huang, Prasan Kumar Sahoo, Jeng-Fu You, Sum-Fu Chiang, Djeane Debora Onthoni, Yih-Jong Chern, Kuo-Yu Chao, Jy-Ming Chiang, Chien-Yuh Yeh, et al. Colon tissues classification and localization in whole slide images using deep learning. *Diagnostics*, 11(8):1398, 2021.
- [311] Ruiwei Feng, Xuechen Liu, Jintai Chen, Danny Z Chen, Honghao Gao, and Jian Wu. A deep learning approach for colonoscopy pathology wsi analysis: accurate segmentation and classification. *IEEE Journal of Biomedical and Health Informatics*, 25(10):3700–3708, 2020.
- [312] Saman Farahmand, Aileen I Fernandez, Fahad Shabbir Ahmed, David L Rimm, Jeffrey H Chuang, Emily Reisenbichler, and Kourosh Zarringhalam. Deep learning trained on hematoxylin and eosin tumor region of interest predicts her2 status and trastuzumab treatment response in her2+ breast cancer. *Modern Pathology*, 35(1):44–51, 2022.
- [313] Ozan Ciga, Tony Xu, and Anne Louise Martel. Self supervised contrastive learning for digital histopathology. *Machine Learning with Applications*, 7:100198, 2022.
- [314] Nicole Bussola, Alessia Marcolini, Valerio Maggio, Giuseppe Jurman, and Cesare Furlanello. Ai slipping on tiles: Data leakage in digital pathology. In *International Conference on Pattern Recognition*, pages 167–182. Springer, 2021.
- [315] Afaf Alharbi, Yaqi Wang, and Qianni Zhang. Trans-attention multiple instance learning for cancer tissue classification in digital histopathology images. In *International Conference on Biomedical Signal and Image Processing*, pages 79–84, 2021.
- [316] Junlong Cheng, Shengwei Tian, Long Yu, Chengrui Gao, Xiaojing Kang, Xiang Ma, Weidong Wu, Shijia Liu, and Hongchun Lu. Resganet: Residual group attention network for medical image classification and segmentation. *Medical Image Analysis*, 76:102313, 2022.
- [317] Eu Wern Teh and Graham W Taylor. Learning with less labels in digital

- pathology via scribble supervision from natural images. *arXiv preprint arXiv:2201.02627*, 2022.
- [318] Andrew Su, HoJoon Lee, Xiao Tan, Carlos J Suarez, Noemi Andor, Quan Nguyen, and Hanlee P Ji. A deep learning model for molecular label transfer that enables cancer cell identification from histopathology images. *NPJ precision oncology*, 6(1):1–11, 2022.
- [319] Jiawei Yang, Hanbo Chen, Yuan Liang, Junzhou Huang, Lei He, and Jianhua Yao. Concl: Concept contrastive learning for dense prediction pre-training in pathology images. In *European Conference on Computer Vision*, pages 523–539. Springer, 2022.
- [320] Chuanqi Tan, Fuchun Sun, Tao Kong, Wenchang Zhang, Chao Yang, and Chunfang Liu. A survey on deep transfer learning. In *International conference on artificial neural networks*, pages 270–279. Springer, 2018.
- [321] Thomas N. Kipf and Max Welling. Semi-supervised classification with graph convolutional networks. In *International Conference on Learning Representations*. OpenReview.net, 2017.
- [322] Yonghang Guan, Jun Zhang, Kuan Tian, Sen Yang, Pei Dong, Jinxi Xiang, Wei Yang, Junzhou Huang, Yuyao Zhang, and Xiao Han. Node-aligned graph convolutional network for whole-slide image representation and classification. In *Proceedings of the IEEE/CVF Conference on Computer Vision and Pattern Recognition*, pages 18813–18823, 2022.
- [323] Richard J Chen, Ming Y Lu, Muhammad Shaban, Chengkuan Chen, Tiffany Y Chen, Drew FK Williamson, and Faisal Mahmood. Whole slide images are 2d point clouds: Context-aware survival prediction using patch-based graph convolutional networks. In *International Conference on Medical Image Computing and Computer-Assisted Intervention*, pages 339–349. Springer, 2021.
- [324] Alexey Dosovitskiy, Lucas Beyer, Alexander Kolesnikov, Dirk Weissenborn, Xiaohua Zhai, Thomas Unterthiner, Mostafa Dehghani, Matthias Minderer, Georg Heigold, Sylvain Gelly, et al. An image is worth 16x16 words: Transformers for image recognition at scale. In *International Conference on Learning Representations*.
- [325] Daniel Bug, Steffen Schneider, Anne Grote, Eva Oswald, Friedrich Feuerhake, Julia Schüller, and Dorit Merhof. Context-based normalization of histological stains using deep convolutional features. In *Deep Learning in Medical Image Analysis and Multimodal Learning for Clinical Decision Support*, pages 135–142. Springer, 2017.
- [326] Zeyu Gao, Bangyang Hong, Xianli Zhang, Yang Li, Chang Jia, Jialun Wu, Chunbao Wang, Deyu Meng, and Chen Li. Instance-based vision transformer for subtyping of papillary renal cell carcinoma in histopathological image. In *International Conference on Medical Image Computing and Computer-Assisted Intervention*, pages 299–308. Springer, 2021.
- [327] Kelei He, Chen Gan, Zhuoyuan Li, Islem Rekik, Zihao Yin, Wen Ji, Yang Gao, Qian Wang, Junfeng Zhang, and Dinggang Shen. Transformers in medical image analysis. *Intelligent Medicine*, 3(1):59–78, 2023.
- [328] Yun Jiang, Li Chen, Hai Zhang, and Xiao Xiao. Breast cancer histopathological image classification using convolutional neural networks with small se-resnet module. *PLoS one*, 14(3):e0214587, 2019.
- [329] Yi Li and Wei Ping. Cancer metastasis detection with neural conditional random field. *arXiv preprint arXiv:1806.07064*, 2018.
- [330] Artem Pimkin, Gleb Makarchuk, Vladimir Kondratenko, Maxim Pisov, Egor Krivov, and Mikhail Belyaev. Ensembling neural networks for digital pathology images classification and segmentation. In *International Conference Image Analysis and Recognition*, pages 877–886. Springer, 2018.
- [331] Sara Hosseinzadeh Kassani, Peyman Hosseinzadeh Kassani, Michal J Wesolowski, Kevin A Schneider, and Ralph Deters. Classification of histopathological biopsy images using ensemble of deep learning networks. In *International Conference on Computer Science and Software Engineering*, pages 92–99, 2019.
- [332] Wenqi Lu, Simon Graham, Mohsin Bilal, Nasir Rajpoot, and Fayyaz Minhas. Capturing cellular topology in multi-gigapixel pathology images. In *IEEE/CVF Conference on Computer Vision and Pattern Recognition Workshops*, pages 260–261, 2020.
- [333] Jiatai Lin, Guoqiang Han, Xipeng Pan, Hao Chen, Danyi Li, Xiping Jia, Zhenwei Shi, Zhizhen Wang, Yanfen Cui, Haiming Li, et al. Pdbl: Improving histopathological tissue classification with plug-and-play pyramidal deep-broad learning. *arXiv preprint arXiv:2111.03063*, 2021.
- [334] Zakaria Senousy, Mohammed M Abdelsamea, Mohamed Medhat Gaber, Moloud Abdar, U Rajendra Acharya, Abbas Khosravi, and Saeid Nahavandi. Mcua: Multi-level context and uncertainty aware dynamic deep ensemble for breast cancer histology image classification. *IEEE Transactions on Biomedical Engineering*, 69(2):818–829, 2021.
- [335] Sai Chandra Kosaraju, Jie Hao, Hyun Min Koh, and Mingon Kang. Deep-hipo: Multi-scale receptive field deep learning for histopathological image analysis. *Methods*, 179:3–13, 2020.
- [336] Olaf Ronneberger, Philipp Fischer, and Thomas Brox. U-net: Convolutional networks for biomedical image segmentation. In *International Conference on Medical Image Computing and Computer-Assisted Intervention*, pages 234–241. Springer, 2015.
- [337] Le Hou, Ayush Agarwal, Dimitris Samaras, Tahsin M Kurc, Rajarsi R Gupta, and Joel H Saltz. Robust histopathology image analysis: to label or to synthesize? pages 8533–8542, 2019.
- [338] Hoo-Chang Shin, Holger R Roth, Mingchen Gao, Le Lu, Ziyue Xu, Isabella Nogue, Jianhua Yao, Daniel Mollura, and Ronald M Summers. Deep convolutional neural networks for computer-aided detection: Cnn architectures, dataset characteristics and transfer learning. *IEEE Transactions on Medical Imaging*, 35(5):1285–1298, 2016.
- [339] Quoc Dang Vu, Simon Graham, Tahsin Kurc, Minh Nguyen Nhat To, Muhammad Shaban, Talha Qaiser, Navid Alemi Koohbanani, Syed Ali Khurram, Jayashree Kalpathy-Cramer, Tianhao Zhao, et al. Methods for segmentation and classification of digital microscopy tissue images. *Frontiers in Bioengineering and Biotechnology*, page 53, 2019.
- [340] Kemeng Chen, Ning Zhang, Linda Powers, and Janet Roveda. Cell nuclei detection and segmentation for computational pathology using deep learning. In *Spring Simulation Conference (SpringSim)*, pages 1–6. IEEE, 2019.
- [341] Tian Bai, Jiayu Xu, and Fuyong Xing. Multi-field of view aggregation and context encoding for single-stage nucleus recognition. In *International Conference on Medical Image Computing and Computer-Assisted Intervention*, pages 382–392. Springer, 2020.
- [342] Xinpeng Xie, Jiawei Chen, Yuexiang Li, Linlin Shen, Kai Ma, and Yefeng Zheng. Instance-aware self-supervised learning for nuclei segmentation. In *International Conference on Medical Image Computing and Computer-Assisted Intervention*, pages 341–350. Springer, 2020.
- [343] Amal Lahiani, Jacob Gildenblat, Irina Klamann, Nassir Navab, and Eldad Klaiman. Generalizing multistain immunohistochemistry tissue segmentation using one-shot color deconvolution deep neural networks. *arXiv preprint arXiv:1805.06958*, 2018.
- [344] Gabriel Jiménez and Daniel Racoceanu. Deep learning for semantic segmentation versus classification in computational pathology: Application to mitosis analysis in breast cancer grading. *Frontiers in Bioengineering and Biotechnology*, 7:145, 2019.
- [345] Tasleem Kausar, Wang MingJiang, M Adnan Ashraf, and Adeeba Kausar. Smallmitosis: Small size mitotic cells detection in breast histopathology images. *IEEE Access*, 2020.
- [346] David Joon Ho, Narasimhan P Agaram, Peter J Schüffler, Chad M Vanderbilt, Marc-Henri Jean, Meera R Hameed, and Thomas J Fuchs. Deep interactive learning: an efficient labeling approach for deep learning-based osteosarcoma treatment response assessment. In *International Conference on Medical Image Computing and Computer-Assisted Intervention*, pages 540–549. Springer, 2020.
- [347] Suzanne C Wetstein, Allison M Onken, Christina Luffman, Gabrielle M Baker, Michael E Pyle, Kevin H Kensler, Ying Liu, Bart Bakker, Ruud Vlutters, Marinus B van Leeuwen, et al. Deep learning assessment of breast terminal duct lobular unit involution: Towards automated prediction of breast cancer risk. *PLoS one*, 15(4):e0231653, 2020.
- [348] Hammad Qureshi, Olcay Sertel, Nasir Rajpoot, Roland Wilson, and Metin Gurcan. Adaptive discriminant wavelet packet transform and local binary patterns for meningioma subtype classification. In *International Conference on Medical Image Computing and Computer-Assisted Intervention*, pages 196–204. Springer, 2008.
- [349] Rokshana Stephny Gered, Abishika Sivanandarajah, Emily Rita Brouwer, Geoffrey A Wood, Dimitrios Androustos, Hala Faragalla, and April Khademi. pinet—an automated proliferation index calculator framework for ki67 breast cancer images. *Cancers*, 13(1):11, 2021.
- [350] David Schuchmacher, Stephanie Schoerner, Claus Kuepper, Frederik Grosserueschkamp, Carlo Sternemann, Celine Lugnier, Anna-Lena Kraeft, Hendrik Juette, Andrea Tannapfel, Anke Reinacher-Schick, et al. A framework for falsifiable explanations of machine learning models with an application in computational pathology. *medRxiv*, 2021.
- [351] Jaime Gallego, Zaneta Swiderska-Chadaj, Tomasz Markiewicz, Michifumi Yamashita, M Alejandra Gabaldon, and Arkadiusz Gertych. A

- u-net based framework to quantify glomerulosclerosis in digitized pas and h&e stained human tissues. *Computerized Medical Imaging and Graphics*, 89:101865, 2021.
- [352] Jianghua Wu, Changling Liu, Xiaoqing Liu, Wei Sun, Linfeng Li, Nannan Gao, Yajun Zhang, Xin Yang, Junjie Zhang, Haiyue Wang, et al. Artificial intelligence-assisted system for precision diagnosis of pd-11 expression in non-small cell lung cancer. *Modern Pathology*, pages 1–9, 2021.
- [353] Pingjun Chen, Yun Liang, Xiaoshuang Shi, Lin Yang, and Paul Gader. Automatic whole slide pathology image diagnosis framework via unit stochastic selection and attention fusion. *Neurocomputing*, 453:312–325, 2021.
- [354] Abdala Nour, Sherif Saad, and Boubakeur Boufama. Prostate biomedical images segmentation and classification by using u-net cnn model. In *ACM Conference on Bioinformatics, Computational Biology, and Health Informatics*, pages 1–7, 2021.
- [355] Akram Bayat, Connor Anderson, and Pratik Shah. Automated end-to-end deep learning framework for classification and tumor localization from native non-stained pathology images. 11596:115960A, 2021.
- [356] Mahendra Khened, Avinash Kori, Haran Rajkumar, Ganapathy Krishnamurthi, and Balaji Srinivasan. A generalized deep learning framework for whole-slide image segmentation and analysis. *Scientific Reports*, 11(1):1–14, 2021.
- [357] Peter Naylor, Marick Laé, Fabien Reyat, and Thomas Walter. Nuclei segmentation in histopathology images using deep neural networks. pages 933–936, 2017.
- [358] Mihir Sahasrabudhe, Stergios Christodoulidis, Roberto Salgado, Stefan Michiels, Sherene Loi, Fabrice André, Nikos Paragios, and Maria Vakalopoulou. Self-supervised nuclei segmentation in histopathological images using attention. In *International Conference on Medical Image Computing and Computer-Assisted Intervention*, pages 393–402. Springer, 2020.
- [359] Saad Nadeem, Travis Hollmann, and Allen Tannenbaum. Multimarginal wasserstein barycenter for stain normalization and augmentation. In *International Conference on Medical Image Computing and Computer-Assisted Intervention*, pages 362–371. Springer, 2020.
- [360] Nanqing Dong, Michael Kampffmeyer, Xiaodan Liang, Zeya Wang, Wei Dai, and Eric Xing. Reinforced auto-zoom net: Towards accurate and fast breast cancer segmentation in whole-slide images. In *Deep Learning in Medical Image Analysis and Multimodal Learning for Clinical Decision Support*, pages 317–325. Springer, 2018.
- [361] Leander van Eekelen, Hans Pinckaers, Konnie M Hebeda, and Geert Litjens. Multi-class semantic cell segmentation and classification of aplasia in bone marrow histology images. 11320:113200B, 2020.
- [362] Gang Xing, Jianqin Lei, and Xiayu Xu. Fluid segmentation in oct with an improved convolutional neural network. In *The Fifth International Conference on Biological Information and Biomedical Engineering*, pages 1–5, 2021.
- [363] Mina Khoshdeli, Garrett Winkelmaier, and Bahram Parvin. Fusion of encoder-decoder deep networks improves delineation of multiple nuclear phenotypes. *BMC bioinformatics*, 19(1):1–11, 2018.
- [364] Mohamed Abdel-Nasser, Adel Saleh, and Domenc Puig. Channel-wise aggregation with self-correction mechanism for multi-center multi-organ nuclei segmentation in whole slide imaging. In *VISIGRAPP*, pages 466–473, 2020.
- [365] Shengcong Chen, Changxing Ding, and Dacheng Tao. Boundary-assisted region proposal networks for nucleus segmentation. pages 279–288, 2020.
- [366] Simon Graham, Hao Chen, Jevgenij Gamper, Qi Dou, Pheng-Ann Heng, David Snead, Yee Wah Tsang, and Nasir Rajpoot. Mild-net: Minimal information loss dilated network for gland instance segmentation in colon histology images. *Medical Image Analysis*, 52:199–211, 2019.
- [367] Abhinav Agarwalla, Muhammad Shaban, and Nasir M. Rajpoot. Representation-aggregation networks for segmentation of multi-gigapixel histology images. *ArXiv*, abs/1707.08814, 2017.
- [368] Ziqiang Li, Rentuo Tao, Qianrun Wu, and Bin Li. Da-refinenet: A dual input whole slide image segmentation algorithm based on attention. *arXiv*, pages arXiv–1907, 2019.
- [369] Pushpak Pati, Sonali Andani, Matthew Padiaditis, Matheus Palhares Viana, Jan Hendrik Rüschoff, Peter Wild, and Maria Gabriani. Deep positive-unlabeled learning for region of interest localization in breast tissue images. In *Medical Imaging: Digital Pathology*, volume 10581, page 1058107. International Society for Optics and Photonics, 2018.
- [370] Talha Qaiser, Yee-Wah Tsang, Daiki Taniyama, Naoya Sakamoto, Kazuaki Nakane, David Epstein, and Nasir Rajpoot. Fast and accurate tumor segmentation of histology images using persistent homology and deep convolutional features. *Medical Image Analysis*, 55:1–14, 2019.
- [371] Dev Kumar Das, Surajit Bose, Asok Kumar Maiti, Bhaskar Mitra, Gopeshwar Mukherjee, and Pranab Kumar Dutta. Automatic identification of clinically relevant regions from oral tissue histological images for oral squamous cell carcinoma diagnosis. *Tissue and Cell*, 53:111–119, 2018.
- [372] Adam J Shephard, Simon Graham, Saad Bashir, Mostafa Jahanifar, Hanya Mahmood, Ali Khurram, and Nasir M Rajpoot. Simultaneous nuclear instance and layer segmentation in oral epithelial dysplasia. In *IEEE/CVF International Conference on Computer Vision*, pages 552–561, 2021.
- [373] Liuan Wang, Li Sun, Mingjie Zhang, Huigang Zhang, Wang Ping, Rong Zhou, and Jun Sun. Exploring pathologist knowledge for automatic assessment of breast cancer metastases in whole-slide image. In *ACM International Conference on Multimedia*, pages 255–263, 2021.
- [374] Mostafa Jahanifar, Neda Zamani Tajeddin, Navid Alemi Koohbanani, and Nasir M Rajpoot. Robust interactive semantic segmentation of pathology images with minimal user input. In *IEEE/CVF International Conference on Computer Vision*, pages 674–683, 2021.
- [375] Hyeongsu Kim, Hongjoon Yoon, Nishant Thakur, Gyoyeon Hwang, Eun Jung Lee, Chulhong Kim, and Yosep Chong. Deep learning-based histopathological segmentation for whole slide images of colorectal cancer in a compressed domain. *Scientific Reports*, 11(1):1–14, 2021.
- [376] G Murtaza Dogar, Muhammad Moazam Fraz, and Sajid Javed. Feature attention network for simultaneous nuclei instance segmentation and classification in histology images. pages 1–6, 2021.
- [377] Maxime W Lafarge, Josien PW Pluim, Koen AJ Eppenhof, and Mitko Veta. Learning domain-invariant representations of histological images. *Frontiers in medicine*, 6:162, 2019.
- [378] Haibo Wang, Angel Cruz Roa, Ajay N Basavanahally, Hannah L Gilmore, Natalie Shih, Mike Feldman, John Tomaszewski, Fabio Gonzalez, and Anant Madabhushi. Mitosis detection in breast cancer pathology images by combining handcrafted and convolutional neural network features. *Journal of Medical Imaging*, 1(3):034003, 2014.
- [379] Chao Li, Xinggang Wang, Wenyu Liu, and Longin Jan Latecki. Deepmitosis: Mitosis detection via deep detection, verification and segmentation networks. *Medical Image Analysis*, 45:121–133, 2018.
- [380] Chao Li, Xinggang Wang, Wenyu Liu, Longin Jan Latecki, Bo Wang, and Junzhou Huang. Weakly supervised mitosis detection in breast histopathology images using concentric loss. *Medical Image Analysis*, 53:165–178, 2019.
- [381] Meriem Sebai, Xinggang Wang, and Tianjiang Wang. Maskmitosis: a deep learning framework for fully supervised, weakly supervised, and unsupervised mitosis detection in histopathology images. *Medical & Biological Engineering & Computing*, 58(7):1603–1623, 2020.
- [382] Saad Ullah Akram, Talha Qaiser, Simon Graham, Juho Kannala, Janne Heikkilä, and Nasir Rajpoot. Leveraging unlabeled whole-slide-images for mitosis detection. pages 69–77, 2018.
- [383] Maxime W Lafarge, Erik J Bekkers, Josien PW Pluim, Remco Duits, and Mitko Veta. Roto-translation equivariant convolutional networks: Application to histopathology image analysis. *Medical Image Analysis*, 68:101849, 2021.
- [384] Md Zahangir Alom, Theus Aspiras, Tarek M Taha, Tj Bowen, and Vijayan K Asari. Mitosisnet: End-to-end mitotic cell detection by multi-task learning. *IEEE Access*, 8:68695–68710, 2020.
- [385] Hansheng Li, Xin Han, Yuxin Kang, Xiaoshuang Shi, Mengdi Yan, Zixu Tong, Qirong Bu, Lei Cui, Jun Feng, and Lin Yang. A novel loss calibration strategy for object detection networks training on sparsely annotated pathological datasets. In *International Conference on Medical Image Computing and Computer-Assisted Intervention*, pages 320–329. Springer, 2020.
- [386] Pushpak Pati, Antonio Foncubierta-Rodríguez, Orcun Goksel, and Maria Gabriani. Reducing annotation effort in digital pathology: A co-representation learning framework for classification tasks. *Medical Image Analysis*, 67:101859, 2021.
- [387] Nicolas Brieu, Armin Meier, Ansh Kapil, Ralf Schoenmeyer, Christos G Gavriel, Peter D Caie, and Günter Schmidt. Domain adaptation-based augmentation for weakly supervised nuclei detection. *arXiv preprint*

- arXiv:1907.04681*, 2019.
- [388] Thomas J Fuchs, Peter J Wild, Holger Moch, and Joachim M Buhmann. Computational pathology analysis of tissue microarrays predicts survival of renal clear cell carcinoma patients. pages 1–8, 2008.
- [389] Wenyuan Li, Jiayun Li, Karthik V Sarma, King Chung Ho, Shiwen Shen, Beatrice S Knudsen, Arkadiusz Gertych, and Corey W Arnold. Path-rnn for prostate cancer diagnosis and gleason grading of histological images. *IEEE Transactions on Medical Imaging*, 38(4):945–954, 2018.
- [390] Muhammad Nasim Kashif, Shan E Ahmed Raza, Korsuk Sirinukunwattana, Muhammad Arif, and Nasir Rajpoot. Handcrafted features with convolutional neural networks for detection of tumor cells in histology images. In *IEEE International Symposium on Biomedical Imaging*, pages 1029–1032. IEEE, 2016.
- [391] Guillaume Jaume, Pushpak Pati, Valentin Anklin, Antonio Foncubierta, and Maria Gabrani. Histocartography: A toolkit for graph analytics in digital pathology. In *MICCAI Workshop on Computational Pathology*, pages 117–128. PMLR, 2021.
- [392] Sajid Javed, Arif Mahmood, Jorge Dias, Naoufel Werghi, and Nasir Rajpoot. Spatially constrained context-aware hierarchical deep correlation filters for nucleus detection in histology images. *Medical Image Analysis*, 72:102104, 2021.
- [393] Linbo Wang, Hui Zhen, Xianyong Fang, Shaohua Wan, Weiping Ding, and Yanwen Guo. A unified two-parallel-branch deep neural network for joint gland contour and segmentation learning. *Future Generation Computer Systems*, 100:316–324, 2019.
- [394] Bingzhe Wu, Shiwan Zhao, Guangyu Sun, Xiaolu Zhang, Zhong Su, Caihong Zeng, and Zhihong Liu. P3sgd: Patient privacy preserving sgd for regularizing deep cnns in pathological image classification. In *IEEE/CVF Conference on Computer Vision and Pattern Recognition*, pages 2099–2108, 2019.
- [395] Haichun Yang, Ruining Deng, Yuzhe Lu, Zheyu Zhu, Ye Chen, Joseph T Roland, Le Lu, Bennett A Landman, Agnes B Fogo, and Yuankai Huo. Circlenet: Anchor-free glomerulus detection with circle representation. In *International Conference on Medical Image Computing and Computer-Assisted Intervention*, pages 35–44. Springer, 2020.
- [396] Gloria Bueno, M Milagro Fernandez-Carrobles, Lucia Gonzalez-Lopez, and Oscar Deniz. Glomerulosclerosis identification in whole slide images using semantic segmentation. *Computer methods and programs in biomedicine*, 184:105273, 2020.
- [397] Zixiao Lu, Siwen Xu, Wei Shao, Yi Wu, Jie Zhang, Zhi Han, Qianjin Feng, and Kun Huang. Deep-learning-based characterization of tumor-infiltrating lymphocytes in breast cancers from histopathology images and multiomics data. *JCO Clinical Cancer Informatics*, 4:480–490, 2020.
- [398] David Tellez, Diederik Höppener, Cornelis Verhoef, Dirk Grünhagen, Pieter Nierop, Michal Drozdal, Jeroen Laak, and Francesco Ciompi. Extending unsupervised neural image compression with supervised multitask learning. pages 770–783, 2020.
- [399] Mohammed Alawad, Shang Gao, John X Qiu, Hong Jun Yoon, J Blair Christian, Lynne Penberthy, Brent Mumphy, Xiao-Cheng Wu, Linda Coyle, and Georgia Tourassi. Automatic extraction of cancer registry reportable information from free-text pathology reports using multitask convolutional neural networks. *Journal of the American Medical Informatics Association*, 27(1):89–98, 2020.
- [400] Zunlei Feng, Zhonghua Wang, Xinchao Wang, Yining Mao, Thomas Li, Jie Lei, Yuexuan Wang, and Mingli Song. Mutual-complementing framework for nuclei detection and segmentation in pathology image. In *Proceedings of the IEEE/CVF International Conference on Computer Vision*, pages 4036–4045, 2021.
- [401] Ozan Sener and Vladlen Koltun. Multi-task learning as multi-objective optimization. In S. Bengio, H. Wallach, H. Larochelle, K. Grauman, N. Cesa-Bianchi, and R. Garnett, editors, *Advances in Neural Information Processing Systems*, volume 31. Curran Associates, Inc., 2018.
- [402] Amelie Royer, Tijmen Blankevoort, and Babak Ehteshami Bejnordi. Scalarization for multi-task and multi-domain learning at scale. In *Advances in Neural Information Processing Systems*, 2023.
- [403] Jiquan Ngiam, Aditya Khosla, Mingyu Kim, Juhan Nam, Honglak Lee, and Andrew Y Ng. Multimodal deep learning. In *ICML*, 2011.
- [404] Haoyang Mi, Trinity J Bivalacqua, Max Kates, Roland Seiler, Peter C Black, Aleksander S Popel, and Alexander S Baras. Predictive models of response to neoadjuvant chemotherapy in muscle-invasive bladder cancer using nuclear morphology and tissue architecture. *Cell Reports Medicine*, 2(9), 2021.
- [405] Sebastian Foersch, Christina Glasner, Ann-Christin Woerl, Markus Eckstein, Daniel-Christoph Wagner, Stefan Schulz, Franziska Kellers, Aurélie Fernandez, Konstantina Tserea, Michael Kloth, et al. Multistain deep learning for prediction of prognosis and therapy response in colorectal cancer. *Nature medicine*, 29(2):430–439, 2023.
- [406] Zhi Huang, Wei Shao, Zhi Han, Ahmad Mahmoud Alkashash, Carlo De la Sancha, Anil V Parwani, Hiroaki Nitta, Yanjun Hou, Tongxin Wang, Paul Salama, et al. Artificial intelligence reveals features associated with breast cancer neoadjuvant chemotherapy responses from multi-stain histopathologic images. *NPJ Precision Oncology*, 7(1):14, 2023.
- [407] Chunyuan Li, Xinliang Zhu, Jiawen Yao, and Junzhou Huang. Hierarchical transformer for survival prediction using multimodality whole slide images and genomics. In *2022 26th International Conference on Pattern Recognition (ICPR)*, pages 4256–4262. IEEE, 2022.
- [408] Yawen Wu, Michael Cheng, Shuo Huang, Zongxiang Pei, Yingli Zuo, Jianxin Liu, Kai Yang, Qi Zhu, Jie Zhang, Honghai Hong, Daoqiang Zhang, Kun Huang, Liang Cheng, and Wei Shao. Recent advances of deep learning for computational histopathology: Principles and applications. *Cancers (Basel)*, 14(5):1199, February 2022.
- [409] Xinrui Huang, Zhaotong Li, Minghui Zhang, and Song Gao. Fusing hand-crafted and deep-learning features in a convolutional neural network model to identify prostate cancer in pathology images. *Front. Oncol.*, 12:994950, September 2022.
- [410] Mobeen Ur Rehman, Suhail Akhtar, Muhammad Zakwan, and Muhammad Habib Mahmood. Novel architecture with selected feature vector for effective classification of mitotic and non-mitotic cells in breast cancer histology images. *Biomedical Signal Processing and Control*, 71:103212, 2022.
- [411] I Onur Sigirci, Abdulkadir Albayrak, and Gokhan Bilgin. Detection of mitotic cells in breast cancer histopathological images using deep versus handcrafted features. *Multimedia Tools and Applications*, pages 1–24, 2021.
- [412] Wei-Hung Weng, Yuannan Cai, Angela Lin, Fraser Tan, and Po-Hsuan Cameron Chen. Multimodal multitask representation learning for pathology biobank metadata prediction. *arXiv preprint arXiv:1909.07846*, 2019.
- [413] Kevin M Boehm, Pegah Khosravi, Rami Vanguri, Jianjiong Gao, and Sohrab P Shah. Harnessing multimodal data integration to advance precision oncology. *Nature Reviews Cancer*, pages 1–13, 2021.
- [414] Wei Shao, Tongxin Wang, Liang Sun, Tianhan Dong, Zhi Han, Zhi Huang, Jie Zhang, Daoqiang Zhang, and Kun Huang. Multi-task multimodal learning for joint diagnosis and prognosis of human cancers. *Medical Image Analysis*, 65:101795, 2020.
- [415] Zhiqin Wang, Ruiqing Li, Minghui Wang, and Ao Li. Gpbn: deep bilinear network integrating both genomic data and pathological images for breast cancer prognosis prediction. *Bioinformatics*, 37(18):2963–2970, 2021.
- [416] Zhi Huang, Federico Bianchi, Mert Yuksekogonul, Thomas J Montine, and James Zou. A visual-language foundation model for pathology image analysis using medical twitter. *Nature Medicine*, pages 1–10, 2023.
- [417] Wisdom Oluchi Ikezogwo, Mehmet Saygin Seyfioglu, Fatemeh Ghezloo, Dylan Stefan Chan Geva, Fatwir Sheikh Mohammed, Pavan Kumar Anand, Ranjay Krishna, and Linda Shapiro. Quilt-1m: One million image-text pairs for histopathology. *arXiv preprint arXiv:2306.11207*, 2023.
- [418] Linhao Qu, Xiaoyuan Luo, Kexue Fu, Manning Wang, and Zhijian Song. The rise of ai language pathologists: Exploring two-level prompt learning for few-shot weakly-supervised whole slide image classification. *Conference on Computer Vision and Pattern Recognition (CVPR)*, 2023.
- [419] Ming Y. Lu, Bowen Chen, Andrew Zhang, Drew F. K. Williamson, Richard J. Chen, Tong Ding, Long Phi Le, Yung-Sung Chuang, and Faisal Mahmood. Visual language pretrained multiple instance zero-shot transfer for histopathology images. In *Proceedings of the IEEE/CVF Conference on Computer Vision and Pattern Recognition (CVPR)*, pages 19764–19775, June 2023.
- [420] Yann LeCun, Yoshua Bengio, and Geoffrey Hinton. Deep learning. *Nature*, 521(7553):436–444, 2015.
- [421] Abdullah-Al Nahid, Mohamad Ali Mehrabi, and Yinan Kong. Histopathological breast cancer image classification by deep neural network techniques guided by local clustering. *BioMed research interna-*

- tional*, 2018, 2018.
- [422] Zizhao Zhang, Pingjun Chen, Mason McGough, Fuyong Xing, Chunbao Wang, Marilyn Bui, Yuanpu Xie, Manish Sapkota, Lei Cui, Jasreman Dhillon, et al. Pathologist-level interpretable whole-slide cancer diagnosis with deep learning. *Nature Machine Intelligence*, 1(5):236–245, 2019.
- [423] Hongdou Yao, Xuejie Zhang, Xiaobing Zhou, and Shengyan Liu. Parallel structure deep neural network using cnn and rnn with an attention mechanism for breast cancer histology image classification. *Cancers*, 11(12):1901, 2019.
- [424] Bolei Xu, Jingxin Liu, Xianxu Hou, Bozhi Liu, Jon Garibaldi, Ian O Ellis, Andy Green, Linlin Shen, and Guoping Qiu. Look, investigate, and classify: a deep hybrid attention method for breast cancer classification. In *IEEE International Symposium on Biomedical Imaging*, pages 914–918. IEEE, 2019.
- [425] Patricia Raciti, Jillian Sue, Rodrigo Ceballos, Ran Godrich, Jeremy D Kunz, Supriya Kapur, Victor Reuter, Leo Grady, Christopher Kanan, David S Klimstra, et al. Novel artificial intelligence system increases the detection of prostate cancer in whole slide images of core needle biopsies. *Modern Pathology*, 33(10):2058–2066, 2020.
- [426] Aicha BenTaieb and Ghassan Hamarneh. Predicting cancer with a recurrent visual attention model for histopathology images. In *International Conference on Medical Image Computing and Computer-Assisted Intervention*, pages 129–137. Springer, 2018.
- [427] Yushan Zheng, Zhiguo Jiang, Haopeng Zhang, Fengying Xie, and Jun Shi. Tracing diagnosis paths on histopathology wsis for diagnostically relevant case recommendation. In Anne L Martel, Purang Abolmaesumi, Danail Stoyanov, Diana Mateus, and Maria A. Zuluaga, editors, *Medical Image Computing and Computer Assisted Intervention – MICCAI*, volume 12265 of *Lecture Notes in Computer Science*, pages 459–469. Springer, 2020.
- [428] Jing Qi, Girvan Burnside, Paul Charnley, and Frans Coenen. Event-based pathology data prioritisation: a study using multi-variate time series classification. In *PROCEEDINGS OF THE 13TH INTERNATIONAL JOINT CONFERENCE ON KNOWLEDGE DISCOVERY, KNOWLEDGE ENGINEERING AND KNOWLEDGE MANAGEMENT (KDIR), VOL 1.*, volume 1, pages 121–128. SCITEPRESS-Science and Technology Publications, 2021.
- [429] Bolei Xu, Jingxin Liu, Xianxu Hou, Bozhi Liu, Jon Garibaldi, Ian O Ellis, Andy Green, Linlin Shen, and Guoping Qiu. Attention by selection: A deep selective attention approach to breast cancer classification. *IEEE Transactions on Medical Imaging*, 39(6):1930–1941, 2019.
- [430] Ashish Vaswani, Noam Shazeer, Niki Parmar, Jakob Uszkoreit, Llion Jones, Aidan N Gomez, Łukasz Kaiser, and Illia Polosukhin. Attention is all you need. *Advances in neural information processing systems*, 30, 2017.
- [431] Faisal Mahmood, Daniel Borders, Richard J Chen, Gregory N McKay, Kevan J Salimian, Alexander Baras, and Nicholas J Durr. Deep adversarial training for multi-organ nuclei segmentation in histopathology images. *IEEE Transactions on Medical Imaging*, 39(11):3257–3267, 2019.
- [432] Adalberto Claudio Quiros, Roderick Murray-Smith, and Ke Yuan. Pathologygan: Learning deep representations of cancer tissue. *Journal of Machine Learning for Biomedical Imaging*, 2021(4):1–48, 2021.
- [433] Srijay Deshpande, Fayyaz Minhas, Simon Graham, and Nasir Rajpoot. Safron: Stitching across the frontier network for generating colorectal cancer histology images. *Medical Image Analysis*, 77:102337, 2022.
- [434] Hyungjoo Cho, Sungbin Lim, Gunho Choi, and Hyunseok Min. Neural stain-style transfer learning using gan for histopathological images. *arXiv preprint arXiv:1710.08543*, 2017.
- [435] Peter Leonard Schrammen, Narmin Ghaffari Laleh, Amelie Echle, Daniel Truhn, Volkmar Schulz, Titus J Brinker, Hermann Brenner, Jenny Chang-Claude, Elizabeth Alwers, Alexander Brobeil, et al. Weakly supervised annotation-free cancer detection and prediction of genotype in routine histopathology. *The Journal of Pathology*, 256(1):50–60, 2022.
- [436] Rishi R Rawat, Itzel Ortega, Preeyam Roy, Fei Sha, Darryl Shibata, Daniel Ruderman, and David B Agus. Deep learned tissue “fingerprints” classify breast cancers by er/pr/her2 status from h&e images. *Scientific Reports*, 10(1):1–13, 2020.
- [437] Amal Lahiani, Jacob Gildenblat, Irina Klaman, Shadi Albarqouni, Nassir Navab, and Eldad Klaiman. Virtualization of tissue staining in digital pathology using an unsupervised deep learning approach. In *European Congress on Digital Pathology*, pages 47–55. Springer, 2019.
- [438] Amal Lahiani, Nassir Navab, Shadi Albarqouni, and Eldad Klaiman. Perceptual embedding consistency for seamless reconstruction of tile-wise style transfer. In *International Conference on Medical Image Computing and Computer-Assisted Intervention*, pages 568–576. Springer, 2019.
- [439] Thomas E Tavalara, M Khalid Khan Niazi, Vidya Arole, Wei Chen, Wendy Frankel, and Metin N Gurcan. A modular cgan classification framework: Application to colorectal tumor detection. *Scientific Reports*, 9(1):1–8, 2019.
- [440] Bo Hu, Ye Tang, I Eric, Chao Chang, Yubo Fan, Maode Lai, and Yan Xu. Unsupervised learning for cell-level visual representation in histopathology images with generative adversarial networks. *IEEE Journal of Biomedical and Health Informatics*, 23(3):1316–1328, 2018.
- [441] Zhaoyang Xu, Carlos Fernández Moro, Béla Bozóky, and Qianni Zhang. Gan-based virtual re-staining: a promising solution for whole slide image analysis. *arXiv preprint arXiv:1901.04059*, 2019.
- [442] Shahira Abousamra, Rajarsi Gupta, Tahsin Kurc, Dimitris Samaras, Joel Saltz, and Chao Chen. Topology-guided multi-class cell context generation for digital pathology. In *Proceedings of the IEEE/CVF Conference on Computer Vision and Pattern Recognition (CVPR)*, pages 3323–3333, 2023.
- [443] Marco Aversa, Gabriel Nobis, Miriam Hägele, Kai Standvoss, Mihaela Chirica, Roderick Murray-Smith, Ahmed Alaa, Lukas Ruff, Daniela Ivanova, Wojciech Samek, et al. Diffinfinite: Large mask-image synthesis via parallel random patch diffusion in histopathology. *arXiv preprint arXiv:2306.13384*, 2023.
- [444] Abhijeet Patil, Dipesha Tamboli, Swati Meena, Deepak Anand, and Amit Sethi. Breast cancer histopathology image classification and localization using multiple instance learning. In *IEEE International WIE Conference on Electrical and Computer Engineering (WIECON-ECE)*, pages 1–4. IEEE, 2019.
- [445] Caner Mercan, Selim Aksoy, Ezgi Mercan, Linda G Shapiro, Donald L Weaver, and Joann G Elmore. Multi-instance multi-label learning for multi-class classification of whole slide breast histopathology images. *IEEE Transactions on Medical Imaging*, 37(1):316–325, 2017.
- [446] Shujun Wang, Yaxi Zhu, Lequan Yu, Hao Chen, Huangjing Lin, Xiangbo Wan, Xijuan Fan, and Pheng-Ann Heng. Rmdl: Recalibrated multi-instance deep learning for whole slide gastric image classification. *Medical Image Analysis*, 58:101549, 2019.
- [447] Yan Xu, Tao Mo, Qiwei Feng, Peilin Zhong, Maode Lai, I Eric, and Chao Chang. Deep learning of feature representation with multiple instance learning for medical image analysis. In *IEEE International Conference on Acoustics, Speech and Signal Processing (ICASSP)*, pages 1626–1630. IEEE, 2014.
- [448] Yan Xu, Yesu Li, Zhengyang Shen, Ziwei Wu, Teng Gao, Yubo Fan, Maode Lai, I Eric, and Chao Chang. Parallel multiple instance learning for extremely large histopathology image analysis. *BMC bioinformatics*, 18(1):1–15, 2017.
- [449] Jiayun Li, Wenyuan Li, Arkadiusz Gertych, Beatrice S. Knudsen, William Speier, and Corey W. Arnold. An attention-based multi-resolution model for prostate whole slide image classification and localization. *ArXiv*, abs/1905.13208, 2019.
- [450] Asfand Yaar, Amina Asif, Shan E Ahmed Raza, Nasir Rajpoot, and Fayyaz Minhas. Cross-domain knowledge transfer for prediction of chemosensitivity in ovarian cancer patients. In *IEEE/CVF Conference on Computer Vision and Pattern Recognition Workshops*, pages 928–929.
- [451] Marvin Lerousseau, Maria Vakalopoulou, Marion Classe, Julien Adam, Enzo Battistella, Alexandre Carré, Théo Estienne, Théophraste Henry, Eric Deutsch, and Nikos Paragios. Weakly supervised multiple instance learning histopathological tumor segmentation. In *International Conference on Medical Image Computing and Computer-Assisted Intervention*, pages 470–479. Springer, 2020.
- [452] Philip Chikontwe, Meejeong Kim, Soo Jeong Nam, Heounjeong Go, and Sang Hyun Park. Multiple instance learning with center embeddings for histopathology classification. In *International Conference on Medical Image Computing and Computer-Assisted Intervention*, pages 519–528. Springer, 2020.
- [453] Jiawen Yao, Xinliang Zhu, Jitendra Jonnagaddala, Nicholas Hawkins, and Junzhou Huang. Whole slide images based cancer survival prediction using attention guided deep multiple instance learning networks. *Medical Image Analysis*, 65:101789, 2020.

- [454] Ming Y Lu, Richard J Chen, Dehan Kong, Jana Lipkova, Rajendra Singh, Drew FK Williamson, Tiffany Y Chen, and Faisal Mahmood. Federated learning for computational pathology on gigapixel whole slide images. *Medical Image Analysis*, 76:102298, 2022.
- [455] Ming Y Lu, Tiffany Y Chen, Drew FK Williamson, Melissa Zhao, Maha Shady, Jana Lipkova, and Faisal Mahmood. Ai-based pathology predicts origins for cancers of unknown primary. *Nature*, 594(7861):106–110, 2021.
- [456] Robert Jewsbury, Abhir Bhalerao, and Nasir M Rajpoot. A quadtree image representation for computational pathology. In *IEEE/CVF International Conference on Computer Vision*, pages 648–656, 2021.
- [457] Abtin Riasatian, Morteza Babaie, Danial Maleki, Shivam Kalra, Mojtaba Valipour, Sobhan Hemati, Mani Zaveri, Amir Safarpour, Sobhan Shafiei, Mehdi Afshari, et al. Fine-tuning and training of densenet for histopathology image representation using tcga diagnostic slides. *Medical Image Analysis*, 70:102032, 2021.
- [458] Anabik Pal, Zhiyun Xue, Kanan Desai, Adekunbiola Aina F Banjo, Clement Akinfolarin Adepiti, L Rodney Long, Mark Schiffman, and Sameer Antani. Deep multiple-instance learning for abnormal cell detection in cervical histopathology images. *Computers in Biology and Medicine*, 138:104890, 2021.
- [459] Christophe AC Freyre, Stephan Spiegel, Caroline Gubser Keller, Marc Vandemeulebroecke, Holger Hoeffling, Valerie Dubost, Emre Cörek, Pierre Moulin, and Imtiaz Hossain. Biomarker-based classification and localization of renal lesions using learned representations of histology—a machine learning approach to histopathology. *Toxicologic Pathology*, 49(4):798–814, 2021.
- [460] Niccolò Marini, Sebastian Otálora, Francesco Ciompi, Gianmaria Silvello, Stefano Marchesin, Simona Vatrano, Genziana Buttafuoco, Manfred Atzori, and Henning Müller. Multi-scale task multiple instance learning for the classification of digital pathology images with global annotations. In *MICCAI Workshop on Computational Pathology*, pages 170–181. PMLR, 2021.
- [461] Johannes Höhne, Jacob de Zoete, Arndt A Schmitz, Tricia Bal, Emmanuelle di Tomaso, and Matthias Lenga. Detecting genetic alterations in braf and ntrk as oncogenic drivers in digital pathology images: towards model generalization within and across multiple thyroid cohorts. In *MICCAI Workshop on Computational Pathology*, pages 105–116. PMLR, 2021.
- [462] Deepak Anand, Kumar Yashashwi, Neeraj Kumar, Swapnil Rane, Peter H Gann, and Amit Sethi. Weakly supervised learning on unannotated h&e-stained slides predicts braf mutation in thyroid cancer with high accuracy. *The Journal of Pathology*, 255(3):232–242, 2021.
- [463] Zhuchen Shao, Hao Bian, Yang Chen, Yifeng Wang, Jian Zhang, Xiangyang Ji, et al. Transmil: Transformer based correlated multiple instance learning for whole slide image classification. *Advances in Neural Information Processing Systems*, 34:2136–2147, 2021.
- [464] Kailu Li, Ziniu Qian, Yingnan Han, Eric I-Chao Chang, Bingzheng Wei, Maode Lai, Jing Liao, Yubo Fan, and Yan Xu. Weakly supervised histopathology image segmentation with self-attention. *Med. Image Anal.*, 86(102791):102791, 2023.
- [465] Fei Li, Mingyu Wang, Bin Huang, Xiaoyu Duan, Zhuya Zhang, Ziyin Ye, and Bingsheng Huang. Patients and slides are equal: A multi-level multi-instance learning framework for pathological image analysis. In *International Conference on Medical Image Computing and Computer-Assisted Intervention*, pages 63–71. Springer, 2023.
- [466] Ramin Nakhli, Allen Zhang, Ali Mirabadi, Katherine Rich, Maryam Asadi, Blake Gilks, Hossein Farahani, and Ali Bashashati. Co-pilot: Dynamic top-down point cloud with conditional neighborhood aggregation for multi-gigapixel histopathology image representation. In *Proceedings of the IEEE/CVF International Conference on Computer Vision (ICCV)*, pages 21063–21073, October 2023.
- [467] Syed Farhan Abbas, Trinh Thi Le Vuong, Kyungeun Kim, Boram Song, and Jin Tae Kwak. Multi-cell type and multi-level graph aggregation network for cancer grading in pathology images. *Medical Image Analysis*, 90(102936):102936, 2023.
- [468] Jaewon Lee, Keunho Byeon, and Jin Tae Kwak. Centroid-aware feature recalibration for cancer grading in pathology images. In *International Conference on Medical Image Computing and Computer-Assisted Intervention*, pages 212–221. Springer, 2023.
- [469] Puria Azadi, Jonathan Suderman, Ramin Nakhli, Katherine Rich, Maryam Asadi, Sonia Kung, Htoo Oo, Mira Keyes, Hossein Farahani, Calum MacAulay, Larry Goldenberg, Peter Black, and Ali Bashashati. ALL-IN: A local GLOBal graph-based DISTillation model for representation learning of gigapixel histopathology images with application in cancer risk assessment. In *Lecture Notes in Computer Science*, pages 765–775. Springer Nature Switzerland, Cham, 2023.
- [470] Ramin Nakhli, Puria Azadi Moghadam, Haoyang Mi, Hossein Farahani, Alexander Baras, Blake Gilks, and Ali Bashashati. Sparse multi-modal graph transformer with shared-context processing for representation learning of giga-pixel images. In *2023 IEEE/CVF Conference on Computer Vision and Pattern Recognition (CVPR)*. IEEE, 2023.
- [471] Gabriele Campanella, Vitor Werneck Krauss Silva, and Thomas J Fuchs. Terabyte-scale deep multiple instance learning for classification and localization in pathology. *arXiv preprint arXiv:1805.06983*, 2018.
- [472] Hongrun Zhang, Yanda Meng, Yitian Zhao, Yihong Qiao, Xiaoyun Yang, Sarah E Coupland, and Yalin Zheng. Dtd-mil: Double-tier feature distillation multiple instance learning for histopathology whole slide image classification. In *Proceedings of the IEEE/CVF Conference on Computer Vision and Pattern Recognition*, pages 18802–18812, 2022.
- [473] Raia Hadsell, Sumit Chopra, and Yann LeCun. Dimensionality reduction by learning an invariant mapping. In *IEEE Computer Society Conference on Computer Vision and Pattern Recognition (CVPR'06)*, volume 2, pages 1735–1742. IEEE, 2006.
- [474] Florian Schroff, Dmitry Kalenichenko, and James Philbin. Facenet: A unified embedding for face recognition and clustering. In *IEEE Conference on Computer Vision and Pattern Recognition*, pages 815–823, 2015.
- [475] Manuel Tran, Sophia J. Wagner, Melanie Boxberg, and Tingying Peng. S5cl: Unifying fully-supervised, self-supervised, and semi-supervised learning through hierarchical contrastive learning. In Linwei Wang, Qi Dou, P. Thomas Fletcher, Stefanie Speidel, and Shuo Li, editors, *Medical Image Computing and Computer Assisted Intervention – MICCAI 2022*, pages 99–108, Cham, 2022. Springer Nature Switzerland.
- [476] Jacob Carse, Frank Carey, and Stephen McKenna. Unsupervised representation learning from pathology images with multi-directional contrastive predictive coding. In *IEEE International Symposium on Biomedical Imaging*, pages 1254–1258. IEEE, 2021.
- [477] Muhammad Dawood, Kim Branson, Nasir M Rajpoot, and Fayyaz Minhas. Albrt: Cellular composition prediction in routine histology images. In *IEEE/CVF International Conference on Computer Vision*, pages 664–673, 2021.
- [478] Chao Feng, Chad Vanderbilt, and Thomas Fuchs. Nuc2vec: Learning representations of nuclei in histopathology images with contrastive loss. In *Medical Imaging with Deep Learning*, pages 179–189. PMLR, 2021.
- [479] Jiawei Yang, Hanbo Chen, Jiangpeng Yan, Xiaoyu Chen, and Jianhua Yao. Towards better understanding and better generalization of few-shot classification in histology images with contrastive learning. *arXiv preprint arXiv:2202.09059*, 2022.
- [480] Cheng Jiang, Xinhai Hou, Akhil Kondepudi, Asadur Chowdury, Christian W. Freudiger, Daniel A. Orringer, Honglak Lee, and Todd C. Hollon. Hierarchical discriminative learning improves visual representations of biomedical microscopy. In *Proceedings of the IEEE/CVF Conference on Computer Vision and Pattern Recognition (CVPR)*, pages 19798–19808, June 2023.
- [481] Jacob Gildenblat, Anil Yüce, Samaneh Abbasi-Sureshjani, and Konstanty Korski. Deep cellular embeddings: An explainable plug and play improvement for feature representation in histopathology. In *Proceedings of the International Conference on Medical Image Computing and Computer Assisted Intervention (MICCAI)*, October 2023.
- [482] Hritam Basak and Zhaozheng Yin. Pseudo-label guided contrastive learning for semi-supervised medical image segmentation. In *Proceedings of the IEEE/CVF Conference on Computer Vision and Pattern Recognition (CVPR)*, pages 19786–19797, June 2023.
- [483] Okyaz Eminaga, Mahmoud Abbas, Christian Kunder, Andreas M Loening, Jeanne Shen, James D Brooks, Curtis P Langlotz, and Daniel L Rubin. Plexus convolutional neural network (plexusnet): A novel neural network architecture for histologic image analysis. *arXiv preprint arXiv:1908.09067*, 2019.
- [484] Jie Hao, Sai Chandra Kosaraju, Nelson Zange Tsaku, Dae Hyun Song, and Mingon Kang. Page-net: interpretable and integrative deep learning for survival analysis using histopathological images and genomic data. In *Pacific Symposium on Biocomputing*, pages 355–366. World Scientific, 2019.

- [485] Ting-An Yen, Hung-Chun Hsu, Pushpak Pati, Maria Gabrani, Antonio Foncubierta-Rodríguez, and Pau-Choo Chung. NINEPINS: Nuclei instance segmentation with point annotations. *arXiv preprint arXiv:2006.13556*, 2020.
- [486] Sheyang Tang, Mahdi S Hosseini, Lina Chen, Sonal Varma, Corwyn Rowsell, Savvas Damaskinos, Konstantinos N Plataniotis, and Zhou Wang. Probeable darts with application to computational pathology. In *IEEE/CVF International Conference on Computer Vision*, pages 572–581, 2021.
- [487] Edgar Galván and Peter Mooney. Neuroevolution in deep neural networks: Current trends and future challenges. *IEEE Transactions on Artificial Intelligence*, 2(6):476–493, 2021.
- [488] Yuqiao Liu, Yanan Sun, Bing Xue, Mengjie Zhang, Gary G Yen, and Kay Chen Tan. A survey on evolutionary neural architecture search. *IEEE transactions on neural networks and learning systems*, 2021.
- [489] Prasanna Balaprakash, Romain Egele, Misha Salim, Stefan Wild, Venkatesh Vishwanath, Fangfang Xia, Tom Brettin, and Rick Stevens. Scalable reinforcement-learning-based neural architecture search for cancer deep learning research. In *International Conference for High Performance Computing, Networking, Storage and Analysis*, pages 1–33, 2019.
- [490] David H Wolpert and William G Macready. No free lunch theorems for optimization. *IEEE transactions on evolutionary computation*, 1(1):67–82, 1997.
- [491] Stavros P Adam, Stamatios-Aggelos N Alexandropoulos, Panos M Pardalos, and Michael N Vrahatis. No free lunch theorem: A review. *Approximation and optimization*, pages 57–82, 2019.
- [492] Narmin Ghaffari Laleh, Hannah Sophie Muti, Chiara Maria Lavinia Loeffler, Amelie Ehle, Oliver Lester Saldanha, Faisal Mahmood, Ming Y Lu, Christian Trautwein, Rupert Langer, Bastian Dislich, et al. Benchmarking weakly-supervised deep learning pipelines for whole slide classification in computational pathology. *Medical image analysis*, 79:102474, 2022.
- [493] Richard Chen, Yating Jing, and Hunter Jackson. Identifying metastases in sentinel lymph nodes with deep convolutional neural networks. *arXiv preprint arXiv:1608.01658*, 2016.
- [494] Forrest N. Iandola, Song Han, Matthew W. Moskewicz, Khalid Ashraf, William J. Dally, and Kurt Keutzer. SqueezeNet: AlexNet-level accuracy with 50x fewer parameters and <0.5mb model size. *arXiv preprint arXiv:1602.07360*, 2016.
- [495] Laith Alzubaidi, Omran Al-Shamma, Mohammed A Fadhel, Laith Farhan, Jinglan Zhang, and Ye Duan. Optimizing the performance of breast cancer classification by employing the same domain transfer learning from hybrid deep convolutional neural network model. *Electronics*, 9(3):445, 2020.
- [496] Mai Bui Huynh Thuy and Vinh Truong Hoang. Fusing of deep learning, transfer learning and GAN for breast cancer histopathological image classification. In *International Conference on Computer Science, Applied Mathematics and Applications*, pages 255–266. Springer, 2019.
- [497] Amirhossein Kiani, Bora Uyumazturk, Pranav Rajpurkar, Alex Wang, Rebecca Gao, Erik Jones, Yifan Yu, Curtis P Langlotz, Robyn L Ball, Thomas J Montine, et al. Impact of a deep learning assistant on the histopathologic classification of liver cancer. *NPJ Digital Medicine*, 3(1):1–8, 2020.
- [498] Nicolas Coudray, Paolo Santiago Ocampo, Theodore Sakellaropoulos, Navneet Narula, Matija Snuderl, David Fenyó, Andre L Moreira, Narges Razavian, and Aristotelis Tsirigos. Classification and mutation prediction from non-small cell lung cancer histopathology images using deep learning. *Nature medicine*, 24(10):1559–1567, 2018.
- [499] Stan Benjamins, Pranavsingh Dhunoo, and Bertalan Meskó. The state of artificial intelligence-based fda-approved medical devices and algorithms: an online database. *NPJ Digital Medicine*, 3(1):1–8, 2020.
- [500] Alec Radford, Jong Wook Kim, Chris Hallacy, Aditya Ramesh, Gabriel Goh, Sandhini Agarwal, Girish Sastry, Amanda Askell, Pamela Mishkin, Jack Clark, et al. Learning transferable visual models from natural language supervision. In *International conference on machine learning*, pages 8748–8763. PMLR, 2021.
- [501] Xiaohua Zhai, Xiao Wang, Basil Mustafa, Andreas Steiner, Daniel Keyser, Alexander Kolesnikov, and Lucas Beyer. Lit: Zero-shot transfer with locked-image text tuning. In *Proceedings of the IEEE/CVF Conference on Computer Vision and Pattern Recognition*, pages 18123–18133, 2022.
- [502] Amanpreet Singh, Ronghang Hu, Vedanuj Goswami, Guillaume Couairon, Wojciech Galuba, Marcus Rohrbach, and Douwe Kiela. Flava: A foundational language and vision alignment model. In *Proceedings of the IEEE/CVF Conference on Computer Vision and Pattern Recognition*, pages 15638–15650, 2022.
- [503] Michiel Bakker, Martin Chadwick, Hannah Sheahan, Michael Tessler, Lucy Campbell-Gillingham, Jan Balaguer, Nat McAleese, Amelia Glaese, John Aslanides, Matt Botvinick, and Christopher Summerfield. Fine-tuning language models to find agreement among humans with diverse preferences. In S. Koyejo, S. Mohamed, A. Agarwal, D. Belgrave, K. Cho, and A. Oh, editors, *Advances in Neural Information Processing Systems*, volume 35, pages 38176–38189. Curran Associates, Inc., 2022.
- [504] Alexey Dosovitskiy, German Ros, Felipe Codevilla, Antonio Lopez, and Vladlen Koltun. Carla: An open urban driving simulator. In *Conference on robot learning*, pages 1–16. PMLR, 2017.
- [505] Steve Borkman, Adam Crespi, Saurav Dhakad, Sujoy Ganguly, Jonathan Hogins, You-Cyuan Jhang, Mohsen Kamalzadeh, Bowen Li, Steven Leal, Pete Parisi, et al. Unity perception: Generate synthetic data for computer vision. *arXiv preprint arXiv:2107.04259*, 2021.
- [506] Viktor Makoviychuk, Lukasz Wawrzyniak, Yunrong Guo, Michelle Lu, Kier Storey, Miles Macklin, David Hoeller, Nikita Rudin, Arthur Allshire, Ankur Handa, et al. Isaac gym: High performance gpu-based physics simulation for robot learning. *arXiv preprint arXiv:2108.10470*, 2021.
- [507] Gregory Griffin, Alex Holub, and Pietro Perona. Caltech-256 object category dataset. 2007.
- [508] Alex Krizhevsky, Ilya Sutskever, and Geoffrey E Hinton. Imagenet classification with deep convolutional neural networks. *Advances in neural information processing systems*, 25, 2012.
- [509] Guansong Pang, Chunhua Shen, Longbing Cao, and Anton Van Den Hengel. Deep learning for anomaly detection: A review. *ACM Comput. Surv.*, 54(2), mar 2021.
- [510] Mahdi S Hosseini, Lyndon Chan, Weimin Huang, Yichen Wang, Daniah Hasan, Corwyn Rowsell, Savvas Damaskinos, and Konstantinos N Plataniotis. On transferability of histological tissue labels in computational pathology. In *European Conference on Computer Vision*, pages 453–469. Springer, 2020.
- [511] Yuchen Lu and Peng Xu. Anomaly detection for skin disease images using variational autoencoder. *CoRR*, abs/1807.01349, 2018.
- [512] Andre Esteva, Brett Kuprel, Roberto A Novoa, Justin Ko, Susan M Swetter, Helen M Blau, and Sebastian Thrun. Dermatologist-level classification of skin cancer with deep neural networks. *nature*, 542(7639):115–118, 2017.
- [513] Dimitris K Iakovidis, Spiros V Georgakopoulos, Michael Vasilakakis, Anastasios Koulaouzidis, and Vassilis P Plagianakos. Detecting and locating gastrointestinal anomalies using deep learning and iterative cluster unification. *IEEE Transactions on Medical Imaging*, 37(10):2196–2210, 2018.
- [514] CAMELYON16 ISBI challenge on cancer metastasis detection in lymph node. Available at: <https://camelyon16.grand-challenge.org/> (accessed June 11, 2021), 2016.
- [515] Qi Qi, Yanlong Li, Jitian Wang, Han Zheng, Yue Huang, Xinghao Ding, and Gustavo Kunde Rohde. Label-efficient breast cancer histopathological image classification. *IEEE Journal of Biomedical and Health Informatics*, 23(5):2108–2116, 2018.
- [516] Mathilde Caron, Hugo Touvron, Ishan Misra, Hervé Jégou, Julien Mairal, Piotr Bojanowski, and Armand Joulin. Emerging properties in self-supervised vision transformers. In *Proceedings of the IEEE/CVF international conference on computer vision*, pages 9650–9660, 2021.
- [517] Chen Sun, Abhinav Shrivastava, Saurabh Singh, and Abhinav Gupta. Revisiting unreasonable effectiveness of data in deep learning era. In *Proceedings of the IEEE international conference on computer vision*, pages 843–852, 2017.
- [518] Alhanoof Althnani, Duaa AlSaeed, Heyam Al-Baity, Amani Samha, Alanoud Bin Dris, Najla Alzakari, Afnan Abou Elwafa, and Heba Kurdi. Impact of dataset size on classification performance: an empirical evaluation in the medical domain. *Applied Sciences*, 11(2):796, 2021.
- [519] Alireza Abdollahi, Hiva Saffar, and Hana Saffar. Types and frequency of errors during different phases of testing at a clinical medical laboratory of a teaching hospital in tehran, iran. *North American journal of medical sciences*, 6(5):224, 2014.
- [520] Frederick A Meier, Ruan C Varney, and Richard J Zarbo. Study of

- amended reports to evaluate and improve surgical pathology processes. *Advances in anatomic pathology*, 18(5):406–413, 2011.
- [521] Teresa P Darcy, Samuel P Barasch, Rhona J Souers, and Peter L Perrotta. Test cancellation: a college of american pathologists q-probes study. *Archives of pathology & laboratory medicine*, 140(2):125–129, 2016.
- [522] Raouf E Nakhleh. A prelude to error reduction in anatomic pathology. *American journal of clinical pathology*, 124(4):489–490, 2005.
- [523] Raouf E Nakhleh. Error reduction in surgical pathology. *Archives of pathology & laboratory medicine*, 130(5):630–632, 2006.
- [524] Raouf E Nakhleh. Patient safety and error reduction in surgical pathology. *Archives of pathology & laboratory medicine*, 132(2):181–185, 2008.
- [525] Raouf E Nakhleh, Vania Nosé, Carol Colasacco, Lisa A Fatheree, Tamara J Lillemo, Douglas C McCrory, Frederick A Meier, Christopher N Otis, Scott R Owens, Stephen S Raab, et al. Interpretive diagnostic error reduction in surgical pathology and cytology: guideline from the college of american pathologists pathology and laboratory quality center and the association of directors of anatomic and surgical pathology. *Archives of Pathology & Laboratory Medicine*, 140(1):29–40, 2016.
- [526] Raouf E Nakhleh. Role of informatics in patient safety and quality assurance. *Surgical Pathology Clinics*, 8(2):301–307, 2015.
- [527] Anobel Y Odisho, Briton Park, Nicholas Altieri, John DeNero, Matthew R Cooperberg, Peter R Carroll, and Bin Yu. Natural language processing systems for pathology parsing in limited data environments with uncertainty estimation. *JAMIA open*, 3(3):431–438, 2020.
- [528] Pilar López-Úbeda, Teodoro Martín-Noguerol, José Aneiros-Fernández, and Antonio Luna. Natural language processing in pathology: Current trends and future insights. *The American Journal of Pathology*, 2022.
- [529] Yoojoong Kim, Jeong Hyeon Lee, Sunho Choi, Jeong Moon Lee, Jong-Ho Kim, Junhee Seok, and Hyung Joon Joo. Validation of deep learning natural language processing algorithm for keyword extraction from pathology reports in electronic health records. *Scientific reports*, 10(1):1–9, 2020.
- [530] John X Qiu, Hong-Jun Yoon, Paul A Fearn, and Georgia D Tourassi. Deep learning for automated extraction of primary sites from cancer pathology reports. *IEEE journal of biomedical and health informatics*, 22(1):244–251, 2017.
- [531] Amir R Zamir, Alexander Sax, William Shen, Leonidas J Guibas, Jitendra Malik, and Silvio Savarese. Taskonomy: Disentangling task transfer learning. In *Proceedings of the IEEE conference on computer vision and pattern recognition*, pages 3712–3722, 2018.
- [532] Yu Zhang and Qiang Yang. A survey on multi-task learning. *IEEE Transactions on Knowledge and Data Engineering*, 2021.
- [533] Keith Bonawitz, Hubert Eichner, Wolfgang Grieskamp, Dzmityr Huba, Alex Ingerman, Vladimir Ivanov, Chloe Kiddon, Jakub Konečný, Stefano Mazzocchi, Brendan McMahan, et al. Towards federated learning at scale: System design. *Proceedings of machine learning and systems*, 1:374–388, 2019.
- [534] Peter Kairouz, H Brendan McMahan, Brendan Avent, Aurélien Bellet, Mehdi Bennis, Arjun Nitin Bhagoji, Kallista Bonawitz, Zachary Charles, Graham Cormode, Rachel Cummings, et al. Advances and open problems in federated learning. *Foundations and Trends® in Machine Learning*, 14(1–2):1–210, 2021.
- [535] Bastiaan S. Veeling, Jasper Linmans, Jim Winkens, Taco Cohen, and Max Welling. Rotation equivariant cnns for digital pathology. In Alejandro F. Frangi, Julia A. Schnabel, Christos Davatzikos, and Carlos Alberola-López, editors, *Medical Image Computing and Computer Assisted Intervention – MICCAI*, volume 11071 of *Lecture Notes in Computer Science*, pages 210–218. Springer, 2018.
- [536] Peter J Schüffler, Luke Geneslaw, D Vijay K Yarlagadda, Matthew G Hanna, Jennifer Samboy, Evangelos Stamelos, Chad Vanderbilt, John Philip, Marc-Henri Jean, Lorraine Corsale, et al. Integrated digital pathology at scale: A solution for clinical diagnostics and cancer research at a large academic medical center. *Journal of the American Medical Informatics Association*, 28(9):1874–1884, 2021.
- [537] Matthew G Hanna, Victor E Reuter, Meera R Hameed, Lee K Tan, Sarah Chiang, Carlie Sigel, Travis Hollmann, Dilip Giri, Jennifer Samboy, Carlos Moradel, et al. Whole slide imaging equivalency and efficiency study: experience at a large academic center. *Modern Pathology*, 32(7):916–928, 2019.
- [538] Matthew G Hanna, Victor E Reuter, Jennifer Samboy, Christine Eng-land, Lorraine Corsale, Samson W Fine, Narasimhan P Agaram, Evangelos Stamelos, Yukako Yagi, Meera Hameed, et al. Implementation of digital pathology offers clinical and operational increase in efficiency and cost savings. *Archives of pathology & laboratory medicine*, 143(12):1545–1555, 2019.
- [539] Jonhan Ho, Stefan M Ahlers, Curtis Stratman, Orly Aridor, Liron Pantanowitz, Jeffrey L Fine, John A Kuzmishin, Michael C Montalto, and Anil V Parwani. Can digital pathology result in cost savings? a financial projection for digital pathology implementation at a large integrated health care organization. *Journal of pathology informatics*, 5(1):33, 2014.
- [540] Rudenko Ekaterina Evgenievna, Demura Tatiana Alexandrovna, Vekhova Ksenia Andreevna, Lobanova Olga Andreevna, Yumashva Valentina Alekseevna, Zhakota Dmitrii Anatolevich, Anoshkin Kirill, Remez Alexey, Untesco Maksim, Kroman Nikolay, et al. Analysis of the three-year work of a digital pathomorphological laboratory built from the ground. *Journal of Pathology Informatics*, 13:100111, 2022.
- [541] Shidan Wang, Tao Wang, Lin Yang, Donghan M Yang, Junya Fujimoto, Faliu Yi, Xin Luo, Yikun Yang, Bo Yao, Shin Yi Lin, et al. Convpath: A software tool for lung adenocarcinoma digital pathological image analysis aided by a convolutional neural network. *EBioMedicine*, 50:103–110, 2019.
- [542] Mike Isaacs, Jochen K Lennerz, Stacey Yates, Walter Clermont, Joan Rossi, and John D Pfeifer. Implementation of whole slide imaging in surgical pathology: A value added approach. *Journal of Pathology Informatics*, 2(1):39, 2011.
- [543] Guy Pare, Julien Meyer, Marie-Claude Trudel, and Bernard Tetu. Impacts of a large decentralized telepathology network in canada. *Telematics and e-Health*, 22(3):246–250, 2016.
- [544] Sten Thorstenson, Jesper Molin, and Claes Lundström. Implementation of large-scale routine diagnostics using whole slide imaging in sweden: Digital pathology experiences 2006-2013. *Journal of pathology informatics*, 5(1):14, 2014.
- [545] Chee Leong Cheng, Rafay Azhar, Shi Hui Adeline Sng, Yong Quan Chua, Jacqueline Siok Gek Hwang, Jennifer Poi Fun Chin, Waih Khuen Seah, Janel Chui Ling Loke, Roy Hang Leng Ang, and Puay Hoon Tan. Enabling digital pathology in the diagnostic setting: navigating through the implementation journey in an academic medical centre. *Journal of clinical pathology*, 69(9):784–792, 2016.
- [546] Nikolas Stathonikos, Mitko Veta, André Huisman, and Paul J van Diest. Going fully digital: Perspective of a dutch academic pathology lab. *Journal of pathology informatics*, 4(1):15, 2013.
- [547] Liron Pantanowitz, John H Sinard, Walter H Henricks, Lisa A Fatheree, Alexis B Carter, Lydia Contis, Bruce A Beckwith, Andrew J Evans, Avtar Lal, and Anil V Parwani. Validating whole slide imaging for diagnostic purposes in pathology: guideline from the college of american pathologists pathology and laboratory quality center. *Archives of Pathology and Laboratory Medicine*, 137(12):1710–1722, 2013.
- [548] Esther Abels and Liron Pantanowitz. Current state of the regulatory trajectory for whole slide imaging devices in the usa. *Journal of pathology informatics*, 8(1):23, 2017.
- [549] Anil V Parwani, Lewis Hassell, Eric Glassy, and Liron Pantanowitz. Regulatory barriers surrounding the use of whole slide imaging in the united states of america. *Journal of pathology informatics*, 5, 2014.
- [550] Andrew Janowczyk and Anant Madabhushi. Deep learning for digital pathology image analysis: A comprehensive tutorial with selected use cases. *Journal of Pathology Informatics*, 7, 2016.
- [551] Sivaramkrishnan Sankarapandian, Saul Kohn, Vaughn Spurrier, Sean Grullon, Rajath E Soans, Kameswari D Ayyagari, Ramachandra V Chamarthi, Kiran Motaparathi, Jason B Lee, Wonwoo Shon, et al. A pathology deep learning system capable of triage of melanoma specimens utilizing dermatopathologist consensus as ground truth. In *Proceedings of the IEEE/CVF International Conference on Computer Vision*, pages 629–638, 2021.
- [552] Saeed Alshieban and Khaled Al-Surimi. Reducing turnaround time of surgical pathology reports in pathology and laboratory medicine departments. *BMJ Open Quality*, 4(1):u209223–w3773, 2015.
- [553] Raouf E Nakhleh and Patrick L Fitzgibbons. *Quality management in anatomic pathology: promoting patient safety through systems improvement and error reduction*. College of American Pathologists, 2005.
- [554] David M Metter, Terence J Colgan, Stanley T Leung, Charles F Timmons, and Jason Y Park. Trends in the us and canadian pathologist

- workforces from 2007 to 2017. *JAMA network open*, 2(5):e194337–e194337, 2019.
- [555] Wouter Bulten, Kimmo Kartasalo, Po-Hsuan Cameron Chen, Peter Ström, Hans Pinckaers, Kunal Nagpal, Yuannan Cai, David F Steiner, Hester van Boven, Robert Vink, et al. Artificial intelligence for diagnosis and gleason grading of prostate cancer: the panda challenge. *Nature medicine*, 28(1):154–163, 2022.
- [556] Martyn Peck, David Moffat, Bruce Latham, and Tony Badrick. Review of diagnostic error in anatomical pathology and the role and value of second opinions in error prevention. *Journal of clinical pathology*, 71(11):995–1000, 2018.
- [557] John HF Smith. Cytology, liquid-based cytology and automation. *Best Practice & Research Clinical Obstetrics & Gynaecology*, 25(5):585–596, 2011.
- [558] Erin Brender, Alison Burke, and Richard M Glass. Frozen section biopsy. *Jama*, 294(24):3200–3200, 2005.
- [559] Sudha Ayyagari, Anusha Potnuru, Sk Aamer Saleem, and Pavani Marapaka. Analysis of frozen section compared to permanent section: a 2 year study in a single tertiary care hospital. *Journal of Pathology of Nepal*, 11(2):1854–1858, 2021.
- [560] Stephan W Jahn, Markus Plass, and Farid Moifar. Digital pathology: advantages, limitations and emerging perspectives. *Journal of Clinical Medicine*, 9(11):3697, 2020.
- [561] Chamidu Atupelage, Hiroshi Nagahashi, Fumikazu Kimura, Masahiro Yamaguchi, Tokiya Abe, Akinori Hashiguchi, and Michiie Sakamoto. Computational cell classification methodology for hepatocellular carcinoma. In *International Conference on Advances in ICT for Emerging Regions (ICTer)*, pages 21–27. IEEE, 2013.
- [562] Peter Bankhead, Maurice B Loughrey, José A Fernández, Yvonne Dombrowski, Darragh G McArt, Philip D Dunne, Stephen McQuaid, Ronan T Gray, Liam J Murray, Helen G Coleman, et al. Qupath: Open source software for digital pathology image analysis. *Scientific reports*, 7(1):1–7, 2017.
- [563] S Rathore, M Iftikhar, M Nasrallah, M Gurcan, N Rajpoot, and Z Mourelatos. Tmod-35. prediction of overall survival, and molecular markers in gliomas via analysis of digital pathology images using deep learning. *Neuro-oncology*, 21(Suppl 6):vi270–vi270, 2019.
- [564] Wei Wang, John A Ozolek, and Gustavo K Rohde. Detection and classification of thyroid follicular lesions based on nuclear structure from histopathology images. *Cytometry Part A: The Journal of the International Society for Advancement of Cytometry*, 77(5):485–494, 2010.
- [565] Charlotte Srykh, Arnaud Abreu, Nadia Amara, Aurore Siegfried, Véronique Maisongrosse, François X Frenois, Laurent Martin, Cédric Rossi, Camille Laurent, and Pierre Brousset. Accurate diagnosis of lymphoma on whole-slide histopathology images using deep learning. *NPJ Digital Medicine*, 3(1):1–8, 2020.
- [566] Yalu Cheng, Pengchong Qiao, Hongliang He, Guoli Song, and Jie Chen. Hard-boundary attention network for nuclei instance segmentation. In *ACM Multimedia Asia*, pages 1–7. 2021.
- [567] Blanca Maria Priego-Torres, Daniel Sanchez-Morillo, Miguel Angel Fernandez-Granero, and Marcial Garcia-Rojo. Automatic segmentation of whole-slide h&e stained breast histopathology images using a deep convolutional neural network architecture. *Expert Systems With Applications*, 151:113387, 2020.
- [568] Christophe Avenel, Anna Tolf, Anca Dragomir, and Ingrid B Carlbohm. Glandular segmentation of prostate cancer: An illustration of how the choice of histopathological stain is one key to success for computational pathology. *Frontiers in Bioengineering and Biotechnology*, 7:125, 2019.
- [569] Richard J Chen, Ming Y Lu, Jingwen Wang, Drew FK Williamson, Scott J Rodig, Neal I Lindeman, and Faisal Mahmood. Pathomic fusion: an integrated framework for fusing histopathology and genomic features for cancer diagnosis and prognosis. *IEEE Transactions on Medical Imaging*, 2020.
- [570] Goce Ristanoski, Jon Emery, Javiera Martinez Gutierrez, Damien McCarthy, and Uwe Aickelin. Handling uncertainty using features from pathology: opportunities in primary care data for developing high risk cancer survival methods. In *Australasian Computer Science Week Multiconference*, pages 1–7, 2021.
- [571] Jia-Ren Chang, Ching-Yi Lee, Chi-Chung Chen, Joachim Reischl, Talha Qaiser, and Chao-Yuan Yeh. Hybrid aggregation network for survival analysis from whole slide histopathological images. In *International Conference on Medical Image Computing and Computer-Assisted Intervention*, pages 731–740. Springer, 2021.
- [572] Fengling Li, Yongquan Yang, Yani Wei, Ping He, Jie Chen, Zhongxi Zheng, and Hong Bu. Deep learning-based predictive biomarker of pathological complete response to neoadjuvant chemotherapy from histological images in breast cancer. *Journal of translational medicine*, 19(1):1–13, 2021.
- [573] Nathalie Harder, Ralf Schönmeier, Katharina Nekolla, Armin Meier, Nicolas Brieu, Carolina Vanegas, Gabriele Madonna, Mariaelena Capone, Gerardo Botti, Paolo A Ascierto, et al. Automatic discovery of image-based signatures for ipilimumab response prediction in malignant melanoma. *Scientific Reports*, 9(1):1–19, 2019.
- [574] Anant Madabhushi, Xiangxue Wang, Cristian Barrera, and Vamsidhar Velcheti. Predicting response to immunotherapy using computer extracted features of cancer nuclei from hematoxylin and eosin (hande) stained images of non-small cell lung cancer (nslc), July 6 2021. US Patent 11,055,844.
- [575] Fang Zhang, Su Yao, Zhi Li, Changhong Liang, Ke Zhao, Yanqi Huang, Ying Gao, Jinrong Qu, Zhenhui Li, and Zaiyi Liu. Predicting treatment response to neoadjuvant chemoradiotherapy in local advanced rectal cancer by biopsy digital pathology image features. *Clinical and translational medicine*, 10(2):e110, 2020.
- [576] National Cancer Institute. Cancer stat facts: Common cancer sites. Available at: <https://seer.cancer.gov/statfacts/html/common.html> (accessed Feb 12, 2023).
- [577] Stacey A Kenfield, Esther K Wei, Meir J Stampfer, Bernard A Rosner, and Graham A Colditz. Comparison of aspects of smoking among the four histological types of lung cancer. *Tobacco control*, 17(3):198–204, 2008.
- [578] American Cancer Society. Survival rates for breast cancer. Available at: <https://www.cancer.org/cancer/breast-cancer/understanding-a-breast-cancer-diagnosis/breast-cancer-survival-rates.html> (accessed Feb 9, 2023).
- [579] Cancer Center. Bladder cancer types. Available at: <https://www.cancercenter.com/cancer-types/bladder-cancer/types> (accessed Feb 10, 2023).
- [580] American Cancer Society. Survival rates for bladder cancer. Available at: <https://www.cancer.org/cancer/bladder-cancer/detection-diagnosis-staging/survival-rates.html> (accessed Feb 10, 2023).
- [581] BK Andreassen, B Aagnes, R Gislefoss, M Andreassen, and R Wahlqvist. Incidence and survival of urothelial carcinoma of the urinary bladder in norway 1981–2014. *BMC cancer*, 16:1–11, 2016.
- [582] American Cancer Society. Liver cancer survival rates. Available at: <https://www.cancer.org/cancer/liver-cancer/detection-diagnosis-staging/survival-rates.html> (accessed Feb 10, 2023).
- [583] Zachary D Goodman. Neoplasms of the liver. *Modern Pathology*, 20:S49–S60, 2007.
- [584] LA Gloeckler Ries, JL Young, GE Keel, MP Eisner, YD Lin, MJ Horner, et al. Seer survival monograph: cancer survival among adults: Us seer program, 1988–2001, patient and tumor characteristics. *National Cancer Institute, SEER Program, NIH Pub*, 7:133–144, 2007.
- [585] National Cancer Institute. Cancer stat facts: Ovarian cancer. Available at: <https://seer.cancer.gov/statfacts/html/ovary.html> (accessed Feb 14, 2023).
- [586] American Cancer Society. Survival rates for kidney cancer. Available at: <https://www.cancer.org/cancer/kidney-cancer/detection-diagnosis-staging/survival-rates.html> (accessed Feb 9, 2023).
- [587] Donald P Bottaro and W Marston Linehan. Multifocal renal cancer: genetic basis and its medical relevance. *Clinical Cancer Research*, 11(20):7206–7208, 2005.
- [588] Victor Srougi, Raphael B Kato, Fernanda A Salvatore, Pedro PM Ayres, Marcos F Dall’Oglio, and Miguel Srougi. Incidence of benign lesions according to tumor size in solid renal masses. *International braz j urol*, 35:427–431, 2009.
- [589] American Cancer Society. Survival rates for colorectal cancer. Available at: <https://www.cancer.org/cancer/colon-rectal-cancer/detection-diagnosis-staging/survival-rates.html> (accessed Feb 9, 2023).
- [590] Andrea Remo, Matteo Fassan, Alessandro Vanoli, Luca Reggiani Bonetti, Valeria Barresi, Fabiana Tatangelo, Roberta Gafà, Guido Giordano, Massimo Pancione, Federica Grillo, et al. Morphology and molecular features of rare colorectal carcinoma histotypes. *Cancers*,

- 11(7):1036, 2019.
- [591] American Cancer Society. Survival rates for prostate cancer. Available at: <https://www.cancer.org/cancer/prostate-cancer/detection-diagnosis-staging/survival-rates.html> (accessed Feb 8, 2023).
- [592] Abul K. Abbas, Jon C. Aster, and Vinay Kumar. *Robbins and Cotran pathologic basis of disease*. Saunders/Elsevier, 2010.
- [593] American Cancer Society. Lung cancer survival rates. Available at: <https://www.cancer.org/cancer/lung-cancer/detection-diagnosis-staging/survival-rates.html> (accessed Feb 11, 2023).
- [594] World Health Organization. Cancer. Available at: <https://www.who.int/news-room/fact-sheets/detail/cancer> (accessed Feb 13, 2023).
- [595] David Clunie, Dan Hosseinzadeh, Mikael Wintell, David De Mena, Nieves Lajara, Marcial Garcia-Rojo, Gloria Bueno, Kiran Saligrama, Aaron Stearrett, David Toomey, et al. Digital imaging and communications in medicine whole slide imaging connectathon at digital pathology association pathology visions 2017. *Journal of Pathology Informatics*, 9, 2018.
- [596] Kamyar Nazeri, Azad Aminpour, and Mehran Ebrahimi. Two-stage convolutional neural network for breast cancer histology image classification. In *International Conference Image Analysis and Recognition*, pages 717–726. Springer, 2018.
- [597] Turki Turki, Anmar Al-Sharif, and Yh Taguchi. End-to-end deep learning for detecting metastatic breast cancer in axillary lymph node from digital pathology images. *medRxiv*, 2021.
- [598] Zihan Xiong, Yixuan Zheng, and Jiayue Qiu. Processing tissue microarray images using machine learning techniques as preparation for determining gleason grade of prostate cancer. In *International Conference on Bioinformatics Research and Applications*, pages 34–41, 2021.
- [599] Xiangyu Zhang, Xinyu Zhou, Mengxiao Lin, and Jian Sun. Shufflenet: An extremely efficient convolutional neural network for mobile devices. In *2018 IEEE/CVF Conference on Computer Vision and Pattern Recognition*, pages 6848–6856, 2018.
- [600] Metin N Gurcan, Anant Madabhushi, and Nasir Rajpoot. Pattern recognition in histopathological images: An icpr 2010 contest. In *International Conference on Pattern Recognition*, pages 226–234. Springer, 2010.
- [601] Liron Pantanowitz, Walter H Henricks, and Bruce A Beckwith. Medical laboratory informatics. *Clinics in laboratory medicine*, 27(4):823–843, 2007.
- [602] Priya Lakshmi Narayanan, Shan E Ahmed Raza, Allison H Hall, Jeffrey R Marks, Lorraine King, Robert B West, Lucia Hernandez, Mitch Dowsett, Barry Gusterson, Carlo Maley, et al. Unmasking the tissue microecology of ductal carcinoma in situ with deep learning. *BioRxiv*, page 812735, 2019.
- [603] Zhengfeng Lai, Chao Wang, Luca Cerny Oliveira, Brittany N Dugger, Sen-Ching Cheung, and Chen-Nee Chuah. Joint semi-supervised and active learning for segmentation of gigapixel pathology images with cost-effective labeling. In *IEEE/CVF International Conference on Computer Vision*, pages 591–600, 2021.
- [604] Mousumi Roy, Jun Kong, Satyananda Kashyap, Vito Paolo Pastore, Fusheng Wang, Ken CL Wong, and Vandana Mukherjee. Convolutional autoencoder based model histocae for segmentation of viable tumor regions in liver whole-slide images. *Scientific Reports*, 11(1):1–10, 2021.
- [605] YQ Jiang, JH Xiong, HY Li, XH Yang, WT Yu, M Gao, X Zhao, YP Ma, W Zhang, YF Guan, et al. Recognizing basal cell carcinoma on smartphone-captured digital histopathology images with a deep neural network. *British Journal of Dermatology*, 182(3):754–762, 2020.
- [606] Shidan Wang, Donghan M Yang, Ruichen Rong, Xiaowei Zhan, and Guanghua Xiao. Pathology image analysis using segmentation deep learning algorithms. *The American journal of pathology*, 189(9):1686–1698, 2019.
- [607] Hiroki Tokunaga, Yuki Teramoto, Akihiko Yoshizawa, and Ryoma Bise. Adaptive weighting multi-field-of-view cnn for semantic segmentation in pathology. In *IEEE/CVF Conference on Computer Vision and Pattern Recognition*, pages 12597–12606, 2019.
- [608] Hye Yoon Chang, Chan Kwon Jung, Junwoo Isaac Woo, Sanghun Lee, Joonyoung Cho, Sun Woo Kim, and Tae-Yeong Kwak. Artificial intelligence in pathology. *Journal of pathology and translational medicine*, 53(1):1, 2019.
- [609] Tiange Xiang, Yang Song, Chaoyi Zhang, Dongnan Liu, Mei Chen, Fan Zhang, Heng Huang, Lauren O’Donnell, and Weidong Cai. Dsnet: A dual-stream framework for weakly-supervised gigapixel pathology image analysis. *arXiv preprint arXiv:2109.05788*, 2021.
- [610] Chetan L Srinidhi and Anne L Martel. Improving self-supervised learning with hardness-aware dynamic curriculum learning: An application to digital pathology. In *IEEE/CVF International Conference on Computer Vision*, pages 562–571, 2021.
- [611] Syed Hamad Shirazi, Saeeda Naz, Muhammad Imran Razzak, Arif Iqbal Umar, and Ahmad Zaib. Automated pathology image analysis. In *Soft Computing Based Medical Image Analysis*, pages 13–29. Elsevier, 2018.
- [612] James A Diao, Jason K Wang, Wan Fung Chui, Victoria Mountain, Sai Chowdary Gullapally, Ramprakash Srinivasan, Richard N Mitchell, Benjamin Glass, Sara Hoffman, Sudha K Rao, et al. Human-interpretable image features derived from densely mapped cancer pathology slides predict diverse molecular phenotypes. *Nature communications*, 12(1):1–15, 2021.
- [613] Réka Hollandi, Ákos Diósi, Gábor Hollandi, Nikita Moshkov, and Péter Horváth. Annotatorj: an imagej plugin to ease hand annotation of cellular compartments. *Molecular biology of the cell*, 31(20):2179–2186, 2020.
- [614] Andrew H Beck, Ankur R Sangoi, Samuel Leung, Robert J Marinelli, Torsten O Nielsen, Marc J Van De Vijver, Robert B West, Matt Van De Rijn, and Daphne Koller. Systematic analysis of breast cancer morphology uncovers stromal features associated with survival. *Science translational medicine*, 3(108):108ra113–108ra113, 2011.
- [615] Prathamesh M Kulkarni, Eric J Robinson, Jaya Sarin Pradhan, Robyn D Gartrell-Corrado, Bethany R Rohr, Megan H Trager, Larisa J Geskin, Harriet M Kluger, Pok Fai Wong, Balazs Acs, et al. Deep learning based on standard h&e images of primary melanoma tumors identifies patients at risk for visceral recurrence and death. *Clinical Cancer Research*, 26(5):1126–1134, 2020.
- [616] Peizhen Xie, Ke Zuo, Yu Zhang, Fangfang Li, Mingzhu Yin, and Kai Lu. Interpretable classification from skin cancer histology slides using deep learning: A retrospective multicenter study. *arXiv preprint arXiv:1904.06156*, 2019.
- [617] Steven N Hart, William Flotte, Andrew P Norgan, Kabeer K Shah, Zachary R Buchan, Taofic Mounajjed, and Thomas J Flotte. Classification of melanocytic lesions in selected and whole-slide images via convolutional neural networks. *Journal of Pathology Informatics*, 10, 2019.
- [618] Angel Alfonso Cruz-Roa, John Edison Arevalo Ovalle, Anant Madabhushi, and Fabio Augusto González Osorio. A deep learning architecture for image representation, visual interpretability and automated basal-cell carcinoma cancer detection. pages 403–410, 2013.
- [619] Joshua J Levy, Christopher R Jackson, Aravindhan Sriharan, Brock C Christensen, and Louis J Vaickus. Preliminary evaluation of the utility of deep generative histopathology image translation at a mid-sized nci cancer center. *bioRxiv*, 2020.
- [620] Bo Tang, Ao Li, Bin Li, and Minghui Wang. Capsurv: capsule network for survival analysis with whole slide pathological images. *IEEE Access*, 7:26022–26030, 2019.
- [621] Justin Kirby. MICCAI 2014 Grand Challenges. Available at: <https://wiki.cancerimagingarchive.net/display/Public/MICCAI2014GrandChallenges> (accessed June 10, 2021).
- [622] Petteri Teikari, Marc Santos, Charissa Poon, and Kullervo Hynynen. Deep learning convolutional networks for multiphoton microscopy vasculature segmentation. *arXiv preprint arXiv:1606.02382*, 2016.
- [623] Benjamin Liechty, Zhuoran Xu, Zhilu Zhang, Cheyanne Slocum, Cagla D Bahadir, Mert R Sabuncu, and David J Pisapia. Machine learning can aid in prediction of idh mutation from h&e-stained histology slides in infiltrating gliomas. *Scientific Reports*, 12(1):22623, 2022.
- [624] Gloria Bueno, Lucia Gonzalez-Lopez, Marcial Garcia-Rojo, Arvydas Laurinavicius, and Oscar Deniz. Data for glomeruli characterization in histopathological images. *Data in brief*, 29:105314, 2020.
- [625] Michael Gadermayr, Ann-Kathrin Dombrowski, Barbara Mara Klinkhammer, Peter Boor, and Dorit Merhof. Cnn cascades for segmenting sparse objects in gigapixel whole slide images. *Computerized Medical Imaging and Graphics*, 71:40–48, 2019.
- [626] Gabriel Tjio, Xulei Yang, Jia Mei Hong, Sum Thai Wong, Vanessa Ding, Andre Choo, and Yi Su. Accurate tumor tissue region detection with accelerated deep convolutional neural networks. *arXiv preprint arXiv:2004.08552*, 2020.
- [627] Pietro Antonio Cicalese, Aryan Mobiny, Pengyu Yuan, Jan Becker,

- Chandra Mohan, and Hien Van Nguyen. Stypath: Style-transfer data augmentation for robust histology image classification. In *Medical Image Computing and Computer Assisted Intervention – MICCAI*, volume 12265 of *Lecture Notes in Computer Science*, page 351–361. Springer, Sep 2020.
- [628] Richard J Chen, Ming Y Lu, Tiffany Y Chen, Drew FK Williamson, and Faisal Mahmood. Synthetic data in machine learning for medicine and healthcare. *Nature Biomedical Engineering*, 5(6):493–497, 2021.
- [629] Jiří Borovec, Jan Kybic, Ignacio Arganda-Carreras, Dmitry Sorokin, Gloria Bueno, Alexander Khvostikov, Spyridon Bakas, Eric Chang, Stefan Heldmann, Kimmo Kartasalo, Leena Latonen, Johannes Lotz, Michelle Noga, Sarthak Pati, Kumaradevan Punithakumar, Pekka Ruusuvoori, Andrzej Skalski, Nazanin Tahmasebi, Masi Valkonen, and Arate Muñoz-Barrutia. Anhir: Automatic non-rigid histological image registration challenge. *IEEE Transactions on Medical Imaging*, PP:1–1, 04 2020.
- [630] Fei Wu, Pei Liu, Bo Fu, and Feng Ye. Deepgcnmil: Multi-head attention guided multi-instance learning approach for whole-slide images survival analysis using graph convolutional networks. In *2022 14th International Conference on Machine Learning and Computing (ICMLC)*, pages 67–73, 2022.
- [631] Brendon Lutnick, David Manthey, Jan U Becker, Brandon Ginley, Katharina Moos, Jonathan E Zuckerman, Luis Rodrigues, Alexander J Gallan, Laura Barisoni, Charles E Alpers, et al. A user-friendly tool for cloud-based whole slide image segmentation with examples from renal histopathology. *Communications medicine*, 2(1):105, 2022.
- [632] CAMELYON17. Available at: <https://camelyon17.grand-challenge.org/Organisers/> (accessed June 11, 2021), 2017.
- [633] Yongxiang Huang and Albert Chi-shing Chung. Improving high resolution histology image classification with deep spatial fusion network. In *Computational Pathology and Ophthalmic Medical Image Analysis*, pages 19–26. Springer, 2018.
- [634] MITOS-ATYPIA-14 Grand Challenge. Available online: <https://mitos-atypia-14.grand-challenge.org/> (accessed June 10, 2021).
- [635] Ludovic Roux, Daniel Racoceanu, Nicolas Loménie, Maria Kulikova, Humayun Irshad, Jacques Klossa, Frédérique Capron, Catherine Genestie, Gilles Le Naour, and Metin N Gurcan. Mitosis detection in breast cancer histological images an icpr 2012 contest. *Journal of Pathology Informatics*, 4, 2013.
- [636] Gabriele Campanella, Matthew G Hanna, Edi Brogi, and Thomas J Fuchs. Breast metastases to axillary lymph nodes. *Cancer Imaging Arch*, 2019.
- [637] Kenneth Clark, Bruce Vendt, Kirk Smith, John Freymann, Justin Kirby, Paul Koppel, Stephen Moore, Stanley Phillips, David Maffitt, Michael Pringle, et al. The cancer imaging archive (tcia): maintaining and operating a public information repository. *Journal of digital imaging*, 26(6):1045–1057, 2013.
- [638] Kosmas Dimitropoulos, Panagiotis Barmpoutis, Christina Zioga, Athanasios Kamas, Kalliopi Patsiaoura, and Nikos Grammalidis. Grading of invasive breast carcinoma through grassmannian vlad encoding. *PLoS one*, 12(9):e0185110, 2017.
- [639] C Zioga, A Kamas, K Patsiaoura, K Dimitropoulos, P Barmpoutis, and N Grammalidis. Breast carcinoma histological images from the department of pathology, “agios pavlos” general hospital of thessaloniki. *Greece*, July, 2017.
- [640] Brady Kieffer, Morteza Babaie, Shivam Kalra, and Hamid R Tizhoosh. Convolutional neural networks for histopathology image classification: Training vs. using pre-trained networks. In *International Conference on Image Processing Theory, Tools and Applications (IPTA)*, pages 1–6. IEEE, 2017.
- [641] Puspanjali Mohapatra, Baldev Panda, and Samikshya Swain. Enhancing histopathological breast cancer image classification using deep learning. *Int J Innov Technol Explor Eng*, 8:2024–2032, 2019.
- [642] Andrew Janowczyk, Scott Doyle, Hannah Gilmore, and Anant Madabhushi. A resolution adaptive deep hierarchical (radhical) learning scheme applied to nuclear segmentation of digital pathology images. *Computer Methods in Biomechanics and Biomedical Engineering: Imaging & Visualization*, 6(3):270–276, 2018.
- [643] Angel Cruz-Roa, Hannah Gilmore, Ajay Basavanahally, Michael Feldman, Shridar Ganesan, Natalie NC Shih, John Tomaszewski, Fabio A González, and Anant Madabhushi. Accurate and reproducible invasive breast cancer detection in whole-slide images: a deep learning approach for quantifying tumor extent. *Scientific Reports*, 7(1):1–14, 2017.
- [644] Mustafa I Jaber, Bing Song, Clive Taylor, Charles J Vaske, Stephen C Benz, Shahrooz Rabizadeh, Patrick Soon-Shiong, and Christopher W Szeto. A deep learning image-based intrinsic molecular subtype classifier of breast tumors reveals tumor heterogeneity that may affect survival. *Breast Cancer Research*, 22(1):1–10, 2020.
- [645] Alberto Corvo, Humberto Simon Garcia Caballero, Michel A Westenberg, Marc A van Driel, and Jarke van Wijk. Visual analytics for hypothesis-driven exploration in computational pathology. *IEEE Transactions on Visualization and Computer Graphics*, 2020.
- [646] Mitko Veta, Paul J Van Diest, Stefan M Willems, Haibo Wang, Anant Madabhushi, Angel Cruz-Roa, Fabio Gonzalez, Anders BL Larsen, Jacob S Vestergaard, Anders B Dahl, et al. Assessment of algorithms for mitosis detection in breast cancer histopathology images. *Medical Image Analysis*, 20(1):237–248, 2015.
- [647] Babak Ehteshami Bejnordi, Guido Zuidhof, Maschenka Balkenhol, Meyke Hermsen, Peter Bult, Bram van Ginneken, Nico Karssemeijer, Geert Litjens, and Jeroen van der Laak. Context-aware stacked convolutional neural networks for classification of breast carcinomas in whole-slide histopathology images. *Journal of Medical Imaging*, 4(4):044504, 2017.
- [648] Babak Ehteshami Bejnordi, Maeve Mullooly, Ruth M Pfeiffer, Shaoqi Fan, Pamela M Vacek, Donald L Weaver, Sally Herschorn, Louise A Brinton, Bram van Ginneken, Nico Karssemeijer, et al. Using deep convolutional neural networks to identify and classify tumor-associated stroma in diagnostic breast biopsies. *Modern Pathology*, 31(10):1502–1512, 2018.
- [649] Mohammad Peikari, Mehrdad J Gangeh, Judit Zubovits, Gina Clarke, and Anne L Martel. Triaging diagnostically relevant regions from pathology whole slides of breast cancer: A texture based approach. *IEEE transactions on medical imaging*, 35(1):307–315, 2015.
- [650] Guillaume Jaume, Pushpak Pati, Antonio Foncubierto-Rodríguez, Florinda Feroce, Giosuè Scognamiglio, Anna Maria Anniciello, Jean-Philippe Thiran, Orcun Goksel, and Maria Gabrani. Towards explainable graph representations in digital pathology. In *ICML*, pages 1–5, 2020.
- [651] Guillaume Jaume, Pushpak Pati, Behzad Bozorgtabar, Antonio Foncubierto, Anna Maria Anniciello, Florinda Feroce, Tilman Rau, Jean-Philippe Thiran, Maria Gabrani, and Orcun Goksel. Quantifying explainers of graph neural networks in computational pathology. In *IEEE/CVF Conference on Computer Vision and Pattern Recognition*, pages 8106–8116, 2021.
- [652] Nadia Brancati, Anna Maria Anniciello, Pushpak Pati, Daniel Riccio, Giosuè Scognamiglio, Guillaume Jaume, Giuseppe De Pietro, Maurizio Di Bonito, Antonio Foncubierto, Gerardo Botti, et al. Bracs: A dataset for breast carcinoma subtyping in h&e histology images. *arXiv preprint arXiv:2111.04740*, 2021.
- [653] Andrew Lagree, Audrey Shiner, Marie Angeli Alera, Lauren Fleshner, Ethan Law, Brianna Law, Fang-I Lu, David Dodington, Sonal Gandhi, Elzbieta A Slodkowska, et al. Assessment of digital pathology imaging biomarkers associated with breast cancer histologic grade. *Current Oncology*, 28(6):4298–4316, 2021.
- [654] Mohamed Amgad, Habiba Elfandy, Hagar Hussein, Lamees A Atteya, Mai AT Elsebaie, Lamia S Abo Elnasr, Rokia A Sakr, Hazem SE Salem, Ahmed F Ismail, Anas M Saad, et al. Structured crowdsourcing enables convolutional segmentation of histology images. *Bioinformatics*, 35(18):3461–3467, 2019.
- [655] Mathias Uhlen, Cheng Zhang, Sunjae Lee, Evelina Sjöstedt, Linn Fagerberg, Gholamreza Bidkhori, Rui Benfeitas, Muhammad Arif, Zhengtao Liu, Fredrik Edfors, et al. A pathology atlas of the human cancer transcriptome. *Science*, 357(6352):eaan2507, 2017.
- [656] Ponkrshnan Thiagarajan, Pushkar Khairnar, and Susanta Ghosh. Explanation and use of uncertainty quantified by bayesian neural network classifiers for breast histopathology images. *IEEE Transactions on Medical Imaging*, 41(4):815–825, 2021.
- [657] Zabit Hameed, Begonya Garcia-Zapirain, José Javier Aguirre, and Mario Arturo Isaza-Ruget. Multiclass classification of breast cancer histopathology images using multilevel features of deep convolutional neural network. *Scientific Reports*, 12(1):1–21, 2022.
- [658] Pinky A Bautista and Yukako Yagi. Staining correction in digital pathology by utilizing a dye amount table. *Journal of digital imaging*, 28(3):283–294, 2015.

- [659] B Albertina, M Watson, C Holback, R Jarosz, S Kirk, Y Lee, and J Lemmerman. Radiology data from the cancer genome atlas lung adenocarcinoma [tcga-luad] collection. *The Cancer Imaging Archive*, 2016.
- [660] National Lung Screening Trial Research Team. The national lung screening trial: overview and study design. *Radiology*, 258(1):243–253, 2011.
- [661] The Lung Cancer SPORE. Available at: <https://www.mdanderson.org/research/departments-labs-institutes/spores/lung-cancer-spore.html> (accessed June 10, 2021).
- [662] Cheng Lu, Can Koyuncu, German Corredor, Prateek Prasanna, Patrick Leo, XiangXue Wang, Andrew Janowczyk, Kaustav Bera, James Lewis Jr, Vamsidhar Velcheti, et al. Feature-driven local cell graph (FLoCK): New computational pathology-based descriptors for prognosis of lung cancer and hpv status of oropharyngeal cancers. *Medical Image Analysis*, 68:101903, 2021.
- [663] Anne Laure Le Page, Elise Ballot, Caroline Truntzer, Valentin Derangère, Alis Ilie, David Rageot, Frederic Bibeau, and Francois Ghiringhelli. Using a convolutional neural network for classification of squamous and non-squamous non-small cell lung cancer based on diagnostic histopathology hes images. *Scientific Reports*, 11(1):1–8, 2021.
- [664] Zaneta Swiderska-Chadaj and Francesco Ciompi. Lyon19- lymphocyte detection test set (version v1) [data set]. <https://zenodo.org/record/3385420#XW-6JygzYuW>, 2019. [Accessed 18-Mar-2023].
- [665] Zaneta Swiderska-Chadaj, Hans Pinckaers, Mart van Rijthoven, Maschenka Balkenhol, Margarita Melnikova, Oscar Geessink, Quirine Manson, Mark Sherman, Antonio Polonia, Jeremy Parry, et al. Learning to detect lymphocytes in immunohistochemistry with deep learning. *Medical image analysis*, 58:101547, 2019.
- [666] Nadia Brancati, Giuseppe De Pietro, Maria Frucci, and Daniel Riccio. A deep learning approach for breast invasive ductal carcinoma detection and lymphoma multi-classification in histological images. *IEEE Access*, 7:44709–44720, 2019.
- [667] Jeppe Thagaard, Søren Hauberg, Bert van der Veegt, Thomas Ebstrup, Johan D Hansen, and Anders B Dahl. Can you trust predictive uncertainty under real dataset shifts in digital pathology? In *International Conference on Medical Image Computing and Computer-Assisted Intervention*, pages 824–833. Springer, 2020.
- [668] Muhammad Shaban, Syed Ali Khurram, Muhammad Moazam Fraz, Najah Alsuaibie, Iqra Masood, Sajid Mushtaq, Mariam Hassan, Asif Loya, and Nasir M Rajpoot. A novel digital score for abundance of tumour infiltrating lymphocytes predicts disease free survival in oral squamous cell carcinoma. *Scientific Reports*, 9(1):1–13, 2019.
- [669] Jonathan Folmsbee, Xulei Liu, Margaret Brandwein-Weber, and Scott Doyle. Active deep learning: Improved training efficiency of convolutional neural networks for tissue classification in oral cavity cancer. In *IEEE International Symposium on Biomedical Imaging*, pages 770–773. IEEE, 2018.
- [670] Wouter Bulten, Péter Bándi, Jeffrey Hoven, Rob van de Loo, Johannes Lotz, Nick Weiss, Jeroen van der Laak, Bram van Ginneken, Christina Hulsbergen-van de Kaa, and Geert Litjens. Epithelium segmentation using deep learning in h&e-stained prostate specimens with immunohistochemistry as reference standard. *Scientific reports*, 9(1):864, 2019.
- [671] Martin Köbel, Steve E Kaloger, Patricia M Baker, Carol A Ewanowich, Jocelyne Arseneau, Viktor Zhrebitskiy, Soran Abdulkarim, Samuel Leung, Máire A Duggan, Dan Fontaine, et al. Diagnosis of ovarian carcinoma cell type is highly reproducible: a transcanadian study. *The American journal of surgical pathology*, 34(7):984–993, 2010.
- [672] Yuri Tolkach, Tilmann Dohmgörgen, Marieta Toma, and Glen Kristiansen. High-accuracy prostate cancer pathology using deep learning. *Nature Machine Intelligence*, 2(7):411–418, 2020.
- [673] Eirini Arvaniti, Kim S Fricker, Michael Moret, Niels Rupp, Thomas Hermans, Christian Fankhauser, Norbert Wey, Peter J Wild, Jan H Rueschoff, and Manfred Claassen. Automated gleason grading of prostate cancer tissue microarrays via deep learning. *Scientific Reports*, 8(1):1–11, 2018.
- [674] Eirini Arvaniti and Manfred Claassen. Coupling weak and strong supervision for classification of prostate cancer histopathology images. *ArXiv*, abs/1811.07013, 2018.
- [675] Jian Ren, Ilker Hacihaliloglu, Eric A Singer, David J Foran, and Xin Qi. Unsupervised domain adaptation for classification of histopathology whole-slide images. *Frontiers in Bioengineering and Biotechnology*, 7:102, 2019.
- [676] Davood Karimi, Guy Nir, Ladan Fazli, Peter C Black, Larry Goldenberg, and Septimiu E Salcudean. Deep learning-based gleason grading of prostate cancer from histopathology images—role of multiscale decision aggregation and data augmentation. *IEEE Journal of Biomedical and Health Informatics*, 24(5):1413–1426, 2019.
- [677] Chaoyang Yan, Kazuaki Nakane, Xiangxue Wang, Yao Fu, Haoda Lu, Xiangshan Fan, Michael D Feldman, Anant Madabhushi, and Jun Xu. Automated gleason grading on prostate biopsy slides by statistical representations of homology profile. *Computer methods and programs in biomedicine*, 194:105528, 2020.
- [678] Scott Doyle, James Monaco, Michael Feldman, John Tomaszewski, and Anant Madabhushi. An active learning based classification strategy for the minority class problem: application to histopathology annotation. *BMC bioinformatics*, 12(1):1–14, 2011.
- [679] Scott Doyle, Michael D Feldman, Natalie Shih, John Tomaszewski, and Anant Madabhushi. Cascaded discrimination of normal, abnormal, and confounder classes in histopathology: Gleason grading of prostate cancer. *BMC bioinformatics*, 13(1):1–15, 2012.
- [680] Kunal Nagpal, Davis Foote, Yun Liu, Po-Hsuan Cameron Chen, Ellery Wulczyn, Fraser Tan, Niels Olson, Jenny L Smith, Arash Mohtashamian, James H Wren, et al. Development and validation of a deep learning algorithm for improving gleason scoring of prostate cancer. *NPJ Digital Medicine*, 2(1):1–10, 2019.
- [681] Adrian B Levine, Jason Peng, David Farnell, Mitchell Nursey, Yiping Wang, Julia R Naso, Hezhen Ren, Hossein Farahani, Colin Chen, Derek Chiu, et al. Synthesis of diagnostic quality cancer pathology images by generative adversarial networks. *The Journal of Pathology*, 252(2):178–188, 2020.
- [682] Birgid Schömig-Markiefka, Alexey Pryalukhin, Wolfgang Hulla, Andrey Bychkov, Junya Fukuoka, Anant Madabhushi, Viktor Achter, Lech Nieroda, Reinhard Büttner, Alexander Quaas, et al. Quality control stress test for deep learning-based diagnostic model in digital pathology. *Modern Pathology*, 34(12):2098–2108, 2021.
- [683] Julio Silva-Rodríguez, Adrián Colomer, María A Sales, Rafael Molina, and Valery Naranjo. Going deeper through the gleason scoring scale: An automatic end-to-end system for histology prostate grading and cribriform pattern detection. *Computer Methods and Programs in Biomedicine*, 195:105637, 2020.
- [684] Hossein Farahani, Jeffrey Boschman, David Farnell, Amirali Darband-sari, Allen Zhang, Pouya Ahmadvand, Steven JM Jones, David Huntsman, Martin Köbel, C Blake Gilks, et al. Deep learning-based histotype diagnosis of ovarian carcinoma whole-slide pathology images. *Modern Pathology*, 35(12):1983–1990, 2022.
- [685] Wouter Bulten, Geert Litjens, Hans Pinckaers, Peter Ström, Martin Eklund, Kimmo Kartasalo, Maggie Demkin, and Sohier Dane. The PANDA challenge: Prostate cANcer graDe Assessment using the Gleason grading system, March 2020.
- [686] Jakob Nikolas Kather, FG Zöllner, F Bianconi, SM Melchers, LR Schad, T Gaiser, A Marx, and CA Weis. Collection of textures in colorectal cancer histology. *Zenodo*, 5281, 2016.
- [687] Korsuk Sirinukunwattana, Josien PW Pluim, Hao Chen, Xiaojuan Qi, Pheng-Ann Heng, Yun Bo Guo, Li Yang Wang, Bogdan J Matuszewski, Elia Bruni, Urko Sanchez, et al. Gland segmentation in colon histology images: The glas challenge contest. *Medical Image Analysis*, 35:489–502, 2017.
- [688] Muhammad Shaban, Ruqayya Awan, Muhammad Moazam Fraz, Ayesha Azam, Yee-Wah Tsang, David Snead, and Nasir M Rajpoot. Context-aware convolutional neural network for grading of colorectal cancer histology images. *IEEE Transactions on Medical Imaging*, 39(7):2395–2405, 2020.
- [689] Jun Xu, Xiaofei Luo, Guanhao Wang, Hannah Gilmore, and Anant Madabhushi. A deep convolutional neural network for segmenting and classifying epithelial and stromal regions in histopathological images. *Neurocomputing*, 191:214–223, 2016.
- [690] University of Leeds. Welcome to the university of leeds virtual pathology project website. Available at: <https://www.virtualpathology.leeds.ac.uk/> (accessed June 10, 2021).
- [691] Francesco Ponzio, Giacomo Deodato, Enrico Macii, Santa Di Cataldo, and Elisa Ficarra. Exploiting “uncertain” deep networks for data cleaning in digital pathology. In *IEEE International Symposium on Biomedical Imaging*, pages 1139–1143. IEEE, 2020.
- [692] Francesco Ciompi, Oscar Geessink, Babak Ehteshami Bejnordi,

- Gabriel Silva De Souza, Alexi Baidoshvili, Geert Litjens, Bram Van Ginneken, Iris Nagtegaal, and Jeroen Van Der Laak. The importance of stain normalization in colorectal tissue classification with convolutional networks. In *IEEE International Symposium on Biomedical Imaging*, pages 160–163. IEEE, 2017.
- [693] Cigdem Gunduz-Demir, Melih Kandemir, Akif Burak Tosun, and Cen Sokmensuer. Automatic segmentation of colon glands using object-graphs. *Medical image analysis*, 14(1):1–12, 2010.
- [694] Jonas KloECKner, Tatiana K Sansonowicz, Áttila L Rodrigues, and Tatiana WN Nunes. Multi-categorical classification using deep learning applied to the diagnosis of gastric cancer. *Jornal Brasileiro de Patologia e Medicina Laboratorial*, 56, 2020.
- [695] Huu-Giao Nguyen, Annika Blank, Alessandro Lugli, and Inti Zlobec. An effective deep learning architecture combination for tissue microarray spots classification of h&e stained colorectal images. In *IEEE International Symposium on Biomedical Imaging*, pages 1271–1274. IEEE, 2020.
- [696] Rasoul Sali, Lubaina Ehsan, Kamran Kowsari, Marium Khan, Christopher A Moskaluk, Sana Syed, and Donald E Brown. Celiacnet: Celiac disease severity diagnosis on duodenal histopathological images using deep residual networks. In *IEEE International Conference on Bioinformatics and Biomedicine (BIBM)*, pages 962–967. IEEE, 2019.
- [697] Rasoul Sali, Sadiq Adewole, Lubaina Ehsan, Lee A Denson, Paul Kelly, Beatrice C Amadi, Lori Holtz, Syed Asad Ali, Sean R Moore, Sana Syed, et al. Hierarchical deep convolutional neural networks for multi-category diagnosis of gastrointestinal disorders on histopathological images. In *IEEE International Conference on Healthcare Informatics (ICHI)*, pages 1–6. IEEE, 2020.
- [698] Bin Kong, Shanhu Sun, Xin Wang, Qi Song, and Shaoting Zhang. Invasive cancer detection utilizing compressed convolutional neural network and transfer learning. In *International Conference on Medical Image Computing and Computer-Assisted Intervention*, pages 156–164. Springer, 2018.
- [699] Zhigang Song, Shuangmei Zou, Weixun Zhou, Yong Huang, Liwei Shao, Jing Yuan, Xiangnan Gou, Wei Jin, Zhanbo Wang, Xin Chen, et al. Clinically applicable histopathological diagnosis system for gastric cancer detection using deep learning. *Nature communications*, 11(1):1–9, 2020.
- [700] Alexander Ian Wright, Catriona Marie Dunn, Michael Hale, Gordon Hutchins, and Darren Treanor. The effect of quality control on accuracy of digital pathology image analysis. *IEEE Journal of Biomedical and Health Informatics*, 2020.
- [701] Mohsin Bilal, Shan E Ahmed Raza, Ayesha Azam, Simon Graham, Mohammad Ilyas, Ian A Cree, David Snead, Fayyaz Minhas, and Nasir M Rajpoot. Development and validation of a weakly supervised deep learning framework to predict the status of molecular pathways and key mutations in colorectal cancer from routine histology images: a retrospective study. *The Lancet Digital Health*, 3(12):e763–e772, 2021.
- [702] Kevin Thandiackal, Boqi Chen, Pushpak Pati, Guillaume Jaume, Drew FK Williamson, Maria Gabrani, and Orcun Goksel. Differentiable zooming for multiple instance learning on whole-slide images. *arXiv preprint arXiv:2204.12454*, 2022.
- [703] Sara P Oliveira, Pedro C Neto, João Fraga, Diana Montezuma, Ana Monteiro, João Monteiro, Liliana Ribeiro, Sofia Gonçalves, Isabel M Pinto, and Jaime S Cardoso. Cad systems for colorectal cancer from wsi are still not ready for clinical acceptance. *Scientific Reports*, 11(1):1–15, 2021.
- [704] Chuang Zhu, Wenkai Chen, Ting Peng, Ying Wang, and Mulan Jin. Hard sample aware noise robust learning for histopathology image classification. *IEEE transactions on medical imaging*.
- [705] Philipp Kainz, Martin Urschler, Samuel Schuler, Paul Wohlhart, and Vincent Lepetit. You should use regression to detect cells. In *International Conference on Medical Image Computing and Computer-Assisted Intervention*, pages 276–283. Springer, 2015.
- [706] Ramraj Chandradevan, Ahmed A Aljudi, Bradley R Drumheller, Nilakshan Kumananthaseelan, Mohamed Amgad, David A Gutman, Lee AD Cooper, and David L Jaye. Machine-based detection and classification for bone marrow aspirate differential counts: initial development focusing on nonneoplastic cells. *Laboratory Investigation*, 100(1):98–109, 2020.
- [707] Arthur O Frankel, Melvin Lathara, Celine Y Shaw, Owen Wogmon, Jacob M Jackson, Mattie M Clark, Navah Eshraghi, Stephanie E Keenen, Andrew D Woods, Reshma Purohit, et al. Machine learning for rhabdomyosarcoma histopathology. *Modern Pathology*, pages 1–11, 2022.
- [708] Xueyi Zheng, Ruixuan Wang, Xinke Zhang, Yan Sun, Haohuan Zhang, Zihan Zhao, Yuanhang Zheng, Jing Luo, Jiangyu Zhang, Hongmei Wu, et al. A deep learning model and human-machine fusion for prediction of ebv-associated gastric cancer from histopathology. *Nature communications*, 13(1):1–12, 2022.
- [709] Ye Tian, Li Yang, Wei Wang, Jing Zhang, Qing Tang, Mili Ji, Yang Yu, Yu Li, Hong Yang, and Airong Qian. Computer-aided detection of squamous carcinoma of the cervix in whole slide images. *arXiv preprint arXiv:1905.10959*, 2019.
- [710] Jevgenij Gamper, Navid Alemi Koohbanani, Ksenija Benet, Ali Khuram, and Nasir Rajpoot. Pannuke: an open pan-cancer histology dataset for nuclei instance segmentation and classification. In *European Congress on Digital Pathology*, pages 11–19. Springer, 2019.
- [711] Jevgenij Gamper, Navid Alemi Koohbanani, Simon Graham, Mostafa Jahanifar, Syed Ali Khuram, Ayesha Azam, Katherine Hewitt, and Nasir M. Rajpoot. Pannuke dataset extension, insights and baselines. *CoRR*, abs/2003.10778, 2020.
- [712] Le Hou, Rajarsi Gupta, John S Van Arnem, Yuwei Zhang, Kaustubh Sivalenka, Dimitris Samaras, Tahsin M Kurc, and Joel H Saltz. Dataset of segmented nuclei in hematoxylin and eosin stained histopathology images of ten cancer types. *Scientific data*, 7(1):1–12, 2020.
- [713] Cheng Jiang, Jun Liao, Pei Dong, Zhaoxuan Ma, De Cai, Guoan Zheng, Yueping Liu, Hong Bu, and Jianhua Yao. Blind deblurring for microscopic pathology images using deep learning networks. *CoRR*, abs/2011.11879, 2020.
- [714] Robert J Marinelli, Kelli Montgomery, Chih Long Liu, Nigam H Shah, Wijan Prapong, Michael Nitzberg, Zachariah K Zachariah, Gavin J Sherlock, Yasodha Natkunam, Robert B West, et al. The stanford tissue microarray database. *Nucleic acids research*, 36(suppl_1):D871–D877, 2007.
- [715] Narayan Hegde, Jason D Hipp, Yun Liu, Michael Emmert-Buck, Emily Reif, Daniel Smilkov, Michael Terry, Carrie J Cai, Mahul B Amin, Craig H Mermel, et al. Similar image search for histopathology: Smily. *NPJ Digital Medicine*, 2(1):1–9, 2019.
- [716] James A Diao, Wan Fung Chui, Jason K Wang, Richard N Mitchell, Sudha K Rao, Murray B Resnick, Abhik Lahiri, Chirag Maheshwari, Benjamin Glass, Victoria Mountain, et al. Dense, high-resolution mapping of cells and tissues from pathology images for the interpretable prediction of molecular phenotypes in cancer. *bioRxiv*, 2020.
- [717] Yiqing Shen and Jing Ke. A deformable crf model for histopathology whole-slide image classification. In *International Conference on Medical Image Computing and Computer-Assisted Intervention*, pages 500–508. Springer, 2020.
- [718] Benoît Schmauch, Alberto Romagnoni, Elodie Pronier, Charlie Saillard, Pascale Maillé, Julien Calderaro, Aurélie Kamoun, Meriem Sefta, Sylvain Toldo, Mikhail Zaslavskiy, et al. A deep learning model to predict rna-seq expression of tumours from whole slide images. *Nature communications*, 11(1):1–15, 2020.
- [719] Andrew A Borkowski, Marilyn M Bui, L Brannon Thomas, Catherine P Wilson, Lauren A DeLand, and Stephen M Mastorides. Lung and colon cancer histopathological image dataset (lc25000). *arXiv preprint arXiv:1912.12142*, 2019.
- [720] Jeongun Ryu, Aaron Valero Puche, JaeWoong Shin, Seonwook Park, Biagio Brattoli, Jinhee Lee, Wonkyung Jung, Soo Ick Cho, Kyunghyun Paeng, Chan-Young Ock, Donggeun Yoo, and Sérgio Pereira. Ocelot: Overlapped cell on tissue dataset for histopathology. In *Proceedings of the IEEE conference on computer vision and pattern recognition*, 2023.
- [721] Christian Matek, Simone Schwarz, Karsten Spiekermann, and Carsten Marr. Human-level recognition of blast cells in acute myeloid leukaemia with convolutional neural networks. *Nature Machine Intelligence*, 1(11):538–544, 2019.
- [722] Jeffrey J Nirschl, Andrew Janowczyk, Eliot G Peyster, Renee Frank, Kenneth B Margulies, Michael D Feldman, and Anant Madabhushi. A deep-learning classifier identifies patients with clinical heart failure using whole-slide images of h&e tissue. *PLoS one*, 13(4):e0192726, 2018.
- [723] Julia Höhn, Eva Kriehoff-Henning, Tanja B Jutz, Christof von Kalle, Jochen S Utikal, Friedegund Meier, Frank F Gellrich, Sarah Hobelsberger, Axel Hauschild, Justin G Schlager, et al. Combining cnn-based histologic whole slide image analysis and patient data to improve skin cancer classification. *European Journal of Cancer*, 149:94–101, 2021.

- [724] Felipe Giuste, Mythreye Venkatesan, Conan Zhao, Li Tong, Yuanda Zhu, Shriprasad R Deshpande, and May D Wang. Automated classification of acute rejection from endomyocardial biopsies. In *Proceedings of the 11th ACM International Conference on Bioinformatics, Computational Biology and Health Informatics*, pages 1–9, 2020.
- [725] Eliot G Peyster, Sara Arabyarmohammadi, Andrew Jancowczyk, Sepideh Azarianpour-Esfahani, Miroslav Sekulic, Clarissa Jansoll, Luke Blower, Anil Parwani, Priti Lal, Michael D Feldman, et al. An automated computational image analysis pipeline for histological grading of cardiac allograft rejection. *European Heart Journal*, 42(24):2356–2369, 2021.
- [726] Juan C Caicedo, Allen Goodman, Kyle W Karhohs, Beth A Cimini, Jeanelle Ackerman, Marzieh Haghighi, CherKeng Heng, Tim Becker, Minh Doan, Claire McQuin, et al. Nucleus segmentation across imaging experiments: the 2018 data science bowl. *Nature methods*, 16(12):1247–1253, 2019.
- [727] Ruggero Donida Labati, Vincenzo Piuri, and Fabio Scotti. All-idx: The acute lymphoblastic leukemia image database for image processing. In *2011 18th IEEE international conference on image processing*, pages 2045–2048. IEEE, 2011.
- [728] Angelo Genovese, Mahdi S Hosseini, Vincenzo Piuri, Konstantinos N Plataniotis, and Fabio Scotti. Histopathological transfer learning for acute lymphoblastic leukemia detection. In *2021 IEEE International Conference on Computational Intelligence and Virtual Environments for Measurement Systems and Applications (CIVEMSA)*, pages 1–6. IEEE, 2021.
- [729] Henrik Failmezger, Sathya Muralidhar, Antonio Rullan, Carlos E de Andrea, Erik Sahai, and Yinyin Yuan. Topological tumor graphs: a graph-based spatial model to infer stromal recruitment for immunosuppression in melanoma histology. *Cancer research*, 80(5):1199–1209, 2020.
- [730] Zahraa Al-Milaji, Ilker Ersoy, Adel Hafiane, Kannappan Palaniappan, and Filiz Bunyak. Integrating segmentation with deep learning for enhanced classification of epithelial and stromal tissues in h&e images. *Pattern Recognition Letters*, 119:214–221, 2019.
- [731] Mehmet Günhan Ertosun and Daniel L Rubin. Automated grading of gliomas using deep learning in digital pathology images: a modular approach with ensemble of convolutional neural networks. In *AMIA Annual Symposium Proceedings*, volume 2015, page 1899. American Medical Informatics Association, 2015.
- [732] Saima Rathore, Tamim Niazi, Muhammad Aksam Iftikhar, and Ahmad Chaddad. Glioma grading via analysis of digital pathology images using machine learning. *Cancers*, 12(3):578, 2020.
- [733] James S Lewis Jr, Sahirzeeshan Ali, Jingqin Luo, Wade L Thorstad, and Anant Madabhushi. A quantitative histomorphometric classifier (qubhc) identifies aggressive versus indolent p16-positive oropharyngeal squamous cell carcinoma. *The American journal of surgical pathology*, 38(1):128, 2014.
- [734] Sara Hosseinzadeh Kassani, Peyman Hosseinzadeh Kassani, Michal J Wesolowski, Kevin A Schneider, and Ralph Deters. Breast cancer diagnosis with transfer learning and global pooling. In *International Conference on Information and Communication Technology Convergence (ICTC)*, pages 519–524. IEEE, 2019.
- [735] SanaUllah Khan, Naveed Islam, Zahoor Jan, Ikram Ud Din, and Joel JP C Rodrigues. A novel deep learning based framework for the detection and classification of breast cancer using transfer learning. *Pattern Recognition Letters*, 125:1–6, 2019.
- [736] Ümit Budak, Zafer Cömert, Zryan Najat Rashid, Abdulkadir Şengür, and Musa Çıbuk. Computer-aided diagnosis system combining fcn and bilstm model for efficient breast cancer detection from histopathological images. *Applied Soft Computing*, 85:105765, 2019.
- [737] Fabio A Spanhol, Luiz S Oliveira, Paulo R Cavalin, Caroline Petitjean, and Laurent Heutte. Deep features for breast cancer histopathological image classification. In *IEEE International Conference on Systems, Man, and Cybernetics (SMC)*, pages 1868–1873. IEEE, 2017.
- [738] David Joon Ho, Dig VK Yarlagadda, Timothy M D’Alfonso, Matthew G Hanna, Anne Grabenstetter, Peter Ntiamoah, Edi Brogi, Lee K Tan, and Thomas J Fuchs. Deep multi-magnification networks for multi-class breast cancer image segmentation. *Computerized Medical Imaging and Graphics*, 88:101866, 2021.
- [739] Mira Valkonen, Kimmo Kartasalo, Kaisa Liimatainen, Matti Nykter, Leena Latonen, and Pekka Ruusuvoori. Dual structured convolutional neural network with feature augmentation for quantitative characterization of tissue histology. In *IEEE International Conference on Computer Vision Workshops*, pages 27–35, 2017.
- [740] Yu Liang, Jinglong Yang, Xiongwen Quan, and Han Zhang. Metastatic breast cancer recognition in histopathology images using convolutional neural network with attention mechanism. In *Chinese Automation Congress (CAC)*, pages 2922–2926. IEEE, 2019.
- [741] Angel Cruz-Roa, Ajay Basavanhalay, Fabio González, Hannah Gilmore, Michael Feldman, Shridar Ganesan, Natalie Shih, John Tomaszewski, and Anant Madabhushi. Automatic detection of invasive ductal carcinoma in whole slide images with convolutional neural networks. In *Medical Imaging: Digital Pathology*, volume 9041, page 904103. International Society for Optics and Photonics, 2014.
- [742] Md Zahangir Alom, Chris Yakopcic, Mst Nasrin, Tarek M Taha, Vijayan K Asari, et al. Breast cancer classification from histopathological images with inception recurrent residual convolutional neural network. *Journal of digital imaging*, 32(4):605–617, 2019.
- [743] Majid Nawaz, Adel A Sewissy, and Taysir Hassan A Soliman. Multi-class breast cancer classification using deep learning convolutional neural network. *Int. J. Adv. Comput. Sci. Appl.* 9(6):316–332, 2018.
- [744] Ziba Gandomkar, Patrick C Brennan, and Claudia Mello-Thoms. Modern: Multi-category classification of breast histopathological image using deep residual networks. *Artificial intelligence in medicine*, 88:14–24, 2018.
- [745] Zhongyi Han, Benzhen Wei, Yuanjie Zheng, Yilong Yin, Kejian Li, and Shuo Li. Breast cancer multi-classification from histopathological images with structured deep learning model. *Scientific Reports*, 7(1):1–10, 2017.
- [746] Pendar Alirezazadeh, Behzad Hejrati, Alireza Monsef-Esfahani, and Abdolhossein Fathi. Representation learning-based unsupervised domain adaptation for classification of breast cancer histopathology images. *Biocybernetics and Biomedical Engineering*, 38(3):671–683, 2018.
- [747] Zhu Meng, Zhicheng Zhao, and Fei Su. Multi-classification of breast cancer histology images by using gravitation loss. In *IEEE International Conference on Acoustics, Speech and Signal Processing (ICASSP)*, pages 1030–1034. IEEE, 2019.
- [748] Alexander Rakhlin, Alexey Shvets, Vladimir Iglovikov, and Alexandr A Kalinin. Deep convolutional neural networks for breast cancer histology image analysis. In *International Conference Image Analysis and Recognition*, pages 737–744. Springer, 2018.
- [749] Yeeleng S Yang, Zhen Chen, and Xiaohui Xie. Deep learning framework for multi-class breast cancer histology image classification. In *International Conference Image Analysis and Recognition*, pages 914–922. Springer, 2018.
- [750] Abdullah-Al Nahid and Yinan Kong. Histopathological breast-image classification using local and frequency domains by convolutional neural network. *Information*, 9(1):19, 2018.
- [751] Eu Wern Teh and Graham W Taylor. Metric learning for patch classification in digital pathology. In *International Conference on Medical Imaging with Deep Learning—Extended Abstract Track*, 2019.
- [752] Ruqayya Awan, Navid Alemi Koohbanani, Muhammad Shaban, Anna Lisowska, and Nasir Rajpoot. Context-aware learning using transferable features for classification of breast cancer histology images. In *International Conference Image Analysis and Recognition*, pages 788–795. Springer, 2018.
- [753] Tomas Iesmantas and Robertas Alzbutas. Convolutional capsule network for classification of breast cancer histology images. In *International Conference Image Analysis and Recognition*, pages 853–860. Springer, 2018.
- [754] Kaushiki Roy, Debapriya Banik, Debotosh Bhattacharjee, and Mita Nasipuri. Patch-based system for classification of breast histology images using deep learning. *Computerized Medical Imaging and Graphics*, 71:90–103, 2019.
- [755] Gaoyi Lei, Yuanqing Xia, Di-Hua Zhai, Wei Zhang, Duanduan Chen, and Defeng Wang. Staincnn: An efficient stain feature learning method. *Neurocomputing*, 406:267–273, 2020.
- [756] Amjad Khan, Manfredo Atzori, Sebastian Otálora, Vincent Andrearczyk, and Henning Müller. Generalizing convolution neural networks on stain color heterogeneous data for computational pathology. In *Medical Imaging: Digital Pathology*, volume 11320, page 113200R. International Society for Optics and Photonics, 2020.
- [757] Dorsa Ziaei, Weizhe Li, Samuel Lam, Wei-Chung Cheng, and Weijie Chen. Characterization of color normalization methods in digital pathol-

- ogy whole slide imaging. In *Medical Imaging: Digital Pathology*, volume 11320, page 1132017. International Society for Optics and Photonics, 2020.
- [758] X. Guo, F. Wang, G. Teodoro, A. B. Farris, and J. Kong. Liver steatosis segmentation with deep learning methods. In *IEEE International Symposium on Biomedical Imaging*, pages 24–27, 2019.
- [759] Yongxiang Huang and Albert Chung. Evidence localization for pathology images using weakly supervised learning. In *International Conference on Medical Image Computing and Computer-Assisted Intervention*, pages 613–621. Springer, 2019.
- [760] Şaban Öztürk and Bayram Akdemir. Hic-net: A deep convolutional neural network model for classification of histopathological breast images. *Computers & Electrical Engineering*, 76:299–310, 2019.
- [761] Karin Stacke, Gabriel Eilertsen, Jonas Unger, and Claes Lundström. A closer look at domain shift for deep learning in histopathology. *arXiv preprint arXiv:1909.11575*, 2019.
- [762] Jacob Gildenblat and Eldad Klaiman. Self-supervised similarity learning for digital pathology. *arXiv preprint arXiv:1905.08139*, 2019.
- [763] Sebastian Otálora, Manfredo Atzori, Amjad Khan, Oscar Jimenez-del Toro, Vincent Andrearczyk, and Henning Müller. Systematic comparison of deep learning strategies for weakly supervised gleason grading. In *Medical Imaging: Digital Pathology*, volume 11320, page 113200L. International Society for Optics and Photonics, 2020.
- [764] Jiayun Li, Karthik V Sarma, King Chung Ho, Arkadiusz Gertych, Beatrice S Knudsen, and Corey W Arnold. A multi-scale u-net for semantic segmentation of histological images from radical prostatectomies. 2017:1140, 2017.
- [765] Juan S. Lara, Victor H. Contreras O., Sebastián Otálora, Henning Müller, and Fabio A. González. Multimodal latent semantic alignment for automated prostate tissue classification and retrieval. In *Medical Image Computing and Computer Assisted Intervention – MICCAI*, volume 12265 of *Lecture Notes in Computer Science*, page 572–581. Springer, Sep 2020.
- [766] Ethan H Nguyen, Haichun Yang, Ruining Deng, Yuzhe Lu, Zheyu Zhu, Joseph T Roland, Le Lu, Bennett A Landman, Agnes B Fogo, and Yuankai Huo. Circle representation for medical object detection. *IEEE transactions on medical imaging*, 41(3):746–754, 2021.
- [767] Saif Almansouri and Susan Zwyea. Early prognosis of human renal cancer with kaplan-meier plotter data analysis model. In *Journal of physics: conference series*, volume 1530, page 012051. IOP Publishing, 2020.
- [768] Simon Graham, Muhammad Shaban, Talha Qaiser, Navid Alemi Koohbanani, Syed Ali Khurram, and Nasir Rajpoot. Classification of lung cancer histology images using patch-level summary statistics. In *Medical Imaging: Digital Pathology*, volume 10581, page 1058119. International Society for Optics and Photonics, 2018.
- [769] Germán Corredor, Paula Toro, Kaustav Bera, Dylan Rasmussen, Vidya Sankar Viswanathan, Christina Buzzy, Pingfu Fu, Lisa M Barton, Edana Stroberg, Eric Duval, et al. Computational pathology reveals unique spatial patterns of immune response in h&e images from covid-19 autopsies: preliminary findings. *Journal of Medical Imaging*, 8(S1):017501, 2021.
- [770] Mohammed Adnan, Shivam Kalra, and Hamid R Tizhoosh. Representation learning of histopathology images using graph neural networks. In *IEEE/CVF Conference on Computer Vision and Pattern Recognition Workshops*, pages 988–989, 2020.
- [771] Miriam Hägele, Philipp Seegerer, Sebastian Lapuschkin, Michael Bockmayr, Wojciech Samek, Frederick Klauschen, Klaus-Robert Müller, and Alexander Binder. Resolving challenges in deep learning-based analyses of histopathological images using explanation methods. *Scientific Reports*, 10(1):1–12, 2020.
- [772] Yves-Rémi Van Eycke, Cédric Balsat, Laurine Verset, Olivier Debeir, Isabelle Salmon, and Christine Decaestecker. Segmentation of glandular epithelium in colorectal tumours to automatically compartmentalise the biomarker quantification: A deep learning approach. *Medical Image Analysis*, 49:35–45, 2018.
- [773] Yan Xu, Yang Li, Yipei Wang, Mingyuan Liu, Yubo Fan, Maode Lai, I Eric, and Chao Chang. Gland instance segmentation using deep multichannel neural networks. *IEEE Transactions on Biomedical Engineering*, 64(12):2901–2912, 2017.
- [774] Jakob Kather, Cleo-Aron Weis, Francesco Bianconi, Susanne Melchers, Lothar Schad, Timo Gaiser, Alexander Marx, and Frank Zöllner. Multi-class texture analysis in colorectal cancer histology. *Scientific Reports*, 6:27988, 06 2016.
- [775] Chaofeng Wang, Jun Shi, Qi Zhang, and Shihui Ying. Histopathological image classification with bilinear convolutional neural networks. In *International Conference of the IEEE Engineering in Medicine and Biology Society (EMBC)*, pages 4050–4053. IEEE, 2017.
- [776] Łukasz Rączkowski, Marcin Możejko, Joanna Zambonelli, and Ewa Szczurek. Ara: accurate, reliable and active histopathological image classification framework with bayesian deep learning. *Scientific Reports*, 9(1):1–12, 2019.
- [777] Srinath Jayachandran and Ashlin Ghosh. Deep transfer learning for texture classification in colorectal cancer histology. In *IAPR Workshop on Artificial Neural Networks in Pattern Recognition*, pages 173–186. Springer, 2020.
- [778] Adrien Foucart, Olivier Debeir, and Christine Decaestecker. Snow: Semi-supervised, noisy and/or weak data for deep learning in digital pathology. In *IEEE International Symposium on Biomedical Imaging*, pages 1869–1872. IEEE, 2019.
- [779] Amal Lahiani, Irina Klaman, Nassir Navab, Shadi Albarqouni, and Eldad Klaiman. Seamless virtual whole slide image synthesis and validation using perceptual embedding consistency. *IEEE Journal of Biomedical and Health Informatics*, 2020.
- [780] Meng-Yao Ji, Lei Yuan, Shi-Min Lu, Meng-Ting Gao, Zhi Zeng, Na Zhan, Yi-Juan Ding, Zheng-Ru Liu, Ping-Xiao Huang, Cheng Lu, et al. Glandular orientation and shape determined by computational pathology could identify aggressive tumor for early colon carcinoma: a triple-center study. *Journal of translational medicine*, 18(1):1–12, 2020.
- [781] Hang Chang, Ju Han, Cheng Zhong, Antoine M Snijders, and Jian-Hua Mao. Unsupervised transfer learning via multi-scale convolutional sparse coding for biomedical applications. *IEEE Transactions on Pattern Analysis and Machine Intelligence*, 40(5):1182–1194, 2017.
- [782] Jacob S Sarnecki, Kathleen H Burns, Laura D Wood, Kevin M Waters, Ralph H Hruban, Denis Wirtz, and Pei-Hsun Wu. A robust nonlinear tissue-component discrimination method for computational pathology. *Laboratory Investigation*, 96(4):450–458, 2016.
- [783] Corentin Gueréndel, Phil Arnold, and Ben Torben-Nielsen. Creating small but meaningful representations of digital pathology images. In *MICCAI Workshop on Computational Pathology*, pages 206–215. PMLR, 2021.
- [784] Huisi Wu, Zhaoze Wang, Youyi Song, Lin Yang, and Jing Qin. Cross-patch dense contrastive learning for semi-supervised segmentation of cellular nuclei in histopathologic images. In *Proceedings of the IEEE/CVF Conference on Computer Vision and Pattern Recognition*, pages 11666–11675, 2022.
- [785] Soufiane Belharbi, Jérôme Rony, Jose Dolz, Ismail Ben Ayed, Luke McCaffrey, and Eric Granger. Deep interpretable classification and weakly-supervised segmentation of histology images via max-min uncertainty. *IEEE Transactions on Medical Imaging*, 41(3):702–714, 2021.
- [786] Parmida Ghahremani, Joseph Marino, Ricardo Dodds, and Saad Nadeem. DeepLiif: An online platform for quantification of clinical pathology slides. In *Proceedings of the IEEE/CVF Conference on Computer Vision and Pattern Recognition*, pages 21399–21405, 2022.
- [787] Pushpak Pati, Antonio Foncubierta-Rodríguez, Orcun Goksel, and Maria Gabrani. Reducing annotation effort in digital pathology: A co-representation learning framework for classification tasks. *Medical Image Analysis*, 67:101859, 2021.
- [788] Yiqing Shen, Dinggang Shen, and Jing Ke. Identify representative samples by conditional random field of cancer histology images. *IEEE Transactions on Medical Imaging*, 41(12):3835–3848, 2022.
- [789] Chuang Zhu, Wenkai Chen, Ting Peng, Ying Wang, and Mulan Jin. Hard sample aware noise robust learning for histopathology image classification. *IEEE Transactions on Medical Imaging*, 41(4):881–894, 2021.
- [790] Ming Y Lu, Drew FK Williamson, Tiffany Y Chen, Richard J Chen, Matteo Barbieri, and Faisal Mahmood. Data-efficient and weakly supervised computational pathology on whole-slide images. *Nature Biomedical Engineering*, 5(6):555–570, 2021.
- [791] Chetan L Srinidhi, Seung Wook Kim, Fu-Der Chen, and Anne L Martel. Self-supervised driven consistency training for annotation efficient histopathology image analysis. *Medical Image Analysis*, 75:102256, 2022.
- [792] Yu’Ang Zhu, Yuxin Zheng, and Zhao Chen. Cell detection by robust self-trained networks. In *International Conference on Pattern Recognition and Intelligent Systems*, pages 64–67, 2021.
- [793] Soufiane Belharbi, Jérôme Rony, Jose Dolz, Ismail Ben Ayed, Luke Mc-

- Caffrey, and Eric Granger. Deep interpretable classification and weakly-supervised segmentation of histology images via max-min uncertainty. *IEEE Transactions on Medical Imaging*, 2021.
- [794] Simon Graham, David Epstein, and Nasir Rajpoot. Dense steerable filter cnns for exploiting rotational symmetry in histology images. *IEEE Transactions on Medical Imaging*, 39(12):4124–4136, 2020.
- [795] Shamima Nasrin, Md Zahangir Alom, Tarek M Taha, and Vijayan K Asari. Pcolornet: investigating the impact of different color spaces for pathological image classification. In *Medical Imaging: Digital Pathology*, volume 11320, page 113201A. International Society for Optics and Photonics, 2020.
- [796] Le Hou, Dimitris Samaras, Tahsin M Kurc, Yi Gao, James E Davis, and Joel H Saltz. Patch-based convolutional neural network for whole slide tissue image classification. In *Proceedings of the IEEE conference on computer vision and pattern recognition*, pages 2424–2433, 2016.
- [797] Massimo Salvi, Nicola Michielli, and Filippo Molinari. Stain color adaptive normalization (scan) algorithm: separation and standardization of histological stains in digital pathology. *Computer methods and programs in biomedicine*, 193:105506, 2020.
- [798] Shivam Kalra, Hamid R Tizhoosh, Sulmaan Shah, Charles Choi, Savvas Damaskinos, Amir Safarpour, Sobhan Shafiei, Morteza Babaie, Phedias Diamandis, Clinton JV Campbell, et al. Pan-cancer diagnostic consensus through searching archival histopathology images using artificial intelligence. *NPJ Digital Medicine*, 3(1):1–15, 2020.
- [799] Ali Mirzazadeh, Arshawn Mohseni, Sahar Ibrahim, Felipe O Giuste, Yuanda Zhu, Bahig M Shehata, Shriprasad R Deshpande, and May D Wang. Improving heart transplant rejection classification training using progressive generative adversarial networks. In *IEEE EMBS International Conference on Biomedical and Health Informatics (BHI)*, pages 1–4. IEEE, 2021.
- [800] Youqing Mu, Hamid R Tizhoosh, Rohollah Moosavi Tayebi, Catherine Ross, Monalisa Sur, Brian Leber, and Clinton JV Campbell. A bert model generates diagnostically relevant semantic embeddings from pathology synopses with active learning. *Communications Medicine*, 1(1):1–13, 2021.
- [801] Tathagato Rai Dastidar and Renu Ethirajan. Whole slide imaging system using deep learning-based automated focusing. *Biomedical Optics Express*, 11(1):480–491, 2020.
- [802] Pinky A Bautista and Yukako Yagi. Detection of tissue folds in whole slide images. In *2009 Annual International Conference of the IEEE Engineering in Medicine and Biology Society*, pages 3669–3672. IEEE, 2009.
- [803] Joseph Boyd, Mykola Liashuha, Eric Deutsch, Nikos Paragios, Stergios Christodoulidis, and Maria Vakalopoulou. Self-supervised representation learning using visual field expansion on digital pathology. In *IEEE/CVF International Conference on Computer Vision*, pages 639–647, 2021.

9. Appendix

9.1. Clinical Pathology Workflow

Sample Collection Tissue samples are categorized into two general types a) *small specimens*, normally obtained to diagnose disease and guide subsequent treatment and b) *large specimens*, surgically removed to treat the disease after diagnosis. *Small specimen* biopsies are performed by different specialties in different settings, which can vary from family doctors sampling skin lesions to head and neck specialists performing panendoscopic biopsies under anesthesia. Based on the type of sample required and its originating site, small specimen samples are obtained by different methods: 1) core biopsies, 2) cytological specimens, 3) small excisions, and 4) pincer biopsies. In contrast, *large specimens* are mostly resections performed by surgeons for treatment purposes once the diagnosis has already been obtained. Large specimens are significantly more complex than small specimens and require a high-level of expertise to process before reaching the microscopic interpretation step.

Accessioning The patient-care team fills out request forms which are tagged to the pathology specimen and sent along with the sample to the pathology department to enter the specimen and patient information into the laboratory information system (LIS). Depending on the institution, the LIS can then be linked to the electronic medical records (EMR) system to populate basic demographic data, and to a slide tracking system (STS) to locate and time each event in pathology. Ensuring that accessioning is done correctly is essential, as specimen mix-ups or incorrect data entry from request forms are a large source of errors in the workflow [519].

Specimen Preparation Most samples arrive at the pathology lab having already been preserved in a 4% formalin solution. Other preservation media are used for specific pathology objectives; notably using Roswell Park Memorial Institute medium (RPMI) to preserve cells for flow cytometry and glutaraldehyde preservation for electronic microscopy [557]. Sometimes, the samples are sent to the pathology lab without a preservation medium, and in this “fresh” state the tissue will undergo cold ischemia changes until the pathologist can assess the sample, perform specimen preparation, and fix the tissue in the preservation media. Indeed, each of these events has an impact on the quality of the tissue, which in turn significantly affects the quality of the final WSI. Specifically, large specimens are almost always processed by a pathologist who will open the container, take basic measurements, and open the organ to ensure uniform formalin penetration.

At some medical centers, intra-operative consultations for resection samples are processed in a frozen section procedure, which allows for more rapid diagnosis of the tissue specimens while trading off diagnostic accuracy when compared to fixation in formalin [558, 559]. Frozen section samples will be rapidly frozen after the preceding *grossing* step, therefore they arrive in the lab unprocessed and remain unprocessed until after grossing, undergoing the aforementioned cold ischemia changes in the meantime.

Grossing Once the basic specimen preparation has occurred, the tissue is analyzed by the pathology team without the use of a microscope; a step called grossing. Smaller specimens are often grossed by technicians who fill out a template-based description notably highlighting the number, size, and appearance of the fragments. After grossing, the tissue fragments are placed into tissue cassettes for final fixation. Grossing larger specimens is much more complex, and is usually performed by pathologists, pathologist-assistants, medical residents, or fellows who have undergone extensive training. The grossing starts by orienting the specimen according to the surgical procedure. By cross-referencing the clinical findings and the EMR reports, the operator will localize the disease, locate the pathological landmarks, describe these landmarks, and measure the extent of the disease. Specific sampling of these landmarks is performed, and these samples are then put into cassettes for the final fixation.

Final Tissue and Slide Preparation For non-frozen section samples, the final fixation step will accrue all the samples put into cassettes and will add a last phase of fixation in formalin. Afterwards, the tissue cassettes are removed from formalin and inserted into a tissue processor which dehydrates the tissue through alcohol gradients, subsequently replacing the liquid with melted paraffin wax. These samples are removed from the tissue processor and placed into a mold filled with paraffin which solidifies into a block. A technician then cuts the blocks with a microtome into $4\mu\text{m}$ slices and places them onto positively charged slides. Slides are then deparaffinized, rehydrated by an inverse alcohol gradient, and stained with pigments such as Hematoxylin and Eosin (H&E), or further processed for ancillary testing by immunohistochemistry. Once these steps are complete, the tissue is dehydrated, cleared, and mounted with a coverslip. Note that significant variations will affect the final quality of the slides based on the performance of the prior steps, the experience of the technician who cut the slides, and batch effects from the reagents which are often reused for multiple slides prior to being replaced—known as cross-contamination.

Frozen section samples are rapidly frozen using a freezing medium such as liquid nitrogen, dry ice, or isopentane [558, 174, 175, 559]. After freezing, the tissue is cut using a microtome and fixed immediately, most often with formalin [174, 175]. Slides are then stained and covered with a glass coverslip and stored at -80°C [175].

Slide Scanning and Image Processing The stained slides are cleaned of excess mounting media and scanned with a whole-slide scanner. They are then loaded onto the image management software, which has previously been linked to the LIS and the STS [560].

Interpretation After a slide is processed and prepared, a pathologist views the slide to analyze and interpret the sample. The approach to interpretation varies depending on the specimen type. Interpretation of smaller specimens is focused on diagnosis of any

disease. Analysis is performed in a decision-tree style approach to add diagnosis-specific parameters, e.g. esophagus biopsy → type of sampled mucosa → presence of foveolar-type mucosa → identify Barrett’s metaplasia → identify degree of dysplasia. Once the main diagnosis has been identified and characterized, the pathologist sweeps the remaining tissue for secondary diagnoses which can also be characterized depending on their nature. Larger specimens are more complex and the focus is on characterizing the tissue and identifying unexpected diagnoses beyond the prior diagnosis from a small specimen biopsy. Microscopic interpretation of large specimens is highly dependent on the quality of the grossing and the appropriate detection and sampling of landmarks. Each landmark (e.g., tumor surface, tumor at deepest point, surgical margins, lymph node in mesenteric fat) is characterized either according to guidelines, if available, or according to the pathologist’s judgment. After the initial microscopic interpretation additional deeper cuts (“levels”), special stains, immunohistochemistry, and/or molecular testing may be performed to hone the diagnosis by generating new material or slides from the original tissue block.

Pathology Report The pathologist synthesizes a diagnosis by aggregating their findings from grossing and microscopic examination in combination with the patient’s clinical information, all of which are included in a final pathology report. The classic sections of a pathology report are patient information, a list of specimens included, clinical findings, grossing report, microscopic description, final diagnosis, and comment. The length and degree of complexity of the report again depends on the specimen type. Small specimen reports are often succinct, clearly and unambiguously listing relevant findings which guide treatment and follow-up. Large specimen reports depend on the disease, for example, in cancer resection specimens the grossing landmarks are specifically targeted at elements that will guide subsequent treatment.

In the past, pathology reports had no standardized format, usually taking a narrative-free text form. Free text reports can omit necessary data, include irrelevant information, and contain inconsistent descriptions [69]. To combat this, synoptic reporting was introduced to provide a structured and standardized reporting format specific to each organ and cancer of interest [69, 70]. Over the last 15 years, synoptic reporting has enabled pathologists to communicate information to surgeons, oncologists, patients, and researchers in a consistent manner across institutions and even countries. The College of American Pathologists (CAP) and the International Collaboration on Cancer Reporting (ICCR) are the two major institutions publishing synoptic reporting protocols. The parameters included in these protocols are determined and updated by CAP and ICCR respectively to remain up-to-date and relevant for diagnosis of each cancer type. For the field of computational pathology, synoptic reporting provides a significant advantage in dataset and model creation, as a pre-normalized set of labels exist across a variety of cases and slides in the form of the synoptic parameters filled out in each report. Additionally, suggestion or prediction of synoptic report values are a possible CPath application area.

9.2. Diagnostic Tasks

Here we provide some examples of diagnostic tasks where CPath has been applied, for the reader to understand the variety of diagnostic problems that CPath can be used to address.

Detection A machine learning framework for detecting cancerous tissue regions and predicting scan-level diagnosis is proposed in [273], wherein thresholding and statistical analysis used to abstain from making a decision in uncertain cases. In contrast to directly predicting the presence of cancers, feature-focused detection tasks can be highly useful in patient diagnosis and treatment planning. For example, identifying microsatellite instability is a crucial factor in determining if immunotherapy will be effective on a patient, and deep learning methods were shown to be effective at detecting microsatellite instability in [294]. Similarly, the detection of fibrous regions in liver WSIs is a precursor step to liver tumor classification and a computational approach to detection was demonstrated in [561]. Furthermore, the first automatic detection algorithm for keratin pearls, which are valuable biomarkers for oral squamous cell carcinoma grading is presented in [371]. Future research into automated detection methods for similar cancer biomarkers could be a valuable step towards developing AI-based pathologist support tools. As an example, lymphocytes, a type of white blood cell, can be detected and quantified to assess the overall health of the immune system. However, manually detecting these cells is a time-consuming task and pathologists rarely identify and count lymphocytes. Thus several computational approaches, including open source tools such as QuPath [562] and deep learning based approaches, are used to provide lymphocyte counts to pathologists [205]. Likewise, counting nuclei can contribute towards diagnoses, however, nuclei detection is a difficult task because of the large variations in the shape of different types of nuclei, such as nuclear clutter, heterogeneous chromatin distribution, and irregular and fuzzy boundaries. Addressing these issues, for example, spatially constrained context-aware correlation filters with hierarchical deep features extracted from multiple layers of a pre-trained network were proposed to accurately detect nuclei in [392].

Tissue Subtype Classification Deep neural networks have been shown to be effective at extracting molecular tumor features from histopathology images, opening new avenues for deep learning applications in computational pathology [563]. As an extension of the tissue subtype classification task, ML models are often able to identify important correlations between tissue structures and disease. Work on nuclei classification suggests that features regarding the nuclear inner texture are most relevant for high classification accuracy [561]. Additionally, a classifier discovered unique chromatin patterns associated with specific types of thyroid follicular lesions in [564]. The potential discovery of similar associations makes tissue subtype classification a relevant task to pursue. Another work presented a computational pathology framework that can localize well-known morphological features on WSIs without the need for spatial labels for each feature using attention-based multiple-instance learning on WSI classification [64]. This method outperforms standard weakly-supervised classification algorithms and is adaptable to independent test cohorts,

biopsy/resection samples, and varying tissue content. Additionally, the co-representation learning for classification (CoReL) framework is proposed in [386] to improve state-of-the-art classification performance for nuclei classification, mitosis detection, and tissue type classification with less data [386].

Disease Diagnosis As stated in 2, disease diagnosis can be considered a fine-grained classification problem which subdivides the general positive disease class into finer disease-specific labels based on the organ and patient context. Under this paradigm, research tends to be focused on maximizing performance for reliable clinical applications [497][565][422]. Recently, works have begun implementing different emulations of pathologist behaviour in their proposed models. For instance, multi-scale receptive fields were proposed for use in networks to simulate the pathologist viewing process of slides at varying zoom levels [335]. Alternatively, weighted slide-level features were used to classify Barrett's esophagus and esophageal adenocarcinoma, similar to a pathologist assessing the overall impact of various cancer biomarkers [295]. To emulate how pathologists isolate and focus on salient regions of the slide, the concept of visual attention can be applied to identify the most important regions of tissue slides, thus ignoring diagnostically-irrelevant image regions [424][444][429]. Such methods indicate a positive step towards the clinical implementation of AI-based CAD tools by reinforcing and emulating tested methodologies in pathology. Further, differential diagnoses in complicated cases of metastatic tumors and cancer of unknown primary (CUPs) can require many clinical tests to narrow a differential diagnosis, and a method called Tumor Origin Assessment via Deep Learning (TOAD) is introduced as an assistive tool to assign a differential diagnosis [309]. This work uses digitized H&E slides of tumors with known primary origins to train a model with transfer learning and weakly supervised multitask learning to simultaneously identify the tumorous or metastatic regions and predicts the site of origin.

Segmentation Segmentation CAD tools can capture characteristics of individual glands, nuclei, and tumor regions. The wide generalizability of this task to various disease types makes it a particularly suitable tool for computational pathology, on which many studies have been conducted [337][357][338][284][339]. For example, models that use segmentation to determine nuclear characteristics including size and shape can help pathologists distinguish between various cell types and consequently, disease severity [241][207]. To address segmentation challenges in histopathology tissue, aIn [356], a generalized deep learning-based framework was proposed in [356], using which uses a sequence of novel techniques for in the preprocessing, training, and inference steps which in conjunction improve the efficiency and the generalizability of model. Similarly, a new framework for WSI analysis in colonoscopy pathology, including lesion segmentation and tissue diagnosis was developed and includes an improved U-Net with a VGG net as the backbone, as well as two training and inference schemes to address the challenge of high resolution images analysis [311].

There are also some instances of segmentation in different organs. For example, an interactive segmentation model was proposed in which the user-provided squiggles guide the model toward semantic segmentation of tissue regions [374]. Also, they proposed four novel techniques to automatically extract minimalistic and human-drawn-like guiding signals from Ground Truth (GT) masks so that they can be used during the model's training. Similarly for the eye, macular edema (ME) is a common disease where analyzing the fluid lesions is a critical stage of the diagnostic process. The optical coherence tomography (OCT) technique can potentially investigate three fluid types and a novel pipeline for segmentation of the three types of fluid lesions in OCT was proposed in [362]. They presented a multi-layer segmentation to detect the ROI and presented an FCN architecture with attention gate (AG) and spatial pyramid pooling (SPP) module to improve the feature extraction. To predict cellular composition from images, ALBRT is proposed in [477], using contrastive learning to learn a compressed and rotation-invariant feature representation which first detects the presence of different cell types in an image patch and then provides cell counts for each type. Another novel deep learning model was developed for simultaneous nuclei instance segmentation in [376]. The model is based on an encoder-decoder architecture design that performs nuclei segmentation by predicting the distance of pixels from their nuclei centers along with the nuclei probability masks and predicts nuclei classes when nuclei type annotations are available. Another work in nuclei segmentation is the hard-boundary attention network (HBANet), which identifies hard-boundaries between nuclei, a difficult problem due to overlapped nuclei [566]. It presents a background weaken module (BWM) to improve the model's attention to the foreground, and integrates low-level features containing more detailed information into deeper feature layers. Furthermore, a gradient-based boundary adaptive strategy (GS) is designed to generate boundary-weakened data as extra inputs and train the model in an adversarial manner. Finally, segmentation has also been applied to delineate tumorous tissue regions for a variety of cancer types, such as breast [285][567], colorectal [370][142], and prostate cancer [483][568]. Such works assist in the efficient isolation of tumor tissue, which is a crucial task for making accurate disease predictions.

9.3. Prognosis

Prognostic models must predict the likely development of a disease based on patient features. For instance, a prognostic model was developed by adjusting a tumor microenvironment-based spatial map with clinical variables such as patient age, gender, health history, and cancer stage [541]. This multi-domain data analysis approach is advanced by another work, which uses both histopathological image data and cancer genomic data in their novel deep learning framework [484][569]. In [570], the authors discussed the correlation between platelets and other haematological measures to cancer by assessing patient status and considering the patient features in the primary care dataset, such as age and sex. They demonstrate the model performance with the plot of survival analysis per age group for platelets. Experiments on the publicly available TCGA data demonstrates that prognostic accuracy was maximized when both forms of data were simultaneously considered. Merging information from multiple WSIs of a patient allowed a

hybrid aggregation network (HANet), consisting of a self-aggregation module and a WSI-aggregation module, to predict survival risks [571].

9.4. Prediction of Treatment Response

A deep learning-based biomarker using H&E-stained images was developed to predict pathological complete response (pCR) of breast cancer patients receiving neoadjuvant chemotherapy, which demonstrates a strong prediction ability for guiding treatment decisions [572]. The developed model outperforms conventional biomarkers including stromal tumor-infiltrating lymphocytes and subtype. In another work, the authors propose a method using convolutional neural networks to discover image-based signatures for ipilimumab response prediction in malignant melanoma patients [573]. An immunotherapy response prediction in patients with non-small cell lung cancer from H&E-stained images was proposed in [574]. Similarly, a deep learning method was developed to predict the treatment response to neoadjuvant chemoradiotherapy in local advanced rectal cancer patients, which can provide assistance in making personalized treatment plans [575].

Oral epithelial dysplasia (OED) segmentation is critical for early identification and effective treatment and HoVer-Net+ is a model to simultaneously perform nuclear instance segmentation (and classification) and semantic segmentation of epithelial layers based on H&E stained histopathology slides of the oral mucosa [372]. This model achieves the state-of-the-art performance in both tasks (0.839 dice score) and is the first method for simultaneous nuclear instance segmentation and semantic tissue segmentation.

9.5. Cancer Statistics

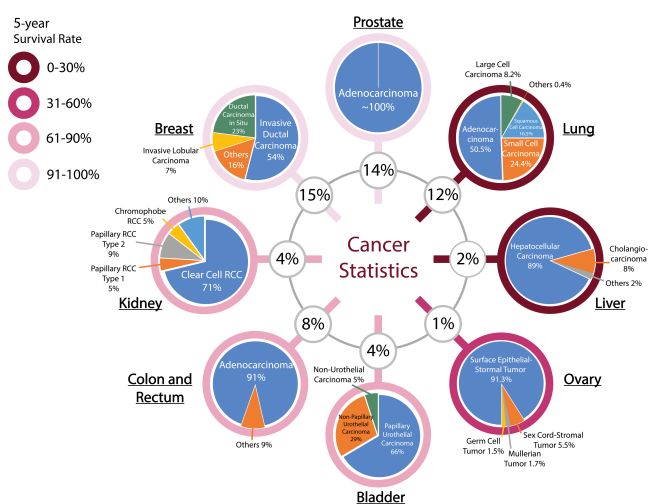


Fig. 12: Demonstration of the cancer statistics, featuring both the 5-Year Survival Rate and Incidence of each cancer in addition to incidence percentage of each subtype. The grey inner circle shows the incidence percentage of the respective cancer. The colored circle around each cancer corresponds to the respective 5-Year Survival Rate bin, showcasing the severity of the cancer. Darker shades (lower survival rate) means fewer people will survive the cancer after 5 years period and the cancer has poor prognosis. On the other hand, lighter shades (higher survival rates) mean more people will survive after 5 years and the cancer has good prognosis. [576, 577, 578, 579, 580, 581, 582, 583, 584, 585, 586, 587, 588, 589, 590, 98, 591, 592, 593]

Cancer remains the leading cause of global mortality in 2020, claiming nearly 10 million lives or approximately 1 in 6 deaths [594]. The grey circle in Figure 12 illustrates the prominence of Breast, Prostate, Colon, and Rectum, as well as Lung cancers, which collectively account for half of all diagnosed cases. The mounting volume of pathology cases poses a significant challenge in clinical workflows. This underscores the pivotal role of computational pathology in streamlining processes, aiding pathologists in coping with overwhelming workloads. Notably, certain cancers not only exhibit high prevalence but also contribute substantially to the overall mortality rates. Lung cancer, for instance, represents approximately 12% of cancer cases in the United States, with its prognosis falling within the lowest range, as depicted in Figure 12 (0 – 30%). Computational pathology proves instrumental, particularly in lung cancer, by facilitating classification and prognosis tasks due to distinct variations among its types in terms of presentation, prognosis, and treatment strategies. Conversely, there are less prevalent cancers like liver cancer characterized by poor prognoses. CPath’s ability to compile specialized datasets for such cancers not only aids pathologists but also supports clinicians in devising personalized treatment plans. Understanding disease statistics and severity is paramount when designing a Computer-Aided Diagnosis (CAD) tool in Computational Pathology (CPath) or curating datasets. By factoring in disease prevalence, mortality rates, and severity across various cancer types, CAD tools can be optimized to prioritize detection, prognosis, and treatment planning for the most prevalent and severe cases, aligning computational pathology advancements with the urgent needs of patients and healthcare practitioners.

Table 1: The following table lists commercially available WSI Scanners grouped by manufacturing company and their respective available compression slide formats.

| Company: Scanner Model (Slide Format) |
|---|
| Leica Biosystems: Aperio AT2 / CS2 / GT450 (TIFF (SVS)) |
| Hamamatsu: Nanozoomer SQ / S60 / S360 / S210 (JPEG) |
| F. Hoffmann-La Roche AG: Ventana DP200 / iScan HT / iScan Coreo (BIF, TIFF, JPG2000, DICOM) |
| Huron Digital Pathology: TissueScope 1Q / LE / LE120 (BigTIFF, DICOM compliant) |
| Philips: Ultra-Fast Scanner (iSyntax Philips proprietary file) |
| 3DHistech: Panoramic Series (MRXS, JPG, JPG2000) |
| Mikrosan Technologies: SL5 (TIFF) |
| Olympus: SL5 (JPEG, vsi, TIFF) |
| Somagen Diagnostics: Sakura VisionTek (BigTIFF, TIFF, JPG2000) |
| Akoya Biosciences: Vectra Polaris (JPEG, single-layer TIFF, BMP, or PNG) |
| Meyer Instruments: EASYSKAN PRO 6 (SVS, MDS, JPEG, JPEG2000) |
| Kfbio: KF-PRO (JPEG, JPEG2000, BMP, TIFF) |
| Motic: EasyScan Pro (JPEG, JPEG2000, Aperio Compatible) |
| Precipoint: PreciPoint O8 (GTIF) |
| Zeiss: Zeiss Axio (Not specified) |
| Objective Imaging: Glissando (SVS, BigTIFF) |
| Microvisioneer: manualWSI (Not specified) |

9.6. Whole Slide Imaging

Generally, a WSI scanning device is composed of four major components [180]: (1) a light source; (2) a slide stage; (3) an objective lens; and (4) a digital camera. In order to produce a WSI that is in focus, which is especially important for CPath works, appropriate focal points must be chosen across the slide either using a depth map or by selecting arbitrarily spaced tiles in a subset [187]. Once focal points are chosen, the image is scanned by capturing tiles or linear scans of the image, these individual components are then stitched together to form the full image known as the big flat TIFF image [180, 187]. To reduce the area needed to be scanned, a segmentation algorithm can be used within the scanner to separate tissue regions from extraneous background regions [198]. Additionally, slide can also be scanned at various magnification levels depending on the downstream task and analysis required. The vast majority of WSIs are scanned at $20\times$ ($\sim 0.5\mu\text{m}/\text{pixel}$) or $40\times$ ($\sim 0.25\mu\text{m}/\text{pixel}$) magnification as these are the most useful in practice for general pathologist [180].

WSI Storage and Standards

WSIs are in giga-pixel dimension format [30, 188]. For instance a tissue in $1\text{cm} \times 1\text{cm}$ size scanned @ $0.25\mu\text{m}/\text{pixel}$ resolution can produce a 4.8GB image (uncompressed) with a $50,000 \times 50,000$ pixels. Due to this large size, hardware constraints may not support viewing entire WSIs at full resolution [189]. Therefore, WSIs are most often stored in a tiled format, so that only the viewed portion of the image (tile) is loaded into memory and rendered [189]. Additionally, to support efficient zooming, WSIs are stored in a pyramidal structure, where higher levels of the pyramid represent lower magnification levels. The highest level of the pyramid is generally a very low resolution thumbnail snapshot of the WSI, while the lowest is the full resolution image (i.e. big-flat TIFF). In this way, different zoom levels can be captured and displayed in a WSI format efficiently—artificially replicating different zooming levels from optical microscopy [193, 189]. Additionally, WSIs can be compressed before storage to reduce their filesize, often using JPEG, JPEG 2000, or LZW algorithms, which can reduce an image size by more than seven times [180]. Alongside the WSI, metadata regarding patient, tissue specimen, scanner, and WSI information is stored for reference [30, 188, 190]. Due to their clinical use and importance, it is important to develop effective storage solutions for these WSI data files and metadata, allowing for robust data management, querying of WSIs, and efficient data retrieval [191, 192].

To develop CPath CAD tools in a widespread and general manner, a standardized format for WSIs and their corresponding metadata is essential [188]. However, there is a general lack of standardization for WSI formats outputted by various scanners, as shown in Table 1, especially regarding metadata storage. The Digital Imaging and Communications in Medicine (DICOM) standard provides a framework for biomedical image format and data management and has been extended to the CPath field through Supplement 145 [190, 193]. Some research has shown that the use of the DICOM standard allows for efficient data access and greater interoperability between different centres and different CPath-related devices [188]. However there is currently a lack of widespread adoption [188, 30, 595, 190], reflected in Table 1 where only two recorded scanners are DICOM-compliant. Notably, with regards to metadata, DICOM provides a systematic format detailing a variety of relevant medical information, consistent with DICOM standards in other medical imaging fields [190]. The expansion through Supplement 145 also adds pyramid-tiling for WSIs, a format that is directly beneficial to creation of CPath and CAD tools. While many scanners have adopted the pyramid-type scheme for image data, they have not fully adopted the DICOM image format, outputting in either TIFF, BigTIFF format, or in TIFF-derivatives such as SVS or GTIFF. While the TIFF format allows for semi-structured metadata [189], the consistency in metadata structure offered by DICOM is an advantage over the former [190].

Apart from storage format, a general system for storing and distributing WSIs is also an important pillar for CPath. Whereas in other medical imaging fields such as radiology, images are often stored in a picture archiving and communications systems (PACS) in a standardized DICOM format, with DICOM storage and retrieval protocols [189], the need for standardization persists in

pathology for WSI storage solutions. Few works have proposed solutions to incorporate DICOM-based WSIs in a PACS, although some research has successfully implemented a WSI PACS consistent using the DICOM standard using a web-based service for viewing and image querying [189].

9.7. *Organs and Diseases*

The following Appendix section is a supplement to section 2.5. Details are provided for several notable works in CPath for the organ types listed in the subsection.

Breast

- A subset of breast-focused research studies the correlation between tissue morphology and molecular differences. Molecular testing can often be preferred over tissue morphology assessments when selecting breast cancer treatments as it provides objective and reproducible disease classifications. For instance, the connection between epithelial patterns with various molecular predictions and heatmaps was used to clearly visualize this correlation in [436].
- In [349] a proposed U-NET based architecture called piNET is used for cell detection and classification in order to calculate the proliferation index (PI) of the Ki67 biomarker. The network classifies cells as Ki67+/Ki67- and uses this classification to calculate the PI. The architecture is able to achieve a PI accuracy of 85.2%, higher than the accuracies of other models [349].
- A two-stage CNN, one for patch-level feature extraction and the other for classification, was proposed and achieved 95% accuracy for classifying normal, benign, in situ carcinoma, and invasive carcinomas [596].
- In [597], several well-known models (DenseNet121, ResNet50, VGG16, and Xception), are compared with their own CNN model named lightweight convolutional neural network (LCNN) for the detection of breast cancer metastasis to axillary lymph nodes (ALN).
- Further research has proposed an automated patient-level tumor segmentation and classification system that takes full use of diagnosis information hints from pathologists [373]. A multi-level view DeepLabV3+ (MLV-DeepLabV3+) was created to investigate the differentiating aspects of cell characteristics between tumor and normal tissue for tumor segmentation. Furthermore, expert segmentation models were chosen and merged using Pareto-front optimization to mimic expert consultation and provide a flawless diagnosis.

Prostate

- Most works focus on prostate aim to classify cancer based on Gleason scoring. To aid in that effort, a U-Net model for object semantic segmentation is created in [354], with the goal of precisely labeling each pixel in an image as belonging to either foregrounds, which may contain glands, or background.
- A method is proposed in [389] that trains a model on both epithelial cell detection and Gleason grade prediction tasks to achieve better performance in both tasks than models trained on either of the tasks alone. Further, some works have investigated epithelial cell detection to explore data augmentation and stain/color normalization techniques [199, 204] which demonstrates the importance of epithelial cell features as an indicator for prostate cancer detection.
- Work in [598] focused on classifying glands, gland boundary regions, and stroma. The authors opted for two classic classifiers: support vector machines (SVM) and Convolutional Neural Networks (CNNs), finding the SVM to perform best by offering high accuracy and good indicators of regions which are present with high probability. The output of the SVM classifier could help pathologists locate existing glands, saving them a significant amount of time from actively searching for them.

Lung

- To further aid diagnosis, prognosis, and treatment decisions, a novel method for nuclei detection and characterization is introduced in [241] using an unsupervised autoencoder network to learn without the use of any annotations. The unsupervised autoencoder is used to construct a CNN that only requires 5% of training data to generate comparable results to the SOTA on supervised lymphocyte and nuclei tasks, thereby reducing the need for extremely large annotated datasets.
- In [498], the work not only classifies adenocarcinoma and squamous cell carcinoma, but also predicts the 10 most commonly mutated genes in adenocarcinoma. The findings indicate the presence of genotype-phenotype correlations for lung cancer tissues, and paves the way for cancer classification and mutation predictions of other types of less common lung cancers.

Colon and Rectum

- An interesting detection application for MSI is implemented in [294]. In this work, ResNet-18 is used to predict MSI from H&E slides with an AUC of 0.84, although performance was reduced with tissue samples from different ethnicities. As MSI requires extensive additional testing which is not always performed [294], the study highlights the applicability of deep learning in detecting this important prognosis indicator.
- The work in [435] presents a weakly-supervised model named the Slide Level Annotation Model (SLAM) based on ShuffleNet [599] that can be trained to detect genetic/molecular changes, including MSI or BRAF mutation, in colorectal WSIs. The results show improvement over SOTA models, and a visualization heatmap is generated which allow for improved result interpretability and analysis.

Bladder

- In [422], bladder cancer grade classification is explored using a large dataset of 915 WSIs which ends up outperforming 17 pathologists by an average of 10%. The model in this study has been integrated into an end-to-end diagnostic tool that provides interpretable cellular-level ROI visualization and natural language descriptions of histology slides. However, there was also a diagnostic disagreement of 23% between the system and pathologists, which could hinder the diagnostic process and consequently limit the overall productivity.

Kidney

- For effective patient prognosis, tissue microarray analysis is typically used to identify biomarkers. Currently, this process is time-consuming and prone to error, especially due to the heterogeneity of nuclei. A random forest classifier was proposed to more efficiently detect cancerous nuclei in MIB-1 stained tissue micro-array spots and predict the survival rate for renal cell carcinoma (RCC) patients in [388]. The results show that there is a significant difference in survival times for patients with high and low proliferating tumors, and further state MIB-1 staining as a key prognostic factor for the survival chance of RCC.
- To aid in determining donor organ acceptance in kidney transplants, [84] uses frozen kidney sections as input data to identify the percentage of glomerulosclerosis.

Brain

- The achieved state-of-the-art SOTA classification accuracy on the 2014 MICCAI Grand Challenge dataset was achieved in [76]. However, on completely unseen datasets, performance varied from 84% to 93%. This shows the complexity of the diseases; low grade glioma (LGG) versus glioblastoma multiforme (GBM) classification is not a trivial task. Not only do their appearances vary in pathological samples, the diagnosis is often made from a few distinct features in a small slide region [76].

Liver

- A notable work for liver cancer classification evaluates a pathologist's performance using a liver cancer diagnostic tool for the diagnosis of HCC and cholangiocarcinoma [497]. Despite lower performance than pathologists, the tool's decisions directly affected pathologists' decisions. Correct model predictions increased pathologists' average accuracy, while incorrect predictions lowered average accuracy. Furthermore, pathologists frequently consulted the model's predictions for difficult cases. This confirms the potential use of deep learning models as an AI diagnostic tool to provide knowledgeable second opinions.

Lymph Nodes

- One of the earliest histopathology challenges, ICPR2010, targets lymphocyte and centroblast counting [600].
- The importance of the lymph nodes in cancer diagnosis is notably addressed in the CAMELYON16 and CAMELYON17 Challenges, in which participants classify lymph node metastases [271]. Metastases in breast regional lymph nodes are classified based on size: micrometastasis, macrometastasis, and isolated tumour cells (ITCs). The ITC classification accuracy was less than 40% for all top teams. This indicates that there was extreme difficulty in detecting ITCs, most likely due to the small size and variability. These results suggest that further improvements can be made by introducing more true positives of ITC data, or incorporating IHC stain information as an additional layer of information to improve detection robustness.

Organ Agnostic

- Nuclei segmentation of epithelial, inflammatory, fibroblast and miscellaneous tissues is performed across seven different organs in [284]. The method attempts to generalize across a large variety of datasets for increased usability and scalability in a clinical setting.

Table 2: Commercially available annotation software along with their manufacturing company and available input slide formats.

| Company: Annotation Tool (Input Format) |
|---|
| Leica Biosystems: Aperio eSlide Manage (JFIF, JPEG2000, PMM) |
| Pathcore: Sedeen Viewer (Aperio SVS, Leica SVN, TIFF, JPEG2000) |
| Indica: Halo (TIFF/SVS) |
| Objective Pathology: MyObjective (Scanner-wide compatibility) |
| ASAP: ASAP (Multiple formats through OpenSlide) |
| SiliconLotus: SiliconLotus (Not specified) |
| Augmentiqs: Annotation Software Suite (Not specified) |
| QuPath: QuPath (Multiple formats, Bio-formats and OpenSlide) |
| Proscia: Concentriq (Not specified) |
| Visiopharm A/S: VisioPharm (Not specified) |
| Hamamatsu: NDP (JPEG) |
| Roche: Ventana Companion Image Analysis (BIF, TIFF, JPG2000, DICOM compliant) |
| Huron: HuronViewer (BigTIFF, FlatTIFF, DICOM compliant) |
| Philips: Intellisite (iSyntax Philips proprietary file) |
| 3DHistech: CaseViewer (JPG, PNG, BMP, TIFF) |
| AnnotatorJ [613]: AnnotatorJ (JPG, PNG, TIFF) |
| NuClick [168]: NuClick (Not specified) |

9.8. Ground Truth Labelling and Annotation

Patient-level Annotation Patient-level annotations assign a single label to a single patient and come from case reports that can address multiple WSIs from a primary organ site. In addition to the WSIs, the Laboratory Information System (LIS) may also contain additional metadata, diagnostic information, and analytical or synoptic report information [601]. Notably, the LIS can store specimen type, molecular and genetic tests, patient medical history, and clinical variables such as the patient’s age and gender [602, 603].

Slide-level Annotation Slide-level annotations designate labels for a single WSI, which encompasses diagnosis and cancer information [309, 275]. In comparison to the patient-level, this level of focus provides a more precise tissue location for the provided diagnosis [323, 457, 604].

ROI-level Annotation ROI-level annotation identifies regions within a slide that can be of either diagnostic or analytical relevance to a pathologist. Regions themselves can be designated using two methods: (1) bounding boxes [169, 213, 226] or (2) pixel-wise masks that are augmented on the WSIs [605, 227, 61]. Importantly, each ROI is considered to be a single class [606], but the labels represent more detailed tissue structures providing more specific and detailed diagnostic information than patient and slide levels [64], ultimately being more applicable in disease diagnosis tasks [372].

Patch-level Annotation Patch-level annotation is done on mosaic tiles (usually in a square shape) extracted from the WSI/ROI with a given field of view (FOV). Most deep-learning models are trained at the patch level, which contains anatomical structures of tissues and cells. Patches are either single-labeled or multi-labeled according to the taxonomical labeling workflow [387]. One key aspect for patch-level annotation is determining the optimum FOV to encompass enough tissue classes [607], as considering smaller or bigger FOV can provide different advantages, as demonstrated in Figure 7 for the patch-level.

Patch-Size Selection The choice of the patch size is limited by the computational complexity of the hardware that is used for training CAD tools. For instance, the majority of deep learning pipelines accept image sizes of less than 300×300 pixels [608, 609, 475, 610, 64]. The size of the FOV needs to be determined such that acceptable levels of morphological tissues will be covered within that patch. Accordingly, the pixel resolution is determined given a certain FOV and patch size. Given the above factors, if a larger FOV is required, then pixel resolution is limited which translates to information loss. In comparison, if higher pixel resolution is required, then the FOV will be limited accordingly which may exclude cellular/architectural relevance pertaining to the underlying class representation [386]. To mitigate this tradeoff, larger image dimensions are required which consequently increases the computational power required for patch processing (e.g. high RAM GPU memory or parallelized multi-GPU processing) [607].

Pixel-level Sizing Pixel-level annotation requires labelling each pixel as a specified class. In this level, features are simple to extract and sufficient for describing the images as they encompass color and texture information [611]. However, there is a lack of biological interpretability as the other levels of annotation more appropriately describe characteristics of the cellular and tissue structures [276]. A solution based on human-interpretable image features can include histological knowledge and expert annotations that can describe different cell anatomies such as the stroma, the nuclei of the cells, and the size and shape of tumor regions, as well as the texture of the tissues and the location of tumor-infiltrating lymphocytes [612].

Pixel-wise masks are differentiated from pixel-level annotations in that when an ROI mask of this type is tiled into multiple instances (i.e. patches), each sample is considered a single class. The ROI-level is in contrast to the pixel-level annotations, wherein the latter is defined to include all annotations where each patch can contain several class types.

9.9. Surveyed Datasets

9.9.1. Table Creation Details

For each dataset recorded in the literature, a collection of information was collected. This information was organized into 10 categories, listed below. The full table is given in Table 9.11:

1. *Dataset Name*: The name of the dataset, if given. If no name is given, then a name was given for book-keeping purposes.
2. *References*: The works that use this dataset are listed.
3. *Availability*: A hyperlink to the dataset, when publicly available or available for request directly is provided.
4. *Stain type*: The type of stain used.
5. *Size*: Describes the number of WSIs, where this information is available, or the number of patches present in the dataset.
6. *Resolution (μm)/ Magnification*: Presents the resolution, in micrometers along with the magnification in the format $\mu\text{m}/\text{Magnification}$. If a piece of information is unavailable (either resolution or magnification) this information is omitted from the table.
7. *Annotation Type*: Describes the annotation granularity present in the dataset (patient, slide, ROI/ROI mask, patch, pixel) where available.
8. *Label Structure*: Whether each image in the dataset has a single label associated with it, or multiple. Datasets, where each image has only a single label associated with it, are labeled with *S*, whereas those with multiple labels are labeled with *M*.
9. *Classes*: The number of classes available, where this count is meaningful. Where it is more helpful to describe the format of ground truth (ex. nucleus pixel locations), this is written instead.
10. *Class Balance (CB)*: Datasets which are balanced are marked with a *B*, whereas those which are imbalanced are marked as *I*. Those where this information is unavailable are marked with an *U*.

9.10. Organ Overview

For each paper recorded in the literature, a collection of information about their specific goal was collected. This information was categorized by organ and arranged into a table, the organs being: Basal/Epithelium, Bladder, Brain, Mouth/Esophagus, Breast, Liver, Lymph Node, Prostate/Ovary, Kidney, Lung, Pancreas, Thyroid, Stomach/Colon. Below will be the explanation of each column in Table 9.11:

1. *References*: Reference number of the paper that involved the specified task.
2. *Tasks*: Specific target goal that the work wanted to achieve, this range from different types of detection, classification, and segmentation to prognosis and diagnosis.
3. *Disease Specification*: Describes the pathology of the target goal of the paper.
4. *Methods*: Define the different machine learning methods used to achieve the proposed target task of the paper.

9.11. Technicalities by Task

For each paper recorded in the literature, a collection of information on the Neural Network architectures used was organized and categorized by its specific task. It was found that across the majority of papers, the following five tasks were the most prevalent: Detection, Disease Diagnosis, Segmentation, WSI Processing, and Patient Prognosis. At the end of the table, an **Other Task** section was added to attach other works that don't follow the selected tasks. Below will be the explanation of each column in Table 9.11:

1. *References*: Reference number of the paper that involved the specified task.
2. *Tasks Specification*: Describes the pathology of the target goal of the paper.
3. *Architecture*: Defines the different Neural Network architectures used to achieve the proposed target task of the paper.
4. *Datasets*: Name of the datasets used for the specified task (see Table 9.11 for information on datasets).

| Dataset Name | References | Availability | Stain Type | Size | Res(μm)/ Mag | Annotation | Label | Class | CB |
|-------------------------|------------|--------------|-------------------------------------|--------------------------------|---------------------------------|--------------|-------|-------|------|
| Basal/Epithelium | | | | | | | | | |
| NKI-VGH | [614] | Link | H&E | 158 ROIs | N/A | Pixel | S | 2 | U |
| AJ-Epi-Seg | [550] | Link | H&E | 42 ROIs | 20x | Pixel | S | 2 | U |
| TCGA-Phil | [277] | TCGA | H&E | 50 WSIs | 40x | Pixel | S | 4 | I |
| MOIC | [605] | N/A | N/A | 6 610 MOIs | 10x | Slide | S | 2 | U |
| MOIS | [605] | N/A | N/A | 1 436 MOIs | 10x | Pixel | S | 2 | U |
| Jiang et al. | [605] | N/A | N/A | 128 WSIs | 40x | Pixel | S | 2 | U |
| MIP | [615] | N/A | H&E | 108 Patients | 40x | Patient | S | 2 | I |
| YSM | [615] | N/A | H&E | 104 Patients | 40x | Patient | S | 2 | I |
| GHS | [615] | N/A | H&E | 51 Patients | 40x | Patient | S | 2 | I |
| DKI | [304] | N/A | H&E | 695 WSIs | 40x | Slide | S | 2 | I |
| Y/CSUXH-TCGA | [616] | N/A | H&E | 2 241 WSIs | 0.275/40x, 0.5/20x, 1/10x, 5/4x | Slide | S | 4 | U |
| BE-Hart | [617] | N/A | H&E | 300 WSIs | 40x | Patch | S | 2 | I |
| BE-Cruz-Roa | [618] | N/A | H&E | 308 ROI, 1 417 Patches | 10x | Patch | S | 2 | U |
| DLCS | [172] | N/A | H&E | 5 070 WSIs | 0.25/40x | Slide | S | 4 | U |
| BE-TF-Florida-MC | [172] | N/A | H&E | 13 537 WSIs | 0.24/20x, 0.5/20x, 0.55/20x | Slide | S | 4 | U |
| Bladder | | | | | | | | | |
| TCGA+UFHSH | [422] | By Req. | H&E | 913 WSIs | 40x | Slide, ROI | S | 2 | I |
| TCGA-Woerl | [146] | TCGA | H&E | 407 WSIs | 40x | ROI | S | 4 | I |
| Bla-NHS-LTGU | [387] | N/A | IF | 75 ROIs | N/A | Pixel | S | 2 | U |
| CCC-EMN MIBC | [146] | N/A | H&E | 16 WSIs | 40x | ROI | S | 4 | I |
| UrCyt | [619] | N/A | ThinStrip | 217 WSIs | 40x | Pixel | S | 3 | U |
| AACHEN-BLADDER | [492] | N/A | H&E | 183 Patients | N/A | Patient | S | 2 | I |
| Brain | | | | | | | | | |
| TCGA-Shirazi | [85] | N/A | H&E | 654 WSIs, 849 ROIs | 0.5 | ROI | M | 4 | I |
| TCGA-GBM-Tang | [620] | TCGA | N/A | 209 Patients, 424 WSIs | 0.5/20x | Patient | S | 2 | I |
| MICCAI14 | [621, 76] | N/A | H&E | 45 WSIs | N/A | Slide | S | 2 | B |
| M-Qureshi | [348] | N/A | H&E | 320 ROIs | N/A | ROI | S | 4 | B |
| Lai et al. | [603] | N/A | Amyloid-β antibody | 30 WSIs | 20x | Slide, Pixel | S | 2, 3 | I, U |
| Vessel | [622] | Link | H&E, PAS-H, Masson trichrome, Jones | 226 WSIs | 0.25/40x | ROI | M | 3 | I |
| WCM | [623] | N/A | H&E | 87 WSIs | N/A | Patch | S | 2 | U |
| Esophagus | | | | | | | | | |
| ESO-DHMC | [295] | N/A | H&E | 180 WSIs, 379 ROIs | 20x | ROI | S | 4 | U |
| Kidney | | | | | | | | | |
| AIDPATH _A | [624, 396] | Link | PAS | 31 WSIs | 20x | Pixel | S | 3 | U |
| AIDPATH _B | [624, 396] | Link | PAS | 2 ~ 340 Patches | 20x | Patch | S | 2 | B |
| M-Gadermayr | [625] | N/A | PAS | 24 WSIs | 20x | ROI | S | 2 | U |
| TCGA-RCC-Lu | [64] | TCGA | H&E | 884 WSIs | 20x, 40x | Slide | S | 3 | I |
| BWH-CRCC | [64] | N/A | H&E | 135 WSIs | 10x, 20x | Slide | S | 3 | I |
| BWH-BRCC | [64] | N/A | H&E | 92 WSIs | 40x | Slide | S | 3 | I |
| BWH-RCC | [64] | N/A | H&E | 135 WSIs | 40x | Slide | S | 3 | I |
| Kid-Wu | [394] | N/A | N/A | 1 216 Patients, 60 800 Patches | N/A | Patch | S | 2 | U |
| UHZ-Fuchs | [388] | N/A | MIB-1 | 133 Patients | 0.23/40x | Patient | S | 9 | I |
| WUPAX | [84] | N/A | H&E | 48 WSIs | 0.495 | ROI | S | 2 | I |
| Pantomics | [626] | N/A | H&E | 21 349 Patches | 0.5/20x | Patch | S | 2 | U |
| RUMC | [152] | N/A | PAS | 50 WSIs | 0.24/20x | Pixel | S | 10 | I |
| Mayo | [152] | N/A | PAS | 10 WSIs | 0.49/20x | Pixel | S | 10 | I |
| UHZ-RCC | [296] | N/A | MIB-1 | 1 272 Patches | N/A | Patch | S | 2 | I |
| Kid-Cicalese | [627] | N/A | PAS | 1 503 ROIs | N/A | ROI | S | 2 | I |
| Kid-Yang | [395] | N/A | H&E, PAS, Jones | 949 WSIs | 0.25 | ROI | S | 2 | U |
| Kid-BWH-TCGA | [454] | N/A | H&E | 1 184 WSIs | 20x | Slide | S | 3 | I |
| WTH | [428] | N/A | N/A | 3 734 Patients | N/A | Patient | S | 3 | I |
| TCGA-RCC-Chen | [628] | N/A | N/A | 45K ROIs | 20x | ROI | S | 3 | B |

Table 9.11 Continued on Next Page

Data Compilation (Continued)

| Continuation of Data Compilation Table 9.11 | | | | | | | | | | |
|---|-----------------|--------------|---|---------------------------|--|---------------------|-------|---------|----|--|
| Dataset Name | References | Availability | Stain Type | Size | Res(µm)/ Mag | Annotation | Label | Class | CB | |
| BWH-RCC-Chen | [628] | N/A | N/A | 1 661 ROIs | 20× | ROI | S | 3 | I | |
| MC-Gallego | [351] | N/A | H&E, PAS | 20 WSIs, 1 184 ROIs | 20×, 40× | ROI | S | 2 | I | |
| AACHEN-RCC | [492] | N/A | H&E | 249 Patients | N/A | Patient | S | 3 | I | |
| ANHIR | [629] | Link | H&E, MAS, PAS, and PASM | 50 WSIs | 0.1 to 0.2/40× | Slide | S | 8 | I | |
| Glomeruli renal biopsies | [630] | N/A | H&E, PAS or Jones | 42 WSIs | 0.25 | ROI | S | 2 | I | |
| Hubmap Glom | [631] | Link | H&E, PAS, PAS-H, Silver, Jones, Van Gieson, etc | 3712 WSIs | 0.13 to 0.25/40× | ROI | S | 2 | U | |
| KPMP | [631] | Link | PAS-H | 26 WSIs | 0.25/40× | ROI | M | 2 | U | |
| Breast | | | | | | | | | | |
| BreakHis | [233, 235] | By Req. | H&E | 82 Patients, 7 909 ROIs | 40×, 100×, 200×, 400× | ROI | S | 2 | I | |
| CAMELYON 16 | [514, 238, 61] | link | H&E | 399 WSIs | 0.243/20×, 0.226/40× | Slide, ROI | S | 3 | I | |
| BACH18 | [227, 596] | Link | H&E | 40 WSIs, 400 Patches | 0.42, 0.467 | Patch, Pixel | S | 4 | B | |
| TUPAC16 | [272] | Link | H&E | 821 WSIs | 40× | Slide | S | 3 | I | |
| TUPAC16-Mitoses | [272] | Link | H&E | 73 WSIs | 0.25/40× | ROI | S | 2 | U | |
| TUPAC16-ROIs | [272] | Link | H&E | 148 WSIs | 40× | ROI | S | 2 | U | |
| CAMELYON 17 | [632, 61, 239] | Link | H&E | 1 399 WSIs | 0.23, 0.24, 0.25 | Patient, Slide, ROI | S | 5, 4, 3 | I | |
| BiolImaging | [263, 633] | N/A | H&E | 285 WSIs | 0.42/200× | Slide | S | 4 | B | |
| Ext-BiolImaging | [264] | N/A | H&E | 1 568 WSIs | 0.42/200× | Slide | S | 4 | I | |
| MITOS-ATYPIA14 | [634, 381] | Link | H&E | 1 696 HPFs | 40× | Pixel | S | 2 | U | |
| MITOS12 | [635, 381] | Link | H&E | 50 HPFs | 0.185/40×, 0.2273/40×, 0.22753/40×, 0.2456/40× | Pixel | S | 2 | U | |
| AJ-Lymphocyte | [550, 397] | Link | H&E | 100 ROIs | 40× | Pixel | S | 2 | U | |
| MSK | [636, 637, 62] | Link | H&E | 130 WSIs | 0.5/20× | Slide | S | 2 | I | |
| CCB | [357] | Link | H&E | 33 Patches | 40× | Pixel | S | 2 | U | |
| BIDMC-MGH | [26] | Link | H&E | 167 Patients, 167 WSIs | 0.25/40× | Patient | S | 4 | I | |
| PUIH | [213] | N/A | H&E | 4 020 WSIs | 100×, 200× | Slide | S | 4 | I | |
| HASHI | [226] | Link | H&E | 584 WSIs | 0.2456/40×, 0.23/40× | ROI | S | 2 | U | |
| TNBC-CI | [260] | Link | H&E | 50 Patches | 40× | Pixel | S | 2 | U | |
| AP | [638, 639] | Link | H&E | 300 ROIs | 40× | ROI | S | 3 | I | |
| KIMIA Path24 | [640] | Link | N/A | 28 380 Patches | 0.5/20×, 0.25/40× | Patch | S | 24 | U | |
| BCSC | [261, 445] | By Req. | H&E | 240 WSIs | 40× | Slide, ROI | M | 14 | I | |
| AJ-IDC | [550, 302, 641] | Link | H&E | 162 WSIs, 277 524 Patches | 40× | Patch | S | 2 | I | |
| PCam | [535] | Link | H&E | 327 680 Patches | 10× | Patch | S | 2 | I | |
| AJ-N | [642] | N/A | H&E | 141 ROIs | 40× | Pixel | S | 2 | U | |
| TCGA-Cruz-Roa | [643] | TCGA | H&E | 195 WSIs | 0.25/40× | ROI | M | 5 | U | |
| TCGA-Jaber | [644] | TCGA | H&E | 1 142 WSIs | 20× | Patch | S | 2 | I | |
| TCGA-Corvò | [645] | TCGA | H&E | 91 WSIs | N/A | ROI | S | 4 | U | |
| TCGA-Lu-Xu | [397] | TCGA | H&E | 1K WSIs | N/A | ROI | S | 2 | I | |
| AMIDA13 | [646, 380] | N/A | H&E | 606 ROIs | 0.25/40× | Pixel | S | 2 | U | |
| MICCAI16/17 | [337] | N/A | H&E | 64 WSIs | N/A | Pixel | S | 2 | U | |
| MICCAI18 | [337] | N/A | H&E | 33 WSIs | N/A | Pixel | S | 2 | U | |
| RUMC-Litjens | [71] | N/A | H&E | 271 WSIs | 0.24/20× | ROI | S | 2 | U | |
| ABCTB | [436] | N/A | H&E | 2 531 WSIs | 20× | Patient | S | 3 | U | |
| NHO-1 | [97] | N/A | H&E | 110 WSIs | 40× | Slide | S | 2 | I | |
| RUMC-Bejnordi | [647] | N/A | H&E | 221 WSIs | 0.243/20× | Slide, ROI | S | 3 | I | |
| UVLCM-UVMC | [648] | N/A | H&E | 2 387 WSIs | 0.455/20× | Slide | S | 6 | I | |
| HUP | [643] | N/A | H&E | 239 WSIs | 0.25/40× | ROI | M | 5 | U | |
| UHCMC-CWRU | [643] | N/A | H&E | 110 WSIs | 0.23/40× | ROI | M | 5 | U | |
| CINJ | [643] | N/A | H&E | 40 WSIs | 0.25/40× | ROI | M | 5 | U | |
| Bre-Steiner | [27] | N/A | H&E, IHC | 70 WSIs | 0.25 | Slide | S | 4 | I | |
| NMCS | [72] | N/A | N/A | 108 WSIs | 0.24 | Slide | S | 4 | I | |
| BC-Priego-Torres | [567] | N/A | H&E | 12 WSIs | 0.2524/40× | Pixel | S | 2 | U | |
| BIRL-SRI | [649] | N/A | H&E | 65 WSIs, 5 151 Patches | 2/5×, 1/10× | ROI | S | 2 | U | |
| BWH-Lymph | [64] | N/A | H&E | 133 WSIs | 40× | Slide | S | 2 | B | |
| NHS-Wetstein | [347] | N/A | H&E | 92 WSIs | 0.16/40× | ROI | S | 3 | U | |

Table 9.11 Continued on Next Page

| Continuation of Data Compilation Table 9.11 | | | | | | | | | | |
|---|-----------------|--------------|--|-------------------------------------|-------------------|-------------------|---------|-------|----|--|
| Dataset Name | References | Availability | Stain Type | Size | Res(μm)/ Mag | Annotation | Label | Class | CB | |
| BRE-Parvatikar | [259] | N/A | H&E | 93 WSIs, 1 441 ROIs | 0.5/20× | ROI | S | 2 | I | |
| BWH-TCGA-Breast | [454] | N/A | H&E | 2 126 WSIs | 20× | Slide | S | 2 | I | |
| Bre-Brieu | [387] | N/A | H&E | 30 ROIs | N/A | Pixel | S | 2 | U | |
| Duke | [602] | N/A | H&E | 140 WSIs | 0.5/20× | ROI | S | 2 | U | |
| TransATAC | [602] | N/A | H&E | 30 WSIs | 0.45/20× | ROI | S | 2 | U | |
| BRACS | [650, 651, 652] | By req. | H&E | 547 WSIs, 4 539 ROIs | 0.25/40× | Slide, ROI | S | 7 | I | |
| Post-NAT-BRCA | [653] | Link | H&E | 138 Patients | 40× | Patient | S | 3 | I | |
| BCSS | [654] | Link | H&E | 151 WSIs, 20K ROIs | 0.25 | ROI | M | 20 | I | |
| Amgad et al. | [374] | N/A | H&E | 151 WSIs, 20 340 ROIs | 0.25/40× | ROI | S | 5 | U | |
| SMH+OVC | [349] | N/A | Ki67 | 30 TMAs, 660 Patches | 20× | Pixel | S | 2 | U | |
| DeepSlides | [349] | Link | Ki67 | 452 Patches | 40× | Pixel | S | 2 | U | |
| Protein Atlas | [349, 655] | Link | Ki67 | 56 TMAs | 20× | Slide | S | 3 | U | |
| Yale HER2 | [349] | N/A | H&E | 188 WSIs | 20× | ROI | S | 3 | U | |
| Yale Response | [349] | N/A | H&E | 85 WSIs | N/A | ROI | S | 2 | U | |
| TCGA-Farahmand | [349] | N/A | H&E | 187 WSIs | N/A | ROI | S | 2 | U | |
| Breast Histopathology Images | [656] | Link | H&E | 162 WSIs | 40× | Patch | S | 2 | I | |
| Colsanitas | [657] | N/A | H&E | 544 WSIs | 0.46/40× | ROI | M | 4 | I | |
| Pancreas | | | | | | | | | | |
| Pan-Bai | [341] | N/A | Ki67 IHC | 203 TMAs | Max. of 20× | Pixel | S | 3 | I | |
| Liver | | | | | | | | | | |
| SUMC | [497] | N/A | H&E | 80 WSIs | 0.25/40× | Slide | S | 2 | B | |
| MGH | [658] | N/A | H&E | 10 WSIs | 0.46/20× | ROI | S | 4 | U | |
| Liv-Atupelage | [561] | N/A | H&E | 305 ROIs | 20× | ROI | S | 5 | I | |
| IHC-Seg | [343] | N/A | H&E, PD1, CD163/CD68, CD8/CD3, CEA, Ki67/CD3, Ki67/CD8, FoxP3, PRF/CD3 | 77 WSIs | 20× | Pixel | S | 4 | I | |
| Lung | | | | | | | | | | |
| TCGA-Gertych | [247] | IDs | H&E | 27 WSIs, 209 ROIs | 0.5/20×, 0.25/40× | ROI, Pixel | S | 4 | I | |
| TCGA-Brieu | [387] | TCGA | H&E | 142 ROIs | N/A | Pixel | S | 2 | U | |
| TCGA-Wang | [659, 637, 541] | TCGA | H&E | 1 337 WSIs | 20×, 40× | ROI | S | 3 | U | |
| NLST-Wang | [660, 541] | By Req. | H&E | 345 WSIs | 40× | ROI | S | 3 | U | |
| TCGA-Wang-Rong | [659, 637, 214] | TCGA | H&E | 431 WSIs | 40× | ROI | S | 6 | U | |
| NLST-Wang-Rong | [660, 214] | By Req. | H&E | 208 WSIs | 40× | Pixel | S | 7 | U | |
| SPORE | [661, 541] | N/A | H&E | 130 WSIs | 20× | ROI | S | 3 | U | |
| CHCAMS | [541] | N/A | H&E | 102 WSIs | 20× | ROI | S | 3 | U | |
| TCGA-Hou-2 | [241] | TCGA | H&E | 23 356 Patches | 0.5/20× | Patch | S | 2 | I | |
| TCGA-LUSC-Tang | [620] | TCGA | N/A | 98 Patients, 305 WSIs | 0.5/20× | Patient | S | 2 | I | |
| TCGA-CPTAC-Lu | [64] | TCGA, CPTAC | H&E | 1 967 WSIs | 20×, 40× | Slide | S | 2 | I | |
| DHMC | [75] | N/A | H&E | 422 WSIs, 4 161 ROIs, 1 068 Patches | 20× | Slide, ROI, Patch | M, S, S | 6 | I | |
| Lung-NHS-LTGU | [387] | N/A | IF | 29 ROIs | N/A | Pixel | S | 2 | U | |
| CSMC | [247] | N/A | H&E | 91 WSIs, 703 ROIs | 0.5/20× | ROI, Pixel | S | 4 | I | |
| MIMW | [247] | N/A | H&E | 88 WSIs, 1 026 ROIs | 0.389/20× | ROI, Pixel | S | 4 | I | |
| NSCLC-Wang | [89] | N/A | H&E | 305 Patients | 20× | Patient | S | 2 | I | |
| ES-NSCLC | [662] | N/A | H&E | 434 Patients, 434 TMAs | 20× | Patient | S | 2 | I | |
| BWH-NSCLC-CL | [64] | N/A | H&E | 131 WSIs | 20× | Slide | S | 2 | I | |
| BWH-NSCLC-BL | [64] | N/A | H&E | 110 WSIs | 40× | Slide | S | 2 | B | |
| BWH-NSCLC-RL | [64] | N/A | H&E | 131 WSIs | 20×, 40× | Slide | S | 2 | I | |
| VCCC | [570] | N/A | N/A | 472 Patients | N/A | Patient | S | 3 | I | |
| Dijon+Caen | [663] | N/A | HES | 197 WSIs | 20× | ROI | S | 2 | U | |
| PKUCH+TMUCH | [352] | N/A | IHC | 239 WSIs, 677 ROIs | 20× | ROI | S | 2 | U | |
| Lymph Nodes | | | | | | | | | | |

Table 9.11 Continued on Next Page

Data Compilation (Continued)

| Continuation of Data Compilation Table 9.11 | | | | | | | | | | |
|---|-----------------|--------------|---|-----------------------------|------------------------------------|----------------|-------|-------|------|--|
| Dataset Name | References | Availability | Stain Type | Size | Res(µm)/ Mag | Annotation | Label | Class | CB | |
| LYON19 | [664, 168, 665] | Link | IHC | 441 ROIs | 0.24 | Pixel | S | 2 | U | |
| AJ-Lymph | [550, 666] | Link | H&E | 374 WSIs | 40× | Slide | S | 3 | I | |
| TUCI-DUH | [565] | N/A | H&E | 378 WSIs | 0.24/20× | Slide | S | 2 | I | |
| Thagaard-2 | [667] | N/A | H&E, IHC | 56 Patches | 20× | Patch | S | 2 | I | |
| Thagaard-3 | [667] | N/A | H&E, IHC | 135 Patches | 20× | Patch | S | 2 | B | |
| Thagaard-4 | [667] | N/A | H&E, IHC | 81 Patches | 20× | Patch | S | 2 | I | |
| Thagaard-5 | [667] | N/A | H&E, IHC | 60 Patches | 20× | Patch | S | 2 | I | |
| Zhongshan Hospital | [166] | N/A | H&E | 595 WSIs | 0.5/20× | ROI | M | 2 | I | |
| Mouth/Esoophagus | | | | | | | | | | |
| SKMCH&RC | [668] | N/A | H&E | 70 WSIs, 193 ROIs | 0.275/40× | ROI | S | 2 | I | |
| SKMCH&RC-M | [668] | N/A | H&E | 30 WSIs | 0.275/40× | ROI | S | 4 | U | |
| ECMC | [669] | N/A | H&E | 143 WSIs | 0.172/40×, 0.345/20×, 0.689/10× | Pixel | S | 7 | U | |
| BCRWC | [371] | N/A | N/A | 126 WSIs | 1.163/50× | Pixel | S | 4 | U | |
| LNМ-OSCC | [32] | N/A | H&E | 217 WSIs | 0.2467/20×, 0.25/40× | ROI | S | 2 | U | |
| OP-SCC-Vanderbilt | [662] | N/A | H&E | 50 Patients | 40× | Patient | S | 2 | B | |
| Sheffield University | [372] | N/A | H&E | 43 WSIs | 0.4952/20× | Slide | S | 4 | I | |
| Prostate/Ovary | | | | | | | | | | |
| PCa-Bulten | [670] | Link | H&E, IHC | 102 WSIs, 160 ROIs | 0.24/20× | Pixel | S | 2 | U | |
| OV-Kobel | [671] | Link | H&E, Ki-67, Mammoglobin B, ER, Mesothelin, MUC5, WT1, p16, p53, Vimentin, HNF-1b | 168 WSIs, 88 TMAs | N/A | Slide | S | 6 | I | |
| TCGA-Tolkach | [672] | TCGA | H&E | 389 WSIs | 0.25/40× | ROI | S | 3 | U | |
| UHZ | [673] | Link | H&E | 886 TMAs | 0.23/40× | ROI | S | 5 | U | |
| SMS-TCGA | [483] | N/A | H&E | 310 WSIs | 20×, 40× | ROI | S | 2 | U | |
| TCGA-Arvaniti | [674] | TCGA | H&E | 447 WSIs | 20×, 40× | Slide | S | 2 | I | |
| TCGA-Yaar | [450] | TCGA | H&E | 220 Patients | 20× | Patient | S | 2 | I | |
| Pro-RUMC | [71] | N/A | H&E | 225 WSIs | 0.16/40× | ROI | S | 2 | B | |
| UHZ-PCa | [296] | N/A | MIB-1 | 826 Patches | N/A | Patch | S | 2 | I | |
| SUH | [208] | N/A | H&E | 230 WSIs, 1 103 160 Patches | 10× | ROI | S | 4 | I | |
| CSMC | [389, 449] | N/A | H&E | 513 Patches | 0.5/20× | Pixel | S | 4 | U | |
| HUH | [73] | N/A | H&E | 28 WSIs | 0.22 | Pixel | S | 2 | U | |
| RCINJ | [675] | N/A | H&E | 83 WSIs | 20× | Slide | S | 2 | I | |
| Pro-Raciti | [425] | N/A | H&E | 304 WSIs | 0.5/20× | Slide, ROI | S | 2 | I, U | |
| VPC | [676] | N/A | H&E | 333 TMAs | 40× | Pixel | S | 4 | U | |
| Pro-Campanella | [195] | N/A | H&E | 137 376 Patches | 20× | Patch | S | 6 | U | |
| UPenn-Yan | [677] | N/A | H&E | 43 WSIs | 40× | ROI | S | 2 | U | |
| Pro-Doyle | [678] | N/A | H&E | 12K ROIs | 0.25/40× | ROI | S | 2 | U | |
| UPenn-Doyle | [679] | N/A | H&E | 214 WSIs | 40× | ROI | S | 7 | U | |
| RUMC-Bulten | [274] | N/A | H&E | 1 243 WSIs | 0.24 | Slide | S | 2 | U | |
| VGH | [119] | N/A | H&E | 305 WSIs | N/A | ROI | S | 5 | U | |
| NMCSД+MML+TCGA | [680] | N/A | H&E | 1 557 WSIs | 0.25/40×, 0.5/20× | Slide, ROI | S | 4 | I, U | |
| OVCARE | [681] | N/A | H&E | 354 WSIs | 40× | ROI | S | 5 | U | |
| CWU | [682] | Link | H&E | 478 WSIs, 120K Patches | 0.504/20× | Patch | S | 3 | I | |
| UHC | [682] | Link | H&E | 157 WSIs, 120K Patches | 0.231/40× | Patch | S | 3 | I | |
| HWN | [682] | Link | H&E | 51 WSIs, 120K Patches | 0.264/40× | Patch | S | 3 | I | |
| CSMC | [354] | N/A | N/A | 625 Patches | N/A | Pixel | S | 4 | U | |
| DiagSet-A | [273] | By Req. | H&E | 2 604 206 Patches | 5×, 10×, 20×, 40× | Patch | S | 9 | I | |
| DiagSet-B | [273] | By Req. | H&E | 4 675 WSIs | 0.25/40× | Slide | S | 2 | I | |
| DiagSet-C | [273] | By Req. | H&E | 46 WSIs | 0.25/40× | Slide | S | 3 | U | |
| SICAPv2 | [391, 683] | Link | H&E | 182 WSIs | 40× | Slide, Pixel | S | 4 | I, U | |
| OVCARE-Farahani | [684] | N/A | H&E | 485 Patients, 948 WSIs | 40× | Patient, Slide | S | 5 | I | |
| University of Calgary | [684] | N/A | H&E | 60 Patients, 60 WSIs | 40× | Patient, Slide | S | 5 | I | |
| PANDA | [685] | Link | H&E | 11 000 WSIs | 40× | ROI | S | 5 | I | |

Table 9.11 Continued on Next Page

| Continuation of Data Compilation Table 9.11 | | | | | | | | | | |
|---|----------------|--------------|----------------------|--------------------------|--------------|--------------|---------|-------|------|--|
| Dataset Name | References | Availability | Stain Type | Size | Res(μm)/ Mag | Annotation | Label | Class | CB | |
| Thyroid | | | | | | | | | | |
| UPMC | [564] | N/A | Feulgen | 10-20 WSIs | 0.074 | Pixel | S | 3 | U | |
| Chen et al. | [353] | N/A | N/A | 600 WSIs | 40x | Slide | S | 3 | I | |
| TCGA-Hoehne | [461] | TCGA | H&E | 482 WSIs | 40x | Slide | S | 4 | I | |
| DEC | [461] | N/A | H&E | 224 WSIs | 40x | Slide | S | 4 | I | |
| ACQ | [461] | N/A | H&E | 100 WSIs | 40x | Slide | S | 4 | I | |
| Stomach & Colon | | | | | | | | | | |
| UMCM | [227, 686] | Link | H&E | 5K Patches | 0.495/20x | Patch | S | 8 | B | |
| GLaS | [687, 83] | Link | H&E | 165 WSIs | 0.62/20x | ROI | S | 5 | I | |
| CRCHistoPhenotypes | [77, 284] | Link | H&E | 10 WSIs, 100 Patches | 0.55/20x | Pixel | S | 4 | I | |
| DACHS | [435] | N/A | H&E | 3 729 WSIs | 20x | Slide | S | 3 | I | |
| NCT-CRC-HE-100K | [686, 86, 475] | Link | H&E | 86 WSIs, 100K Patches | 0.5 | Patch | S | 9 | I | |
| NCT-CRC-HE-7K | [686, 86, 475] | Link | H&E | 25 WSIs, 7 180 Patches | 0.5 | Patch | S | 9 | I | |
| CoNSep | [284] | Link | H&E | 16 WSIs, 41 Patches | 40x | Pixel | S | 7 | I | |
| OSU | [439] | Link | H&E, Pan-Cytokeratin | 115 WSIs | 0.061/40x | ROI | S | 2 | U | |
| Warwick-CRC | [169, 688] | Link | H&E | 139 ROIs | 20x | ROI | S | 3 | I | |
| HUH | [689] | Link | EGFR | 27 TMAs, 1 377 ROIs | 20x | ROI | S | 2 | I | |
| CRAG | [169] | N/A | H&E | 38 WSIs, 139 Patches | 0.275/20x | Patch | S | 3 | I | |
| ULeeds | [690, 691] | Link | H&E | 27 WSIs | N/A | Slide | S | 3 | B | |
| Kather et al. | [294] | Link | H&E | 11 977 Patches | 0.5 | Patch | S | 3 | U | |
| ZU | [142] | By Req. | H&E | 717 ROIs | 0.226/40x | ROI | S | 6 | I | |
| KCCH | [294] | N/A | H&E | 185 Patients | N/A | Patient | S | 3 | I | |
| SC-Takahama | [285] | N/A | H&E | 1 019 WSIs | Max. of 20x | Pixel | S | 2 | U | |
| HUCH | [88] | N/A | H&E | 420 Patients | 0.22 | Patient | S | 2 | I | |
| RC-Ciampi | [692] | N/A | H&E | 74 WSIs | 0.455/200x | ROI | S | 9 | U | |
| DHMC-Korbar | [78] | N/A | H&E | 1 962 WSIs | 200x | Slide | S | 6 | U | |
| CRC-TP | [286] | N/A | H&E | 20 WSIs, 280K Patches | 20x | ROI | S | 7 | U | |
| CRC-CDC | [286] | N/A | H&E | 256 Patches | 20x | Pixel | S | 5 | I | |
| SC-Xu | [447] | N/A | N/A | 60 WSIs | N/A | ROI | S | 2 | U | |
| FAHZU-Xu | [448] | N/A | H&E | 13 838 WSIs | 40x | Slide | S | 2 | I | |
| Bilkent | [83, 693] | N/A | H&E | 72 Patches | 20x | Pixel | S | 2 | U | |
| DHMC-Wei | [300] | N/A | H&E | 1 230 WSIs | 20x | Slide | S | 3 | I | |
| Warwick-UHCW | [370] | N/A | H&E | 75 WSIs | 0.275/40x | ROI | S | 2 | U | |
| Warwick-Osaka | [370] | N/A | H&E | 50 WSIs | 0.23/40x | Slide | S | 6 | I | |
| GNUCH | [335] | N/A | H&E | 94 WSIs, 343 ROIs | N/A | Slide, ROI | S | 4, 2 | I | |
| SPSCI | [694] | N/A | H&E | 55 WSIs, 251 ROIs | 0.19/40x | ROI | S | 5 | I | |
| WSGI | [446] | N/A | H&E | 608 WSIs | 0.2517/40x | Slide, Pixel | S | 3, 2 | I, U | |
| TBB | [695] | N/A | H&E | 44 TMAs | N/A | Slide | S | 3 | I | |
| UV | [696] | N/A | H&E | 456 WSIs | 40x | Slide | S | 4 | U | |
| SC-Sali | [697] | N/A | H&E | 1 150 WSIs | N/A | Slide | S | 7 | I | |
| SC-Holland | [303] | N/A | H&E | 10 WSIs, 1K Patches | 40x, 100x | Slide | S | 2 | B | |
| SC-Kong | [698] | N/A | H&E | 272 WSIs | 40x | ROI | S | 2 | U | |
| SSMH-STAD | [243] | N/A | H&E | 50 WSIs | N/A | Slide | S | 2 | B | |
| HIUH | [231] | N/A | H&E | 8 164 WSIs | 20x | Slide, ROI | S | 3 | I | |
| HAH | [231] | N/A | H&E | 1K WSIs | 20x | Slide | S | 3 | I | |
| SC-Galjart | [398] | N/A | H&E | 363 Patients, 1 571 WSIs | 0.25 | Slide | S | 2 | U | |
| SC-Zheng | [427] | N/A | H&E | 983 WSIs, 10 030 ROIs | 0.96/10x | ROI | S | 5 | U | |
| CRC-I-Chikontwe | [452] | N/A | H&E | 173 WSIs | 40x | Slide | S | 2 | I | |
| CRC-II-Chikontwe | [452] | N/A | H&E | 193 WSIs | 40x | Slide | S | 2 | I | |
| PLAGH | [699] | N/A | H&E | 2 123 WSIs | 0.238/40x | Pixel | S | 4 | U | |
| QUASAR | [700] | N/A | H&E | 106 268 ROIs | 0.5 | ROI | S | 2 | U | |
| CGMH | [310] | N/A | H&E | 297 WSIs | 0.229/40x | ROI | S | 2 | U | |
| AOEC-RUMC-I | [460] | N/A | H&E | 2 131 WSIs | 5x-10x | Slide | M | 5 | I | |
| AOEC-RUMC-II | [460] | N/A | H&E | 192 WSIs | 5x-10x | Slide, ROI | M, S | 4 | I, U | |

Table 9.11 Continued on Next Page

Data Compilation (Continued)

| Continuation of Data Compilation Table 9.11 | | | | | | | | | | |
|---|-----------------|--------------|--|-----------------------------|--|----------------|-------|-------|------|--|
| Dataset Name | References | Availability | Stain Type | Size | Res(μm)/ Mag | Annotation | Label | Class | CB | |
| Lizard | [267] | Link | H&E | 291 WSIs, | 0.5/20× | Pixel | S | 6 | I | |
| YCR-BCIP | [435] | N/A | H&E | 889 WSIs | 20× | Slide | S | 2 | I | |
| MHIST | [262] | By Req. | H&E | 3 152 Patches | 40× | Patch | S | 2 | I | |
| YSMH | [375] | N/A | H&E | 390 WSIs | 20× | Slide, ROI | S | 5 | I, U | |
| ColonPredict-Plus-2 | [350] | N/A | H&E | 200 Patients, 2 537 Patches | N/A | Pixel | S | 2 | U | |
| PAIP | [701] | By Req. | H&E | 47 WSIs | N/A | ROI | S | 2 | U | |
| Li et al. | [276] | N/A | N/A | 10 894 WSIs, 200 Patches | 0.5/20× | Slide, Pixel | S | 2 | I | |
| Stanford Hospital | [318] | Link | H&E, p53 IHC | 70 WSIs | 20× | Slide | S | 2 | U | |
| IMP Diagnostics Lab. | [702, 703] | By Req. | H&E | 1133 WSIs | 40× | Slide | S | 3 | I | |
| Chaoyang | [704] | Link | H&E | 6 160 patches | N/A | Patch | S | 8 | I | |
| BERN-GASTRIC-MSI | [492] | N/A | H&E | 302 Patients | N/A | Patient | S | 2 | I | |
| BERN-GASTRIC-EBV | [492] | N/A | H&E | 304 Patients | N/A | Patient | S | 2 | I | |
| Bone Marrow | | | | | | | | | | |
| BM-MICCAI15 | [705] | Link | H&E | 11 WSIs | N/A | Pixel | S | 3 | U | |
| MICCAI15-Hu | [440] | N/A | H&E | 11 WSIs, 1 995 Patches | N/A | Patch | S | 4 | I | |
| FAHZU-Hu | [440] | N/A | H&E | 24 WSIs, 600 Patches | N/A | Patch | S | 3 | B | |
| BM-Hu | [440] | N/A | H&E | 84 WSIs | N/A | Slide | S | 2 | I | |
| RUMC-Eekelen | [361] | N/A | PAS | 24 WSIs | 0.25 | Pixel | S | 6 | U | |
| MSKCC | [346] | N/A | H&E | 1 578 WSIs | 0.5025, 0.5031/20× | Pixel | S | 7 | I | |
| EUH | [706] | N/A | Wright's Stain | 9 230 ROIs | 0.25/40× | ROI | S | 12 | I | |
| Frankel et al. | [707] | N/A | H&E | 424 WSIs | 40× | Slide | S | 9 | I | |
| Internal-STAD | [708] | N/A | H&E | 203 WSIs | 0.25/40× | ROI | S | N/A | U | |
| MultiCenter-STAD | [708] | N/A | H&E | 417 WSIs | 0.46/40× | ROI | S | N/A | U | |
| Cervix | | | | | | | | | | |
| TCGA-Idlahcen | [268] | TCGA | H&E | 10 WSIs | 2.5×-40× | Slide | S | 2 | B | |
| XH-FMMU | [709] | N/A | H&E | 800 WSIs | 4×-40× | ROI | S | 2 | U | |
| Pap-Cytology | [168] | N/A | N/A | 42 ROIs | 20× | Pixel | S | 2 | U | |
| Chen et al. | [353] | N/A | N/A | 372 WSIs | 40× | Slide | S | 2 | I | |
| OAUTHC | [458] | N/A | H&E | 1 331 ROIs | N/A | ROI | S | 2 | I | |
| Multi-organ | | | | | | | | | | |
| MoNuSeg | [265] | Link | H&E | 30 WSIs | 40× | Pixel | S | 2 | U | |
| UHN | [257] | Link | H&E | 1 656 WSIs, 838 644 Patches | 0.504/20× | Slide, Patch | S | 74 | I | |
| CPM-15 | [284] | Link | H&E | 15 Patches | 20×, 40× | Pixel | S | 2 | U | |
| CPM-17 | [284] | Link | H&E | 32 Patches | 20×, 40× | Pixel | S | 2 | U | |
| ADP | [167, 307] | By Req. | H&E | 100 WSIs, 17 668 Patches | 0.25/40× | Patch | M | 57 | I | |
| Bándi-Dev-Set | [198] | Link | H&E, Sirius Red, PAS, Ki-67, AE1/AE3, CK8-18 | 100 WSIs | 0.2275, 0.2278, 0.2431, 0.25, 0.2525, 0.5034 | Pixel | S | 6 | U | |
| Bándi-Dis-Set | [198] | Link | H&E, Alcian Blue, Von Kossa, Perls, CAB, Grocott | 8 WSIs | 0.2431 | ROI | S | 4 | U | |
| PanNuke | [710, 711] | Link | H&E | 20K WSIs, 205 343 ROIs | 40× | ROI | S | 5 | I | |
| Salvi-SCAN | [668] | Link | H&E | 270 ROIs | 10×, 20×, 40× | Pixel | S | 2 | U | |
| TCGA-Nuclei | [712, 637, 337] | Link | H&E | 5 060 WSIs, 1 356 Patches | 0.25/40× | Pixel | S | 14 | U | |
| MO-Khoshdeli | [363] | Link | H&E | 32 WSIs, 32 Patches | 0.5 | Pixel | S | 2 | U | |
| FocusPath | [196] | Link | H&E, Trichrome, IRON(Fe), Mucicarmine, CR, PAS, AFB, Grocott | 9 WSIs, 8 640 Patches | 0.25/40× | Patch | S | 15 | U | |
| Cheng-Jiang | [713] | Link | H&E, TCT, IHC | 20 521 WSIs | 10× | Slide | 4 | S | I | |
| Stanford-TMA | [714, 297] | By Req. | H&E, IHC | 6 402 TMAs | N/A | Slide | S | 4 | I | |
| TCGA-Courtiol | [87] | TCGA | H&E | 56 Patients, 56 WSIs | N/A | Patient, Slide | S | 3 | I | |
| BreCaHAD | [74] | link | H&E | 170 ROIs | 40× | ROI | S | 2 | U | |
| TCGA-Hegde | [715] | TCGA | H&E | 60 WSIs | 10× | ROI | S | 10 | U | |
| TCGA-Diao | [716] | TCGA | H&E | 2 917 WSIs | 20×, 40× | ROI, Pixel | S | 4, 6 | I | |
| TCGA-Levine | [681] | TCGA | H&E | 668 WSIs | N/A | ROI | S | 5 | U | |
| TCGA@Focus | [196] | Link | H&E | 1K WSIs, 14 371 Patches | N/A | Patch | S | 2 | I | |

Table 9.11 Continued on Next Page

| Continuation of Data Compilation Table 9.11 | | | | | | | | | | |
|---|------------|--------------|--------------------|----------------------------|--|----------------|-------|-------|----|--|
| Dataset Name | References | Availability | Stain Type | Size | Res(μ m)/ Mag | Annotation | Label | Class | CB | |
| TCGA-Shen | [717] | TCGA | H&E | 1 063 WSIs | 20 \times | Patch | S | 3 | U | |
| TCGA-Lerousseau | [451] | TCGA | H&E | 6 481 WSIs | 20 \times | Pixel | S | 3 | U | |
| TCGA-Schmauch | [718] | TCGA | H&E | 10 514 WSIs | N/A | Slide | S | 28 | I | |
| MO-Khan | [202] | N/A | H&E | 60 WSIs | 20 \times , 40 \times | Pixel | S | 3 | U | |
| MESOPATH/ MESOBANK | [87] | N/A | HES | 2 981 Patients, 2 981 WSIs | 40 \times | Patient, Slide | S | 3 | U | |
| Mo-Campanella | [195] | N/A | H&E, SDF-1, TOM20 | 249 600 Patches | 20 \times | Patch | S | 6 | U | |
| BWH-TCGA-MO | [455] | N/A | H&E | 25 547 WSIs | N/A | Slide | S | 18 | I | |
| BWH-Lu | [309] | N/A | H&E | 19 162 WSIs | 20 \times , 40 \times | Slide | 2 | I | | |
| Feng et al. | [478] | N/A | H&E, IHC | 500 WSIs | 20 \times | Slide | S | 10 | B | |
| SegSet | [273] | N/A | H&E | 30 WSIs | 0.25/40 \times | Pixel | S | 2 | U | |
| LC25000 | [719] | Link | H&E | 25 000 Patches | N/A | Patch | S | 5 | B | |
| OCELOT-CELL | [720] | Link | H&E | 306 WSIs, 673 Patches | 0.2 | ROI | S | 2 | I | |
| OCELOT-TISSUE | [720] | Link | H&E | 306 WSIs, 673 Patches | 0.2 | Pixel | S | 3 | I | |
| Other | | | | | | | | | | |
| MUH | [475, 721] | N/A | N/A | 18 365 Patches | 14.14/100 \times | Patch | S | 15 | I | |
| UPenn | [722] | N/A | H&E | 209 Patients | 20 \times | Patient | S | 2 | I | |
| CMTHis | [306] | N/A | H&E | 352 ROIs | 40 \times , 100 \times , 200 \times , 400 \times | ROI | S | 2 | I | |
| Heidelberg University | [723] | N/A | H&E | 431 WSIs | N/A | ROI | S | 2 | U | |
| CHOA | [724] | N/A | H&E | 43 WSIs | 10 \times | Slide | S | 4 | I | |
| Han-Wistar Rats | [459] | N/A | H&E, ISH | 349 WSIs | 40 \times | Slide | S | 2 | U | |
| Osteosarcoma | [486] | Link | H&E | 1 144 ROIs | 10 \times | ROI | S | 3 | I | |
| UPenn+OSU+UH | [725] | N/A | H&E | 2 358 WSIs | 40 \times | Slide | S | 4 | I | |
| Kaggle 2018 Data Science Bowl | [726] | Link | DAPI, Hoechst, H&E | 670 WSIs | N/A | Pixel | S | 2 | U | |
| ALL-IDB2 | [727, 728] | By Req. | N/A | 260 ROIs | 300 \times - 500 \times | Slide | S | 2 | B | |
| End of Table 9.11 | | | | | | | | | | |

Compilation of tasks found in different Co-Path papers categorized by organ (see 9.10)

| References | Tasks | Disease Specification | Methods |
|-------------------------|--|---|---|
| Basal/Epithelium | | | |
| [605] | Detection | Metastasis | End-to-end classifier using cascaded CNNs |
| [618] | Detection | Metastasis | Unsupervised learning via auto-encoder |
| [616] | Disease diagnosis | Melanoma, intra-dermal, compound, junctional nevus | CNN-based patch classifier |
| [729] | Nuclei subtype classification | lymphocyte, stromal, artefact, cancer | CRImage and TTG/CNx for cell identification and classification |
| [730] | Tissue subtype classification | Epithelial, stromal tissues, Spitz, conventional melanocytic lesions | Integration of CNN and HFCM segmentation |
| [617] | Tissue subtype classification | Epithelial, stromal tissues, Spitz, conventional melanocytic lesions | CNN-based classifier with transfer learning |
| [87] | Patient prognosis | Epithelioid, sarcomatoid, biphasic in mesothelium, distant metastatic recurrence | ResNet classifier with transfer learning |
| [266] | Patient prognosis | Epithelioid, sarcomatoid, biphasic in mesothelium, distant metastatic recurrence | Combination of DNN and RNN for feature processing |
| [277] | Tumor segmentation | Tumor, epidermis, dermis, background | FCN based segmentation |
| [304] | Classification | Nevi, melanoma | CNN-based classifier |
| Bladder | | | |
| [422] | Classification | Papillary urothelial carcinoma LG/HG | Combination of CNN and LSTM |
| [387] | Segmentation | Voronoi objects, edges, background regions | CycleGAN with U-Net segmentation |
| [265] | Nuclei Segmentation | Nuclear, Non-nuclear, Boundary | CNN-based classifier with AJI evaluation |
| [146] | Tissue Subtype Classification | Double negative, basal, luminal, luminal p53-like | ResNet variation classifier |
| Brain | | | |
| [76] | Classification | Glioblastoma multiforme, LG glioma | Elastic net classifier with weighted voting |
| [731] | Classification | LGG Grade II/III, GBM | Modular CNN-ensemble network |
| [142] | Classification | LGG and GBM | CNN-based classifier with transfer learning |
| [732] | Classification | Glioma grading III,IV,V | SVM classifier |
| [257] | Classification | Tissue feature correlation analysis | CNN-based classifier with transfer learning |
| [623] | Patient prognosis | Tissue feature correlation analysis | Densenet121 classifiers, initialized with imageNet pre-trained weights |
| [245] | Patient prognosis | IDH mutation | Survival CNN with genetic biomarker data integration |
| [85] | Patient prognosis | Survival period for glioblastoma | CNN-based patch classifier |
| [484] | Patient prognosis | GBM prognostic index | Fusion network of genome, histopathology, and demography |
| [620] | Patient prognosis | Glioblastoma Multiforme | Custom CNN classifier |
| [563] | Patient prognosis/Tissue sub-type classification | Oligodendroglioma, IDH-mutant/wild type astrocytoma | CNN-based classifier |
| [603] | Segmentation | Superior Middle Temporal Gyri in the temporal cortex | Semi-supervised active learning(SSL) |
| Mouth/Esophagus | | | |
| [669] | Tissue subtype classification | Stroma, lymphocytes, tumor, mucosa, kerClassificationatin pearls, blood, adipose | Modified AlexNet patch classifier with active learning |
| [295] | Disease Diagnosis | Barrett esophagus no dysplasia, esophageal adenocarcinoma, normal, Barrett esophagus with dysplasia | Attention based classifier |
| [733] | Patient prognosis | Oropharyngeal squamous cell carcinoma | Computational cell cluster graph |
| [372] | Segmentation | Oral epithelial dysplasia (OED) | HoVer-Net+, a deep learning framework consists of an encoder branch, and three decoder branches |
| Breast | | | |
| [199, 496] | Detection | Benign, malignant | CNN-based patch classifier |
| [306, 734, 735] | Detection | Benign, malignant | CNN classifier with transfer learning |
| [643] | Detection | Benign, malignant | CNN-based pixel classifier |
| [515] | Detection | Benign, malignant | Pre-trained AlexNet with automatic label query |
| [736] | Detection | Benign, malignant | Pre-trained AlexNet with Bi-LSTM classifier |
| [330] | Detection | Benign, malignant | Combination of CNN classifier and U-Net segmentation |
| [737] | Detection | Benign, malignant | CNN-based classifier |
| [424] | Detection | Benign, malignant | 3 stage LSTM-RNN classifier |
| [444] | Detection | Benign, malignant | Attention-based MIL model |
| [302] | Detection | Benign, malignant | Tri-branched ResNet model |
| [234] | Detection | Benign, malignant | Combination of CNN and hand-crafted features |
| [226] | Detection | | Custom CNN classifier with Quasi-Monte Carlo sampling |
| [397] | Detection, Patient Prognosis | Tumor, Normal/ Tumor-infiltrating lymphocytes | U-Net based classifier |
| [345] | Detection | Mitosis | Multi-scale custom CNN classifier |
| [656] | Detection | Invasive Ductal Carcinoma | Bayesian Convolution Neural Networks |

Table 9.11 Continued on Next Page

| Continuation of Organ Overview Table 9.11 | | | |
|---|---------------------------------------|--|---|
| References | Tasks | Disease Specification | Methods |
| [597] | Binary classification | Breast cancer to axillary lymph nodes (ALNs) | Pre-trained architectures: DenseNet121, ResNet50, VGG16, Xception and lightweight convolutional neural network (LCNN) |
| [373] | Tumor Segmentation and Classification | Breast Cancer Metastases | SOTA methods,designed MLVDeepLabV3+ |
| [653] | Segmentation | Segmentation of the malignant nuclei within each tumor bed | Mask regional convolutional neural network (Mask R-CNN) |
| [738] | Segmentation | Segmentation of multiple subtypes on breast images | Deep Multi Magnification Network (DMMN), CNN architecture |
| [305] | Detection | Metastasis/ Micro, Macro | CNN-based pixel classifier |
| [426] | Detection | Metastasis/ Micro, Macro | Resnet with transfer learning |
| [739] | Detection | Metastasis/ Micro, Macro | Combination of CNNs with LSTM-RNN, DCNN-based classifier |
| [329] | Detection | Cancer metastasis detection | MIL+RNN classifier, Neural conditional random field |
| [740] | Detection | Cancer metastasis detection | CNN with attention mechanism |
| [493] | Detection | Metastasis in sentinel lymph node | CNN with Random Forest classifier |
| [741] | Detection | Invasive ductal carcinoma | CNN-based patch classifier |
| [298] | Detection | Invasive ductal carcinoma | ResNet with transfer learning |
| [641] | Detection | Invasive ductal carcinoma | CNN-based random forest classifier |
| [666] | Detection | Invasive ductal carcinoma | Autoencoder network |
| [72] | Detection | Macrometastasis, micrometastasis, isolated tumor cells, negative | Customized InceptionV3 classifier |
| [225] | Detection | Mitosis detection | CNN classifier with two-phase training |
| [269] | Detection | Mitosis detection | Task-based CNN ensemble |
| [378] | Detection | Mitosis detection | CNN-based random forest classifier |
| [344] | Detection | Mitosis detection | CNN classifier with transfer learning |
| [379] | Detection | Mitosis detection | Multi-stage RCNN classifier |
| [380] | Detection | Mitosis detection | FCN classifier |
| [381] | Detection | Mitosis detection | Adaptive Mask RCNN |
| [382] | Detection | Mitosis detection | CNN-based patch classifier |
| [200] | Detection | Mitosis detection | Combination of DCNN network |
| [384] | Detection | Mitosis detection | R2U-Net based regression model |
| [235] | Classification | Epithelium, Stroma | Magnification invariant CNN classifier |
| [236] | Classification | Benign, malignant | CNN classifier interleaved with squeeze-excitation modules (SENet) |
| [742] | Classification | Adenosis, fibroadenoma, phyllodes tumors, tubular adenoma, ductal, lobular, mucinous, papillary | Inception Recurrent Residual Convolutional Neural Network (IRRCNN) |
| [743] | Classification | Adenosis, fibroadenoma, phyllodes tumors, tubular adenoma, ductal, lobular, mucinous, papillary | Custom DenseNet classifier |
| [657] | Classification | normal tissue, benign lesion, in situ carcinoma, and invasive carcinoma | Custom multiclass dense layer classifier based on Xception network |
| [744] | Disease diagnosis | Adenosis, fibroadenoma, phyllodes tumors, tubular adenoma, ductal, lobular, mucinous, papillary | Two-stage ResNet classifier (MuDeRN) |
| [331] | Disease diagnosis | Benign, malignant | Ensemble of CNN classifiers |
| [301] | Disease diagnosis | Adenosis, fibroadenoma, phyllodes tumors, tubular adenoma, ductal, lobular, mucinous, papillary | CNN-based classifier with transfer learning |
| [745] | Disease diagnosis | Adenosis, fibroadenoma, phyllodes tumors, tubular adenoma, ductal, lobular, mucinous, papillary | Class structured DCNN |
| [429] | Disease diagnosis | Adenosis, fibroadenoma, phyllodes tumors, tubular adenoma, ductal, lobular, mucinous, papillary | Two stage classification and selection network |
| [746] | Disease diagnosis | Adenosis, fibroadenoma, phyllodes tumors, tubular adenoma, ductal, lobular, mucinous, papillary | Domain adaptation based on representation learning |
| [747] | Disease diagnosis | Benign, in-situ, invasive carcinoma | CNN-based classifier with gravitational loss |
| [748] | Disease diagnosis | Benign, in-situ, invasive carcinoma | CNN ensemble with LightGBM |
| [749] | Disease diagnosis | Benign, in-situ, invasive carcinoma | InceptionV3 classifier using dual path network |
| [26] | Disease diagnosis | Usual ductal hyperplasia, ductal carcinoma in situ | Logistic regression with Lasso regularization |
| [369] | Disease diagnosis | Proliferation score (1, 2, or 3) | Encoder-decoder with Gaussian Mixture model |
| [259] | Disease diagnosis | Low risk/High risk | Logistic regression using morphological features |
| [495] | Disease diagnosis | normal, benign, in situ carcinoma, invasive carcinoma | Hybrid CNN classifier |
| [648] | Disease diagnosis | Proliferative without atypia, atypical hyperplasia, ductal / lobular carcinoma in situ, invasive carcinoma | Cascade of VGG-Net like classifier |
| [750] | Disease diagnosis | Benign, malignant | CNN-based classifier with fourier pre-processing |
| [421] | Disease diagnosis | Benign, malignant | Combination of CNN and LSTM classifiers |

Table 9.11 Continued on Next Page

Organ Overview (Continued)

| Continuation of Organ Overview Table 9.11 | | | |
|---|--|---|---|
| References | Tasks | Disease Specification | Methods |
| [751] | Disease diagnosis | Tumour, normal | Metric learning using similarities |
| [227] | Classification | Clinically relevant classes | CNN-based patch classifier with aggregation |
| [263] | Classification | Benign, in-situ, invasive carcinoma | Scale-based CNN classifier |
| [596] | Classification | Normal, benign, in situ, invasive carcinoma | Combination of patch and image level CNN |
| [647] | Classification | Normal, benign, DCIS, invasive ductal carcinoma (IDC) | Context-aware stacked CNN |
| [752] | Classification | Benign, in-situ, invasive carcinoma | CNN-based classifier with dimensionality reduction |
| [63] | Classification | Benign, in-situ, invasive carcinoma | MIL with auto-regression |
| [423] | Classification | Benign, in-situ, invasive carcinoma | Parallel network with CNN-RNN |
| [264] | Classification | Benign, in-situ, invasive carcinoma | Hybrid Convolutional and Recurrent NN |
| [308] | Classification | Benign, in-situ, invasive carcinoma | CNN-based patch classifier |
| [753] | Classification | Benign, in-situ, invasive carcinoma | Convolutional capsule network |
| [633] | Classification | Benign, in-situ, invasive carcinoma | Combination of residual and spatial model |
| [754] | Classification | Benign, in-situ, invasive carcinoma | Custom CNN patch classifier |
| [213] | Classification | Benign, in-situ, invasive carcinoma | CNN classifier with bidirectional LSTM |
| [755] | Classification | Tumor, non-tumor | Custom CNN-based classifier |
| [337] | Nuclei segmentation | N/A | UNet segmentation with GAN patch refinement |
| [387] | Nuclei segmentation | N/A | UNet segmentation with CycleGAN domain transfer |
| [357] | Nuclei segmentation | N/A | Ensemble of several CNNs with different architectures |
| [265] | Nuclei segmentation | Normal, malignant, dysplastic epithelial, fibroblast, muscle, inflammatory, endothelial, miscellaneous | Sequential CNN network |
| [642] | Nuclei segmentation | Normal, malignant, dysplastic epithelial, fibroblast, muscle, inflammatory, endothelial, miscellaneous | Custom encoder-decoder model |
| [602] | Detection, Segmentation | DCIS and invasive cancers | IM-Net for DCIS detection and segmentation |
| [285] | Tumour segmentation | Tumor, Normal | U-Net segmentation with GoogleNet patch level feature extraction |
| [368] | Tumour segmentation | Normal, benign, in situ carcinoma or invasive carcinoma | Global and local ResNet feature extractors, FCN with auto zoom |
| [360] | Tumour segmentation | Normal, benign, in situ carcinoma or invasive carcinoma | Global and local ResNet feature extractors, FCN with auto zoom |
| [374] | Segmentation | Breast cancer | U-Net, Residual Multi-Scale (RMS) |
| [349] | Segmentation | Ki67 detection for breast cancer | U-NET, piNET |
| [567] | Tumour segmentation | Non-tumor, ductal carcinoma in situ (DCIS), invasive ductal carcinoma (IDC), lobular carcinoma in situ (LCIS), invasive lobular carcinoma (ILC) | Ensemble of CNN with atrous spatial pyramid encoding |
| [312] | Classification | Prediction of HER2 status and trastuzumab response | CNN classifier with Inception v3, Transfer learning |
| [315] | Tissue subtype classification | Classifying cancerous tissues | weakly supervised approach, Multiple Instance Learning (MIL) model, Transfer learning pre-trained models (Trans-AMIL), VGG, DenseNet, ResNe |
| [640] | Tissue subtype classification | 24 different tissues | Ensemble of different CNN architectures with transfer learning |
| [445] | Tissue subtype classification | Proliferative without atypia, atypical hyperplasia, ductal / lobular carcinoma in situ, invasive carcinoma | Multi-class MIL |
| [650] | Disease Diagnosis | Normal, Benign, Atypical, Ductal Carcinoma In Situ, Invasive | CNN-based classifier using graphical representation |
| [436] | Tissue subtype classification | Estrogen, Progesterone, Her2 receptor | Style invariant ResNet classifier |
| [27] | Tissue subtype classification | Negative, micrometastasis, macrometastasis, isolated tumor cell cluster (ITC) | Custom CNN-based classifier |
| [347] | Tissue subtype classification | Adipose regions, TDLU regions, acini centroid | UNet based CNN classifier |
| [651] | Classification, Segmentation | Benign, Atypical (flat epithelial atypia, atypical ductal hyperplasia), Malignant (ductal, in situ, invasive) | Graphical neural networks |
| [644] | Tissue subtype classification | Basal-like, HER2-enriched, Luminal A, and Luminal B | CNN-based classifier with PCA |
| [756] | Classification | Malignant, normal | CNN classifier with transfer learning |
| [209] | Segmentation | Stain normalization | Style transfer using CycleGAN, Relevance vector machine |
| [432] | Segmentation | Realistic patch generation | GAN based architecture |
| [757] | Classification | Processing technique comparison | Comparison of color normalization methods |
| [332] | Classification | 19 histological types, HER2-, HER2+, PR+, PR- | Graph CNN slide level classifier |
| [334] | Classification | normal, benign, in situ, and invasive | Dynamic Deep Ensemble CNN |
| [463] | Binary Classification | Breast cancer | Transformer based MIL (TransMIL) |
| Liver | | | |
| [561] | Disease diagnosis, Nuclei segmentation | G0, G1, G2, G3, G4 (HCC grade) | BoF-based classifier |
| [497] | Disease diagnosis | Hepatocellular/cholangio carcinoma | CNN-based end to end diagnostic tool |

Table 9.11 Continued on Next Page

| Continuation of Organ Overview Table 9.11 | | | |
|---|------------------------------------|--|--|
| References | Tasks | Disease Specification | Methods |
| [619] | Nuclei segmentation | N/A | CycleGAN based segmentation |
| [343] | Tissue segmentation | Background, tumor, tissue and necrosis | UNet with color deconvolution |
| [758] | Tissue segmentation | Steatosis droplet | Mask-RCNN segmentation |
| [658] | Classification | Stain normalization | Relevance vector machine |
| [437] | Classification | Hematoxylin, eosin, unstained RBC | Linear discriminant classifier |
| [438] | Classification | Stain style transfer | CycleGAN based architecture, CycleGAN with perceptual embedding consistency loss |
| Lymph Nodes | | | |
| [205] | Detection | Detection and quantification of Lymphocytes | U-Net and SegNet with VGG16 and Resnet50 and pre-trained weights of ImageNet |
| [238] | Detection | Metastasis | Ensemble of CNNs with different architectures |
| [759] | Detection | Metastasis | Custom CNN for discriminative feature learning |
| [271] | Detection | Metastasis | DCNN classifier |
| [97] | Detection | Metastasis | CNN-based patch classifier |
| [760] | Detection | Metastasis (Isolated / micro / macro) | Variants of ResNet/GoogleNet |
| [565] | Disease diagnosis | Hyperplasia, small B cell lymphomas | Bayesian NN with dropout variance |
| [371] | Tissue segmentation | Keratin, subepithelial, epithelial, background | Custom CNN model |
| [367] | Tumor segmentation | normal, metastatic | Representation-Aggregation Network with LSTM |
| [761] | Classification, Segmentation | Domain shift analysis for breast tumour | Comparison of CNN models, data augmentation, and normalization techniques |
| [203] | Classification, Segmentation | Stain normalization | Deep Gaussian mixture color normalization model |
| [434] | Classification, Segmentation | Stain normalization | GAN, stain-style transfer network |
| [762] | Classification, Segmentation | Similar image retrieval | Siamese network |
| [476] | Classification | metastatic tissue | Contrastive predictive coding, Autoregressor PixelCNN |
| [166] | Prognosis of lymph node metastasis | lymph node metastasis of papillary thyroid carcinoma | Transformer-Guided Multi-instance Learning, Attention-based mutual knowledge distillation |
| Prostate/Ovary | | | |
| [598] | Tissue subtype classification | Gland, Gland border region, or Stroma | SVM with RBF kernel, CNN classifiers |
| [354] | Tissue subtype classification | stromal areas (ST), benign/normal (BN), low-grade pattern (G3) and high-grade pattern (G4) cancer | CNN classifiers using a modified U-Net architecture |
| [355] | Detection | Tumor, No-tumor | Generative Adversarial Network named GAN-CS |
| [73, 274] | Detection | Tumor, Normal | CNN-based classifier with transfer learning, MIL model |
| [270] | Detection | Pancreatic adenocarcinoma | Custom CNN classifier |
| [678] | Detection | Probabilistic boosting tree with active learning | |
| [682] | Detection | benign glandular, nonglandular, tumor tissue | Pre-trained and validated model based on InceptionResNetV2 convolutional architecture |
| [389] | Disease diagnosis | Prostate cancer (benign, LG, HG) | Region based CNN classifier |
| [763] | Disease diagnosis | Gleason Score (G6-G10) | Comparison of commonly used CNN models |
| [763] | Disease diagnosis | Gleason Score (0-5) | Active Learning Framework |
| [672] | Disease diagnosis | Invasive carcinoma, Benign (glandular, non-glandular, stromal, seminal vesicles, ejaculatory ducts, high-grade prostatic intraepithelial neoplasia, HGPIN), intraductal carcinoma | NASNetLarge classifier with transfer learning |
| [674] | Disease diagnosis | Gleason grading (3, 4, 5) | ResNet classifier with symmetric domain adaptation |
| [680] | Disease diagnosis | Gleason grading (3, 4, 5) | Two-stage deep learning system |
| [764] | Disease diagnosis | Gleason grading (3, 4, 5) | Multi-scale U-Net for pixel-wise Gleason score prediction |
| [208] | Disease diagnosis | Gleason grading (3, 4, 5) | CNN classifier with CycleGAN |
| [449] | Disease diagnosis | Gleason grading (3, 4, 5) | Attention-based MIL classifier |
| [676] | Disease diagnosis | Benign, Gleason Grades 3-5 | Ensemble of CNN classifiers |
| [677] | Disease diagnosis | Gleason grades 1-5 | K-NN classifier using statistical representation of Homology Profiles |
| [119] | Disease diagnosis | High-grade serous ovarian, clear cell ovarian, endometrioid (ENOC), low-grade serous, mucinous carcinoma | Two-staged CNN with RF classifier |
| [765] | Disease diagnosis | Low risk Gleason score (6-7), high risk (8-10) | Information retrieval using TF-IDF |
| [568] | Gland segmentation | Gleason Score (1-5) | Image analysis using mathematical morphology |
| [273] | Tissue subtype classification | Diagset A : scan background (BG), tissue background (T), normal, healthy tissue (N), acquisition artifact (A), or one of the 1-5 Gleason grades (R1-R5), Diagset B: presence of cancerous tissue on the scan (C) or lack thereof (NC), Diagset C:containing cancerous tissue (C), not containing cancerous tissue (NC), or uncertain and requiring further medical examination (IHC) | CNNs, a variant of fully-convolutional VDSR networks, AlexNet, VGG16/19, ResNet50, InceptionV3 |

Table 9.11 Continued on Next Page

Organ Overview (Continued)

| Continuation of Organ Overview Table 9.11 | | | |
|---|---------------------------------------|--|--|
| References | Tasks | Disease Specification | Methods |
| [204] | Tissue subtype classification | Epithelial, stromal | Multiresolution segmentation |
| [679] | Tissue subtype classification | Gleason grade 3-5, Benign Epithelium (BE), Benign stroma (BS), Tissue atrophy (AT), PIN | Cascaded approach |
| [425] | Clinical validation | Cancer, non-cancerous | Two-stage MIL-RNN classifier |
| [450] | Prediction of treatment response | Positive, negative (response to platinum chemotherapy) | Ensemble of RBF+SVM and MIL-based CNN classifier |
| Kidney | | | |
| [626] | Detection | Tumor, normal | DCNN based classifier |
| [627] | Detection | Antibody mediated rejection | CNN-based classifier |
| [428] | Classification | Abnormalities of blood chemistry, Kidney function and dehydration | k Nearest Neighbour (kNN), Long short-term memory (LSTM) |
| [351] | Classification, Segmentation | Cancer | Modified U-Net CNN model |
| [395] | Detection | Glomeruli boundaries | CNN-based classifier with center point localization |
| [766] | Detection | Glomeruli and Nuclei | Anchor Free Backbone + center point localization |
| [388] | Prognosis | Survival rate for renal cell carcinoma | Random forest classifier for nuclei detection |
| [767] | Prognosis | Survival rate | Kaplan-Meier analysis |
| [84] | Classification | Sclerosed glomeruli, tubulointerstitium | Laplacian-of-Gaussian method for blob detection |
| [394] | Classification | Glomerulus, lymphocytes | Different architectures of standard CNN with patient privacy preservation |
| [396] | Classification | Non-glomerular tissue, normal glomeruli, sclerosed glomeruli | U-Net based classifier |
| [322] | WSI representation and classification | Kidney Chromophobe Renal Cell Carcinoma (KICH), Kidney Renal Clear Cell Carcinoma (KIRC) and Kidney Renal Papillary Cell Carcinoma(KIRP) | hierarchical global-to-local clustering, weakly-supervised |
| [625] | Segmentation | Glomeruli | Cascaded UNet model |
| [152] | Segmentation | Glomeruli, sclerotic glomeruli, empty Bowman's capsules, proximal tubuli, distal tubuli, atrophic tubuli, undefined tubuli, capsules, arteries, interstitium | Ensemble of U-Net |
| [463] | Multiple Classification | 3 cancer types | Transformer based MIL (TransMIL) |
| Lung | | | |
| [241] | Detection | Lymphocyte richness | Unsupervised classifier using convolutional autoencoder |
| [339] | Segmentation, Classification | Mitosis,ND, LUAD, LUSC | Deep residual aggregation network with U-Net |
| [663] | Classification | Squamous and non-squamous non-small cell | Inception V3 |
| [352] | Detection | Tumor, cell Detection | U-Net |
| [570] | Classification | Cancer | Decision Tree, AdaBoost and XGBoost |
| [498] | Disease diagnosis | LUAD, LUSC | Deep CNN with transfer learning |
| [768] | | | CNN ensemble with random forest aggregation |
| [258] | | | ML models with Cox hazard model |
| [339] | | | Deep residual aggregation with U-Net |
| [453] | Prognosis | Malignant, Normal | MIL-based CNN classifier |
| [75] | Disease diagnosis | Lepidic, acinar, papillary, micropapillary, solid, benign | CNN-based patch classifier |
| [247] | Disease diagnosis | Acinar, micropapillary, solid, cribriform, non-tumor | CNN-based classifier |
| [498] | Prognosis | STK11, EGFR, SETBP1, TP53, FAT1, KRAS, KEAP1, LRP1B, FAT4, NF1 | Deep CNN with transfer learning |
| [769] | Segmentation | Characterizing spatial arrangement features of the immune response | Watershed-based model |
| [337, 387, 214] | Segmentation | N/A Nuclei of tumor cells, stromal cells, lymphocytes, macrophages, blood cells, karyorrhexis | UNet segmentation with GAN patch refinement, UNet segmentation with CycleGAN domain transfer Mask-RCNN based classifier |
| [541] | Classification | Tumor cell, stromal cell, lymphocyte | CNN |
| [770] | Classification | LUAD, LUSC | Pre-trained DenseNet |
| [322] | WSI representation and classification | Lung Adenocarcinoma (LUAD) and Lung Squamous Cell Carcinoma (LUSC) | hierarchical global-to-local clustering, weakly-supervised |
| [258] | Prognosis | Pathology grade, non-small cancer | Various ML models with Cox hazard model |
| [89] | | Recurrence prediction for non-small cell cancer | CNN-based classifier |
| [258] | | Lung squamous cell carcinoma | Custom CNN |
| [339] | | Tumor cell, stromal cell, lymphocyte | Cox regression model |
| [571] | Prognosis | Squamous cell | Self-supervised pre-trained model, HANet |

| Continuation of Organ Overview Table 9.11 | | | |
|---|------------------------------|--|--|
| References | Tasks | Disease Specification | Methods |
| [325] | Segmentation | Stain normalization | CNN, LSTM based feature aware normalization |
| [771] | Classification | Cancer, normal | High resolution heatmaps from CNN |
| [463] | Binary Classification | LUSC/LUAD subtypes classification | Transformer based MIL (TransMIL) |
| [463] | Detection | carcinomas and benign tissue | Transfer Learning |
| Pancreas | | | |
| [257] | Classification | Feature correlation analysis Nuclei, antigen, cytoplasm, blood, ECM | CNN-based classifier with transfer learning Non-linear tissue component discrimination |
| [341] | Classification | Immunopositive tumor, immunonegative tumor, non-tumor | U-Net |
| [333] | Tissue Classification | benign lung tissues (LN), lung adenocarcinomas (LAC), lung squamous cell carcinomas (LSCC), benign colonic tissues (CN), and colon adenocarcinomas (CAC) | Pyramid Deep-Broad Learning |
| Thyroid | | | |
| [564] | Classification | Follicular lesion (FA,FTC), normal | Radial based SVM classifier |
| [461] | Classification, Detection | Unknown/have mutation(BRAF+), don't have mutation (BRAF-)/have fusion(NTRK+), don't have fusion (NTRK-) | Attention-based deep multiple instance learning classifier, DenseNet121 |
| [462] | Classification, Detection | Tumor, Healthy/papillary, follicular, poorly differentiated, anaplastic/have mutation(BRAF+), don't have mutation (BRAF-) | Multi Instance Learning (MIL) |
| Stomach/Colon | | | |
| [447, 439, 448] | Detection | Cancer | Combination of CNN and MIL, InceptionV3 classifier with conditional GANs, Generalized mean model with parallel MIL |
| [294] | Detection | Microsatellite instability | ResNet with transfer learning |
| [453] | Prognosis | Malignant, normal | MIL-based CNN classifier |
| [77] | Detection | Nucleus | Space-constrained CNN |
| [243] | Detection | Adenocarcinoma, normal | CNN-based classifier |
| [303] | Detection | Carcinoma, benign | CNN-based classifier |
| [699] | Detection | High-grade intraepithelial neoplasia | Deep learning classifier with ResNet backbone |
| [276] | Detection | Gastric cancer | DLA34, Hybrid and Weak supervision Learning method |
| [435] | Detection | Tumor-bearing tissue, Non-tumor tissue | SuffleNet with end-to-end learning method |
| [228] | Detection | BRAF mutational status and microsatellite instability | Swarm Learning |
| [475] | Classification | N/A | Encoder,Resnet18 |
| [350] | Classification | Colorectal carcinoma, Colorectal cancer | Weakly supervised neural network named comparative segmentation network (CompSegNet), U-Net |
| [333] | Classification of tissue | Cadipose (ADI),background (BACK), debris (DEB), lymphocytes (LYM),mucus (MUC), smooth muscle (MUS), normal colon mucosa (NORM), cancer-associated stroma (STR), and colorectal adenocarcinoma epithelium (TUM) | Pyramid Deep-Broad Learning |
| [375] | Segmentation | colorectal cancer | CNN, Sliding window method, U-Net++ |
| [311] | Segmentation, Classification | Colorectal cancer | U-Net16/19 network with a VGG-16/19 net as backbone |
| [694] | Disease diagnosis | Non-epithelial normal, normal gastric epithelium, neoplastic gastric epithelium/tubular gastric adenocarcinoma, solid-type gastric adenocarcinoma, diffuse/discohesive gastric carcinoma | Custom CNN classifier |
| [142] | Disease diagnosis | Adenocarcinoma, mucinous carcinoma, serrated carcinoma, papillary carcinoma, and cribriform comedo-type carcinoma | CNN-based classifier with transfer learning |
| [231] | Disease diagnosis | Adenocarcinoma, adenoma, non-neoplastic | CNN classifier with RNN aggregation |
| [688] | Disease diagnosis | Colorectal cancer | CNN |
| [300] | Disease diagnosis | Celiac disease, nonspecific duodenitis | ResNet patch classifier |
| [452] | Disease diagnosis | Cancer | Multiple instance learning |
| [335] | Disease diagnosis | Adenocarcinoma, poorly cohesive carcinoma, normal gastric mucosa | Multi-scale receptive field model |
| [446] | Disease diagnosis | Dysplasia, Cancer | Multi-instance deep learning classifier |
| [82] | Disease diagnosis | Healthy, adenomatous, moderately differentiated, moderately-to-poorly differentiated, and poorly differentiated | Multi-task classifier |
| [691] | Disease diagnosis | Adenocarcinoma (AC), tubulovillous adenoma (AD), healthy (H) | Downstream classifiers (ResNet18, SVM) |
| [80, 84, 83] | Segmentation | Benign, malignant | Deep contour-aware networks using transfer learning, CNN |
| [81, 366] | Segmentation | Carcinoma | Random polygon model, Multi-scale CNN with minimal information loss |
| [772, 82] | Segmentation | Lumen, cytoplasm, nuclei | SVM classifier with RBF kernel, Regions containing glandular structures, Multi-task classifier |

Table 9.11 Continued on Next Page

Organ Overview (Continued)

| Continuation of Organ Overview Table 9.11 | | | |
|---|---|--|---|
| References | Tasks | Disease Specification | Methods |
| [393, 773] | Segmentation | Colorectal Cancer | Two-parallel-branch DNN |
| [375] | Segmentation | Colon: adenocarcinoma, high-grade adenoma with dysplasia, low-grade adenoma with dysplasia, carcinoid, and hyperplastic polyp | Ensemble method, wavelet transform (WWE) |
| [267] | Segmentation, Classification | Epithelial cell, Connective tissue cell, Lymphocytes, Plasma cells, Neutrophils, Eosinophils | ResNet-34 network with contrastive learning, HoVerNet |
| [701] | Segmentation, Classification | high/ low mutation density, microsatellite instability/ stability, chromosomal instability/ genomic stability, CIMP-high/ low, BRAF mutation/wild-type, TP53 mutation/ wild-type, KRAS wild-type/ mutation | ResNet-18 network/ Adapted ResNet34/ HoVerNet, Weakly supervised learning |
| [310] | Classification | Colorectal Cancer | customized CNNs, pretrained model VGG, ResNet, Inception, IRV2 |
| [390] | Segmentation | Epithelial, inflammatory, fibroblast, miscellaneous, unassigned | Spatially Constrained CNN |
| [285] | Segmentation | Tumour | U-Net segmentation with GoogleNet patch level feature extraction, Custom CNN with random forest regression |
| [299] | Segmentation | Gastric cancer | CNN models with transfer learning |
| [370] | Segmentation | colon/ adenoma, adenocarcinoma, signet, and healthy cases | combination of PHPs, CNN features |
| [700] | Classification | tumor, stroma | random forests |
| [86] | Prognosis | Stroma | CNN based on neuronal activation in tissues |
| [88] | Prognosis | Five year survival rate | CNN/LSTM based regression classifier |
| [708] | Prognosis | EBV-associated gastric cancer | deep convolutional neural network backbone by ResNet50 |
| [460] | Classification | cancerous, high-grade dysplasia, low-grade dysplasia, hyperplastic polyp, normal glands | CNN based classifier with a Multi-Scale Task Multiple Instance Learning (MuSTMIL) |
| [774, 775, 776, 777, 78] | Classification | Hyperplastic polyp, sessile serrated polyp, traditional serrated / tubular / tubulovillous / villous adenoma | Radial based SVM classifier, CNN classifier with dropout variance and active learning, SqueezeNet with transfer learning ResNet patch classifier |
| [775, 776] | Classification | tumor epithelium, simple stroma, complex stroma, immune cell conglomerates, debris and mucus, normal mucosal glands, adipose tissue, background | Bilinear CNN classifier, Convolutional networks (ConvNets) |
| [695] | Classification | Normal epithelium, normal stroma, tumor | VGG16, hierarchical neural network |
| [231] | Classification | Adenocarcinoma, adenoma, or non-neoplastic | InceptionV3 patch classifier |
| [286] | Classification | Epithelial, Spindle-shaped, Necrotic, Inflammatory | SC-CNN with Delaunay Triangulation |
| [778] | Segmentation | Colorectal cancer, Gastroesophageal junction (dysplastic) lesion, Head and neck carcinoma | DCNN with residual blocks |
| [691] | Classification | Adenocarcinoma, corresponding to noticeable CRC, Tubulovillous adenoma, a precursive lesion of CRC, Healthy tissue | Bayesian CNNs (B-CNNs), |
| [318] | Classification | cancer, non-cancer | Transfer Learning |
| [427] | Disease diagnosis | Gastric cancer | GCN-RNN based feature extraction and encoding |
| [779] | Segmentation | Tumor | GAN |
| [780] | Prognosis | Adenocarcinoma, disease-specific survival time | ECA histomorphometric-based image classifier |
| [433] | Synthesis of large high-resolution images | Colorectal Cancer | Novel framework called SAFRON (Stitching Across the FRONTier Network) |
| Multi-Organ | | | |
| [296] | Classification | Benign, malignant | CNN based classifier |
| [64] | Classification | Kidney, Lymph nodes, Lung/ Chromophobe, clear cell carcinoma, papillary | Weakly supervised ResNet50 with transfer learning |
| [284] | Segmentation | Bladder, Breast, Kidney, Liver, Prostate, Stomach/ Normal, malignant, dysplastic epithelial, fibroblast, muscle, inflammatory, endothelial, miscellaneous | Modified Preact-ResNet50 |
| [265] | Segmentation | Nuclear, non-nuclear, boundary | CNN-based classifier with AJI evaluation |
| [483] | Detection | Liver, Prostate/ Tumor, normal | Custom CNN architecture |
| [689] | Classification | Epithelial, stromal tissues | DCNN classifier |
| [781] | Classification | Brain, Breast, Kidney/ DCIS, ERBB2+, triple negative | Transfer learning using multi-scale convolutional sparse coding |
| [297] | Detection | Bladder, Breast, Lymph nodes, Lung | CNN-based classifier with transfer learning |
| [62] | Detection | Basal, Breast, Prostate/ Cell carcinoma, Metastasis | RNN classifier with multiple instance learning |
| [71] | Classification | Micro/Macro metastasis | RNN classifier with MIL |
| [698] | Detection | Breast, Stomach/ Tumor, normal | Custom CNN classifier |

Table 9.11 Continued on Next Page

| Continuation of Organ Overview Table 9.11 | | | |
|---|--|--|---|
| References | Tasks | Disease Specification | Methods |
| [377] | Segmentation | Bladder, Breast, Liver, Prostate, Kidney, Stomach/ Edge, foreground, background | Domain-Adversarial Neural Network |
| [339] | Segmentation, Classification | Brain, Lung, Esophagus/ Mitosis, Lymphocyte richness, LUAD, LUSC | Deep residual aggregation network with U-Net segmentation |
| [202] | Segmentation | Breast, Esophagus, Liver/ Stain normalization | Relevance vector machine |
| [782] | Classification | colon, kidney, ovarian cancer, lung adenocarcinoma, gastric mucosa, astrocytoma, skin cutaneous melanoma, breast cancer/ Nuclei, antigen, cytoplasm, blood, ECM | Non-linear tissue component discrimination |
| [459] | Classification | Different organs of rats/Exploring the morphological changes in tissue to biomarker level | CNN, MIL, multi-task learning |
| [314] | Classification | Adrenal gland, Bladder, Breast, Liver, Lung, Ovary, Pancreas, Prostate, Testis, Thyroid, Uterus, Heart | CNN models with transfer learning/ ResNet-152 pretrained on ImageNet and GTEx |
| [206] | Classification | Colon, Breast/molecular fingerprint of a deficient mismatch (Microsatellite stability(MSS)/ Microsatellite instability (MSI) | CNN models with transfer learning method |
| [313] | Classification, Segmentation | blood, breast, lymph, colon, bone, prostate, liver, pancreas, bladder, cervix, esophagus, head, neck, kidney, lung, thyroid, uterus, bone marrow, skin, brain, stomach, and ovary | Unsupervised contrastive learning, residual networks pretrained with self-supervised learning |
| [363] | Segmentation | Brain, Breast/ Nuclei | Custom encoder-decoder model |
| [278] | Prognosis | Bladder/ Lung, Low TMB, Medium TMB, High TMB | Deep transfer learning, SVM with Gaussian kernel |
| [783] | Classification | Bladder, Brain, Breast, Bronchus and lung, Connective, subcutaneous and other soft tissues, Kidney, Liver and intrahepatic bile ducts, Pancreas, Prostate gland, Thyroid gland/ Cancer | ResNet18, self-supervised BYOL method, Clustering tiles using k-means clustering |
| [356] | Segmentation, Classification | Colon, Liver, lymph node sections | An ensemble of FCNs architectures/U-Net with DenseNet, ResNet |
| [784] | Segmentation cellular nuclei | Multiple | Cross-patch Dense Contrastive Learning |
| [569] | Prognosis, Cancer Grade Classification | brain and kidney | CNN, GCN, SNN |
| [785] | Segmentation | Colon, Lymph Node | Kullback-Leibler (KL) divergence with classifier |
| [486] | Segmentation | Breast, Bone, Tissue | Performing Neural architecture search(NAS) |
| [786] | Segmentation of nuclei and cytoplasm | Lung, Bladder | Multi-task model |
| [787] | Classification | Axillary lymph nodes, Breast/Metastasis, Colorectal cancer | Adversarial autoencoder, Progressive growing algorithm for GANs, Resnet18 with pre-trained ImageNet weights |
| [612] | Classification, Detection | Skin/ cutaneous melanoma(SKCM), Stomach/ adenocarcinoma(STAD), Breast/ cancer(BRCA), Lung/ adenocarcinoma(LUAD), Lung/ squamous cell carcinoma (LUSC) | Convolutional neural networks(CNNs), Birch clustering |
| [788] | Classification of tissue | Stomach, Colon, Rectum | CNN+ Pathology Deformable Conditional Random Field |
| [479] | Classification of tissue | Liver, Lung, Colon, Rectum | Contrastive learning (CL) with latent augmentation (LA) |
| [789] | Classification | Stomach, Intestine, Lymph node, Colon | label correction + NSHE scheme |
| [790] | Detection | Renal/ cell carcinoma (RCC), lung/nonsmall cell cancer (NSCLC), Breast/cancer lymph node metastasis | Attention-based learning, Instance-level clustering |
| [791] | Classification | Breast, Colon /Tumor metastasis and Tumor cellularity quantification | ResNet-18 |
| [386] | Classification, Detection | Breast cancer, Colorectal adenocarcinoma, Colorectal cancer | Co-representation learning (CoReL), Neighborhood-aware multiple similarity sampling strategy |
| [348] | segmentations | Nuclei in pancreatic, tubules in colorectal, epithelium in breast | U-net |
| [457] | Classification | Brain, Endocrine, Gastro, Gynaeco, Liver, pancreas, Urinary tract, Melanocytic, Pulmonary, Prostate Cancer | DenseNet121, KimiaNet |
| [792] | Detection | cell nuclear | Robust Self-Trained Network(RSTN) trained on distance maps(DMs) |
| [391] | Segmentation, Classification | Nuclei in the breast, prostate/Benign, ADH, DCIS | GNN models |
| [316] | Classification, Segmentation | Lung and Skin/nuclei | ResGANet |
| [662] | Prognosis | HPV+, HPV-, survival class | MIL classifier with discriminant analysis |
| [455] | Detection | 18 primary organ/Tumor | MIL with attention pooling |
| [246] | Detection | Tumor, normal | Sparse coding and transfer learning |
| [74] | Detection | Tumor, normal from 23 cohorts | CNN-based classifier with transfer learning |
| [717] | Detection | Loose non-tumor tissue, dense non-tumor tissue, normal tumor tissue | Custom CNN classifier |
| [383] | Detection | Mitosis centroid | G-CNN for rotational invariance |
| [319] | Detection, Segmentation | Colon, Rectum | Concept Contrastive Learning |

Table 9.11 Continued on Next Page

Organ Overview (Continued)

| Continuation of Organ Overview Table 9.11 | | | |
|---|-------------------------------|---|--|
| References | Tasks | Disease Specification | Methods |
| [309] | Disease diagnosis | Lung, Breast, Colorectal, Glioma, Renal, Endometrial, Skin, Head and neck, Prostate, Bladder, Thyroid, Ovarian, Liver, Germ cell, Cervix, Adrenal/metastatic tumors and Cancer | MIL |
| [280] | Segmentation | Breast, Pancreatic, Colon/Cell Nuclei, Tubules, Epithelium | u-net |
| [207] | Segmentation | prostate, colon, breast, kidney, liver, bladder, stomach/Nuclei | U-Net |
| [478] | Segmentation | Bladder, Breast, Colorectal, Endometrial, Ovarian, Pancreatic, Prostate/Nuclei | Hovernet on tiles, Nuc2Vec with a ResNet34 with contrastive learning method |
| [631] | Segmentation | Brain, Kidney, | semantic segmentation+ Xception |
| [566] | Segmentation | Breast, liver, kidney, prostate, bladder, colon, stomach/Cell boundary pixels, Nuclei | Hard-boundary Attention Network (HBA Net) with background weaken module (BWM) |
| [376] | Segmentation, Classification | Bladder, Breast, Colorectal, Endometrial, Ovarian, Pancreatic, Prostate/Nucleus boundaries/Normal epithelial, malignant/dysplastic epithelial, fibroblast, muscle, inflammatory, endothelial, miscellaneous | CNN pretrained on ImageNe/End-to-end learning |
| [353] | Classification | Thyroid frozen sections, Colonoscopy tissue, Cytological cervical pap smear/ benign, non-benign | VGG16bn, ResNet50, U-net, with stochastic selection and attention fusion |
| [793] | Classification | Colon, Breast/ non-discriminative and discriminative regions | CNN classifier, ResNet18, Weakly supervised learning, Max-Min uncertainty |
| [383] | Classification, Segmentation | Nuclear boundaries, Benign, malignant | G-CNN for rotational invariance |
| [172] | Classification | Basaloid, Melanocytic, Squamous | Multi-stage CNN classifier |
| [794] | Classification | Colorectal glands, Tumor, normal | Dense steerable filter CNN for rotational invariance |
| [451] | Segmentation | Contoured tumor regions | Resnet classifier with transfer learning |
| [716] | Classification | Skin melanoma, stomach adenocarcinoma, breast cancer, lung adenocarcinoma, lung squamous cell carcinoma | Custom CNN using human-interpretable image features (HIF) |
| [795] | Classification | 20 classes for muscle, epithelial, connective tissue | Inception Residual Recurrent CNN |
| [32] | Tissue subtype classification | Adipose (ADI), background (BACK), debris (DEB), lymphocytes (LYM), mucus (MUC), smooth muscle (MUS), normal colon mucosa (NORM), cancer-associated stroma (STR), colorectal adenocarcinoma epithelium (TUM) | ResNet based classifier |
| [392] | Nuclei segmentation | Breast, Colon, Liver, Prostate, Kidney, Stomach, Colorectal, Bladder, Ovarian | CNN model, VGG-19 network |
| [275] | Segmentation | Lung, Breast | Multiple Instance Learning (MIL), self-supervised contrastive learning in SimCLR setting, feature vector aggregation |
| [323] | Prognosis | Prediction of cancer rate survival in the Bladder, Breast, Lung, Uterus, Brain | Graph Convolutional Neural Net (GCN) |
| [207] | Nuclei segmentation | prostate, colon, breast, kidney, liver, bladder, stomach | A convolutional U-Net architecture |
| [340] | Nuclei segmentation | Nuclear boundaries | U-net based architecture |
| [485] | Nuclei segmentation | Nuclear boundaries | Modified HoVer-Net segmentation |
| [358] | Nuclei segmentation | Nuclear boundaries | CNN-based attention network |
| [307] | Segmentation | 3-level hierarchy of histological types | Pixel level semantic segmentation |
| [198] | Segmentation | Tissue, background, edge artifacts, inner artifacts, inner/external margin | Custom FCNN |
| [266] | Segmentation | Lymphocytes, necrosis | Semantic segmentation CNN classifier |
| [169] | Disease diagnosis | usual ductal hyperplasia, ductal carcinoma in-situ | Deep-learning based CAD tool for pathologists |
| [431] | Nuclei segmentation | Positive/negative in nuclei boundaries | Conditional GAN |
| [365] | Nuclei segmentation | Nuclear boundaries | CNN-based Boundary-assisted Region Proposal Network |
| [364] | Nuclei segmentation | Nuclei, other | CNN-based multi-branch network classifier |
| [199] | Detection | Mitosis and metastasis detection | U-Net based normalization |
| [338, 168] | Nuclei segmentation | normal epithelial, myoepithelial, invasive carcinoma, fibroblasts endothelial, adipocytes, macrophages, inflammatory | U-Net with regression loss |
| [342] | Nuclei segmentation | Nuclei body, nuclei boundary, background Background removal Nuclei boundary | UNet based classifier with self-supervised learning UNet with transfer learning Custom encoder-decoder network |
| [120] | Tissue subtype classification | 60 types of tissues from a various datasets | ResNet50 feature encoder/decoder for 11 tasks |
| [667] | Detection | Tumor, normal | ResNet based patch classifier |
| [628] | Classification | Skin/Skin lesions, Chest/ Benign, malignant, Kidney/Chromophobe, clear cell, papillary carcinoma | Conditional Progressive Growing GAN (PG-GAN/ResNet-50) |
| [212] | Classification | Neural image compression for Rectal carcinoma | CNN classifier with encoder compression network |

Table 9.11 Continued on Next Page

| Continuation of Organ Overview Table 9.11 | | | |
|---|---|---|--|
| References | Tasks | Disease Specification | Methods |
| [399] | Pathology report information extraction | Tumor description relating to primary cancer site, laterality, behavior, histological type, and histological grade | Ensemble of multi-task CNN |
| [195] | Detection | Blur detection | Combination of CNN and Random Forest regressor |
| [196] | Classification | 15 types based on focus level | Lightweight CNN |
| [718] | Segmentation | Molecular feature extraction | Multi-layer perceptron with aggregation |
| [713] | Classification | Deblurring | Encoder-decoder with VGG-16 blur type classifier |
| [702] | Classification | WSI Classification | Multi-scale Context-aware MIL, Multi-level Zooming |
| [65] | Classification | BRCA subtyping, NSCLC subtyping, RCC Subtyping | Vision Transformer |
| [796] | Classification | Classification of glioma and non-small-cell lung carcinoma cases into subtypes | Two-level model consisting of an Expectation Maximization based method combined with CNN and a decision fusion model |
| [65] | Prognosis | Survival prediction of IDC, CCRCC, PRCC, LUAD, CRC, and STAD cancer types | Vision Transformer |
| [797] | WSI Processing | Stain normalization | Combination of segmentation and clustering for nuclear/stroma detection |
| [210] | WSI Processing | Stain normalization | Self-supervised cycleGAN |
| [359] | WSI Processing | Stain normalization | Modified Wasserstein Barycenter approach for multiple referencing |
| [681] | WSI Processing | Patch synthesis | Progressive GAN model |
| [798] | WSI Processing | Similar image retrieval | Classifier based on ANN with K-means clustering |
| Other | | | |
| [799] | Detection | Heart/rejection and nonrejection tissue tiles | Progressive Generative Adversarial Network + Inspirational Image Generation with a VGG-19 as a classifier |
| [722] | Detection | Heart failure | CNN based patch classifier |
| [725] | Classification | Heart/Endomyocardial disease | CACHE-Grader, SVM and K-means clustering |
| [723] | Classification | Skin/Cancer | random forest ensemble learning method, feature extractor using ResNeXt50 |
| [362] | Detection | Eye/Macular edema | Fully convolutional neural network (FCN), Improved attention U-Net architecture (IAUNet) |
| [454] | Prognosis | N/A | Custom MIL framework with attention modules |
| [440] | Classification | Bone marrow/Neutrophil, myeloblast, monocyte, lymphocyte | GAN-based classifier |
| [706] | Classification, Detection | Bone marrow/nonneoplastic, myeloid leukemia, myeloma | Two-stage detection and classification model |
| [800] | Detection | Bone marrow/aspirate pathology synopses | BERT-based NLP mode, Active learning |
| [346] | Segmentation | Viable tumor, necrosis with/without bone, normal bone, normal tissue, cartilage, blank | UNet-based multi-magnification network |
| [801] | Diseases diagnosis | Bacterial disease | CNN-based classifier |
| [361] | Segmentation | Bone marrow/Myelopoietic cells, erythropoietic cells, matured erythrocytes, megakaryocytes, bone, lipocytes | Custom CNN |
| [712] | Segmentation | 10 Cancer types | U-Net, Mask R-CNN for quality control |
| [167] | Classification | Level 1 (Epithelial, Connective Proper, Blood, Skeletal, Muscular, Adipose, Nervous, Glandular), Level 2 (23 sub-classes from Level 1), Level 3 (36 sub-classes from Level 2 classes) | Ensemble of different CNN architectures |
| [715] | Classification | Arteries, nerves, smooth muscle, fat | InceptionV3, Deep ranking network |
| [696] | Disease diagnosis | Duodenum/Celiac | CNN-based classifier |
| [268] | Disease diagnosis | Cervical cancer, Squamous cell carcinoma, adenocarcinoma | CNN-based patch classifier |
| [697] | Disease diagnosis | Duodenum/Celiac, environmental enteropathy, Esophagus/EoE, Ileum/Crohn's disease | Hierarchical CNN classifier |
| [709] | Disease diagnosis | Squamous carcinoma | Combinations of CNN classifiers |
| [458] | Classification | Normal, Cervicitis, Squamous Intra-epithelial Lesion- Low and High, Cancer | Deep multiple instance learning |
| [361] | Classification, Segmentation | Bone marrow/Aplasia | SVM classifier with BoW |
| [645] | Detection | Tumor cells, stromal cells, lymphocytes, stromal fibroblasts | k-means, Hierarchical Clustering |
| [398] | Classification | colorectal liver metastasis | Ensemble of 4 MLP and an encoder, supervised multitask learning (MTL) |
| [385] | Detection | Mitosis | Feature pyramid network |
| [728] | Detection | Acute Lymphoblastic (or Lymphocytic) Leukemia (ALL), normal/lymphoblast | Transfer Learning, CNN pretrained on a histopathology dataset, ResNet18 and VGG16 as the backbone |

End of Table 9.11

Compilation of information and Neural Network architectures found in different Co-Path papers categorized by task (see 9.11)

| References | Disease/Organ Specification | Architecture | Datasets |
|--|---|---|--|
| Detection Task | | | |
| [71, 238, 271, 62, 741, 97, 199, 647, 298, 641, 212, 329, 305, 666, 751, 740, 72, 760, 434, 759, 493, 698, 226, 485, 426, 739, 383, 794, 64, 717, 756, 32, 309, 373, 597, 312] | Breast cancer | Custom CNN {15}, Inception {6}, ResNet {14}, VGG {4}, U-Net {2}, Multi-stage CNN {1}, DenseNet {4}, GAN {1}, AlexNet {1}, E-D CNN {1}, CAS-CNN {1}, Attention CNN {3}, HoVer-Net {1}, MLV-DeepLabV3+ {1}, Xception {1}, Lightweight-CNN {1} | RUMC, CAMELYON16, CAMELYON17, MSK, HUP+CINJ, NHO-1, IDC-Moh, AJ-IDC, PCam, NMCSO, HASHI, TCGA, Cancer Imaging Archive, TCGA-BRCA, Yale HER2 dataset, Yale response dataset |
| [71, 62, 73, 425, 678, 274, 672, 309, 598] | Prostate cancer | Custom CNN {2}, ResNet {4}, Inception {1}, Non-DL {1}, NASNetLarge {1} | RUMC, MSK, HUH, Pro-Raciti, Pro-Doyle, CUH, UHB, Gleason 2019 |
| [62, 605, 266, 618, 309, 723] | Skin cancer | ResNet {3}, Inception {1}, Custom CNN {1}, E-D CNN {1}, ResNeXt {1} | SCMOI, YSM, GHS, MIP, MSK, BE-Cruz-Roa, Private |
| [447, 439, 448, 231, 452, 717, 779, 310, 311, 460, 228] | Colon cancer | Custom CNN {2}, Inception {1}, GAN {1}, Novel algorithm {1}, DenseNet {1}, ResNet {2}, Inception-ResNet {1}, U-Net {1}, VGG {1}, Swarm Learning {1} | SC-Xu, FAHZU, OSU, TCGA, CRC-Chikontwe, Novel Dataset, DigestPath 2019, Epi700, DACHS, TCGA-CRC, QUASAR trial, YCR-BCIP |
| [243, 698, 231, 717, 699, 345, 276] | Stomach cancer | AlexNet {1}, ResNet {3}, Inception {3}, DenseNet {1}, DeepLab {1}, VGG {1}, DLA {1}, Custom CNN {1} | TCGA, SSMH-STAD, SC-Kong |
| [278, 309] | Bladder cancer | Inception {1}, ResNet {2} | TCGA |
| [709, 309] | Cervix cancer | Inception {1}, ResNet {2}, Inception-ResNet {1} | XH-FMMU |
| [626] | Kidney cancer | Custom CNN {1} | Pantomics |
| [771, 309, 570, 352, 663] | Lung cancer | Inception {2}, ResNet {1}, DT {1}, AdaBoost {1}, XGBoost {1}, U-Net {1} | TCGA(-LUAD,-LUSC), MedicineInsight, 22c3, Ventana PD-L1, Private |
| [32] | Oral cancer | Custom CNN {1} | LNM-OSCC |
| [377, 199, 225, 269, 378, 344, 379, 200, 380, 381, 382, 383, 384, 385] | Mitosis | Custom CNN {7}, AlexNet {1}, U-Net {2}, Multi-stage CNN {2}, FCN {1}, R-CNN {1}, ResNet {2} | TUPAC16, RUMC, MITOS12, TNBC-JRC, AMIDA13, MITOS-ATYP1A14, CWRU |
| [387, 388, 77, 389, 390, 372, 792, 477, 392, 478, 376, 769] | Nuclei | U-Net {2}, GAN {1}, Non-DL {2}, Custom CNN {2}, Hover-Net {2}, SC-CNN {1}, Robust-Self Trained Network (RSTN) {1}, RCNN {1}, VGG {1}, ResNet {2}, E-D CNN {1} | NHS-LTGU, TNBC-CI, MoNuSeg, UHZ, CRCHistoPhenotypes, TCGA, Private, BCFM, PanNuke, NuCLS, CoNSEP, NCT-CRC-HE-100K, Cleveland Clinic (CC) |
| [80, 393] | Colorectal gland | FCN {2} | GLaS |
| [199] | Epithelial cell | Custom CNN {1} | PCa-Bulten, RUMC |
| [394, 395, 396] | Glomeruli | ResNet {1}, VGG {1}, AlexNet {1}, MobileNet {1} | Kid-Wu, Kid-Yang |
| [722, 725, 799] | Heart failure, Heart Transplant | Custom CNN {1}, K-Means {1}, SVM {1}, VGG {1}, PG-GAN {1} | UPenn, CHOA |
| [371] | Keratin pearl | Custom CNN {1} | BCRWC |
| [561, 604] | Liver, Liver fibrous region | Non-DL {1}, Autoencoder CNN {1} | Liv-Atupelage, PAIP |
| [241] | Lymphocyte-richness | Autoencoder CNN {1} | TCGA |
| [294] | Microsatellite instability | ResNet {1} | TCGA, DACHS, KCCH |
| [397, 602] | Tumor-infiltrating lymphocyte | U-Net {1}, IM-Net {1}, DRDIN {1} | TCGA, DUKE |
| [246, 74, 309, 457, 612, 316] | Multi-organ tumor | KimiaNet {1}, Novel algorithm {1}, ResNet {3}, Inception {1}, DenseNet {1}, Custom CNN {1}, MLV-DeepLabV3+ {1} | AJ-Lymph, TCGA, ISIC2017, LUNA, COVID19-CT |
| [195, 802, 196] | WSI defect | ResNet {2}, DenseNet {1}, Novel algorithm {1}, Custom CNN {1} | Pro-Campanella, MO-Campanella, MGH, TCGA@Focus, FocusPath |
| [728] | Acute Lymphoblastic (or Lymphocytic) Leukemia (ALL) | Custom CNN {1}, ResNet {1}, VGG {1} | ADP, ALL-IDB2 |
| Tissue Subtype Classification Task | | | |
| Table 9.11 Continued on Next Page | | | |

| Continuation of Technicalities by Task Table 9.11 | | | |
|--|------------------------------|---|--|
| References | Disease/Organ Specification | Architecture | Datasets |
| [86, 774, 692, 199, 78, 286, 775, 776, 777, 695, 689, 32, 318] | Colorectal cancer | Non-DL {1}, FCN {1}, ResNet {3}, VGG {3}, AlexNet {1}, Inception {1}, SqueezeNet {2}, BCNN {1}, Capsule CNN {1}, Custom CNN {5}, U-Net {2} | NCT-CRC-HE-100K, NCT-CRC-HE-7K, RUMC, RC-Ciampi, GLaS, CRC-TP, CRC-CDC, UMCM, DHMC-Korbar, TBB, HUH, Stanford Hospital, TCGA |
| [436, 781, 445, 27, 644, 689, 334] | Breast cancer | Custom CNN {1}, ResNet {1}, Novel algorithm {2}, Inception {2}, Novel CNN {1} | US-Biomax, ABCTB, TCGA, Bre-Chang, Bre-Steiner, BCSC, NKI-VGH, BACH |
| [257, 781, 563] | Brain cancer | VGG {1}, Novel algorithm {1}, ResNet {1} | UHN, TCGA |
| [75, 247, 541] | Lung cancer | ResNet {2}, AlexNet {1}, Inception {1}, Custom CNN {1} | DHMC, CSMC, MIMW, TCGA, NLST, SPORE, CHCAMS |
| [204, 296, 679] | Prostate cancer | Non-DL {2}, Custom CNN {1}, ResNet {1} | CPCTR, UHZ-PCa, UPenn |
| [781, 296, 64] | Kidney cancer | Novel algorithm {1}, ResNet {2} | TCGA, UHZ-RCC, BWH |
| [146] | Bladder cancer | ResNet {1} | CCC-EMN MIBC |
| [694] | Stomach cancer | Custom CNN {1} | SPSCI |
| [202, 640, 167, 296, 716, 795, 455, 783, 65] | Multi-organ | Non-DL {1}, Custom CNN {2}, VGG {2}, Inception {3}, ResNet {4}, K-Means {2}, XGBoost {1}, ViT {1} | MO-Khan, KIMIA Path24, ADP, UHZ, TCGA, KIMIA Path960, MO-Diao, BWH-TCGA-MO, CRC-100K, BCSS, BreastPathQ |
| [77, 284, 561, 270, 372, 477] | Nuclei | Custom CNN {3}, ResNet {1}, Non-DL {1}, Hover-Net {2} | CRCHistoPhenotypes, CoNSEp, Liv-Atupelage, PHI, Private, PanNuke, NuCLS |
| [231, 730, 372] | Epithelial | Inception {1}, Custom CNN {1}, Hover-Net+ {1} | HUH-HH, NKI-VGH, TCGA, Private |
| [396] | Glomeruli | AlexNet {1} | AIDPATH _A , AIDPATH _B |
| [440, 361, 706] | Bone marrow | VGG {1}, GAN {1}, FCN {1} | BM-MICCAI15, BM-Hu, FAHZU, RUMC, EUH |
| [564, 617, 259] | Lesion | Non-DL {2}, Inception {1} | UPMC, BE-Hart, Bre-Parvatikar |
| [669] | Oral cavity | AlexNet {1} | ECMC |
| Disease Diagnosis Task | | | |
| [748, 227, 234, 263, 761, 235, 236, 750, 421, 596, 306, 647, 648, 63, 298, 328, 747, 330, 749, 641, 734, 735, 752, 515, 736, 305, 496, 423, 264, 742, 743, 308, 753, 737, 424, 297, 444, 633, 744, 331, 301, 302, 754, 26, 213, 745, 429, 746, 495, 650, 651, 454] | Breast cancer | ResNet {14}, VGG {7}, Inception {9}, Custom CNN {12}, AlexNet {3}, XGBoost {1}, MobileNet {1}, Xception {1}, DenseNet {7}, Multi-stage CNN {3}, Capsule CNN {1}, SENet {1}, Inception-ResNet {1}, VGGNet {2}, Attention CNN {3}, RCNN {1}, CaffeNet {1}, TriResNet {1}, Class Structured Deep CNN {1}, Non-DL {1} | BACH18, BreakHis, BioImaging, Ext-BioImaging, CAMELYON16, CAMELYON17, CMTHis, AP, AJ-IDC, BIDMC-MGH, PUIH, BRACS, TCGA |
| [208, 764, 389, 674, 449, 680, 675, 200, 676, 677, 763, 672, 765] | Prostate cancer | Custom CNN {3}, U-Net {1}, ResNet {2}, VGG {2}, Inception {1}, AlexNet {2}, Non-DL {1}, MobileNet {1}, DenseNet {1}, DCNN {1}, NASNetLarge {1} | SUH, CSMC, TCGA, NMCS-D-MML-TCGA, VPC, UPenn, RCINJ |
| [688, 142, 303, 82, 691] | Colon cancer | Inception {1}, ResNet {4}, SqueezeNet {1}, AlexNet {2}, MobileNet {1}, Xception {1} | Warwick-CRC, Ext-Warwick-CRC, SC-Holland, GLaS, ZU, ULeeds |
| [498, 768, 258, 339, 64, 770, 662] | Lung cancer | Inception {1}, ResNet {3}, Non-DL {2}, DenseNet {1}, GCNN {1} | TCGA, MICCAI17, Stanford-TMA, NYU LMC, BWH, DHMC, ES-NSCLC |
| [76, 142, 731, 732] | Brain cancer | Non-DL {2}, Custom CNN {1}, AlexNet {1} | TCGA, MICCAI14 |
| [497, 561] | Liver cancer | DenseNet {1}, Non-DL {1} | TCGA, SUMC, Liv-Atupelage |
| [335, 446] | Stomach cancer | Custom CNN {1}, Multi-stage CNN {1} | GNUCH, WSGI |
| [304, 616, 172] | Skin cancer | ResNet {2}, VGG {1}, Multi-stage CNN {1} | DKI, Y/CSUXH-TCGA, DLCS, BE-TF-Florida-MC |
| [422] | Bladder cancer | Custom CNN {1}, Inception {1}, Multi-stage CNN {1} | TCGA+UFHSH |
| [268] | Cervix cancer | VGG {1} | TCGA |
| [295] | Esophagus cancer | ResNet {1}, Attention CNN {1} | DHMC |
| [454] | Kidney cancer | Custom CNN {1} | TCGA |
| [297, 353] | Multi-organ cancer | Inception {1}, ResNet {2}, Custom CNN {1}, U-Net {1}, VGG {1} | Stanford-TMA, BIDMC-MGH, Private |
| [662] | Oral cancer | Custom CNN {1} | OP-SCC-Vanderbilt |
| [119] | Ovarian cancer | VGG {1}, Multi-stage CNN {1} | VGH |
| [300, 696, 697] | Non-cancer GI tract disorder | ResNet {2}, VGG {1} | DHMC-Wei, UV, SC-Sali |
| [565, 666] | Lymphoma | E-D CNN {1}, Custom CNN {1} | TUCI-DUH, AJ-Lymph |

Table 9.11 Continued on Next Page

Technicalities by Task (Continued)

| Continuation of Technicalities by Task Table 9.11 | | | |
|---|---|--|--|
| References | Disease/Organ Specification | Architecture | Datasets |
| Segmentation Task | | | |
| [337, 377, 357, 265, 338, 284, 339, 241, 440, 431, 619, 340, 561, 712, 363, 642, 485, 383, 794, 168, 214, 364, 358, 341, 365, 342, 359, 477, 207, 478, 376, 566, 769] | Nuclei | U-Net {6}, Custom CNN {8}, FCN {1}, ResNet {5}, GAN {4}, Non-DL {2}, Multi-stage CNN {1}, E-D CNN {4}, Autoencoder CNN {1}, PangNet {1}, DeconvNet {1}, Hover-Net {3}, multi-branch CNN {1}, Attention(EP, SM) CNN {1}, HBANet {1} | MICCAI15-18, TCGA, TNBC-CI, MoNuSeg, CPM-15, CPM-17, CCB, CRCHistoPhenotypes, CoNSeP, BM-Hu, FAHZU, Liv-Atupelage, DHMC, MO-Khoshdeli, AJ-N, Kumar-TCGA, TCGA-Nuclei, SOX10, UrCyt, NLST, Pan-Bai, PanNuke, NuCLS, Cleveland Clinic (CC) |
| [80, 83, 84, 81, 366, 772, 82, 393, 773, 794, 168] | Gland | FCN {2}, Non-DL {1}, Custom CNN {5}, ResNet {2}, VGG {1}, multi-branch CNN {1}, E-D CNN {1} | GLaS, Bilkent, CRAG, Priv-IHC |
| [285, 330, 643, 367, 368, 567, 360, 369, 373, 374, 312, 738] | Breast tumor | Custom CNN {2}, Inception {2}, U-Net {3}, FCN 1, E-D CNN {1}, RAN {1}, DA-RefineNet {1}, DeepLab {1}, MLV-DeepLabV3 {1} | CAMELYON16, CAMELYON17, BACH18, TCGA, UHCMC-CWU, BC-Priego-Torres, TUPAC16, AMGrad, TCGA-BRCA, Yale HER2 dataset, Yale response dataset |
| [370, 142, 375, 311] | Colon tumor | Custom CNN {1}, VGG {1}, U-Net {2}, Non-DL {1}, AlexNet {1} | Warwick-UHCW, Warwick-Osaka, ZU, DigestPath 2019, Yeouido |
| [483, 343, 604] | Liver tumor | PlexusNet {1}, U-Net {1}, Autoencoder CNN {1} | TCGA, IHC-Seg, PAIP |
| [352] | Lung tumor | U-Net {1} | 22c3, Ventana PD-L1 |
| [483, 568, 354] | Prostate tumor | PlexusNet {1}, Non-DL {1}, U-Net {1} | SMS-TCGA, UUH, Private |
| [285, 299] | Stomach tumor | Inception {1}, U-Net {1}, ResNet {1} | SC-Takahama, SC-Liu |
| [142] | Brain tumor | AlexNet {1} | MICCAI14 |
| [346] | Bone tumor | U-Net {1} | MSKCC |
| [277, 316] | Skin tumor | FCN {1}, ResNet {1}, ResGANet {1} | TCGA, ISIC2018 |
| [451] | Multi-organ tumor | ResNet {1} | TCGA |
| [84, 625, 152, 351] | Kidney tissue structure | Custom CNN {1}, U-Net {1}, cascaded CNN {1} | WUPAX, M-Gadermayr, RUMC, Mayo, AIDPATH |
| [361] | Bone marrow cell | FCN {1} | RUMC |
| [347] | Breast tissue subtype | U-Net {1} | NHS |
| [307] | Histological tissue type | Custom CNN {1} | ADP |
| [758] | Liver steatosis | ResNet {1} | Liv-Guo |
| [344, 345] | Mitosis | U-Net {1}, FCN {1} | MITOS12, MITOS-ATYPIA14, AMIDA13 |
| [371, 372] | Oral mucosa, Oral Epithelial Dysplasia | Custom CNN {1}, Hover-Net+ {1} | BCRWC, Private |
| [266, 602, 205] | Lymphocytes(Tumor-infiltrating, segmentation) | E-D CNN {1}, IM-Net {1}, DRDIN {1}, U-Net {1}, SegNet {1} | TCGA, DUKE, Lymphocyte Detection(from Andrew Janowczyk and Anant Madabhushi) |
| [198, 362] | Tissue region, Fluid Lesions | Custom CNN {1}, FCN {1}, IAUNet {1} | Bánda-Dev-Set, Bánda-Dis-Set, RETOUCH |
| WSI Processing Task | | | |
| [387, 209, 675, 437, 438, 619, 200] | Domain adaptation | GAN {5}, U-Net {1}, AlexNet {1}, Custom CNN {1}, ResNet {5} | NHS-LTGU, MITOS-ATYPIA14, RCINJ, Roche, Liv-Lahiani, TUPAC16, TCGA, DHMC, SOX10, UrCyt |
| [208, 325, 202, 658, 203, 797, 210, 359] | Stain normalization | Custom CNN {2}, ResNet {1}, VGG {1}, U-NET {1}, GAN {3}, E-D CNN {1}, Multi-stage CNN {1}, Non-DL {4} | SUH, Leica Biosystems, MO-Khan, MGH, Lym-Bejnordi, Salvi-SCAN, MITOS-ATYPIA14 |
| [337, 496, 431, 432, 681, 628, 433] | Patch synthesis | Custom CNN {2}, GAN {5}, PG-GAN {2}, ResNet {1}, VGG {1}, U-Net {2} | MICCAI16/17/18, Kumar-TCGA, BreakHis, NKI-VGH, TCGA, OV-CARE, ISIC 2020, ChestXray-NIHCC, CRAG, Digestpath |
| [199, 434, 757, 359] | Processing technique comparison | U-Net {1}, Custom CNN {2}, GAN {2} | RUMC, CAMELYON16, MITOS-ATYPIA14 |
| [212, 398] | WSI compression | Custom CNN {2}, E-D CNN {1}, GAN {1} | N/A |
| [691] | Data cleaning | ResNet {1} | ULeeds |
| [782] | Stain augmentation | VGG {1} | Kid-Cicalese |
| [782] | Tissue component discrimination | Non-DL {1} | TCGA, MO-JHU/US/UB |
| [750] | WSI transformations | Custom CNN {1} | BreakHis |
| [702] | WSI Classification | MIL {1} | IMP Diagnostics Lab., BRIGHT, CAMELYON16 |
| Patient Prognosis Task | | | |

Table 9.11 Continued on Next Page

| Continuation of Technicalities by Task Table 9.11 | | | |
|--|--|--|---|
| References | Disease/Organ Specification | Architecture | Datasets |
| [245, 85, 484, 620, 563] | Brain cancer | Inception {1}, VGG {1}, Custom CNN {2}, Capsule CNN {1}, ResNet {1} | TCGA |
| [258, 620, 541, 214, 453, 662, 571] | Lung cancer | Custom CNN {2}, Non-DL {2}, AttentionMIL {1}, MI-FCN {1}, HANet {1} | Stanford-TMA, TCGA(-LUSC), CHCAMS, NLST, ES-NSCLC |
| [86, 88, 780, 453] | Colon cancer | VGG {2}, Inception {1}, ResNet {1}, Non-DL {1}, AlexNet {1}, SqueezeNet {1}, AttentionMIL {1}, MI-FCN {1} | NCT-CRC-HE-100K, NCT-CRC-HE-7K, HUCH, WRH-WCH, MCO |
| [388, 767, 454] | Kidney cancer | Non-DL {2}, AttentionMIL {1} | UHZ, TCGA, HPA |
| [397, 454] | Breast cancer | U-Net {1}, AttentionMIL {1} | AJ-Lymph, TCGA |
| [680] | Prostate cancer | Inception {1} | NMCS+MML+TCGA |
| [266] | Melanoma | Multi-stage CNN {1} | MIP, YSM, GHS |
| [87] | Mesothelioma | ResNet {1} | MESOPATH, TCGA |
| [323, 65] | Multi-Organ | AttentionMIL {1}, GCN {1}, ViT {1} | TCGA, CRC-100K, BCSS, BreastPathQ |
| [89, 733] | Recurrence prediction | Custom CNN {1}, Non-DL {1} | NSCLC-Wang, ROOHNS |
| Other Tasks | | | |
| [497, 27, 425, 304, 682, 350] | Clinical validation, Stress Test, Quality Control, Explainability | DenseNet {1}, ResNet {2}, Inception {1}, Inception-ResNet {1}, Extended U-Net {1} | SUMC, Bre-Steiner, Pro-Raciti, DKI, TCGA, Private |
| [306, 167, 712, 213, 280, 391, 267, 314, 355, 435, 273, 206, 652, 356] | Dataset creation/curation and annotation, Integrated API and (End-to-End) Toolkits | Custom CNN {1}, GNN {1}, VGG {3}, Inception {3}, AlexNet {1}, FCN {2}, U-Net {4}, ResNet {6}, Hover-Net {1}, DenseNet {1}, MobileNet {1}, DeepLab {1}, SLAM {1} | CMTHis, ADP, TCGA, TCGA-Nuclei, PUIH, BRACS, BACH, UZH, SICAPv2, Lizard, GTE Dataset(V8), BreakHis, HF(Heart failure) Dataset, DACHS, YCR-BCIP, Diagset-A, Diagset-B, Diagset-C, Painter by Numbers, miniImageNet, CRC(DX), CAMELYON(16,17), DigestPath, PAIP, Private |
| [771, 778, 667] | Data deficiency study | Inception {1}, Custom CNN {1}, ResNet {1} | TCGA, GLaS, CAMELYON16, CAMELYON17, Thagaard |
| [715, 762, 427, 765, 456, 375, 783, 459] | Image retrieval/compression, Representation Learning | ResNet {1}, Inception {1}, Non-DL {2}, GCN {1}, AttnMIL {1}, Custom CNN {2}, U-Net++ {1}, Barcodes {1}, XGBoost {1}, K-Means {1} | TCGA, CAMELYON16, SC-Zheng, CRA, Han-Wistar Rats |
| [120, 398, 603, 275, 323, 475, 610, 790, 791, 803, 477, 793, 313, 458, 459, 460, 276, 435, 478, 315, 461, 701, 462, 463] | Multi-(task,instance) learning(MT,MIL), (Weak,Semi,Self)-Supervised Learning, Contrastive Learning | ResNet {9}, GCN {1}, AttentionMIL {2}, MuSTMIL {1}, SimCLR {3}, MIL {2}, D(S)MIL {1}, Pretext-RSP {1}, MoCo {1}, MLP {1}, CLAM {1}, GAN {1}, VGG {2}, DenseNet {2}, Hover-Net {2}, Custom CNN {2}, SLAM {1}, DLA {1}, TransMIL {1} | UHC-WNHST, PanNuke, AJ-Epi-Seg, OSCC, TCGA(-CRC-DX, -THCA, -NSCLC, -RCC), CAMELYON16, CAMELYON17, NCT-CRC-HE-100K, NCT-CRC-HE-7K, CPM-17, AJ-Lymph, M-Qureshi, SKMCH&RC, SKMCH&RC-M, OV-Kobel, MT-Tellez, TUPAC16, SC-Galjart, CT-CRC-HE-100K, Munich AML, MSK, MHIST, CPTAC, Kather multi-class, BreastPathQ, CRC, Novel, PanNuke, NuCLS, GLaS, OAUTHC, DACHS, YCR-BCIP, BreakHis, DEC, TH-TMA17 |
| [269, 212, 349] | Proliferation scoring | Custom CNN {2}, piNET {1} | TUPAC16, DeepSlides |
| [440] | Cell clustering | ResNet {1} | MICCAI15, BM-Hu, FAHZU |
| [440] | Chemosensitivity prediction | Non-DL {1} | TCGA |
| [486] | Neural Architecture Search | DARTS {1} | ADP,BCCS,BACH, Osteosarcoma |
| [257, 762, 476, 604, 612, 478] | Feature extraction/analysis, Unsupervised Learning | VGG {1}, Custom CNN {2}, Hover-Net {1}, PixelCNN {1}, AutoEncoder CNN {1} | CAMELYON16, UHN, TCGA, Private |
| [498, 461, 701, 462] | Gene mutation prediction | VGG {1}, Inception {1}, AttentionMIL {2}, DenseNet {1}, ResNet {1}, Hover-Net {1} | TCGA(-CRC-DX, -THCA), DEC, PAIP, TH-TMA17, Private |
| [747, 394, 386, 311, 392] | Novel loss function, Novel optimizer | ResNet {3}, VGG {3}, MobileNet {1}, DenseNet {1}, U-Net {1} | BACH18, AJ-Lymphocyte, CRCHistoPhenotypes, CoNSEP, ICPRI2, AMIDA13, Kather Multi-class, DigestPath 2019, CT-CRC-HE-100K |
| [689, 610] | Patch triaging | Non-DL {1}, ResNet {1}, Pretext-RSP {1}, MoCo {1}, MLP {1} | BIRL-SRI, CAMELYON16, MSK, MHIST |
| [399, 800] | Pathology report information extraction | BERT {1}, Custom CNN {1} | LTR |
| [332] | Receptor status prediction | Custom CNN {1} | TCGA |
| [278] | TMB prediction | Inception {1} | TCGA |
| [269, 653] | Tumor grading | Mask R-CNN {1}, Custom CNN {1}, Non-DL {1} | TUPAC16, Post-NAT-BRCA, ILC |
| [645] | Visual analytic tool | Non-DL {1} | TCGA |
| End of Table 9.11 | | | |

9.12. Model Card Categorization

For comprehensive review on model cards and updated information, please refer to our GitHub repository for more information. The following lists examples of our model cards used in preparation of our survey paper.

9.12.1. Template

Model-Card for Categorizing Computational Pathology Papers

Step-1) Paper Summarization:

Summarize the paper in terms of (A) Goal/Problem of the paper to be solved; (B) Why the problem introduced by the authors is important to the community in terms of Technical Novelty, Comprehensive Experiment, New Insights, Explainability; and (C) Overall conclusion of the paper.

Step-2) Model Card Table Categorization:

The following is a model-card for each paper to populate the table accordingly. Find relevant information within each category that is reported in the paper. Try to compile it efficiently and populate each sub-type within each category.

| | |
|------------------------------------|---|
| Keywords | comma separated list |
| Organ Application | Organ: Task: |
| Dataset Compilation | Name: Availability: Dataset Size: (#patches/#slides/#images) Image Resolution: Staining Type: Annotation Type: (region/patch/slide-level) Histological Type: (cellular/tissue ROI/etc, I.e., on what basis is it labeled) Label Structure: (single label/multi label) Class Balance: (is size of dataset balanced across each classes) |
| Technicality | Model: (architecture/transfer learning/output format) Training Algorithm: (end-to-end/separately staged) Code Availability: (give source) |
| Data Processing | Image Pre-processing: (patching, data augmentation, color normalization) Output Processing: |
| Performance Summary | Evaluation Metrics: Notable Results: Numerical result for strongest performing model. Comparison to Other Works: Comparison to state-of-the-art models (one sentence) |
| Novelty | Medical Applications/Perspectives: Technical Innovation: (algorithms for processing or deep learning, new metrics) |
| Explainability | Visual Representations: (feature distribution, heatmaps, tsne, gradCAM, pseudocode, etc.) |
| Clinical Validation | Usage in Clinical Settings: Has the work been used by pathologists in clinical setting? Suggested Usage: How can the work be used by pathologists? Performance Comparison: Has the model performance been compared to that of pathologists? |
| Caveats and Recommendations | <ul style="list-style-type: none"> • Personal comments on the paper • Relevant info from other papers • Criticism and limitations of the work |

Step-3) Citation: BibTeX Citation.

9.12.2. Samples

Paper: Pathologist-level classification of histologic patterns on resected lung adenocarcinoma slides with deep neural networks

Summary:

Classification of histological structures in lung adenocarcinoma tissue is important for patient prognosis and treatment plans. Some histological patterns (such as lepidic patterns) are associated with better survival rates, whereas others (micropapillary and solid patterns) are associated with poor prognoses. The identification of these histological patterns is a challenge, as 80% of adenocarcinoma tissue samples contain a mixture of different patterns, and the qualitative classification criteria can result in variance in diagnosis between different pathologists. Automated analysis and classification of tissue structures through convolutional neural networks has been a compelling area of research. This paper presents a variant of ResNet, ResNet18 to perform a patch-based classification amongst the different lung adenocarcinoma histological patterns. A heatmap for the entire WSI is made using the probability score per patch, with low-confidence patches being discarded. The performance of the model is compared with 3 expert pathologists to determine relative performance. The study concludes that the model has high performance, with results on par with expert pathologists.

Categorization:

| | |
|------------------------------------|--|
| Keywords | Deep learning, convolutional neural networks, lung adenocarcinoma, multi class, ResNet |
| Organ Application | Organ: Lung Task: Histologic pattern classification in lung adenocarcinoma |
| Dataset Compilation | Name: Dartmouth-Hitchcock Medical Centre in Lebanon, New Hampshire Availability: Unavailable due to patient privacy constraints. Anonymized version available upon request. Dataset Size: 422 WSIs, 4 161 training ROIs, 1 068 validation patches Image Resolution: 20× magnification Staining Type: H&E Annotation Type: Region-level training set, patch-level validation set, slide-level test set Histological Type: Lepidic, acinar, papillary, micropapillary, solid, and benign. Label Structure: Single label Class Balance: Imbalanced, with significantly fewer papillary patterns in all data. |
| Technicality | Model: ResNet model with 18 layers Training Algorithm: <ul style="list-style-type: none"> • Multi-class cross-entropy loss • Initial learning rate of 0.001 • Learning rate decay by factor of 0.9 per epoch Code Availability: https://github.com/BMIRDS/deepslide |
| Data Processing | Image Pre-processing: <ul style="list-style-type: none"> • Created training ROIs by selectively cropping regions of 245 WSIs. • Spliced 34 validation WSIs into 1 068 224x224 patches. • Colour channel normalization to mean and standard deviation of entire training set. • Data augmentation by rotation; flipping; and random colour jittering on brightness, contrast, hue, and saturation. Output Processing: Low-confidence predictions filtered out for predictions below a threshold. Thresholds are determined by a grid search over classes, optimizing for similarity between the trained model and the validation data. |
| Performance Summary | Evaluation Metrics: F1-Score, AUC Notable Results: F1-Score of 0.904 on validation set, AUC greater than 0.97 for all classes. Comparison to Other Works: ResNet18, 34, 50, 101, 152 compared for performance to choose optimal depth. All had similar accuracies on validation set, so chose ResNet18 for lower model complexity. |
| Novelty | Medical Applications/Perspectives: Potential platform for quality assurance of diagnosis and slide analysis. Technical Innovation: First paper to attempt to classify based on histological lung adenocarcinoma subtypes. |
| Explainability | Visual Representations: Heatmaps for patterns detected, AUC curve for each class |
| Clinical Validation | Usage in Clinical Settings: N/A Suggested Usage: <ul style="list-style-type: none"> • Could be integrated into existing lab information management systems to provide second opinions to diagnoses. • Visualization of a slide could highlight important tissue structures. • Could help facilitate tumour diagnosis process by automatically requesting genetic testing based on histological data for patient. Performance Comparison: <ul style="list-style-type: none"> • On par with pathologists for all evaluated metrics • Model in agreement 66.6% of the time with pathologists on average, with robust agreement (agreement with 2/3 of the pathologists) 76.7% of the time. • WSI region annotation differences between pathologist and model are compared for a sample slide. |
| Caveats and Recommendations | <ul style="list-style-type: none"> • Data taken from one medical centre, so may not be representative of lung adenocarcinoma morphology • Dataset relatively small compared to other deep learning datasets, with some classes having very few instances |

Citation:

```
@article{wei2019pathologist,
title={Pathologist-level classification of histologic patterns on resected lung adenocarcinoma slides with deep neural networks},
author={Wei, Jason W and Tafe, Laura J and Linnik, Yevgeniy A and Vaickus, Louis J and Tomita, Naofumi and Hassanpour, Saeed},
journal={Scientific reports},
volume={9},
number={11},
pages={3358},
year={2019},
publisher={Nature Publishing Group UK London}
}
```

Paper: Classification of lung cancer histology images using patch-level summary statistics

Summary:

The classification of non-small cell lung cancer WSIs as either lung adenocarcinoma (LUAD) or lung squamous cell carcinoma (LUSC) is an important task in diagnosis and treatment planning. Manually classifying these WSIs is a laborious and subjective task that is often complicated by poorly differentiated tissue structures within the slide. Automated classification of WSIs may facilitate the analysis of non-small cell lung cancers. This paper proposes a new 3-class network for effective classification of tissue regions within a WSI. It uses a modification of the ResNet50 architecture, ResNet32 to create probability maps of LUAD/LUSC/non-diagnostic pixels in the WSI. Features from these probability maps are next extracted and fed into a random forest classifier for the final classification. The model achieves the greatest accuracy of 0.81 in the Computational Precision Medicine Challenge and provides a new method of classification for non-small lung cancer histological images.

Categorization:

| | |
|------------------------------------|---|
| Keywords | Non-small cell lung cancer, histology image classification, computational pathology, deep learning |
| Organ Application | Organ: Lung Task: Classification between non-small cell lung cancer types |
| Dataset Compilation | Name: Computational Precision Medicine at MICCAI 2017 Availability: Unavailable, link on MICCAI 2017 website unreachable Dataset Size: 64 WSIs Image Resolution: 20× magnification Staining Type: H&E Annotation Type: Pixel-level and Slide-level Histological Type: <ul style="list-style-type: none"> • At pixel-level, classifies as lung adenocarcinoma (LUAD), lung squamous cell carcinoma (LUSC), and non-diagnostic (ND) • At slide-level, LUAD or LUSC Label Structure: Single label Class Balance: Balanced dataset at the slide level, 32 LUAD and 32 LUSC |
| Technicality | Model: <ul style="list-style-type: none"> • Ensemble ML model • Variant of ResNet50, called ResNet32 with 32 layers and 3x3 kernel, as compared to 7x7 kernel with ResNet50. • 50 statistical and morphological features extracted from probability maps generated by ResNet32. The top 25 are selected for best class separability and used as input to a random forest. Training Algorithm: Separately staged, ResNet32 creates probability maps, then random forest generates final prediction for each WSI Code Availability: Unavailable |
| Data Processing | Image Pre-processing: <ul style="list-style-type: none"> • Splicing of slides into 256×256 patches, then random cropping into 224×224 patches • Reinhard stain normalization • Random crop, flip, rotation data augmentation Output Processing: N/A |
| Performance Summary | Evaluation Metrics: Accuracy Notable Results: <ul style="list-style-type: none"> • ResNet32 with Random Forest achieves 0.81 accuracy over WSI • Results superior to ResNet32 with Maximum Vote, which had 0.78 accuracy. Features for the random forest are tailored for WSI classification, and so can achieve higher performance. Comparison to Other Works: Compared ResNet32 to VGG, GoogLeNet, and ResNet50, with higher average classification accuracy. |
| Novelty | Medical Applications/Perspectives: Automated distinguishing of LUAD tissue from LUSC could be done at scale to assist pathologists in diagnosis and treatment planning for patients. Technical Innovation: <ul style="list-style-type: none"> • First 3-class network for classification of WSI into diagnostic/nondiagnostic areas • Ensemble method resulted in greatest accuracy at the MICCAI 2017 competition. |
| Explainability | Visual Representations: Probability maps for each pixel-level class |
| Clinical Validation | Usage in Clinical Settings: N/A Suggested Usage: Automated distinguishing of LUAD and LUSC slides could aid pathologists in treatment planning. Performance Comparison: N/A |
| Caveats and Recommendations | • Because features for random forest training are chosen based on categorization of lung tissue samples, may not be able to generalize well to other tissue types. |

Citation:

```
@inproceedings{graham2018classification,
title={Classification of lung cancer histology images using patch-level summary statistics},
author={Graham, Simon and Shaban, Muhammad and Qaiser, Talha and Koohbanani, Navid Alemi and Khurram, Syed Ali and Rajpoot, Nasir},
booktitle={Medical Imaging 2018: Digital Pathology},
volume={10581},
pages={327–334},
year={2018},
organization={SPIE}
}
```

Paper: Digital pathology and artificial intelligence (Review)**Summary:**

The advent of cheaper storage solutions, faster network speed, and digitized WSIs has greatly facilitated the presence of digital pathology in modern pathology. Particularly, WSIs allow for the development and integration of automated AI tools for histopathological analysis into the pathologist's workflow. AI tools have the potential to increase the efficiency of diagnostics and improve patient safety and care. However, histological analysis comes with several challenges, including the large size, different potential image magnifications, presence, and variation of stain color information, and z-axis information (in the thickness of the slide). These challenges make it difficult for a human viewer to extract all available information and provide important issues that an AI tool must overcome. This paper outlines several different areas in which AI may be applied in digital pathology, namely education, quality assurance (QA), clinical diagnosis, and image analysis. The potential uses are outlined as follows:

- **Education:** Through the digitization of slides, education can be enhanced. As slides no longer need to be viewed through a microscope, and images can be zoomed into and panned, convenience can be increased without sacrificing the quality of education. Synthetic tissue sample images using GANs can be used to easily create test material in trainees, as well as evaluate cognitive biases in practicing pathologists.
- **Quality Assurance:** Can help pathologists remain updated in their field and check for lab proficiency of diagnoses, as well as monitor for inter-observer variance.
- **Clinical Diagnosis:** AI can aid in the preparation of digital slide imagery, such as in reducing the frequency of out-of-focus areas in slides. Color and stain normalization methods using AI-based models are another possible area of application.
- **Image Analysis:** AI can be used to process the data, including in nuclear segmentation and ROI detection.

AI systems have several different limitations. AI models have been criticized as being black box models. Explainability of decisions will need to be increased. While visualization techniques are being developed, these tend to reduce performance. Additionally, regulatory and economic effects of AI-based systems are unknown at this time. Some areas of future research for AI applications in computational pathology include one-shot learning and reinforcement learning.

Citation:

```
@article{niasi2019digital,
title={Digital pathology and artificial intelligence},
author={Niazi, Muhammad Khalid Khan and Parwani, Anil V and Gurcan, Metin N},
journal={The lancet oncology},
volume={20},
number={5},
pages={e253–e261},
year={2019},
publisher={Elsevier}
}
```